University of Bath

PHD

Fluorescence and Raman spectra of rare earth metaphosphate glasses and pentaphosphate crystals

Farok, Haitham Mohammed

Award date:
1997

Awarding institution:
University of Bath

Link to publication

Alternative formats
If you require this document in an alternative format, please contact:
openaccess@bath.ac.uk

Copyright of this thesis rests with the author. Access is subject to the above licence, if given. If no licence is specified above, original content in this thesis is licensed under the terms of the Creative Commons Attribution-NonCommercial 4.0 International (CC BY-NC-ND 4.0) Licence (https://creativecommons.org/licenses/by-nc-nd/4.0/). Any third-party copyright material present remains the property of its respective owner(s) and is licensed under its existing terms.

Take down policy
If you consider content within Bath's Research Portal to be in breach of UK law, please contact: openaccess@bath.ac.uk with the details. Your claim will be investigated and, where appropriate, the item will be removed from public view as soon as possible.

Download date: 06. May. 2023

IN THE NAME OF GOD, THE MOST GRACIOUS, THE MOST MERCIFUL.

SURELY THE KNOWLEDGE YOU HAVE BEEN GIVEN IS LITTLE.

THE HOLY QURAN.

THIS WORK IS DEDICATED TO

MY FATHER THE GREAT EDUCATOR.

MY MOTHER THE KIND LADY.

MY BROTHERS AND SISTERS.

FLUORESCENCE AND RAMAN SPECTRA OF RARE EARTH METAPHOSPHATE GLASSES AND PENTAPHOSPHATE CRYSTALS

submitted by

HAITHAM MOHAMMED FAROK

for the degree of PhD

of the University of Bath

1997

Copyright

Attention is drawn to the fact that copyright of this thesis rests with its author. This copy of the thesis has been supplied on condition that anyone who consults it is understood to recognise that its copyright rests with its author and no quotation from the thesis and no information derived from it may be published without the prior written consent of the author.

This thesis may be made available for consultation within the University Library and may be photocopied or lent to other libraries for the purposes of consultation.

Signature. 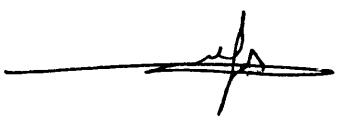 **Date. 23/03/1997**

UMI Number: U529838

All rights reserved

INFORMATION TO ALL USERS
The quality of this reproduction is dependent upon the quality of the copy submitted.

In the unlikely event that the author did not send a complete manuscript
and there are missing pages, these will be noted. Also, if material had to be removed,
a note will indicate the deletion.

UMI U529838
Published by ProQuest LLC 2013. Copyright in the Dissertation held by the Author.
Microform Edition © ProQuest LLC.
All rights reserved. This work is protected against
unauthorized copying under Title 17, United States Code.

ProQuest LLC
789 East Eisenhower Parkway
P.O. Box 1346
Ann Arbor, MI 48106-1346

UNIVERSITY OF BATH
LIBRARY
24 22 SEP 1997
PHD
511545

ACKNOWLEDGEMENTS

I wish to express my great appreciation to my supervisor professor G A Saunders for his guidance, encouragement, advice and value comments and suggestions, without his help and kindness I would not have reached this stage. Many thanks to Mr. B Draper for his technical assistance and for reading the manuscript.

I sincerely wish to thank both Dr. D Adams from the Chemistry Department, Leicester University and Dr. T Beals from STC for their assistance and advice during the first stage of this research which enabled me to make headway into this project.

It has been my privilege to work with Dr. W Poon, Dr. J Crain and Mr. H Vass from the Physics Department, Edinburgh University. I would like to acknowledge their hospitality and thank them for helping me to use their Raman optical set-up.

I am grateful to Dr. W Hönle and Dr. E Schönherr from the Max-Planck-Institut für Festkörperforschung for their assistance in growing the rare earth pentaphosphate crystals.

It is my pleasure to acknowledge the congenial atmosphere and assistance provided by colleagues especially Dr. P Ford, Dr. H Senin, Mr and Mrs. Lambson, Mr. B Chapman, Mr. B Ring and Mr. M Tatar of the School of Physics, University of Bath.

Finally, I must recognise the patience, understanding and support of my family and all my close friends.

ABSTRACT

The details are given of a convenient optical system assembled for use as a precise, rapid and routine instrument for high pressure measurement generated by a diamond anvil cell (DAC), using the fluorescence lines of ruby as a gauge. The system has been successfully used to calibrate the DAC. The system has also been used to measure the fluorescence spectra of rare earth metaphosphate glasses, having the composition $(R_2O_3)_x(P_2O_5)_{1-x}$ (where R represents one of the rare earth elements and the mole fraction x is close to 0.25), and pentaphosphate crystals under hydrostatic pressures up to 50Kbar. Application of pressures up to 50Kbar, using the DAC, to the Eu, Sm and Tb metaphosphate glasses did not alter the positions of the fluorescence bands within the error in the fluorescence wavelength measurements. The shifts ($d\lambda/dp$) in the wavelengths of the fluorescence peaks of the EuP_5O_{14} and SmP_5O_{14} crystals induced by pressure up to 50Kbar in the diamond anvil cell are small but measurable at room temperature. Neither the crystals nor the glasses showed any indication of undergoing a valence change or phase transition up to the highest pressure reached.

The fluorescence spectra of Eu, Sm, Tb and Ho metaphosphate glasses have been measured to examine their valence states. The spectra do not show any obvious sign of divalent rare earth ions in these glasses, only trivalent ion fluorescence being observed. Room temperature absorption spectra of these glasses also evidence only the absorption bands of trivalent rare earth ions.

The laser induced fluorescence spectra of Eu, Sm and Tb pentaphosphate crystals have been measured and compared with the spectra of Eu, Sm and Tb ions incorporated in metaphosphate glasses to investigate their local symmetries. The local symmetry of the europium ion in EuP_5O_{14} crystal fits the low symmetry option (C_s, C_v). At room temperature the crystal field splitting of the energy levels in SmP_5O_{14} is consistent with a pseudocubic local symmetry about the Sm^{3+} ions. At 12K there is a systematic disappearance of the shortest wavelength lines of each fluorescence band consistent with a hypothesis that the local symmetry tends to become closer to being cubic. The local symmetry of the Tb^{3+} ion in TbP_5O_{14} crystal at 12K fits two options, hexagonal and tetragonal. For small distortions

both these local symmetries are close to pseudocubic. These symmetry options of the rare earth ions are in accord with the crystal structure and the shape of the co-ordination polyhedron of the eight oxygen atoms surrounding a rare earth ion which can be thought of as a distorted cube. The metaphosphate glass fluorescence shows aspects which can be related to that of their counterpart crystals, but with inhomogeneous line broadening; the rare earth ion in the metaphosphate glasses can also be thought of as being in the centre of a distorted cube made by the surrounding phosphate tetrahedra.

An alexandrite effect has been found in holmium metaphosphate glass: it's perceived colour changes when it is viewed under different light sources. The colour changes cannot be due to light induced fluorescence. The dominating effect in determining the colour of this glass is related to light transmission through optical windows in its absorption spectrum.

The Raman spectra of some rare earth metaphosphate glasses have been measured in the temperature range 10-300K and compared with the measured spectra of their counterpart rare earth pentaphosphate crystals. The Raman spectra of all the glasses are similar; there exists a common structural skeleton among these glasses: cross-linked chains of PO_4 tetrahedra. The Raman bands of the rare earth metaphosphate glasses have been assigned to vibrational modes. The rare earth ion in these metaphosphate glasses is situated in the centre of a distorted cube made of cross-linked PO_4 tetrahedra. The Raman spectra of the crystals are also similar; the crystals show a higher degree of cross-linking of the PO_4 tetrahedra than the spectra of the glasses. Some of the low frequency Raman modes of the SmP_5O_{14}, EuP_5O_{14} and NdP_5O_{14} crystals show softening with temperature reduction.

The frequency dependence of the coupling constant $C(\omega)$ in the Shuker and Gammon equation at low frequency Raman modes of these glasses has been found to be close to 4; it agrees with the prediction of an ω^4 dependence in the soft potential model for the Stokes Raman scattering intensity of glasses.

CONTENTS

CHAPTER ONE

GENERAL INTRODUCTION

1.1. INTRODUCTION

In modern technological terms the word "glass" (or vitreous in Latin) can be simply defined as an amorphous solid. A material is amorphous when it does not possess the long-range transitional order (periodicity) characteristics of a crystal, that is, when there is no regularity in the arrangement of its molecular constituents on a scale larger than a few times the size of these groups (Pfaender 1983). The uses of glass are numerous and modern technologists are almost continuously proposing new applications. Glass is replacing less abundant and more expensive materials as witnessed by the growing importance of glass in optical and communicational purposes. For example, phosphate glasses find applications such as glass lasers (Weber 1990, Marion and Weber 1991), and optical fibers (Stokowski et al. 1980). Nuclear technology would be unthinkable without radiation shield enclosures with glass viewing windows and there are many areas where recently developed glasses are irreplaceable.

The rare earth metaphosphate glasses $(R_2O_3)_x(P_2O_5)_{1-x}$ (where R represents one of the rare earth elements Ce, Pr, Sm, Nd, Eu, Gd, Tb, Dy, Ho, and Er or La or Y, and the mole fraction x is close to 0.25) have a plethora of fascinating physical properties of fundamental interest and potential application in laser and optoelectronics technology. In general the rare earth ions incorporated into the glass matrix are natural candidates to serve as active ions in solid-state laser materials because they exhibit a wealth of sharp fluorescent transitions representing almost every region of the visible and near-infrared portions of the electromagnetic spectrum (material for laser operation must possess sharp fluorescent lines, strong absorption bands, and a reasonably high quantum efficiency for the fluorescent transition of interest). The sharp fluorescence lines in the spectra of solids (glass or crystal) doped with rare earth ions result from the fact that the electrons involved in transitions (the 4f electrons) in the optical regime are shielded by the outer shells from the

surrounding structure; the corresponding transitions are similar to those of free ions.

Optical absorption and fluorescence spectra of rare earth ions consist of line multiplets in "bands" separated by a wave number difference of the order of $1000cm^{-1}$; within such a group the lines result from transitions to a multiplet of levels having the same total angular momentum (J) and are of order $100cm^{-1}$ apart. Spectral studies provide a direct source of information concerning the energy levels in glasses and crystals. Alternatively, an ion can be used as a probe to determine and measure the type and strength of the crystalline field (Runciman 1958). Learning about the nature of the local structure around rare-earth ions in materials and how it relates to the optical absorption and fluorescence originating from these ions is important for understanding their properties. The association between local structure and fluorescence properties of glasses doped with small concentrations of rare-earth ions, but not the metaphosphates, which contain a very high concentration of these modifying ions, has previously been used to provide information about laser glasses (Hirao and Soga 1985, Belliveau and Simkin 1989).

At low temperatures, the physical properties of glasses are strikingly different from those of the respective crystalline solids. These differences (anomalies) which are attributed to the frozen-in supplementary degrees of freedom during the manufacturing process of glasses, are now being commonly referred to as universal for disordered systems. Some of these effects concern low-energy dynamics and manifest themselves in low-temperature specific heat (Pohl 1981), acoustic, dielectric (Hunklinger and Schickfus 1981), optical (Jäckle 1981), thermal conductivity (Zeller and Pohl 1971), and inelastic scattering experiments (Buchenau et al. 1988, Malinovsky et al. 1990). The most characteristic features are the linear behaviour of the specific heat and the T^2 dependence of the thermal conductivity in the temperature region below 1K, which are well accounted for by the phenomenological tunnelling model of two-level systems (Anderson et al. 1972, Phillips 1972). According to this model, atoms or groups of atom have more than one site in a disordered lattice, and these sites are separated by energy barriers. At low temperatures, atoms or groups of atoms can tunnel through the potential wells separating their possible sites, leading to splitting of the ground state of the two-level systems. An

important conceptual result of the low-energy behaviour is that disordered systems support, in addition to the Debye-like phonons (nondispersive thermal plane waves), some other "excess" modes. Therefore the lowest-energy excitation (corresponding to $T < 1K$) can be successfully described in terms of two-level systems (TLS's), coexisting and interacting with Debye phonons. However, at higher temperatures effects are observed which can not be accounted for by this TLS model. Above 1K the thermal conductivity reaches a plateau (Zeller and Pohl 1971), while the specific heat exhibits further excess over that predicted by the standard Debye model (Lasjaunias et al. 1975), which is manifested in a bump in a C_p/T^3 vs T plot (Jäckle 1981, Carini et al. 1994b). The corresponding total density of vibrational states (DVS) $g(\omega)$, deduced from inelastic neutron scattering measurements, exhibits a broad maximum in a $g(\omega)/\omega^2$ vs ω plot, indicating again a non-Debye behaviour. The excitations responsible have been shown to be soft harmonic vibrations, localised to about 10 or more atoms by a number of inelastic scattering (Buchenau et al. 1986, 1988) and infrared absorption experiments, thus confirming that TLS's alone cannot account for the anomalous properties.

It is plausible to assume that both the two-level systems and these soft harmonic vibrations have a similar structural origin: they have the same vibrational structure (Grace and Anderson 1989, Brand and Löhneysen 1991). A mathematical theory based on the idea of this soft harmonic configurations was developed by Karpov et al. (1983) using a soft-potential model (SPM). In this model, both the tunnelling and the soft vibrational states appear as very similar localised modes with only slightly different potential parameters, the difference being ascribed to the local variation of atomic surroundings. Using the soft-potential model, it has been possible to explain the maximum in $C_p(T)/T^3$, the plateau in the thermal conductivity, as well as the rapid rise of the acoustic absorption around 10K (Buchenau et al. 1992, Ramos et al. 1993, Buchenau 1993), a linear temperature dependence of the sound velocity below 100K (Carini et al. 1994a) and a number of relaxation and heat release phenomena (Parshin and Sahling 1993).

The low-frequency modes which contribute to the specific heat, co-exist with sound waves and show effects in Raman scattering (Shuker and Gammon 1970, Winter-

ling 1975, Malinovsky and Sokolov 1986). Spectral components such as the boson peak, and the so-called light scattering excess (LSE), are observed in the low frequency region Raman spectra of glasses. To find out whether the low-frequency Raman scattering of the rare earth metaphosphate glasses (REMG) are consistent with the predictions of the SPM model, Raman scattering measurements have been made on some of these glasses (Lipinska-Kalita et al. 1995). The measurements has shown that the light scattering excess (LSE) contribution of these REMG decreases with frequency approximately as ω^{-1}, as predicted by the SPM. Further, the reduced Raman intensity have shown that the frequency exponent of the product $C(\omega)$ of the coupling factor $C(\omega)$ and the density of states $g(\omega)$ is about 3.5 in reasonable agreement with an ω^4 dependence predicted by the SPM (Carini et al. 1994). Here we will measure the low temperature Raman spectra of Nd, Eu, and La metaphosphate glasses to add additional support to the findings of Carini et al. (1994) and Lipinska-Kalita et al. (1995).

1.2. RARE EARTH ELEMENTS AND LANTHANIDE CONTRACTION

The rare earth elements, known as lanthanides, are a group of 14 elements that run from cerium (atomic number 58) to lutetium (atomic number 71) inclusively. The electronic configuration of the lanthanides is based on the xenon core, ($1s^2 2s^2 2p^6 3s^2 3p^6 3d^{10} 4s^2 4p^6 4d^{10} 5s^2 5p^6$), denoted as [Xe], plus three electrons in the higher energy 5d and 6s orbitals. The series of the elements is characterised by the gradual filling of the 4f shell from cerium $[Xe]4f^1 5d^1 6s^2$ to lutetium $[Xe]4f^{14} 5d^1 6s^2$. Lanthanum (atomic number 57) is often considered as a rare earth element with zero electron in the 4f shell.

In general, most of the rare earths in compounds are triply ionised. Consequently their electrons are in the closed shell configurations of the xenon structure, except the 4f electrons which runs from zero at La to 14 at Lu with a half-filled shell at Gd. Because of the stability of full and half-filled shells Yb and Eu appear in divalent form while Ce may be quadrivalent. The 4f electrons, which determine the electronic states of interest, are shielded by the closed shells $5s^2\ 5p^6$ from perturbations due to neighbouring ions, so that the effects of the latter are small. On the other

hand the spin-orbit interaction for the 4f electrons, which couples the angular momenta L and S to give a total angular momentum J, is larger than other interactions. As a result J is considered to be a good quantum number in almost all circumstances, and the lowest levels are usually taken to be determined by a single value of J. The effect of the other interactions, such as those with the nucleus or crystal fields, is to lift the (2J+1) degeneracy of the level.

The most striking fact about the rare earths is their similar chemical properties. This arises from the fact that the 4f shell of electrons is deeply buried within the atom therefore play a small role in chemical bonding, while the number of outer valence electrons remains unchanged through out the series. The close resemblance between their chemical and certain physical properties ensures that the rare earth elements occur together in individual minerals, and also accounts for the considerable difficulties in separating them from one another. Because of similar atomic and ion sizes and the same chemical valences, one rare earth ion can readily be replaced in a crystal lattice by another rare earth ion with little strain. Further, the rare earths have very different and striking magnetic properties due to the electrons of the 4f inner shell.

In going from the lightest element of the rare earth elements (La) throughout the series to the heaviest one (Lu), the nuclear charge Z increases, therefore the potential seen by the inner 4f electrons deepens and their orbitals show a systematic contraction in radius; this effect is known as lanthanide contraction. The effect is a result of the imperfect shielding of one 4f electron by another 4f electron (Jørgensen 1955). As the nuclear charge, and thus the 4f electron population, increases, the imperfect shielding induced by the directed nature of these orbitals causes each 4f electron to experience added electrostatic attraction by the nucleus. The result is a decrease in the size of the entire $4f^n$ arrangement, and therefore in the sizes of atom and ions, with increasing atomic number.

1.3. RARE EARTHS VALENCE INSTABILITY

In lanthanides, although the main valency is trivalent, there is the possibility of finding divalent or tetravalent ions. This tendency towards different valencies stems from the fact that in some ions there is no significant difference in the binding energy of the 4f electron and the 5d valence electron. A 4f electron may be raised to the 5d valence shell to make a tetravalent ion, such as Ce, Pr and Tb or a 5d valence electron may be demoted to the 4f shell to create a divalent ion as in Sm, Eu, Tm and also Yb. Therefore, due to this valence instability the lanthanides can exhibit intermediate valence states. A variety of experiments under pressure and optical studies, have shown that in a number of semiconducting rare earth divalent monochalcogenides a transition to the metallic state involving 4f electron delocalization can be induced by pressure (Jayaraman et al. 1970, Hirts 1970, Maple and Wohlleben 1971, Kirk 1972). These involve a change in the valence state from divalent to trivalent state. For example, pressure studies on divalent samarium in SmS (Jayaraman et al. 1975) and SmSe (Welber and Jayaraman 1977) have revealed that the Sm ion in this crystalline compound undergoes a pressure-induced first-order electronic transition from the electronic configuration $4f^6 5d^0$ (divalent) to $4f^6 5d^1$(trivalent). The transition is isostructural but is accompanied by a large volume decrease since the ionic radius of the Sm^{2+} ($4f^6$) has almost 20% larger than Sm^{3+} ($4f^5$). Anomalous reduction in the elastic stiffness under pressure stems from this valence instability, for example, application of pressure up to that (6.5×10^8Pa) at which the first-order transition occur causes marked decreases in the bulk and longitudinal moduli in semiconducting SmS (Tu Hailing et al. 1984). Ultrasonic measurements of samarium and europium metaphosphate glasses have shown anomalous reduction in the elastic stiffness under pressure, negative values obtained for the hydrostatic pressure derivatives $(\partial C11/\partial P)_{T,P=0}$ and $(\partial C_{44}/\partial P)_{T,P=0}$ of the elastic stiffnesses and $(\partial B/\partial P)_{T,P=0}$ of the bulk modulus. The question arises: is anomalous elastic behaviour is a sign of valency instability in these glasses?. To answer this, measurements have been made here of the optical absorption and fluorescence spectra of the rare earth metaphosphate glasses under pressures; results are compared with the spectra reported for 2+ and 3+ rare earth ions.

1.4. RESEARCH OBJECTIVES AND THESIS ORGANISATION

Glasses doped with small quantity of rare earth elements have received great amounts of attention due to their wide range of novel optoelectronic applications. Due to their chemical stability and high quality, interest has grown in applications and in the fundamental physics involved in glasses containing very large concentrations of rare earth ions. This has prompted a collaborative venture between the solid state physics groups at the Universities of Bath, Messina, Trento, Southampton, Kent and Edinburgh to study these glasses using different techniques. The first stage has been to manufacture high quality glasses and characterise them. This stage was accomplished by Senin (1994).

The main objective of the present research is twofold. First, to measure the fluorescence spectra of the rare earth phosphate glasses and crystal under very high pressures using the diamond anvil pressure cell. These measurements should help by providing some knowledge about pressure-induced phase transitions and valence changes. This goal has been accomplished by assembling an optical system to calibrate the pressure cell using the ruby fluorescence lines. The second aim has been to measure the fluorescence and Raman spectra of these glasses and crystals at low temperatures. These fluorescence measurements have enabled the determination of the valency state and the local symmetry of the rare earth ions, while the Raman spectra have provided information about the vibrational states which is of great help in finding out about the connectivity of structural units of these glasses and crystals. This work has been achieved by using a high resolution optical system at The Physics Department, Edinburgh University.

This thesis is organised as follows. In chapter 2 descriptions of the diamond anvil cell, the principle of its operation, the method of alignment of the diamond anvils and accessories needed for loading a sample in the cell, are given. Ruby fluorescence has proved to be a practical pressure gauge to calibrate diamond anvil pressure cells. Chapter 3 gives the details of the calibration procedure with a description of the optical, electrical, and mechanical components of an optical system designed to calibrate the DAC and to measure the fluorescence spectra of the rare earth metaphosphate glasses and pentaphosphate crystals. Chapter 4 describes phosphates and presents a brief review of the previous work reported on the struc-

ture of phosphate glasses. Also in this chapter the manufacturing procedure of making rare earth phosphate glasses and pentaphosphate crystals is given. Chapters 5 through 8 deal specifically with the experimental results obtained on the fluorescence spectra of the rare earth metaphosphate glasses and pentaphosphate crystals at low temperatures and very high pressures. The experimental Raman spectra obtained at room and low temperatures are presented in chapter 9. Finally, in chapter 10, the conclusions of the present findings of the spectral measurements are presented; also in this chapter, directions for future investigation are indicated.

CHAPTER TWO

THE HIGH PRESSURE DIAMOND ANVIL CELL-INTRODUCTION AND TECHNIQUES

2.1 INTRODUCTION

In the last forty years, the concept of using opposed diamond anvils to generate pressure has revolutionised high pressure research both in terms of the range of static pressure that can be reached and the variety of techniques that can be employed to study the behaviour of matter at high pressures. This technique was developed simultaneously and independently by two groups. One at the National Bureau of Standards (N.B.S) and a second at the University of Chicago (Lawson and Tang. 1950). Later the DAC has become a standard tool for the generation of high pressures; as compared with the classic hydraulic piston-cylinder devices, the DAC has found extensive application in extremely high pressure experiments. A few of these include: (i) studies of high pressure phases using x-ray diffraction powder methods, (ii) compressibility studies using both powder and single crystal x-ray diffraction methods, (iii) melting curves, (iv) optical studies, which include measurement of refractive index.

The diamond anvil cell (DAC) has proved to be more suitable than the piston-cylinder pressure cell technique for many experiments at very high pressure for a number of reasons. It is three to four orders of magnitude smaller than the piston-cylinder devices, provides optical access for optical experiments, is completely safe (in contrast with massive hydraulic pressure vessels where great attention must be paid to safety) and can generate static pressures one to two orders of magnitude higher than the previous devices particularly in the pressure range of interest to solid state physicists (0-500Kbar). Another two very important advantages, which have made the DAC the most widely used very high pressure technique are: firstly diamond is the hardest known material, secondly it is highly transparent to a wide

range of electromagnetic radiation. This optical transparency has promoted a number of high pressure spectroscopic studies of DAC, including Raman scattering, Brillioun scattering, absorption, and fluorescence.

The basic principle of operation of a DAC is that a force applied over a small area results in a high stress. The stress in the sample is made hydrostatic, or close to it, by surrounding it with a fluid confined by a gasket.

Originally, the DAC was used to study materials where the sample itself provided the gasket seal (non-gasketed technique). This method extended the pressures obtained up to 300 Kbar. However, the pressure gradients were often severe, and measurements were restricted to only to polycrystalline samples. Later, the pressure cell was used with a metal gasket so that liquids could be contained in a hole. The method of encapsulating liquids within a small diameter hole of metal gasket placed between the flat parallel faces of diamonds was developed by Van Valkenburg (1965). With this technique it was possible to apply pressure to liquids due to the compressible nature of the metal gasket. It was then demonstrated that it was possible to subject a crystal immersed in an appropriate liquid to a purely hydrostatic pressure. This development led initially to the study of optical properties of liquids and solids under pressure and finally to the development of pressure cell designed to study single crystal phases by x-ray diffraction.

In the most of the earlier work with the DAC, pressures were estimated from the applied load. Such estimates give an only an average pressure over the sample in the non-gasketed technique, but are even less reliable using a gasketed sample, since the gasket absorbs an unknown amount of the load. An early approach to pressure measurement in the cell was based upon the shift of an optical absorption band in nickel diamethylglyoxime with pressure (Davies 1968), this has not gained general acceptance due to the limited temperature stability of nickel diamethlylglyoxime, interference with measurement on materials under study, and the complexity of the measuring apparatus. Pressure measurement utilising the change in lattice constant of known materials notably, NaCl, was used extensively in the DAC in x-ray powder studies (Bassett et al. 1967, 1968) but again it was not a convenient technique for making pressure measurements since it is time consuming.

In the early days, pressure measurements in the DAC were seriously hampered due to the lack of a rapid, accurate, and reliable technique to calibrate and determine the pressure generated on the samples. However a preliminary report from N.B.S suggested using the shift of the R-lines fluorescence in ruby as a pressure measuring technique for use in the DAC. A small chip of ruby is placed within the pressure chamber along with the sample and the fluorescent emission spectrum is recorded. In ruby the wavelength shift of the R-lines with pressure is approximately linear (Bassette et al. 1968). As this technique has gained wide support, for many reasons which will be given in chapter 3, it has been adopted by us as well for pressure determination in the DAC.

In this chapter a description of the diamond anvil cell, the principle of its operation, and accessories needed for handling and loading a sample in the cell will be given. The method of alignment of the diamond anvils will be explained in detail, as it is a crucial and essential factor in any pressure run in the DAC. The types and shapes of diamond anvils are also described, taking into consideration optical absorption spectra of the diamonds, knowledge of which is needed in optical measurements.

2.2 DESCRIPTION OF THE DIAMOND ANVIL CELL

The diamond anvil cell (DAC) used for develop pressure and measure its effect on fluorescence spectra of glasses and crystals is shown in Figure 2.1. The cell is cylindrical in shape, 3cm high and 5cm in diameter, and is in the form of a piston-cylinder assembly made of stainless steel. The main parts of the cell with its components are as follows:

1- The cylinder.

This component is the first major part of the cell and, as its name reveals, it has a cylindrical shape. It has an internal diameter of 2.7cm and external diameter of 5cm with a thickness of 2cm and height of 2cm. Inside it is set a beryllium disc, 2.5cm in diameter and 0.5cm in thickness with a conical shaped hole drilled in its centre.

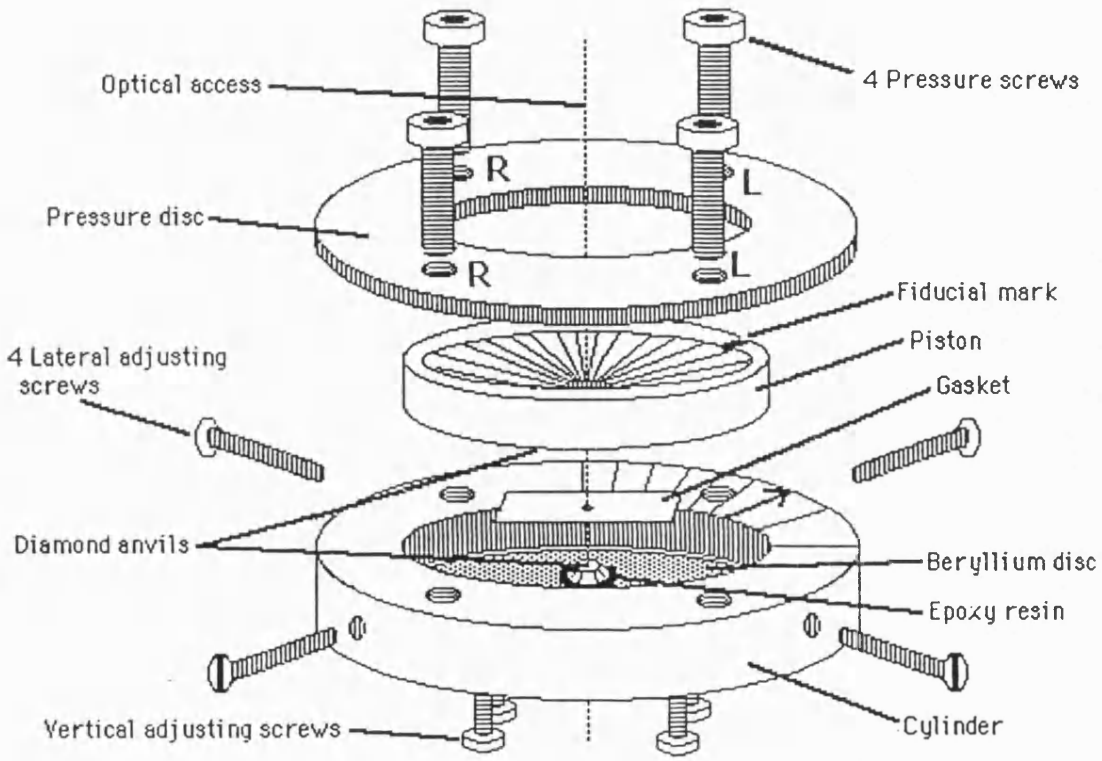

Figure 2.1. The diamond anvil cell design.

This conical hole, which allows optical access through the cell, is 0.1cm in diameter on the internal face and 0.2cm in diameter on the external face. A diamond anvil gem having 3mm table diameter is centred over the internal face of the hole and glued into position with epoxy cement. For the purpose of alignment (which will be discussed later) the beryllium disc can be moved laterally by 4 screws (the lateral adjusting screws) which penetrate the sides of the supporting steel cylinder from the sides. The disc can also be tilted and adjusted by another 4 screws (the vertical adjusting screws), which penetrate the base of the supporting steel cylinder and touch the bottom of the disc to allow this.

2- The piston.

The next major component of the cell to consider is the piston. This is 2.7cm in diameter and 1.1cm in height, and is a press fit into the internal diameter of the cylinder. The piston has a beryllium disc 1.8cm in diameter pressed and glued into it. The beryllium disc has a conical hole in its centre similar to the one in the beryllium disc of the cylinder with nearly the same dimensions and is placed opposite to it. This hole also supports a centred and glued diamond anvil similar to the one on the beryllium disc. On the top surface of the piston there is a groove used as a fiducial mark for alignment of the two diamond faces. The mark is aligned against grooves, denoting angles, on the top surface of the cylinder.

3- The gasket.

The gasket is a thin piece of hard stainless steel with a small hole (about 0.35mm in diametre) drilled in it centre. The gasket dimensions is not very important as long as it is at least five times larger than the hole diametre and fits easily inside the DAC's cylinder.

4- The pressure disc.

This disc has the role of applying pressure on the piston-cylinder assembly. It has an internal diameter less than the external diameter of the piston (about 2.1cm), and sits on top of the piston and is tightened down to the cylinder by four loading screws to generate the high pressure. The pressure disc has four holes to fit the four loading screws corresponding to another 4 threaded holes on the cylinder.

Pairs of holes have different thread directions from the others (two right-handed and two left-handed screws).

2.3 OPERATION PRINCIPLE OF THE DIAMOND ANVIL CELL

The basic principle of the DAC is straight-forward and is shown in Figure 2.2: a force is applied over a small area to produce the high pressure. When a metal gasket is compressed between the small flat faces (flattened by grinding and polishing of the culets) of the two brilliant-cut gem quality diamonds set in opposed anvil configuration, a very high pressure is generated in the gasket hole. To generate a hydrostatic stress on the sample, the hole is usually filled with a pressure transmitting medium.

The reason that very high pressures can be generated in the DAC is that the flat area of the diamond anvil culet is so small, (0.75mm in diameter): the applied load gets multiplied by a large factor (200 to 500), depending on the size of the flat. For successful operation of the DAC, the two anvil flats must be accurately centred and set parallel to each other. The pressure is controlled by the ability of the diamond, gasket, and diamond-backing plates to withstand the applied stresses. Such a cell can be designed in a number of different ways to meet the specific requirements of an experiment. This has given rise to several versions of the DAC and Figure 2.3 illustrates some of the more commonly used types.

2.4 TYPE AND SHAPE SELECTION OF DIAMOND ANVILS

Diamond has two very important characteristics that make it a particularly suitable material for use in generating very high pressure especially for optical studies. It is the hardest substance known and can withstand pressure. It is also makes a good optical window since it is transparent to photons over a wide energy range (infrared, visible, near ultra-violet, energy less than 5ev) and also hard x-rays with energy greater than 10keV.

A number of factors influence the choice of diamond as a material for anvil use; they fall in two groups: (i) those determined by the nature of the experiment, (ii)

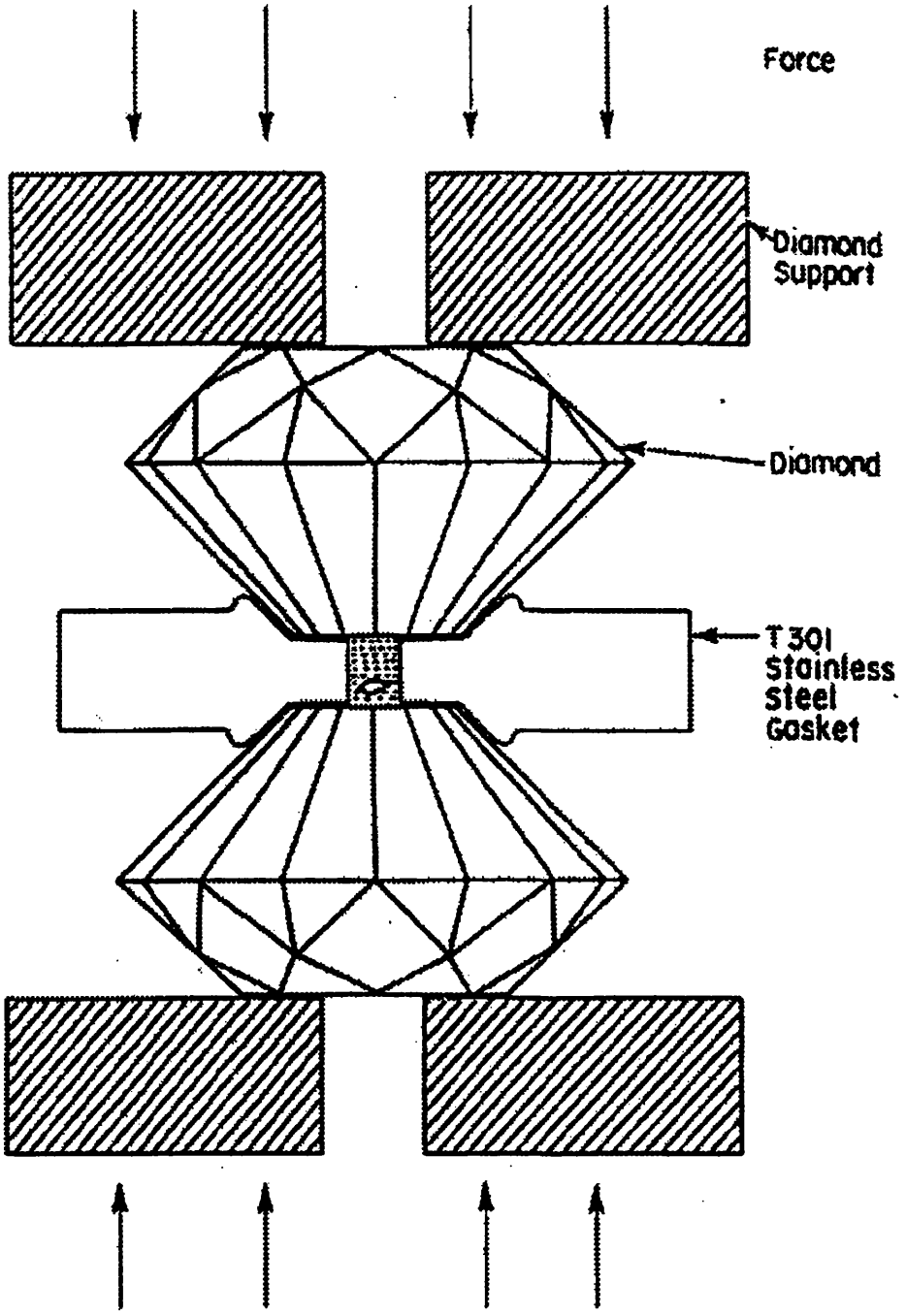

Figure 2.2. The basic principle of the diamond anvil cell.

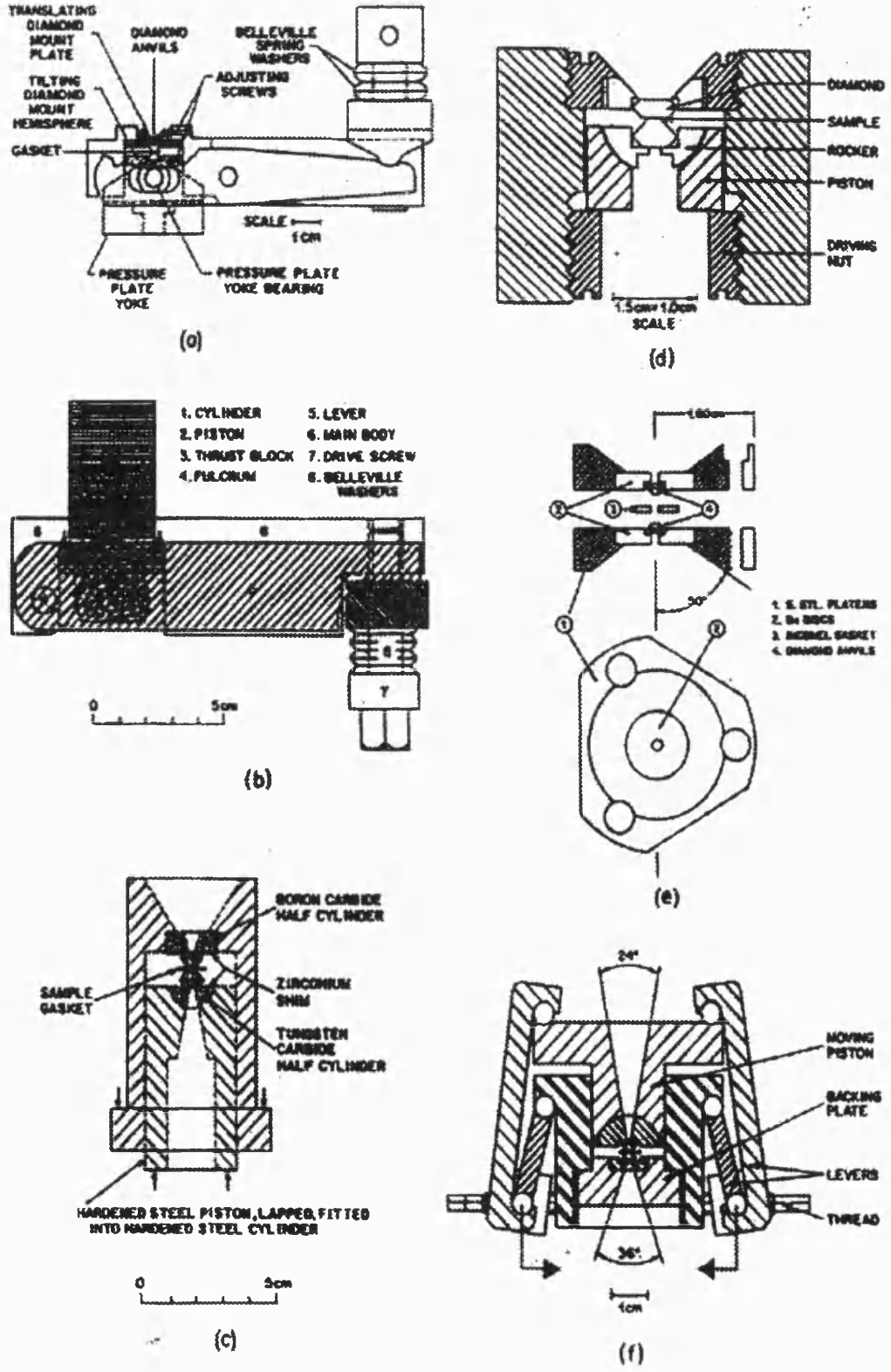

Figure 2.3. Various types of DACs a) Piermarini-Block cell, b) Mao-Bell cell, c) M-B cell piston-cylinder details, d) Bassett cell, e) Merrill-Bassett cell, f) Syassen-Holzapfel cell (after Jayaraman 1986).

those affecting the ultimate pressures achievable in an anvil apparatus. In the first group are such factors as colour (including absorption in the ultraviolet and infra-red). This is of importance in spectra analysis of a sample under high pressures. Another factor in the choice of the diamond is the optical quality. Diamond exists in two types (I and II) differing in their ultraviolet and infrared transmission. Type I diamonds are slightly yellow having an ultraviolet absorption edge at about 3000Å (0.3μm) and show a complex system of broad absorption bands between 7 to 10μm in the infrared (Figure 2.4(a)). Examination of diamonds has shown the presence of nitrogen as a major impurity in type I diamonds, which results in a yellow colour and causes an absorption edge in the 7 to 10μm region of the infrared spectrum (Kaiser and Bond 1959). Type II diamonds are white, having an absorption edge at about 2300Å (0.23μm) and the 7 to 10μm absorption system is absent, an indication of absence of nitrogen, (Figure 2.4(b)). However, they are more expensive than type I. It is recommended that experience be gained at first with these less expensive diamonds, which are usually sufficient for most purposes except in infrared work and at very high pressures.

The diamond anvil shape can be designed in one of two common cuts according to the particular application. The first is the standard eight-sided traditional brilliant cut, which is used for to achieve pressures in the range of 0-100Kbar (Figure 2.5a). The second cut is sixteen-sided; this is more suitable for application of pressures higher than 100Kbar (Figure 2.5b). Diamonds are sold by weight in carats (1/15g), and a typical diamond for use in high pressure studies is about 1/3 carat, giving a table diameter (D) of about 3mm. The size used is partly dictated by cost, but also the larger the diamond, the higher the probability that it will break. The anvil dimension (culet) d is chosen according to the pressure needed; 0.75mm has been used in this laboratory; which allows 100kbar to be reached routinely, and 200kbar without much difficulty. For 300kbar 0.5mm culets would have to be used (Dunstan and Spain 1989).

Because of the wide applications of the diamond anvil cell some other parameters are worth mentioning. An important parameter is the birefringence, which can be used as a criterion for the hardness of the diamond. This arises from the belief that

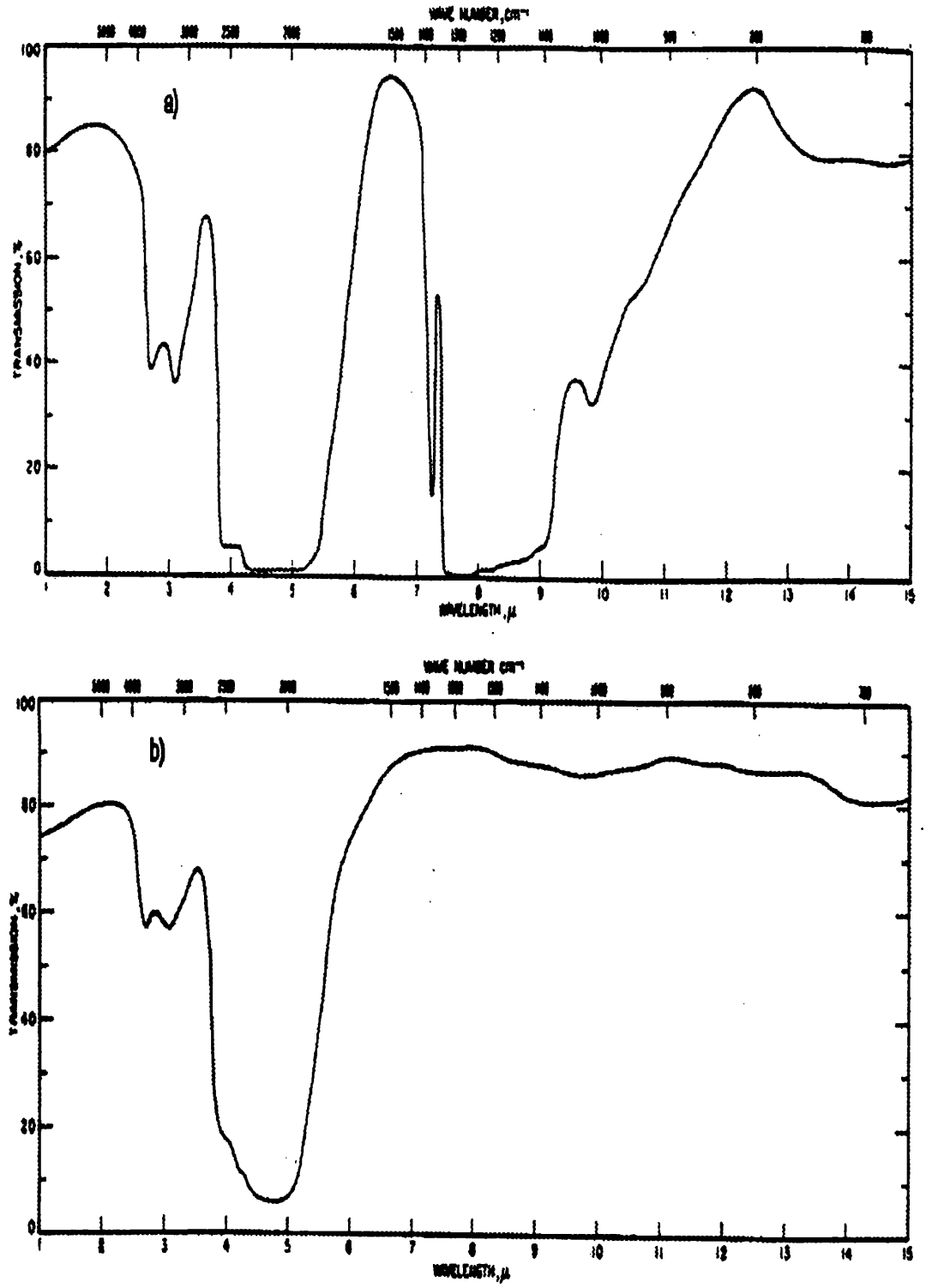

Figure 2.4. Infrared transmission spectra for typical a) type I, b) type II diamonds (after Weir et al. 1959).

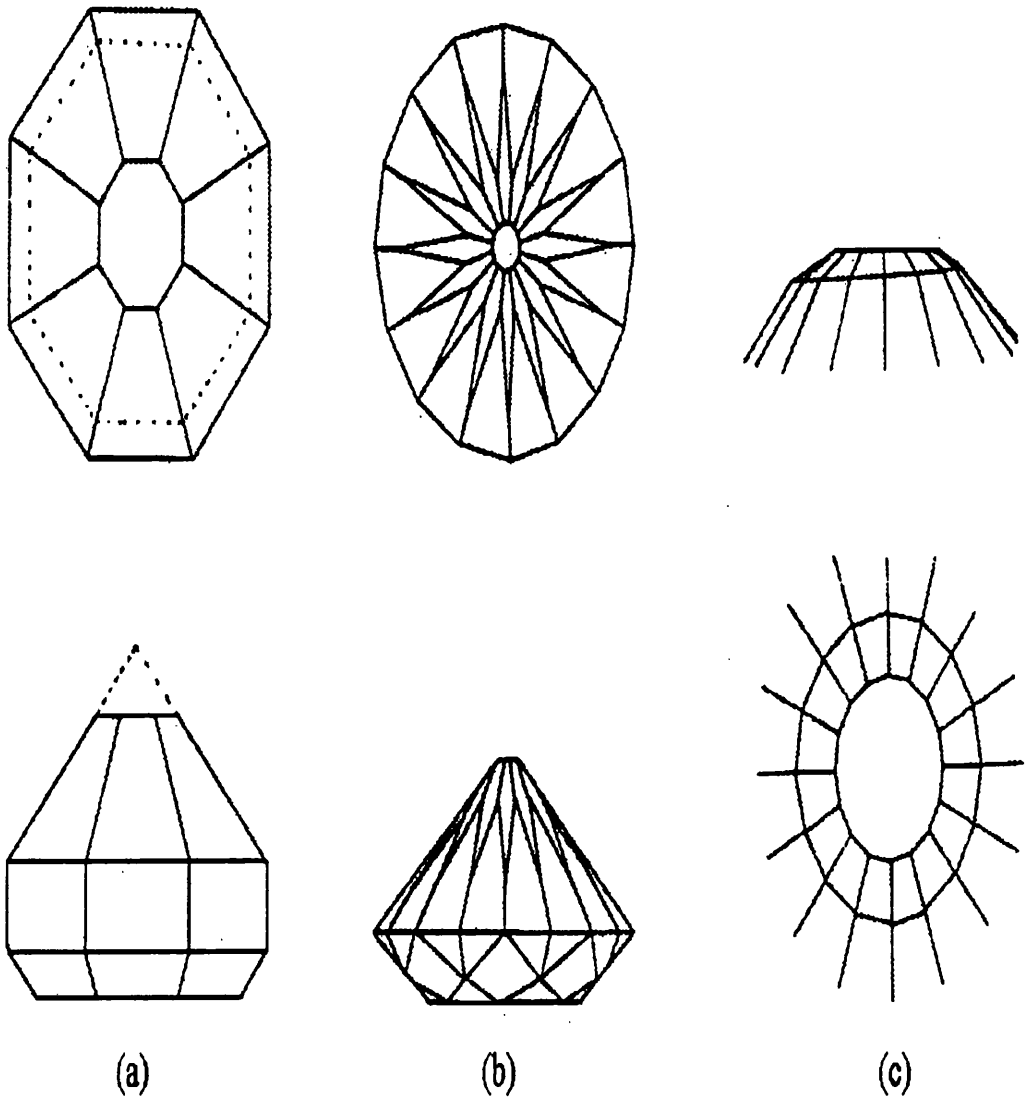

Figure 2.5. Diamond anvil designs. a) eight sided basic design, b) sixteen sided basic design, c) high pressure end-flat diamond anvil bevelled (2-5°) for work above 30Gpa (after Sherman and Stadtmuller 1987).

diamonds with high stress birefringence are weaker than ones with a lower value and thus break at lower pressures. Perfect diamonds (which are cubic with no birefringence) do not occur in nature at all, so all diamonds show some low stress birefringence. Many diamonds show birefringence higher than 0.0005, although it is possible to select diamonds with values as low as 0.00005 (Friedel 1924). Type II diamonds are probably slightly harder than type I and thus should make better anvils. However, type II diamonds also have a much easier and smoother cleavage than type I; therefore small stress concentrations in the contact regions are more likely to produce catastrophic cleavage splitting of type II diamonds. Although detailed investigation is required, it looks as though the highest pressures should be attainable with type II diamonds, ultra clean working conditions, good alignment and careful loading.

Another parameter which effects the choice of the diamond anvil is the thermal conductivity. This is important in applications of the DAC using high and low temperatures where the diamond is used as a heat sink. Diamond has high thermal conductivity arising from the strong bonding and the high Debye temperature. Type II diamonds show higher conductivities than most type I (Burgemeister 1978).

The shape of the culet can be important, particularly in cases where electrical measurements are to be made. One technique is to bevel the edge of the working surface (culet) to facilitate the passage of electrical leads between the diamonds and gasket; this reduces stress concentration at the sharp corners of the working surface (Figure 2.5c). Diamonds with bevelled edges are also often used for studies in the Megabar pressure region, since it allows the stress supporting the diamonds by the gasket to be optimised (Mao and Bell 1978). The results of a stress analysis of bevelled DAC's has been published by Bruno and Dunn (1984) who came to the conclusion that the optimum bevel angle lies in the neighbourhood of 15°.

2.5 MOUNTING AND ALIGNMENT OF THE DIAMOND ANVILS IN THE DAC

To obtain high pressure using a DAC, precise diamond alignment is an essential factor. Misaligned diamond anvils cause premature gasket failure, and may result in

diamond breakage (Hazen and Finger 1984). The alignment operation is performed with the aid of a microscope equipped with upper and lower illumination. The diamond anvils must be strongly attached to the two beryllium discs so epoxy resin is needed. A requirement of the diamond mounting is to centre the gem precisely over the conical hole of the supporting disc, without getting glue into the hole. The way to avoid this is to centre the diamond anvil (using the jig shown in Figure 2.6) over the hole and then put a small drop of glue at the side of the diamond anvil. When dry, more epoxy is put around the diamond. This procedure produces a strong bond, without closing the optical access through the cell. This procedure is repeated for the second diamond anvil on the beryllium disc of the piston. Then the two beryllium discs are ready to be inserted into the piston-cylinder assembly for alignment. The following procedure can be used to align the cell (Adams, 1990).

1- The lower beryllium disc is fixed to the cylinder with the four lateral adjusting screws set into the side of the cell, leaving them barely tightened. There are the four vertical adjusting grub screws in the base of the cell and they must not be in contact with lower beryllium disc. The role of these grub screws is to tilt the disc in order to achieve alignment, while the purpose of the four lateral screws is to translate the disc (relative to the piston) and also to hold it down when they are fully tightened (Figure 2.1). The next stage is to put the diamond cell under the microscope to align the two octagonal culet faces of the diamond anvils relative to each other. This can be done by setting the lower disc at whatever orientation allows coincidence with the anvil of the upper disc of the piston, the scale position of the piston fiducial mark having been first decided (Figure 2.7a). Alternatively, this procedure may be reversed. During this procedure it is necessary to ensure that the two diamond surfaces do not rotate relative to each other when they are in contact. To obtain a symmetrical octagonal figure, which indicates that the two diamond faces are precisely opposed each other, the cell is illuminated from below, and the piston is inserted into the cylinder with a fraction of millimetre retraction to prevent sliding the diamond surfaces over each other. Then the lateral screws are adjusted in opposing pairs until the symmetrical octagonal figure is achieved.

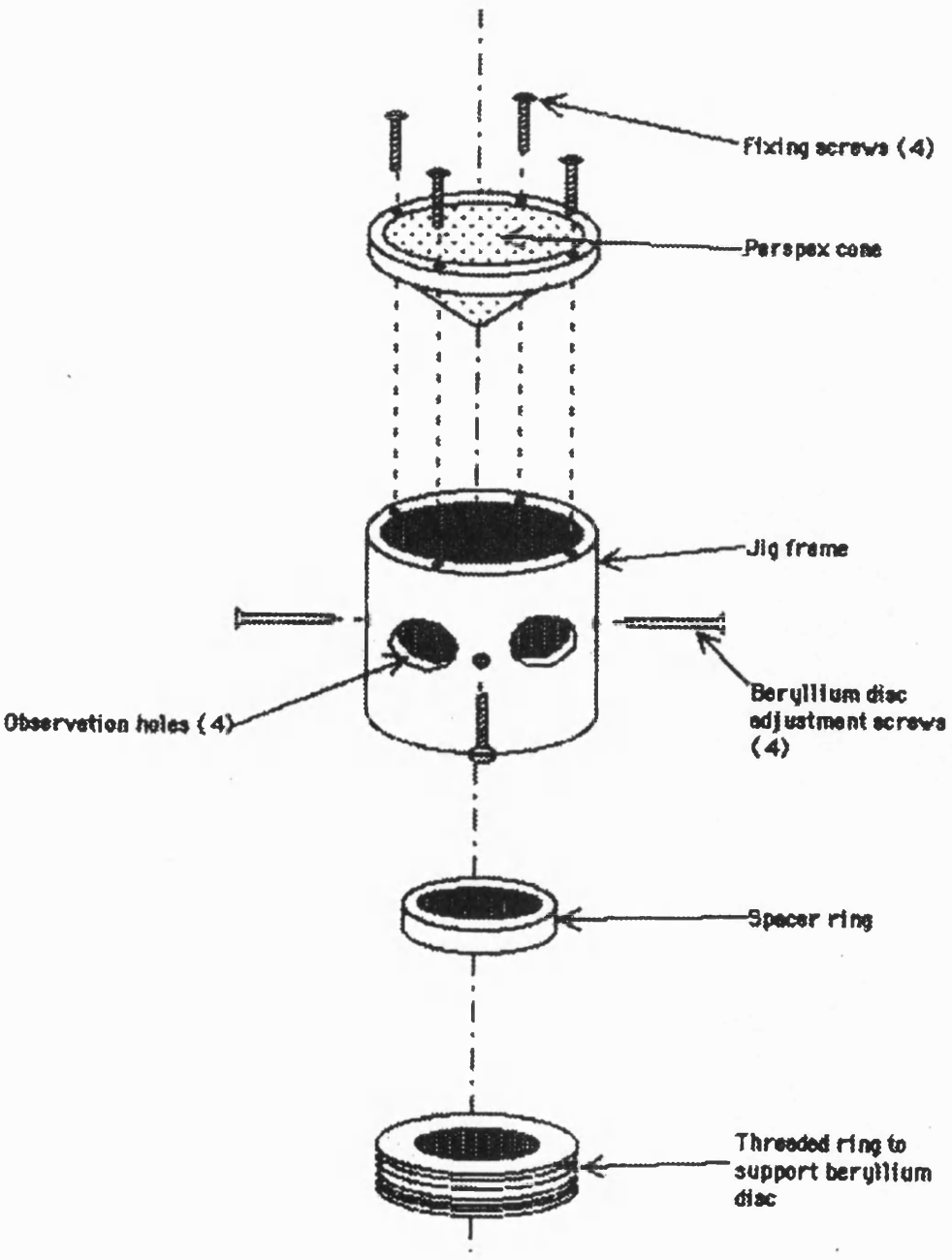

Figure 2.6. Diamond anvil mounting jig design.

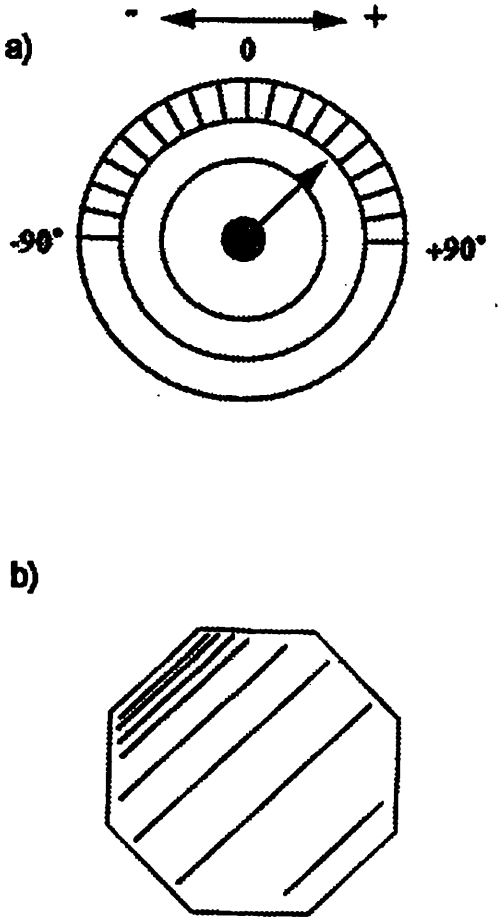

Figure 2.7. A) alignment condition of the cell using the fiducial mark on the piston with the appropriate angle on the cylinder of the cell, b) fringes in a misaligned diamond anvil cell.

2- At this stage the two coincident anvil faces will, in general not be parallel. When the piston is pushed in so that the two diamond anvils are in contact, linear interference fringes are usually seen; the number of the fringes depends upon the degree of misalignment. Figure 2.7b shows the diamond faces with interference fringes generated between them. To get rid of this misalignment, the cell is turned upside down so it rests on its piston; then the four grub screws in the base are adjusted by turning them 1/4 of a turn so as to drive the pattern in the direction of fewer fringes. Eventually, one or two fringes will be left, so only very small adjustments of one or two of the screws are then needed to eliminate the fringes completely. The last touch is to tighten the four lateral screws (in opposing pairs), taking care that the alignment is not upset.

To make a practical check of the alignment, finely ground red mercury iodide (HgI_2) may be used. Mercury iodide is known to undergo a phase transition at 13Kbar which shows up visually as a change in colour from red to yellow. The procedure, which can be followed, is to remove the piston and load a sample of HgI_2 onto the lower diamond anvil face, covering it fairly evenly; then replace the piston ensuring that it is aligned using the scale (by putting the fiducial mark against the appropriate angle of alignment); this procedure is carried out without a gasket. Next a load is applied to the cell by tightening the pressure screws (in opposed pairs) on the pressure disc and at the same time looking through the microscope. A dark patch appears at the centre of the field and with further increase of pressure this central patch turns yellow, and then expands outwards. It is important that the yellow phase appears at the centre of the anvil faces, and that it expands symmetrically, an indication of proper alignment (uniaxial pressure is high in the centre of contact and low on the edges). Figure 2.8 shows the diamond anvils under different pressures with the HgI_2 powder showing the colour change starting from the centre as a yellow and spreading nearly symmetrically outwards. If this is not the case, there are two possibilities, either the sample has been loaded unevenly, or the alignment is out.

The alignment can also be checked at pressures low than 13kbar in a way, which is safer for the diamonds, since at this stage the degree of the alignment of the diamond anvils is not known and application of pressure could result in diamond

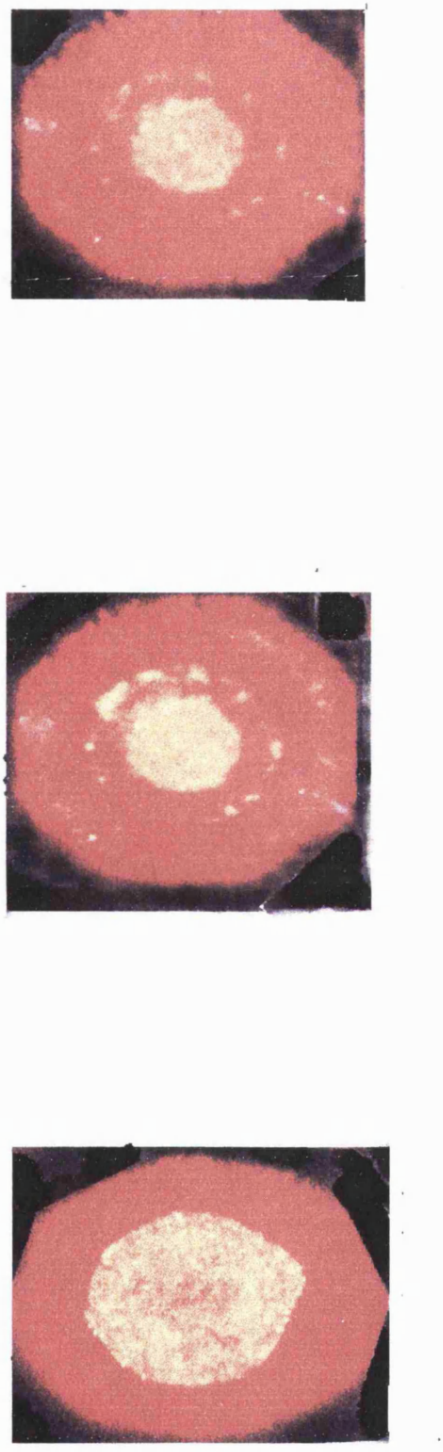

Figure 2.8. Three photographs taken for the diamond anvil cell loaded with HgI_2 under increased pressures under the microscope for alignment checking. The yellow patch starts in the centre of the anvil and spreads nearly symmetrically outwards.

breakage. For this method a small quantity of AgI powder is put between the diamond faces. This powder has a phase transition under the low pressure of 4Kbar. The new phase, when seen under transmitted light, is darker in colour than the yellow atmospheric pressure phase; and symmetric patterns centred on the diamond axis can be used as evidence that good alignment has been achieved (Spain and Dunstan 1989).

It is important to note that optical fringes are often not observed initially after coarse alignment. This is caused by the diamond surfaces being separated by lint particles, so fringes are poor in contrast. The diamond culets need to be cleaned thoroughly with solvent on a cotton tip, and inspected to ensure that cotton fibres have not adhered to the them. After the cell has been aligned, a gasket has to be preindented with successively high force; the alignment has to be checked after each pressing operation. If the diamonds remain well aligned (e.g. to about 1 fringe) after application of the highest rated force, then the cell is ready for use. If the cell becomes misaligned, then the cause of the misalignment (usually poor diamond mounting) needs to be ascertained.

2.6 DIAMOND ANVIL BREAKAGE AND THE AVAILABLE PRESSURE RANGE

The material characteristics of diamond and in the anvil form determine the design of any DAC. Monocrystalline diamond is hard and very strong in compression in certain directions; however it is very weak in tension and in under shear in certain directions. Hence a DAC must be designed to load the diamonds by rectilinear movement along the z axis. Any other movement is likely to break the diamond anvils.

High pressure results from the large force applied to the small area of the diamond culet; the maximum pressure and hence the maximum load, is limited by possible breakage of the diamond culet: the maximum pressure depends on the culet diameter. The limit is not well-defined, but the following working equation has been agreed on:

$$P_{max}\ (Gpa)=12.5/(d_{(mm)})^2 \qquad (2.1)$$

The maximum pressure used in experiments should be somewhat lower than this, such as $0.8P_{max}$. It must be stressed that this formula is only applicable to simple culet shapes. However small values of pressure can also lead to diamond failure if the cell does not enable the diamonds to remain in good alignment or if they are incorrectly mounted (Dunstan and Spain 1989).

2.7 DESCRIPTION OF GASKETS USED IN DAC

Metal gaskets were first used in DACs by Van Valkenburg (1965), and their use has been one of the principal factors which has permitted quantitative measurements to be carried out in DAC. The gasket is a piece of metal with a small hole drilled in it. Thus the gasket is the simplest component of the cell, yet it is a most critical one. This is due to the fact that many diamond cell experiments terminate at high pressure in extreme deformation (i.e. failure) of the gasket. An appropriate gasket is needed, and that is dominated by the selection of the suitable material with the right dimensions.

The purpose of the gasket is to provide a chamber in which a fluid-like substance can be contained between the two diamond anvils used to apply approximately hydrostatic pressures to the sample. An additional purpose is to provide support to the anvils (see Figure 2.1). The gasket is made of a hard metal foil; commonly used foils are Inconal 750X foil, which is a moderately hard nickel alloy, and T301 stainless steel foil, which is a hard stainless steel (Hazen and Finger 1984). The size of the gasket hole depends on the maximum desired pressure as well as on the size of the sample under study. The optimum gasket hole diameter for a sample of 100μ is 0.35mm. When the gasket is squeezed between the diamonds, it deforms plastically and extrudes outwards. The hydrostatic pressure is due to the frictional force between the metal and the anvil. This force is limited by the shear strength of the metal, so that at high pressure the metal does not slide over the diamond, but shears, with a stationary surface layer (Spain and Dunstan 1989). The gasket thickness is a crucial parameter for determining the maximum pressure that is reached. For instance, a stainless steel gasket of thickness 100μ, used with 0.6mm diameter diamond culet, and 200μ diameter gasket hole can only be used up to 100kbar,

while a 40μ thick gasket can reach 200kbar. Therefore it is necessary to carefully select gasket materials and dimensions for a particular experiment. In conclusion, the gasket should always be thin enough so that the sample hole contracts as the pressure is raised. If the hole expands at high pressure, the run must be terminated and a thinner gasket used. The gasket should not be smaller than about five times the culet diameter as excessive distortion will occur, and it is possible for a crack to propagate inwards leading to gasket bursting.

2.8 GASKET PREPARATION TECHNIQUES

There are two methods usually used to prepare the gasket for pressure runs. In the first one, shim steel of the required thickness is used directly (simple gasket). In the second, a much thicker gasket is used, typically 0.5mm, and the required thickness is obtained by a preindentation method. The second method is preferable for the following reasons,

1- A range of different gasket thicknesses is usually required, depending upon factors such as the intended pressure range or the particular sample to be studied.

2- It is not always possible to obtain shim of the required thickness, while preindentation allows any thickness to be obtained from same stock thickness.

3- A preindented gasket provides a thick belt of the metal supporting the material between the culets and also supporting the flanks of the diamonds.

4- Two operations of some delicacy are the centring of the sample and ruby chip on the diamond culet, and the centring of the gasket hole. Preindentation helps by easing these two operation by making an impression of the diamond culet on the gasket. This diamond impression on the gasket can be used as a guide for drilling a hole in its exact centre.

Preindentation allows the automatic selection of the correct gasket thickness, by applying the same load to preindent as that which is subsequently used in the pressure run. The DAC is assembled with the gasket between the two anvil and without any hole drilled in it, returning to zero load repeatedly to relieve stress. The gasket may be removed to measure the thickness and then replaced for further thinning. A

micrometer with small rounded measuring tips is used to measure the indentation thickness. It is essential to apply the load in small steps and reduce it to zero between each step.

Diamonds are more likely to break during reindentation than in a high pressure run. This is because the radial extrusion of the metal is entirely outwards, putting the maximum tensile component of stress in the diamond tips. Although, the indentation procedure may increase the available pressure range in some experiments, there can be difficulty in centring the hole after indenting (Spain and Dunstan 1989). Another way of indenting the gasket is first to place 3mm diameter balls of jeweller's wax on the beryllium disc around the lower diamond. A small speck of dust is then placed at the precise centre of the lower clean diamond face. The gasket is drilled to the desired hole and then pressed onto the wax balls with hole exactly centred over the speck of dust. In this way the gasket is centred. In order to prevent leakage of pressure fluid when the cell is first closed, the gasket must be slightly impressed onto the bottom diamond after centring. This can be done by closing the two halves of the cell together (without fluid) and tightening the four load screws slightly just enough to indent the top surface of the gasket. When reopened, the gasket should reveal a light impression of the top anvil exactly centred over the gasket hole, Figure 2.9. After that the diamond cell is ready for sample mounting. This last method of indentation has been adopted by us for it convenience and easiness.

An alternative method of gasket preparation and mounting is to centre the gasket hole as above, but then clamp down on the gasket until the hole closes down to only 0.1mm diameter. The gasket is then removed and the hole is redrilled to the original size of about 0.35mm diameter. The gasket, which has clean octagonal impressions of both the upper and lower diamonds, is centred over the lower diamond. Though more time-consuming, this redrilling procedure has the advantage of allowing higher pressures with less gasket deformation or shielding when a pre-thinned gasket is used (Hazen and Finger 1984).

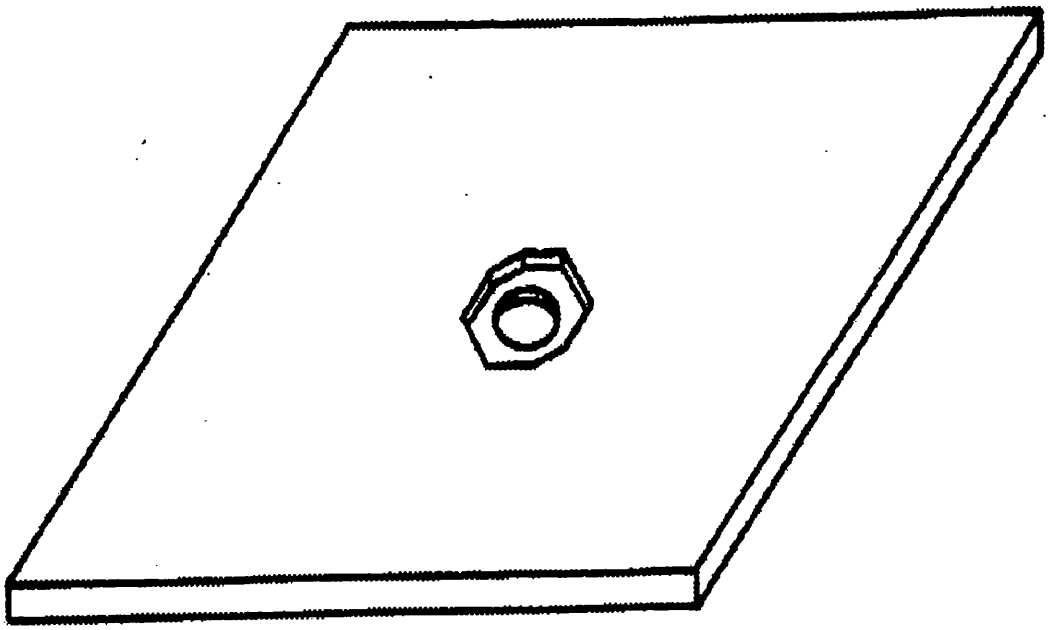

Figure 2.9. Metal foil gasket after indentation by diamond anvils. The gasket hole and the faces of the anvils should be concentric (after Hazen and Finger 1982).

2.9 TOOLS AND MATERIALS FOR SAMPLE HANDLING AND MOUNTING IN THE DAC

The following materials and tools are essential for mounting a sample in the DAC:

1- Binocular microscope (Olympus) with variable magnification up to 60X, a long working distance (10cm) and top and bottom illumination.

2- Drills of 0.35mm, 0.4mm and 0.45mm diameter (ordered from the Titex Plus).

3- Sharp needles with long handles for sample manipulation.

4- Epoxy resin for diamond attachment to beryllium discs (5minute epoxy from the Devcon company).

5- Jeweller's wax to hold the gasket in position from its sides when centring the gasket hole on the diamond culet.

6- Vaseline petroleum jelly for sticking the sample on top of the diamond anvil.

7- Offset and pointed tweezers.

8- Differently shaped surgical blades with handles.

9- Fine wire, 0.1 mm in diameter.

10- Microlitre syringe (obtained from the Hamilton company) for filling the gasket hole with alcohol mix.

11- Ethanol for cleaning the diamond anvils.

12- Soft tissue.

13- Emery cloth to smooth the surround of the gasket hole and remove the burr.

14- Needle file.

15- Allen keys.

2.10 SAMPLE PREPARATION AND HANDLING WHEN MOUNTING IN THE DAC

Samples for high pressure measurement in the DAC must be small enough to remain uncrushed between the diamonds anvils, yet large enough to provide sufficient details about their properties. Typically, the samples used are 50 to 100μ in linear di-

mension and about 20 to 50μ in thickness. It is a delicate procedure to handle and transfer such small samples from whatever surface they were prepared on to the DAC; in fact a fair proportion of samples are lost at this stage. There are two techniques to handle and lift a sample, either using a sharp pointed needle or a piece of fine wire secured in a tubular handle by crimping (we have preferred the second technique). Under the microscope the sample is picked up on the fine wire by electrostatic attraction; in the case of a fairly large sample a smear of grease on the wire can sometimes increase the chance of picking up the sample without the fear of losing it. Then the sample is transferred and deposited on the diamond culet. It is a good practise to place a very small drop of Vaseline petroleum jelly on the lower diamond face (just enough not to embed the sample) to collect the sample; and also an additional smear can be applied to the side of the gasket hole for ruby chip attachment. When the sample is deposited on the diamond face inside the gasket hole, it is pushed around and centred using the sharp needle. Finally, the cell is ready to be filled with fluid and sealed.

2.11 PRESSURE MEDIA FOR HYDROSTATIC PRESSURE GENERATION IN THE DAC

The most meaningful studies of the physical properties of materials subjected to very high pressures require a hydrostatic environment. The use of an encapsulated fluid as a pressure-transmitting medium generally fulfils this requirement as long as the fluid does not solidify in the pressure range considered. Bridgman (1964) and others (Babb et al. 1964, Barnett and Bosco 1969), studied the hydrostatic pressure limits of several organic fluid pressure media and determined the limits by using ruby line broadening, or by measuring the pressure homogeneity with several ruby chips distributed over the area of the gasket hole. They showed that many pure liquids and liquid mixtures slowly vitrify rather than crystallise as pressure is applied, and that some liquids remain hydrostatic to pressures well over 30Kbar. Of the liquids studied, pentane, isopentane, and methanol, were shown to have the smallest increase in viscosity with pressure and to have relatively low absolute values at 30Kbar. It was found that a 1:1 mixture by volume of pentane:isopentane remains hydrostatic up to 60Kbar (Barnett and Bosco 1969). Piermarini et al.

(1973) discovered that a 4:1 methanol-ethanol mixture remains hydrostatic up to 104Kbar at room temperature. A addition of water to methanol-ethanol in the proportion 16:3:1 appears to extend the hydrostatic range of the alcohol mixture to 145Kbar (Table 2.1).

Table 2.1. Various pressure media for hydrostatic conditions in a DAC (after Jayaraman 1983).

Medium	Freezing Pressure (Kbar at RT)	Pressure range for hydrostatic conditions (Kbar)
CH_3OH-EtOH (4:1)	104	~200
H_2O-CH_3OH-EtOH (16:3:1)	145	~200
He	118	>600
Ne	47	160
Ar	12	90
Xe	-	300
H_2	57	>600
N_2	24	130

CHAPTER THREE

THE ASSEMBLY OF AN OPTICAL SYSTEM TO MEASURE THE FLUORESCENCE OF RUBY AND RARE EARTH PHOSPHATE GLASSES AND CRYSTALS UNDER HIGH PRESSURES

3.1 INTRODUCTION

The possibility of making visual microscopic studies in the DAC has transformed it into a quantitative instrument. In 1972 a major development occurred in the calibration of pressure in the DAC. The new technique, which is widely used nowadays, employed ruby fluorescence as a rapid and quite precise pressure gauge for pressure measurements in DAC. For the purpose of calibration a small chip of ruby crystal, together with the sample of interest, is introduced into the pressure chamber of the DAC and a suitable laser source is used to excite the chip to obtain the fluorescence. The approach is to use the pressure dependence of the sharp ruby R lines fluorescence.

In this chapter, a description of the components of an optical system designed to calibrate the DAC (using the ruby fluorescence) and to measure the fluorescence spectra of a set of rare earth phosphate glasses and crystals will be given. It commences with background studies of the development of ruby fluorescence as a pressure gauge and the advantages and disadvantages it has over other gauges. Then it goes on to give the specifications and description of each of the optical and electrical components of the optical system designed for this purpose and their roles. Finally the assembly of the optical system will be given followed by a discussion of the preliminary attempts to calibrate the DAC.

3.2 RUBY HIGH PRESSURE GAUGE

To understand how ruby fluorescence can be used as pressure gauge in the DAC, it is essential to know the corresponding properties together with the interpretation of

its energy level. Chemically, ruby is inert and its strength is much higher than the strength of the materials usually examined in the DAC. Basically, ruby consists of pure corundum (Al_2O_3) which is transparent and a small amount of impurity (Cr_2O_3) which gives ruby its strong red colour (Alonso and Finn 1971). The chromium percentage is usually between 0.05% and 0.5% by weight. At lower concentration the material is pale pink whilst at higher concentrations it becomes deep red. The chromium resides in the lattice in the form of Cr^{3+} ions, and these ions give the crystal specific fluorescent properties.

The chromium ion (Cr^{3+}) has three electrons in the d shell with the lowest levels belonging to the ^4F and the ^2G terms. Within the ruby crystal there is a considerable modification of the energy levels of the chromium ion brought about by the electric field associated with ionic bonding. Figure 3.1 shows the appropriate energy levels of ruby crystal. The ^4F term is split into 3 levels usually designated by the symbols $^4F_1$, $^4F_2$, and $^4A_2$. The ^2G term is split into 4 levels designated by the symbols $^2A_1$, $^2F_1$, $^2F_2$, and ^2E. In addition, the ^2E level is not single but is a pair of closely spaced levels approximately ($29cm^{-1}$) apart. These are usually noted by the symbols 2A and E. In fact, the $^4F_1$ and $^4F_2$ levels are 600Å wide giving rise to a broad absorption band between 3500Å and 6000Å. The widths of the other levels are much smaller, for example the total width of E is about 7Å at 60°C. Optical pumping is used to populate the two levels $^4F_1$ and $^4F_2$ which can then undergo rapid relaxation to the narrow ^2E levels. The transitions from either E or 2A to the ground state are called R_1 and R_2 respectively. At room temperature the wavelength of R_1 is 6943Å, and R_2 is 6928Å (Eastham 1986).

The pressure calibration procedure of the DAC is based on the wavelength shift of the R fluorescence lines of ruby with pressure. The first quantitative study of the ruby pressure monitor was carried out in a gasketed DAC up to 23Kbar and used as fixed calibration points the known freezing pressures of several liquids that are chemically inert (Forman et al. 1972). The calibration was extended subsequently to nearly 100Kbar (Piermarini et al. 1973). Next Piermarini et al. (1975) calibrated the shift of the R_1 line initially at 6942Å produced by pressure up to 195Kbar against the compression of NaCl by using the Decker equation of state for NaCl.

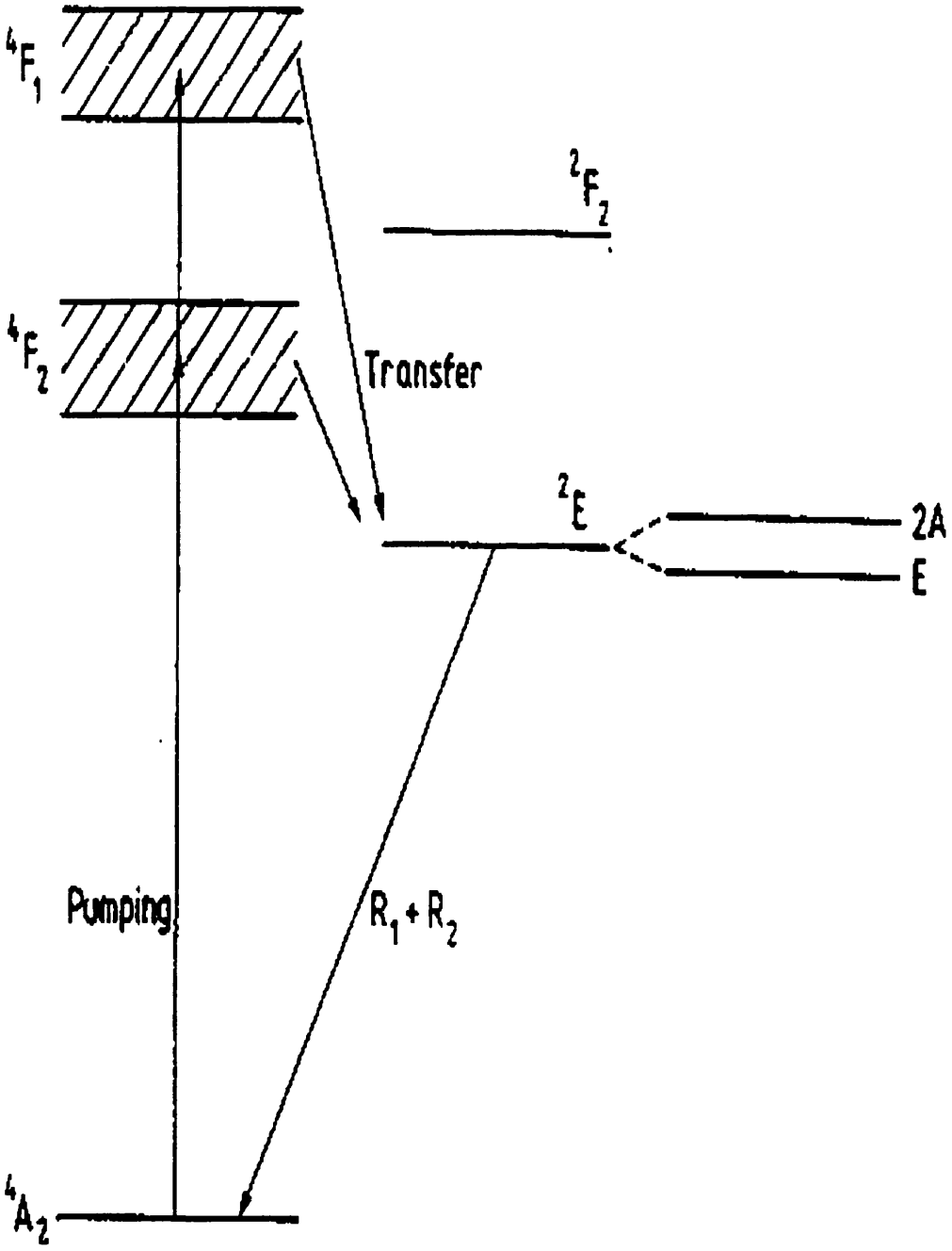

Figure 3.1. Ruby energy levels (after Eastham 1986).

The pressure dependence was found to be linear (Figure 3.2). The generally accepted shift of the wavelength in the pressure range up to 100Kbar is

$$d\lambda/dP = 0.365 \text{ Å/Kbar} \qquad (3.1)$$

where λ is the wavelength of the ruby fluorescence and P is the pressure. According to Bell and Mao (1975), the pressure induced line shift of the ruby fluorescence lines is nearly linear up to pressures of 1Megabar and may be used to measure pressure to a precision equivalent to 0.5Kbar or better (Barnett et al. 1973).

The precise wavelength of the R lines depends on the percentage of Cr_2O_3 in the Al_2O_3, and on the temperature as well as on the pressure. However, within the accuracy of measurements reported, the rate of change of wavelength with pressure is independent of temperature in the range -270 to 87°C, and independent of doping level at least up to 0.5% by weight. The wavelength of the R_1 line does not shift with pressure only but with temperature too towards the red region at a rate of,

$$d\lambda/dT = 0.068\text{Å/°C} \qquad (3.2)$$

where T is the temperature of the ruby chip in the DAC. So when careful measurement with the ruby pressure is required, it is necessary to measure the temperature fairly carefully. An error of 1°C is equivalent to something over 0.1Kbar (Noack and Holzapfel 1978). It is not unusual for pressures derived from room temperature ruby pressure calibrations to be quoted with uncertainties of ±0.2Kbar. At low temperatures, the R_1 line is much sharper and shifts less quickly with temperature. Therefore, the precision of the pressure measurements can be higher for low temperature work, if the performance of the monochromator is good enough.

There are some advantages in using ruby fluorescence lines as a pressure gauge in the DAC which are worth mentioning here. The fluorescence has a high intensity per unit volume: a very small ruby chip can be used as small as 30μ in the DAC,

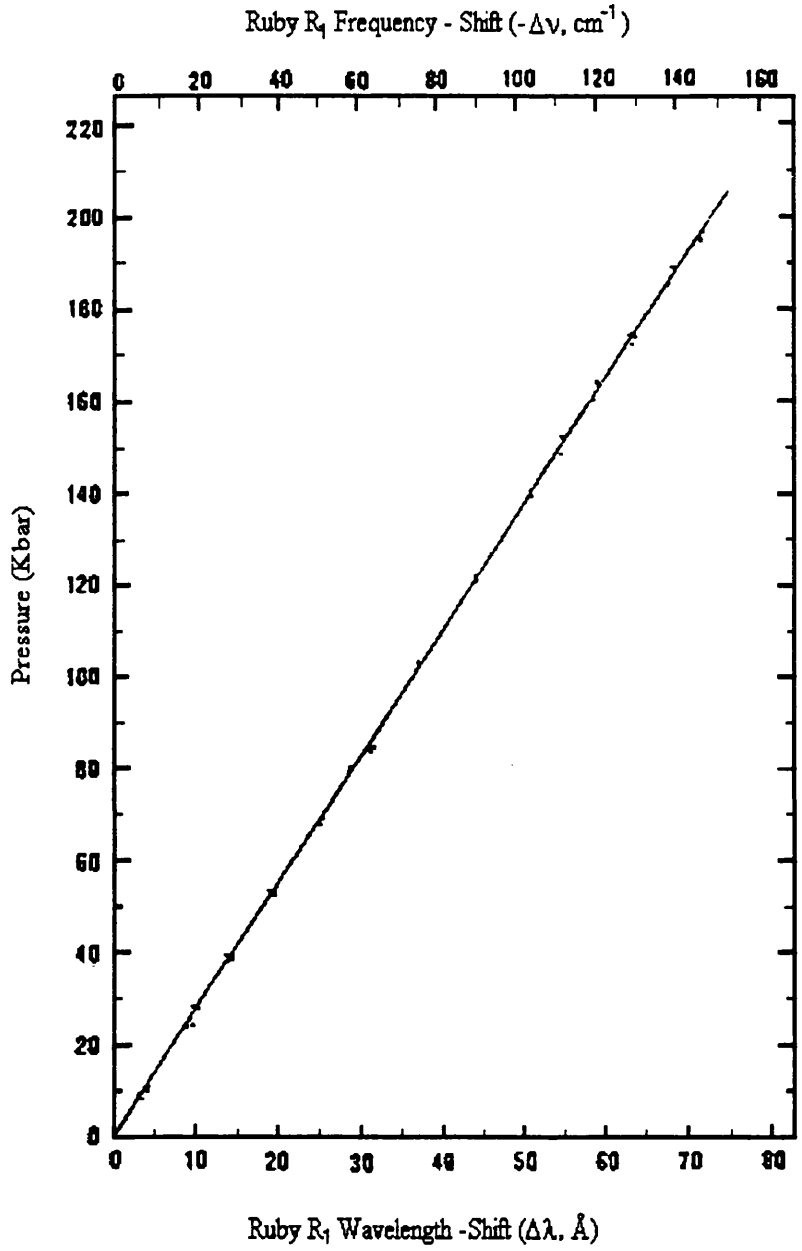

Figure 3.2. The pressure dependence at 25°C of the ruby R_1 fluorescence line at 6942Å as a function of wavelength (Å) and also wavenumber of frequency (cm^{-1}) (after Piermarini et al. 1975).

acceptable pressure dependency (0.365Å/Kbar), sharp line width (7.5Å). It is a rapid and dependable method (pressure can be determined within a short time of 1 to 15 minutes).

However, there are also some disadvantages when using the ruby gauge. It has a doublet rather than singlet fluorescence line with a significant temperature coefficient (0.068Å/°C) in the same direction (red) for both temperature and pressure. It also shows a thermal line broadening with pressure, causing R_1 and R_2 to overlap and limiting the use for pressure calibration when temperature is greater than 300°C. However, the composite line can be used with decreased precision up to 400°C (Barnett et al. 1973).

Workers with DAC have examined other possible materials which could be used as a pressure gauge. However, ruby has been found to be the one which is most suitable for calibration. All other materials investigated have a larger half-width than ruby at room temperature. In general, those materials exhibiting large pressure coefficients also exhibit large temperature coefficients, Table 3.1.

3.3 ARGON ION LASER TUBE

In general, ion lasers produce a number of high power lasing wavelengths ranging from the ultraviolet, through the visible, into the near infrared portion of the electromagnetic spectrum. In particular, the argon ion laser produces strong visible power levels and has up to ten lasing wavelengths in the blue and green portion of the spectrum. This wide region of lasing lines coincides with most of the rare earth glass and crystal absorption bands; this has made this type of ion laser suitable for the current work.

The laser used in the optical system needed for the calibration and fluorescence measurements in the DAC is a water-cooled CW argon ion laser Lexel model 95, capable of reaching a maximum power of 4W in multiline mode. This model has a cavity length of 1m and a beam diameter of 1.3mm at the 5145Å green line. Single line mode can be produced when the back mirror of the laser tube is changed with the prism wavelength selector to select the appropriate laser line suitable for an experiment. The lines can be tuned, as required, by two screws on the back of the la

Table 3.1. Characteristics of selected fluorescence spectra of materials which have been considered for use as a pressure indicator (after Barnett et al. 1973).

Material	Line designation and description	Wavelength (Å)	Relative intensity	dλ/dP (Å/Kbar)	dλ/dT (Å/°C)	Linewidth (Å)
Ruby (Al_2O_3) (0.5%Cr)	R-lines Doublet	6928 6942	very strong	0.36	0.068	7.5
$YAlO_3$ (0.2%Cr)	R-lines Doublet	7228 7251	strong	0.70	0.076	10
YAG (0.38%Cr_2O_3)	R-lines Doublet	6887 6878	medium	0.31	0.105	8
$YAlO_3$ (2.5%Cr)	Pair line Singlet	7320	strong	0.84	0.093	21
MgO (Cr Unknown %)	R-line Singlet	6992	weak	0.35	0.090	10
$YAlO_3$ (Nd unknown %)	R_2-Z_2 line Multiplet	8753	strong	-0.13	0.010	20

ser tube for horizontal and vertical movements of the prism. In the single line mode the maximum laser power varied according to the line chosen, being 1.2 and 1W at 5145Å and 4880Å respectively. The rest of the laser lines have less power than 5145Å and 4880Å ones, and their wavelengths are: 5017, 4965, 4765, 4727, 4658, 4579, 4545Å. The minimum power that can be obtained using this laser model is 100mW.

3.4 PHOTOMULTIPLIER

To choose an appropriate photomultiplier tube for the optical system, certain things have to be considered; e.g. its physical shape, photocathode material, and related optical properties. In general, photomultipliers consist of a photocathode and anode stages connected to a high voltage. The photocathode of photomultiplier tubes converts energy of incident light into electrons. The conversion efficiency (photocathode sensitivity) varies with the wavelength of incident light. The relationship between the photocathode sensitivity and wavelength is called the spectral response.

The photomultiplier chosen is a side-on type R955 from the Hamamatsu company. It has an opaque photocathode (reflection-mode photocathode) and a circular-cage structure. Its spectral response is given by the curve labelled 552S in Figure 3.3; it can be seen that its spectral response ranges from 1600 to 9000Å and it has a peak of radiant sensitivity at 4000Å and a peak of quantum efficiency at 2150Å. By definition, radiant sensitivity is the ratio of the photoelectric current from the photocathode divided by the incident radiant power at a given wavelength, expressed in Amps/Watt. The quantum efficiency (Q.E) of a photomultiplier can be defined as the ratio of the number of incident photons to the number of the resulting photoelectrons emitted from the photocathode, usually given in percent. There are two factors affecting the spectral response of the photomultiplier: the first is related to the photocathode material, the second to the window material. In the photomultiplier used (R955) the photocathode material is multialkali having a high and wide spectral response from the ultraviolet to near infrared region. The window material of the tube is synthetic silica which transmits ultraviolet radiation down to 1600Å. The choice of the R955 photomultiplier was based upon these points:

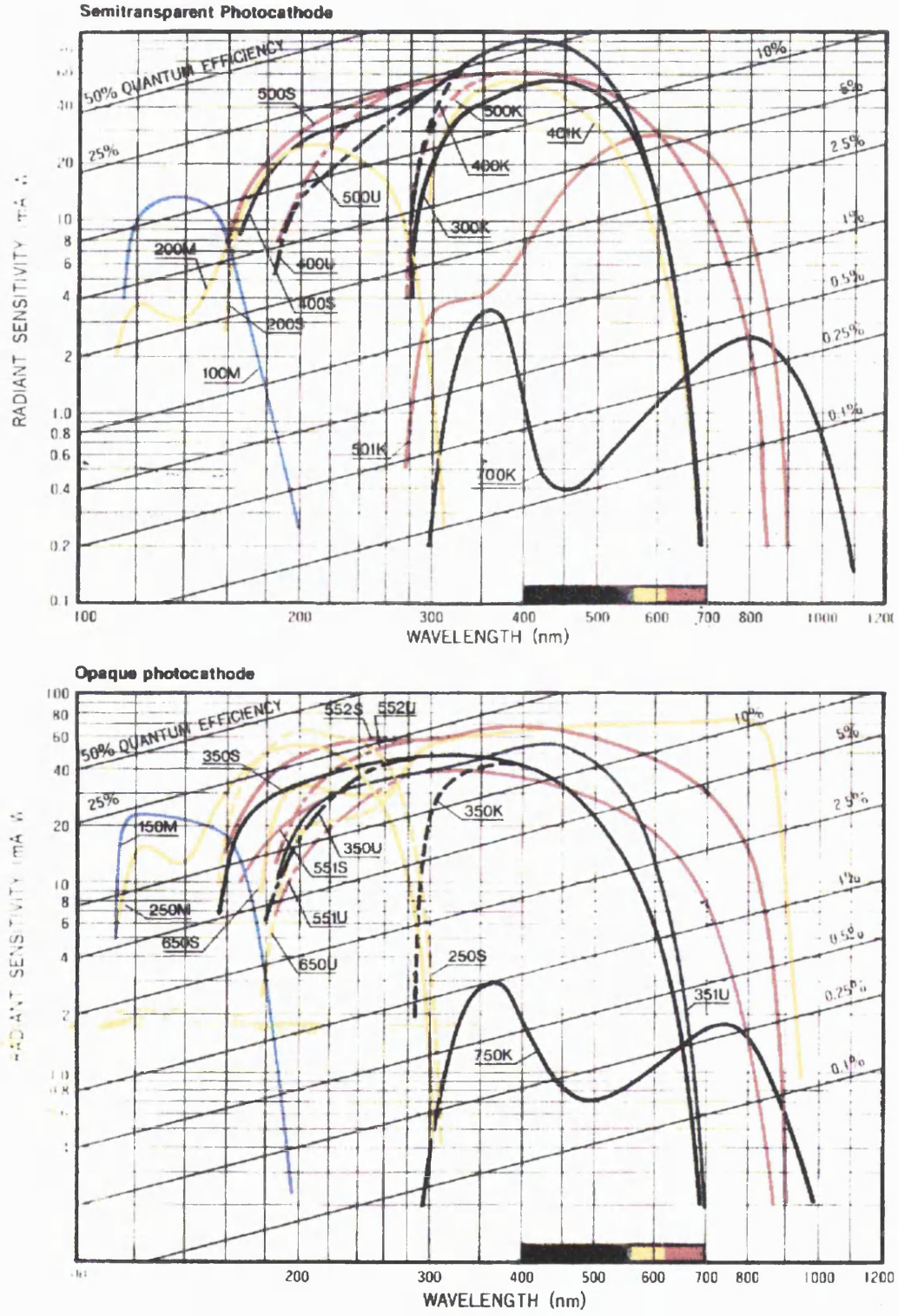

Figure 3.3. The spectral response of the available photomultipliers from the Hamamatsu company. The curve labelled 552S represents the spectral response of the R955 photomultiplier which has been chosen for the optical system.

1- It has a wide spectral response, which covers a wide range of wavelengths. This is consistent with our study of the fluorescent materials which may fluoresce over a wide range of wavelengths.

2- It is sensitive in the red region, the region where the ruby fluorescence is situated, mainly at the two ruby fluorescence peaks (6928Å and 6942Å). In this region the radiant sensitivity is about 30mA/W and the quantum efficiency is nearly 5%, resulting in better sensitivity compared with those of other types of photomultipliers.

3- The photomultiplier tube shape is side-on rather than a head-on; this brings another advantage to the work which comes from the sensitivity to external magnetic field: the side-on type is less susceptible to the external magnetic field than the head-on type.

4- The photocathode of the photomultiplier is opaque while the photocathode available in the head-on photomultipliers is semitransparent. This type of photocathode has a wider and better spectral response than the semitransparent photocathode, as illustrated in the curves of Figure 3.3.

Photomultiplier tubes are extremely sensitive to the effects of magnetic fields and exhibit variations in output and, as a consequence, decrease in the gain. Even the influence of the earth's magnetic field is sufficient to affect appreciably the trajectories of photoelectrons between the anode stages. Therefore it is necessary to cover the tube with a magnetic shield case to minimise the magnetic effect. A shield type E989 from the Hamamatsu company has been used for the photomultiplier. A photomultiplier socket type E717-21 (from the Hamamatsu company) has been incorporated as a potential divider for the anode stages. The driving voltage of the photomultiplier is 1000volts.

3.5 MONOCHROMATOR

A plane grating Monospeck 1000 monochromator from the Rank Hilger company has been used in the optical system construction. It is a symmetrical Czerney-Turner type in which radiation transmitted through the entrance slit is collimated

and directed towards the diffraction grating by a collimating mirror. The diffraction grating disperses the incident radiation and part of the dispersed radiation falls on to a second mirror, which directs and focuses a spectrum at the exit slit. To change the wavelength band passing through the exit slit, the diffraction grating is rotated either manually or by a motor drive. The wavelength of the outgoing radiation is indicated by a mechanical counter. The counter can be read directly to 0.2Å and by interpolation to 0.1Å.

To have a good insight into the characteristics of the monochromator, which are very important in calculating the resolution, it is essential to acquire some knowledge about its diffraction grating. Simply, the diffraction grating consists of a series of parallel grooves ruled on a hard glassy material. The grooves are extremely closely spaced. The general equation for diffraction by a grating is

$$m\lambda = d(\sin\theta + \sin\varphi) \qquad (3.3)$$

where θ and φ are the angles of incidence and diffraction, both measured from the normal to the surface, d is the groove spacing, λ is the wavelength, and m (= 0,1,2,3----) is the order of diffraction. For normal incidence

$$m\lambda = d\sin\varphi \qquad (3.4)$$

The angular dispersion produced by the grating is given by

$$d\varphi/d\lambda = m d\cos\varphi \qquad (3.5)$$

From this equation it is clear that the dispersion increases with the diffraction order. The resolving power (R) of a grating is given by

$$R = mN \qquad (3.6)$$

where N is the total number of grooves. The full resolving power can be achieved, if the incident light covers all the grooves of the grating. Also when high dispersion and high resolution are required from a grating, it is clear from the equations 3.5 and 3.6 that highest possible diffraction order should be used. When using only one order of diffraction, it is very wasteful to reject the radiation diffracted in other orders or that having the same order but on the other side of the incident beam (Figure 3.4a). The radiation can be diffracted preferentially close to a particular angle by using a blazed grating in which the grating grooves have been ruled by a diamond and are normally symmetrically V-shaped so that each has a long and a short side as in Figure 3.4b (Hollas 1987). The monochromator used has such a blazed grating; its specifications are tabulated below:

Focal length	600mm
Grating rulings	1200line/mm
Blaze wavelength	5000Å
Recommended wavelength range	3300 to 1000Å
Reciprocal dispersion	8.2Å/mm
Mirror diameters	120mm
Grating dimensions	110x110x16mm
Smallest reading of the slitwidths	0.01mm
Motor drive speeds for the 1200line/mm grating	from 0.5 to 500Å/min
F/number	F/5

3.6 FILTERS, MIRRORS, AND LENSES USED IN CONSTRUCTION OF THE OPTICAL SYSTEM

To construct the optical system, which is required to calibrate the DAC using ruby fluorescence and to measure the fluorescence spectra of the rare earth phosphate glasses and crystals under very high pressure, special filters, mirrors, and lenses are needed. Figure 3.5 illustrates the optical components, filters, mirrors, and lenses and their functions and locations.

a)

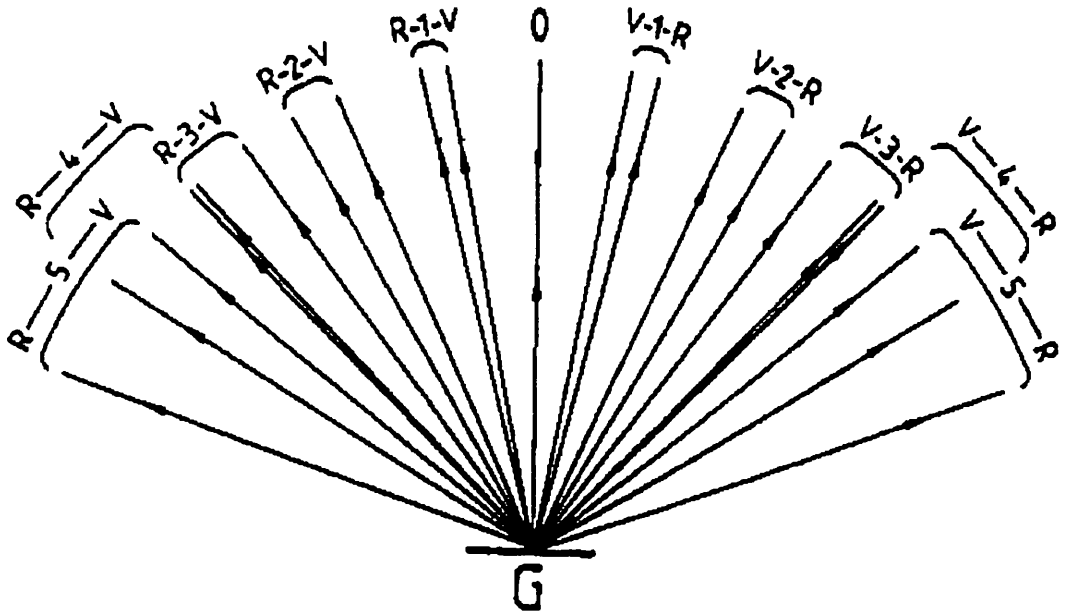

b)

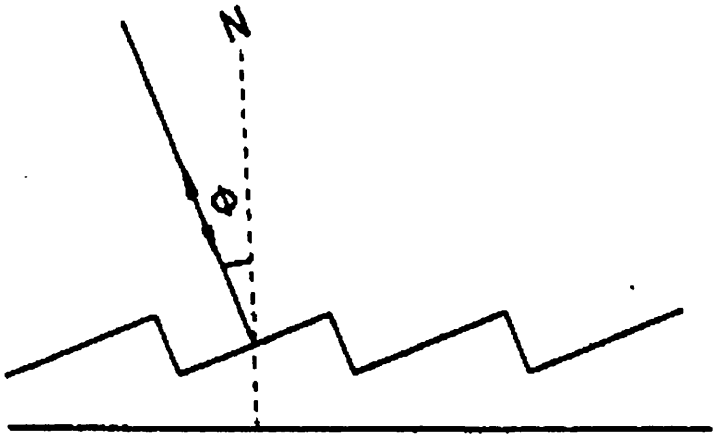

Figure 3.4. A) various orders of diffraction from a plane reflection grating G, b) use of blazed grating at blaze angle φ (after Hollas 1987).

1 Diamond anvil cell
2 Focusing lens
3 Precision RMS focus attachment
4 Tetravar single objective holder
5 Tetravar intermediate component
6 Ruby reflection dichroic mirror
7 Inclined monocular eyepiece holder
8 Two schott coloured glass filters
9 Eyepiece lens
10 RMS thread joint
11 Laser reflection dichroic mirror
12 Condensing lens
13 Monochromator
14 Photomultiplier
15 Lock-in amplifier
16 Chopper frequency unit control
17 Computer
18 Signal digitiser
19 Photomultiplier power supply
20 Plotter
21 Laser tube power supply
22 Laser tube
23 Optical chopper
24 Three neutral density filters
25 Four laser reflecting mirrors
26 Plasma lines blocking filter

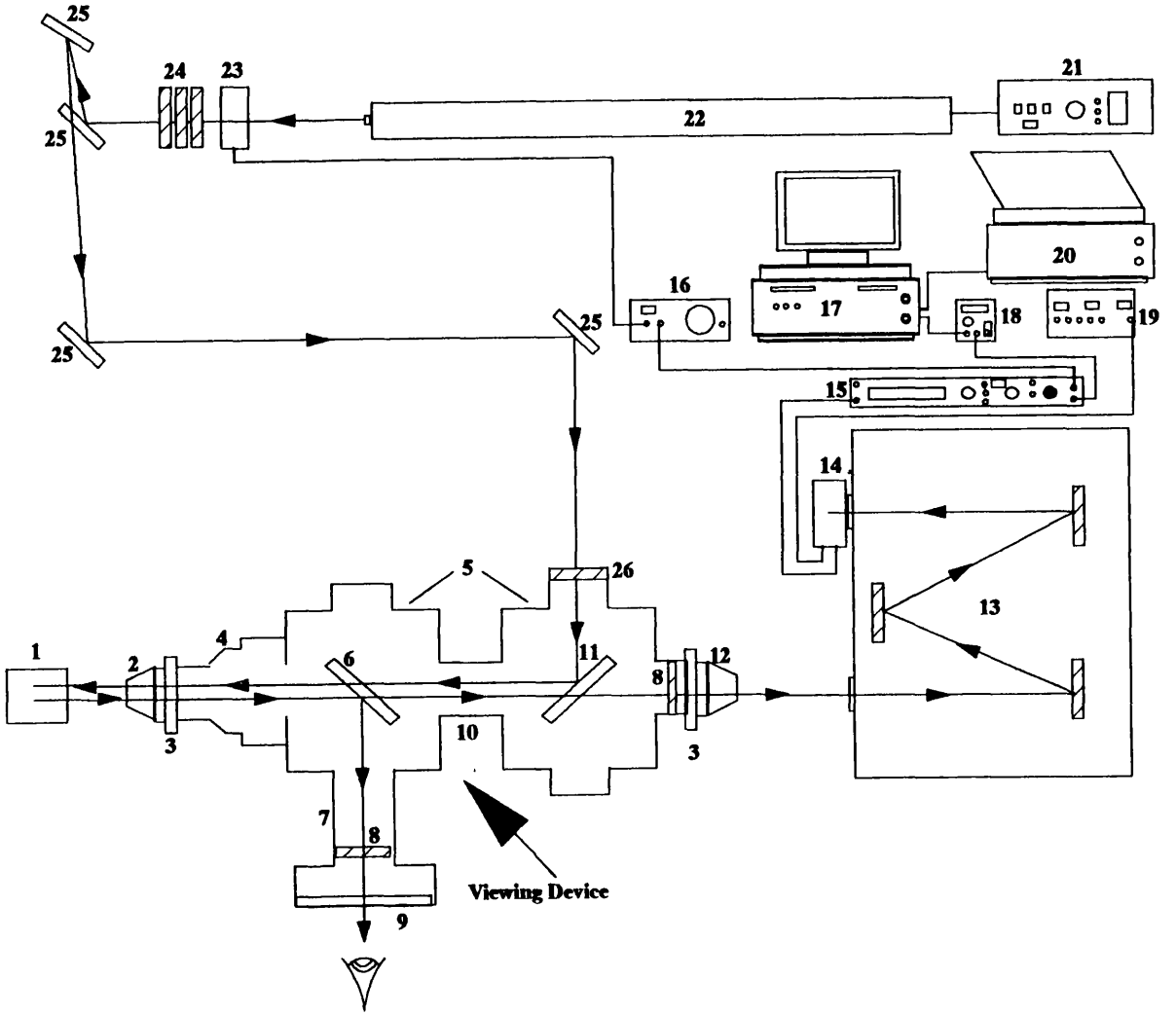

Figure 3.5. The optical system assembled to calibrate the pressure generated in the diamond anvil cell by using the ruby fluorescence lines. The system has also been used to measure the fluorescence of the rare earth metaphosphate glasses and pentaphosphate crystals under high pressures.

The first type of filters used are three neutral density filters put in front of the laser tube (item no.24 in Figure 3.5). They are square in shape with dimensions of 50x50mm. They have the capability of withstanding high power laser without changing their characteristics; each blocks the laser beam intensity by a different amount: 10%, 25%, 50%. These filters are used to lower the intensity of the laser power when necessary, especially when alignment of the optical system is required so work can be done safely without any possibility of damage to the eyes.

The second type of filter (no.26) is an ID901003M type from the Infrared Engineering company having the characteristics shown in Figure 3.6. Its purpose is to block all the plasma glow lines generated inside the laser tube and to pass only the laser lines. It is round in shape having 25mm diameter and 3mm thickness; it is placed normal to the laser beam with the visibly reflective side oriented towards the laser beam.

The third type of filter (there are two of these (no.8) in different locations, one preceding the eyepiece of the viewing device and the other behind the collecting lens) is a round OG-550 Schott coloured glass filter with dimensions of 12.5mm in diameter and 3mm in thickness; its characteristics are shown in Figure 3.7. The role of the first one of these, which is located in the viewing device, is to protect the eye from any laser while at the same time allowing the ruby fluorescence to be observed through the eyepiece. The purpose of the second filter, which is located behind the (condensing) collecting lens, is to block any stray laser light from getting through this lens into the monochromator and causing noise.

From the design of the optical system it can be seen that some laser reflecting mirrors are needed to steer and lift the laser beam to the appropriate height matching the monochromator entrance slit. Four such mirrors were used for this purpose (no.25). These mirrors are broad band, visible type B1004.136 from the Melles Griot company, capable of reflecting a laser beam at 45° angle in the visible range of 4000-7000Å. Their dimensions are 25mm in diameter and 6mm thick. They are made of the material BK7 having reflectance of 99.0% and 2 J/cm^2 in 10ns laser damage threshold. A laser beam-steerer type 07BSD505 from Melles Griot is used to lift and reflect the laser beam in the direction appropriate for the optical set up.

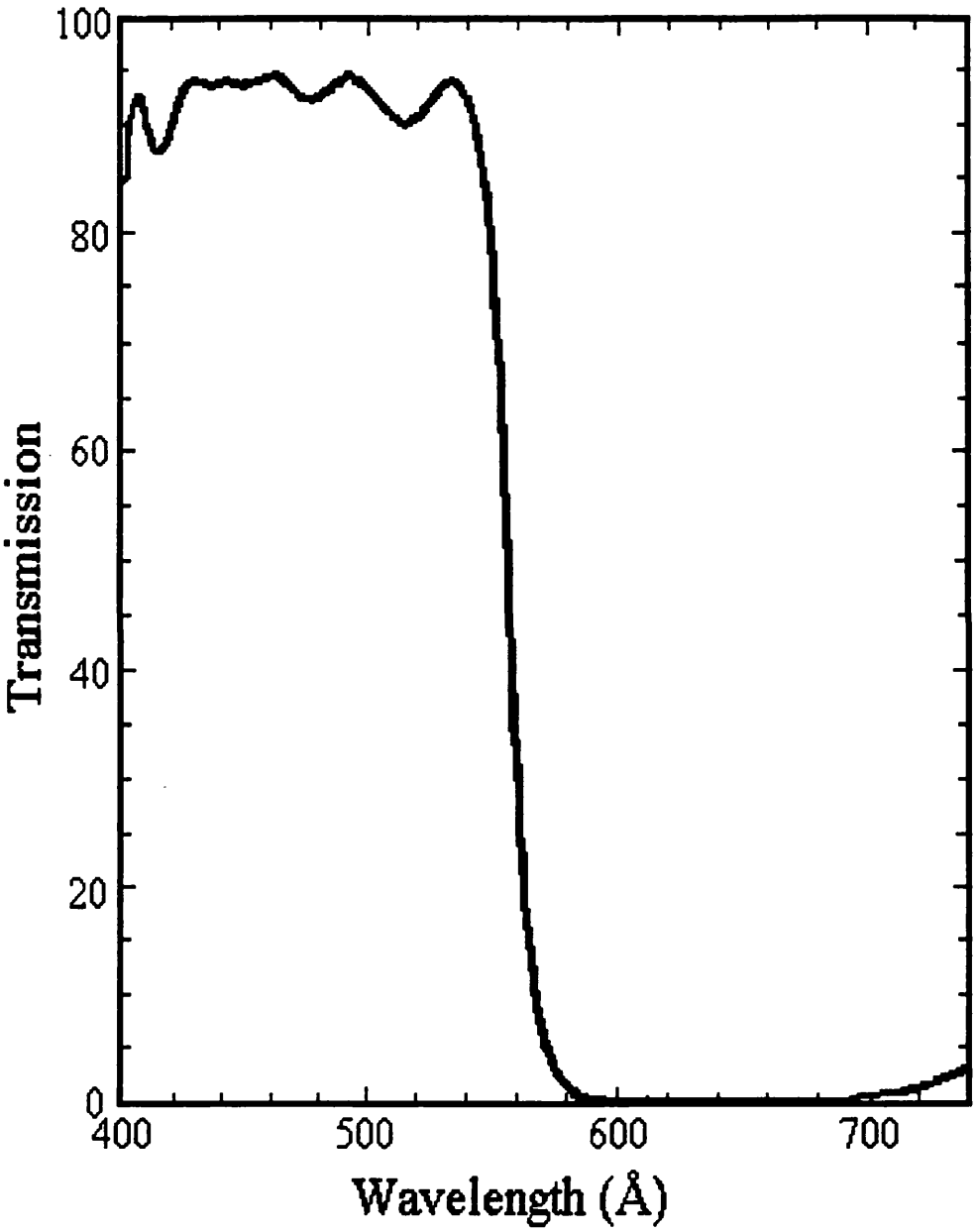

Figure 3.6. The wavelength transmission of the filter ID901003M used to block the plasma glow lines generated inside the laser tube.

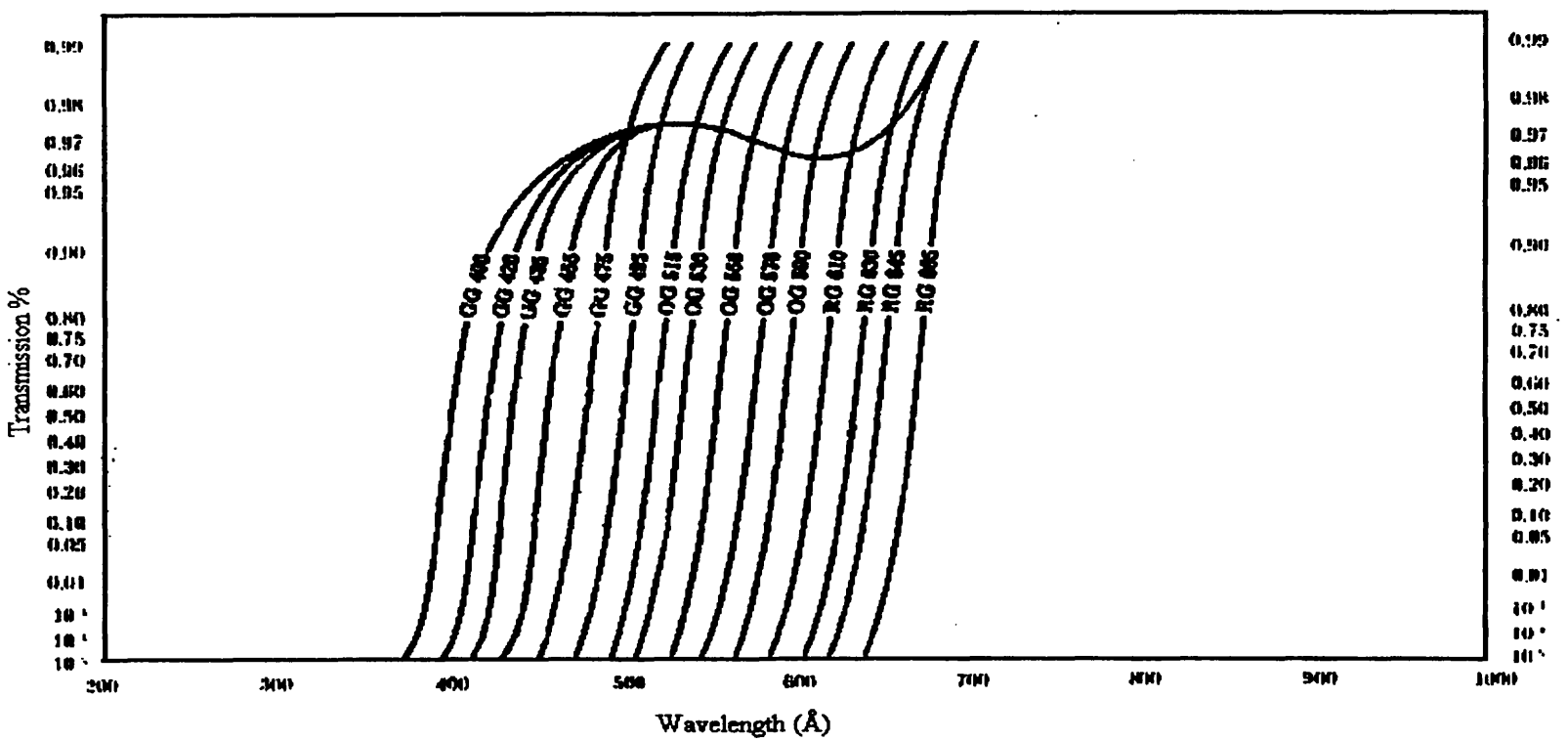

Figure 3.7. The spectral characteristics of the filter OG-550 used to block the argon ion laser lines.

It accommodates the first two of the four laser broad band reflecting mirrors mentioned above.

A steering mirror is needed to bend the laser beam coming from the last laser reflecting mirror through the optical viewing device. A dichroic mirror 25mm diameter, 6mm thickness, highly reflective for the main argon laser lines at 45° is introduced for this purpose (no.11). This mirror passes any other wavelengths: its transmission of wavelengths is shown in Figure 3.8. For the viewing of the ruby sample by the eyepiece, another dichroic mirror is placed inside the viewing device. It is a highly reflecting red mirror, with a polished back surface, 25mm in diameter, and has the property of reflecting the ruby fluorescence at 45° towards the eyepiece (no. 6). These two dichroic mirrors were obtained from the AG-electro optics company.

For the purpose of the imaging and focusing of the laser beam down into the DAC, on the sample, a special objective lens is introduced into the optical system (no.2). This lens is an SLWD PLN Achro from the Nikon company. It has the following specification: 20X magnification, 0.35 numerical aperture, 20mm working distance, 210mm mechanical tube length, 45mm parfocal distance. Such a long working distance lens is needed because of the natural width of the DAC, which is about 10mm distance from the sample location to its outer edge. This would be impossible to image with an ordinary objective lens (normal objective lenses have a short working distance of less than 10mm). The lens used has a special coating to protect it from carbonisation caused by the heating effect of the laser beam. Another lens, part of the viewing device (no.12), is a condensing lens preceeding the monochromator entrance slit. It has a 3mm focal length, 20X magnification made of the Baker company. It has been used as a condensing lens for the fluorescence spectrum coming from the objective lens (no.2).

3.7 OPTICAL CHOPPER, LOCK-IN AMPLIFIER AND DIGITISER

To manipulate and convert the optical signal (generated from the fluorescence of the samples under study by the optical system) to an electrical one, some electrical components are required. An optical chopper, model 300C from Scitec

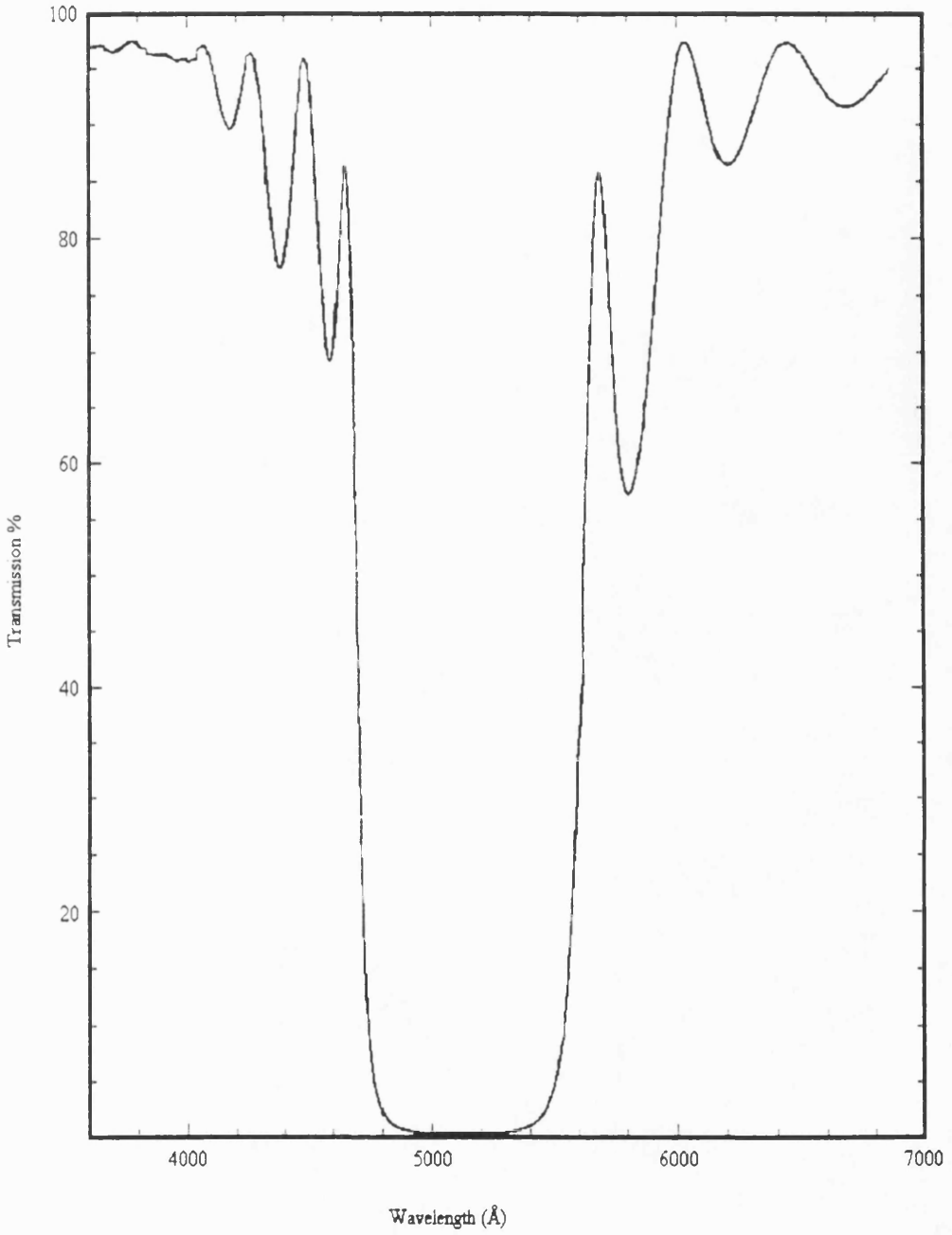

Figure 3.8. The spectral characteristics of the dichroic mirror used to reflect the argon ion laser lines at 45^0.

Instruments, has been used in the optical system setup (item no.23 in Figure 3.5). It consists of a remotely mounted chopping head connected by a cable to a control unit. It has a stability better than 0.01%/°C and manual frequency control via a ten turn potentiometer fitted with dial, which counts turns. It also has four different blades to cover frequency ranges of 5 to 3000Hz. The blades are specially coated to prevent damage by a high power laser beam. A square wave reference signal at the chopping frequency having constant phase relative to the chopping is available from a reference output BNC socket. This signal is standard TTL and is used as a reference frequency signal for the lock-in amplifier.

A single phase lock-in amplifier (model SR510 from Stanford Research Systems) has been used in the optical system (no. 15). It is computer programmable and has a full scale sensitivity from 10nV to 500mV and maximum input voltage of 100V dc, and 10V ac and a current of 10mA. The reference channel unit of the lock-in amplifier has a frequency range of 0.5 to 100kHz and an input impedance of 1MΩ. Phase control of 90° shift and fine shift of 0.025° steps can be achieved in this reference unit. The time constant unit of the lock-in has pretime constants of 1msec to 100sec, and a post time constant of 1sec, 0.1sec, or none. The output signal of 10V corresponds to the full scale meter deflection.

A fully programmable digital storage adapter, Thurlby DSA524, has been used to digitise the output signal (item no.18) from the lock-in amplifier. It is supplied with DSA type software enabling the computer to act as a display device for it, and also provides complete control of the adapter from the computer.

3.8 THE OPTICAL SYSTEM CONSTRUCTED FOR HIGH PRESSURE FLUORESCENCE MEASUREMENT

To begin with, the whole optical system was set on a vibration free optical bench 150x90cm with 5cm thick magnetic stainless steel top from the Photon Control Ltd.

It is evident from Table 3.1 that to examine and use ruby R lines in the calibration operation of the DAC, a good resolution monochromator is essential to preserve the natural linewidth (7.5Å) of the measured fluorescence. Furthermore the small magnitude of the shift of the R-lines with pressure ($d\lambda/dP$ = 0.365 Å/Kbar, equation

3.1) necessitates a high optical dispersion to provide good precision in the pressure measurements. To optimise the magnitude of the measured signals, the light gathering ability of the system is important and, as might be expected, requires a fast monochromator (that is a small F/number). The optical system constructed for this purpose is shown diagrammatically in Figure 3.5. It consists of the argon laser tube sited parallel to the monochromator. The emergent laser beam passes first through the optical chopper, whose purpose is to chop the light into pulses to enable it to be detected and amplified by the lock-in amplifier. At the same time the chopper frequency is used as a reference frequency in the lock-in amplifier. After passing the chopper, the laser beam enters a box containing the three neutral density filters which can be brought into beam path as needed to control the intensity of the beam. The beam then falls on the lower laser reflecting mirror of the beamsteerer, which is angled at 45° to lift the beam up to the second laser beam reflecting mirror; this is angled at 45° also but towards the left hand side. With the help of the other two laser reflecting mirrors the beam is directed towards the viewing device of the optical system. At the entrance of the viewing device, the laser beam passes through the plasma blocking filter, which blocks any plasma glow caused by the high temperature generated inside the laser tube and hence passes only the argon laser lines.

In brief, the viewing device consists of two intermediate tetravars, a tetravar single objective holder, and an inclined monocular eyepiece holder (obtained from Ealing Electro Optics plc.). Inside the first intermediate tetravar sits the high reflecting laser dichroic mirror which is angled at 45°. Its role is to reflect the laser beam parallel to and through the viewing device and also to pass any other wavelengths except the argon laser lines to the right hand side of the viewing device. On the left hand side of the first intermediate tetravar another intermediate tetravar is attached by an RMS thread joint; on its right hand side is attached the condensing lens (or converging lens) by the means of a precision RMS focus attachment (made by Ealing Electro Optics plc.). The laser beam reflected by the laser reflecting dichroic mirror, passes through the second intermediate tetravar, which holds the tetravar single objective holder in the direction of the optical axis; the inclined monocular eyepiece holder is also attached to it at a right angle to the optical axis. The eyepiece holder holds the eye-protection Schott filter to protect the eye from laser light

reflected inside the system, and an eyepiece lens for observation. The second intermediate tetravar has a cover with a mirror holder; this holder can flip up and down. It holds the highly reflecting red dichroic mirror, which has the property of reflecting the ruby fluorescence wavelengths and passing any other wavelengths coming from the sample under study. This mirror is angled at 45° to reflect the ruby fluorescence into the inclined monocular tube so that the excitation and position of the ruby chips and of the sample inside the DAC can be seen. Hence, this mirror must be removed during the pressure measurements, because it blocks the fluorescence of the ruby from passing through the optical system used for the pressure calibration and also because it reduces the intensity of the fluorescence spectrum directed towards the monochromator. Both of the intermediate tetravars with their supplements are supported by a micropositioner with x-z micrometer for alignment with the optical axis. The component next to the second intermediate teravar is the objective lens; this is attached to the tetravar single objective holder by another precision RMS focus attachment. The last component on the left hand of the diagram is the DAC which is mounted on a micropositioner with x-y-z micrometers (obtained from Ealing Electro Optics plc.). Precision translation devices are an integral part of this micropositioner, as they are used to position the tiny sample ($\approx 100\mu$) inside the DAC on the optical axis of the system and focus with laser beam on it. On the right hand side of the viewing device, there is the monochromator to analyse the spectrum of the excitation coming from the sample in the DAC from the left hand side and transfer it to the photomultiplier, which is located on its exit slit. The photomultiplier is supplied with 1000V from the high voltage power supply, and it converts the optical signal to an electrical signal as a voltage across a resistance of 500kΩ. The voltage signal is detected by the lock-in amplifier and matched with the frequency of the optical chopper to maximise it and also to reject any noise. The amplified signal output is sent to the digitiser and then the output is sent from there as a digital signal to a computer for analysis and plotting. Finally the computer output signal is sent to a printer.

To describe how the optical system works, how all the components operate together must be discussed in detail. High resolution spectral measurements in the monochromator require a small entrance slit through which the light must pass.

Thus the converging lens is inserted in to the system preceding the monochromator entrance slit, to reduce the light beam diameter so as to match the entrance slitwidth of the monochromator and also drastically increase the divergence of the beam; this makes necessary the monochromator's small F/number. Also to provide a beam divergence consistent with the F/number of the monochromator, the focal length of the converging lens is carefully selected to meet this requirement. When a spectrum from a ruby chip (or the sample under study) is recorded, the objective and converging lenses act as a light gathering device. The first purpose of the objective lens is to form an image of the ruby chip, or the sample, for viewing with the eyepiece after the light beam has been reflected by the high-reflecting red dichroic mirror. The second purpose of the objective lens is to gather the fluorescence spectrum in a nearly parallel beam and pass it to the converging lens. The third purpose is to concentrate maximum laser light onto the sample at its focal point. The optimal focal length for the converging lens depends on the magnification of the objective lens since latter lens determines the diameter of the near-parallel light beam which falls on the former. The distance of the converging lens from the monochromator slit must be carefully and precisely adjusted for optimum operation. Because resolution of a monochromator is partly a function of how the slit is illuminated, these two lenses must be chosen in accord with the intended sample size. To maximise resolution, there are two requirements for the slit illumination. The sample's image at the entrance slit must be larger than the slit width; and the divergence of the entering light must be greater than or equal to that of the monochromator optics (F/number of incident light = F/number of monochromator).

The first requirement follows from the fact that a recorded spectrum is the coincidence of the image of the entrance slit on the exit slit (the slit function). If the slit is not uniformly illuminated from edge to edge, this slit function will not have the desired Gaussian peak shape, and its centroid will not necessarily represent the true peak position. The second requirement has two parts. The resolution of the grating of the monochromator is limited by the total number of lines N which are used to form the diffracted image, as in equation 3.6. This equation shows that, for a given spectral order m, resolution will decrease when the incident light divergence is insufficient to illuminate the entire width of the grating. This resolution limit, depend-

ing on the limit imposed by the slit width (the half-width of the slit function), can be significant. The function of the converging lens is to gather light to a minimum diameter, not to form an image. This can be accomplished by placing the image of the aperture defined by the objective lens itself at the slit of the monochromator. This location of the converging lens gives near uniform illumination across the slit, ensures that light from all portions of the sample passes through the slit and gives the narrowest beam size at the slit, consistent with the divergence. Furthermore, the amount of light passing into the monochromator does not depend on where the sample image is focused. The converging lens does form an image of the sample a few millimetres away from the slit when they are in their optimum position, as just described. Taking this consideration into account, the requirements for the lenses can be specified. The monochromator under consideration has F-number of F/5 and the slits used are both 150μ. The objective lens used gives a magnification of 20X at a distance equal to 210mm. Therefore, at the converging lens, a 30μ diameter ruby chip will form a 600μ diameter beam to match the F/number of the monochromator. This requires a converging lens with a focal length of about 3mm. A simple lens with such a short focal length would be difficult to obtain, instead, a 20X microscope objective has been used and it is positioned very near to the slit so that the light beam converges to a beam diameter of about 200μ.

3.9 RESULTS AND DISCUSSION OF A PRELIMINARY PRESSURE CALIBRATION OF THE DIAMOND ANVIL CELL

The optical system was set up for calibrating the pressure developed in the DAC, as described in Section 3.8, based upon the shift of the R-lines fluorescence spectrum of ruby with pressure. The calibration procedure was first investigated to verify the linearity (equation 3.1) reported in the early literature. Measurements were taken under pressure, to observe and measure the shift in the wavelengths of the two peaks (R_1 and R_2) of the ruby fluorescence spectrum. A small chip of ruby (about 50μ) was put in a gasket hole of 0.35mm diameter centred on the lower diamond anvil of the DAC. The gasket hole was filled with the 4:1 mixture of methanol-ethanol, used as the hydrostatic pressure medium. Then the cell was closed and squeezed, to apply high pressures on the ruby chip. The detailed techniques and

procedure of the process of loading and applying pressure to the DAC have been thoroughly explained in chapter 2. The loaded DAC was put in its specified place in the optical system, as shown in Figure 3.5. To excite the ruby fluorescence, one of the argon ion laser lines (the 5145Å line at 50mW power) was used and focused down, using the objective lens of the system, into the diamond anvil cell, through the optical access of the cell, onto the ruby chip. The widths of the entrance and exit slits of the monochromator were set to 150μ. The scanning speed of the monochromator was set to 5Å/min, and the plotter folding speed to 10mm/min. Accordingly, the smallest measurable increment on the plotter tracing paper was 0.5Å/mm. The optical signal obtained from the ruby chip was converted to an electrical signal using the photomultiplier and amplified by the lock-in amplifier. The electrical signal was maximised by aligning the optical access of the DAC with the optical axis of the optical system using the micropositioners, in very small steps, relative to the laser beam.

The results of the preliminary attempts to measure the pressure in the DAC using the fluorescence of ruby are shown in Figure 3.9. The curve labelled a in Figure 3.9 shows the fluorescence spectrum obtained for the ruby chip in the gasket hole surrounded by the alcohol mixture and without any pressure applied to the cell (atmospheric pressure). From this curve the R_1 line peak is situated at the wavelength 6943.2Å and the R_2 line peak at 6929.4Å. Curve b in the Figure shows the ruby fluorescence R lines when a pressure was applied to the DAC by pressing the pressure plate of the cell. In this curve the R_1 peak has shifted to the wavelength 6952.6±0.5Å and the R_2 peak to the wavelength 6938.2±0.5Å. By applying equation 3.1 to the R_1 line shift, the amount of the pressure developed in the DAC was obtained as about 25.7Kbar. Curve c shows the ruby fluorescence R-lines when higher pressure was applied to the DAC. The curve reveals an obvious broadening in the widths of the R_1 and R_2 lines caused most probably by improper filling of the gasket with the alcohol mixture. This broadening in the R-lines is a sign that a non-hydrostatic pressure has been applied to the ruby chip in the DAC: there is a pressure gradient. The R_1 peak of this pressure run is situated at about 6968.8±0.5Å and the R_2 peak at about 6950.6±0.5Å; by applying equation 3.1, the pressure inside the cell was calculated to be about 70.1Kbar. An error in the pressure measurement

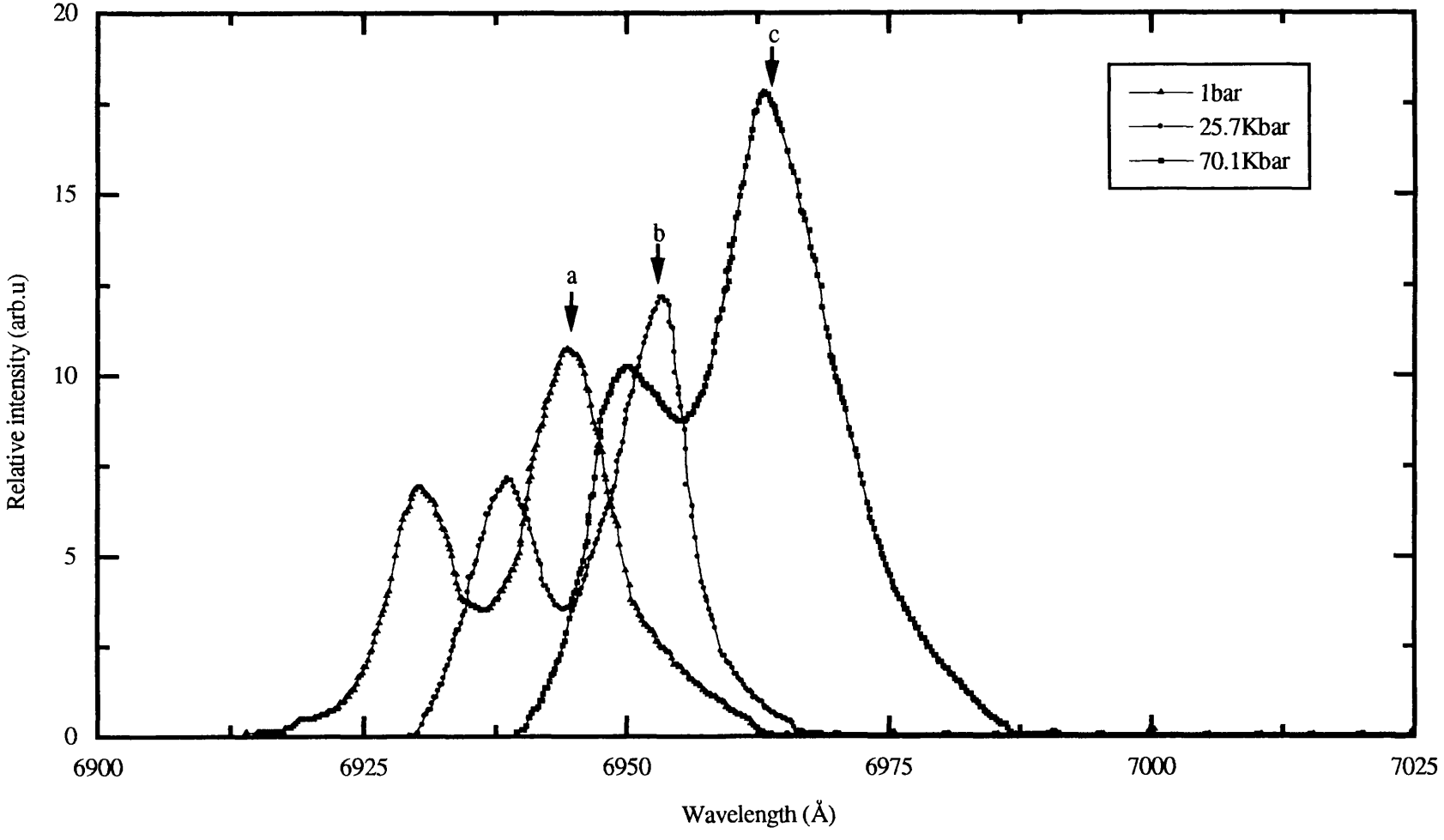

Figure 3.9. The R-line fluorescence spectra of a tiny crystal of ruby in the DAC at different pressures. The spectra show some broadening especially at 70.1Kbar.

was obtained as ±1.37Kbar, which was calculated from the error made in measurement of the wavelength of the R-line peaks (±0.5Å) and applying the equation 3.1.

In these attempts to calibrate the pressure developed in DAC some more errors were determined which come from different sources. First, the rise in the ruby temperature caused by the use of relatively high power laser beam (50mW) shifted the ruby fluorescence peaks to higher wavelength (equation 3.2), in addition to the shift caused by pressure. Secondly, The back-lash of the monochromator read-out counter produced an error of ±1Å in wavelength measurements at the beginning and the end of each scan operation. Thirdly, the monochromator slitwidths were set at 150μ for the ruby fluorescence measurements; such slitwidths produced a linewidth of about 10Å (curve a in Figure 3.9). This is wider than the 7.5Å linewidth reported in the literature.

To tackle some of these errors, the following measures were taken. The lowest laser power possible was used (10mW) to excite the ruby. This reduces the rise in the ruby temperature and causes a smaller shifts in the fluorescence peaks (eq.3.2) which eventually leads to a better determinations of the wavelengths of the R_1 and R_2. Narrower slitwidths (60μ) were used in the monochromator, to preserve the natural line widths of the ruby fluorescence R lines. The back-lash of the monochromator counter was eliminated at the beginning of each scan. The procedure used was to turn the scan control manually until the edge of scan region was reached then the scan motor was switched on.

When the main sources of error were corrected, better results were obtained. In particular sharper line widths for the ruby fluorescence lines were recorded, consistent with the reported line width of a 7.5Å in the literature. This enabled better accuracy in pressure determination since sharper lines give less error in measuring the R-line peaks, equation 3.1, and also resulted in higher resolution in measuring the fluorescence spectra of the rare earth phosphate samples under pressure. The effect of these improvements are reflected in ruby fluorescence spectrum measured at different pressures (Figure 3.10) and the results (detailed in chapter 5,6,7,and 8) obtained for the spectral measurements of the studied rare earth phosphate glasses and crystals under high pressure using the DAC.

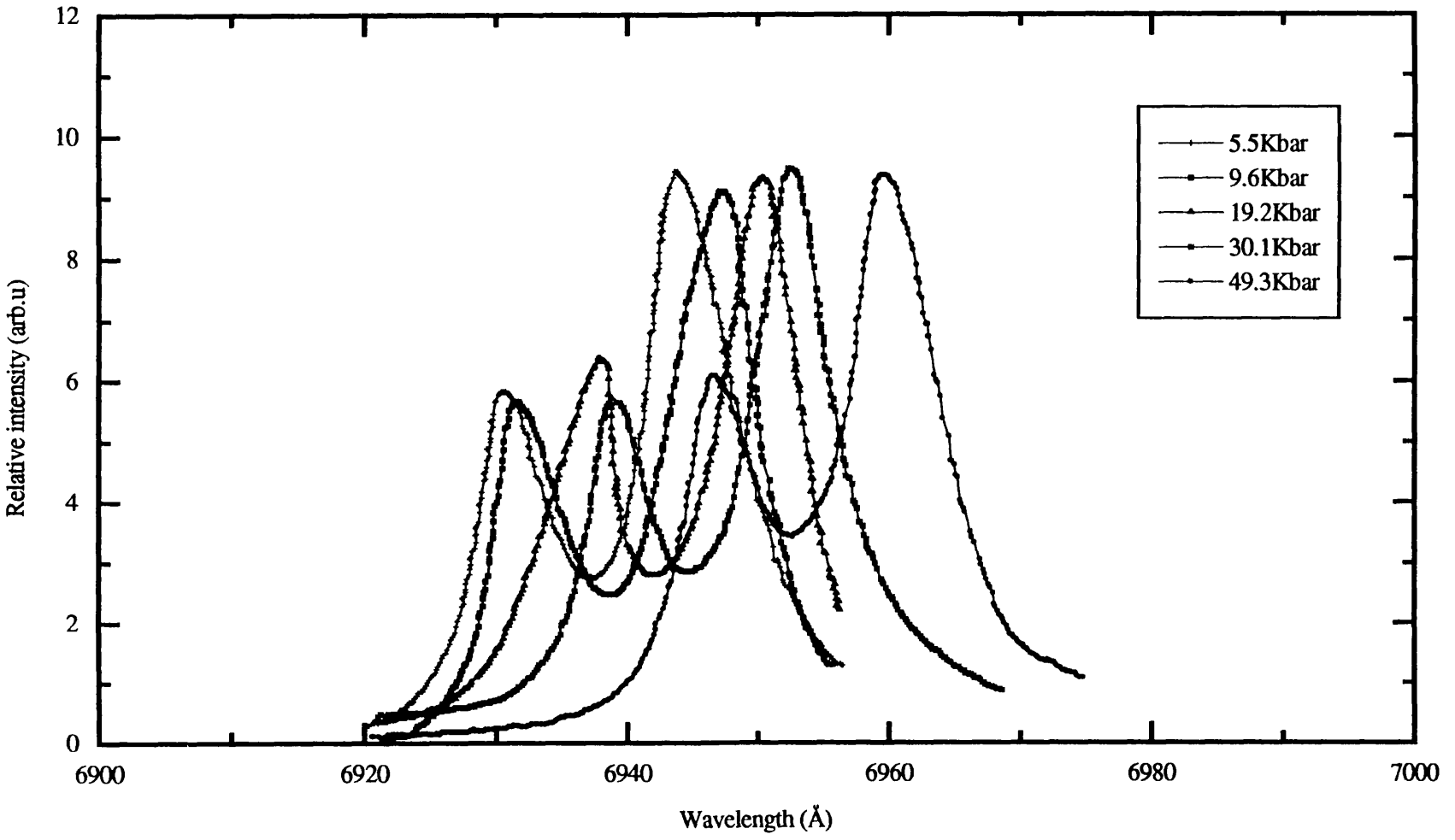

Figure 3.10. The R-line fluorescence spectra of a tiny crystal of ruby in the DAC at different pressures. The spectra have been recorded after the improvements made on the measurements.

CHAPTER FOUR

STRUCTURAL CHARACTERISTICS OF PHOSPHATE GLASSES

4.1. INTRODUCTION

Phosphates, generally, can be defined as compounds which contain P-O linkages. Such compounds may contain either three, four, five or six oxygen atoms linked to a centred phosphorus atom. Traditionally, phosphates are those compounds of phosphorus in the anions of which each atom of phosphorus is surrounded by four oxygen atoms (PO_4) arranged at corners of tetrahedron (Figure 4.1a). By sharing oxygen atoms between tetrahedra, chain, ring, and branched polymers of interconnected PO_4 tetrahedra can be produced.

Pure phosphorus oxide (P_2O_5) is one of five main oxides (the others are the oxides of Si, B, Ge, As), which possess the capability for forming glass if they are cooled quickly after melting (Figure 4.1b). These glass formers also exhibit this behaviour when mixed with other metallic constituents within certain system-dependent compositional limits. Binary phosphate glasses is one example of such mixing, which can be written as $xM_2O.yP_2O_5$ where M_2O may stand for alkali metal, alkaline earth, transition metal, rare earth or actinide, and P_2O_5 is pure pentoxide. The addition of such "glass modifying" components changes bonding relationships and structural groupings resulting in broad physical and chemical characteristics of glasses. This characteristic variation of glasses, as a result, has led to the manufacture of a wide range of glasses and opened a vast field of research.

In this chapter two major aims will be fulfilled. First, to give a general background explaining the necessary conditions to form glasses, and the theory which identifies their atomic arrangement. Second, to give a short review of the previous work reported on the structure of phosphate glasses, as this will be used later as a guide to interpret the experimental results obtained on the rare earth phosphate glasses.

a)

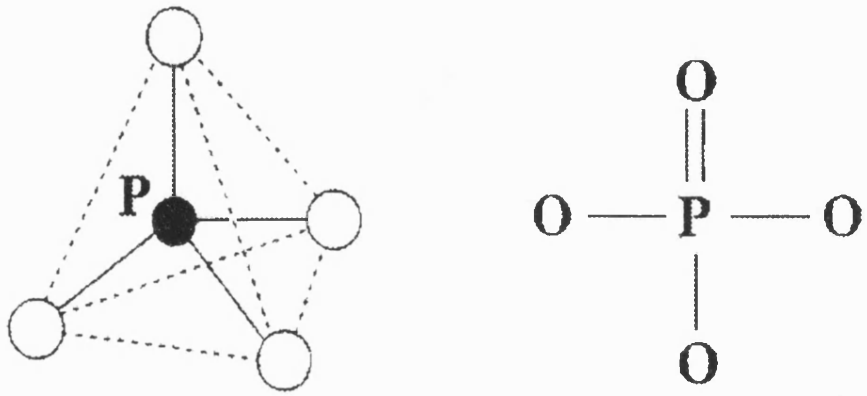

b)

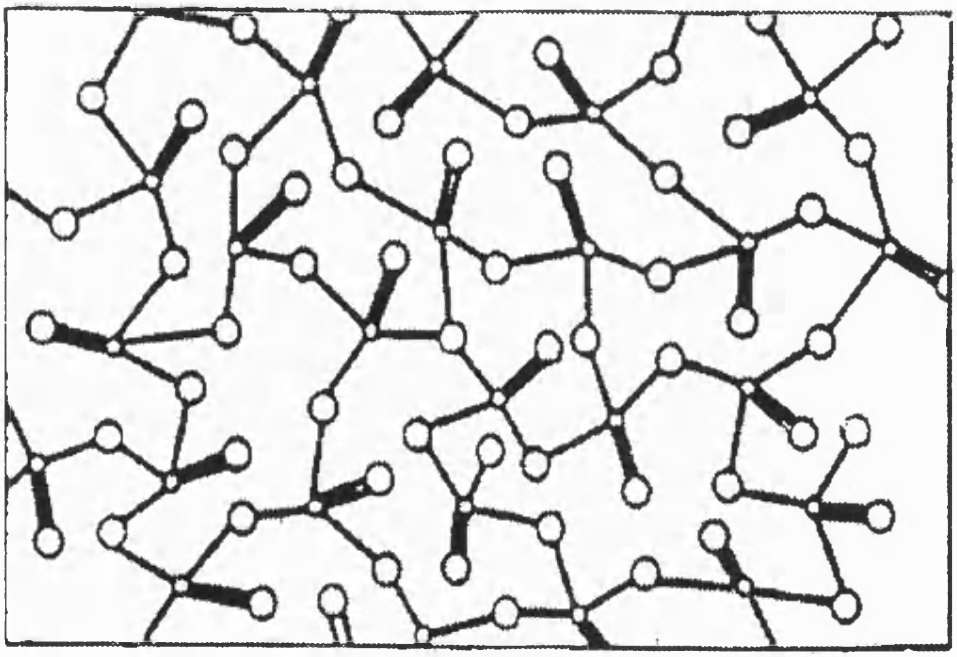

Figure 4.1. Schematic illustrations of a) the PO_4 tetrahedra, b) the pure P_2O_5 glass (after Sales 1990).

4.2. GLASS FORMATION

In principle any substance can be made into a glass by cooling it from the liquid state fast enough to prevent crystallisation. The final temperature must be so low that the molecules move too slowly to rearrange to the more stable crystalline form. In actual practice glass formation has been achieved with a relatively limited number of substances.

When a liquid is cooled, one of two events may occur according to the schematic results of the volume vs. temperature shown in Figure 4.2. Either crystallisation may take place at the melting point T_s (system goes from A to B), or else the liquid will become "supercooled" for temperature below T_s (system goes from A to C), becoming more viscous with decreasing temperature, and may ultimately form a glass. If the cooling is sufficiently slow, it will continue to condense further to point D. So the curve flattens out towards E or F depending on the cooling rate, but it always stays above the line B-G of crystallisation. So at room temperature (T_R), the system does not reach the density of the crystallised system. The crystallisation process is manifested by an abrupt change in volume at T_s whereas glass formation is characterised by a gradual break in slope. The region over which the change of slope occurs is termed the "glass-transition temperature" T_g, the super-cooled glass transforms from a plastic state to a rigid state typical of glass. The movement of the structural elements is very slight here, which is also demonstrated by the high viscosity of glass in this state (Elliott 1990).

Physically, all glasses are energetically unstable compared with a crystal of the same composition. In general, when cooling a molten substance, crystallisation should begin to occur when the temperature falls below the melting point (T_s). The reason this does not occur in glass lies in the fact that the molecular building blocks (as example SiO_4 tetrahedra in silicate glass, Figure 4.3b) are spatially cross-linked to one another. In order to form crystals, the bonds must first be broken in order that crystal nuclei may form. This can only occur at lower temperatures at which the viscosity of the melt hinders the restructuring of the molecules and thereby the growth of crystals. The inclination toward crystallisation generally decreases with increasing speed of the cooling within the critical temperature range below T_s and

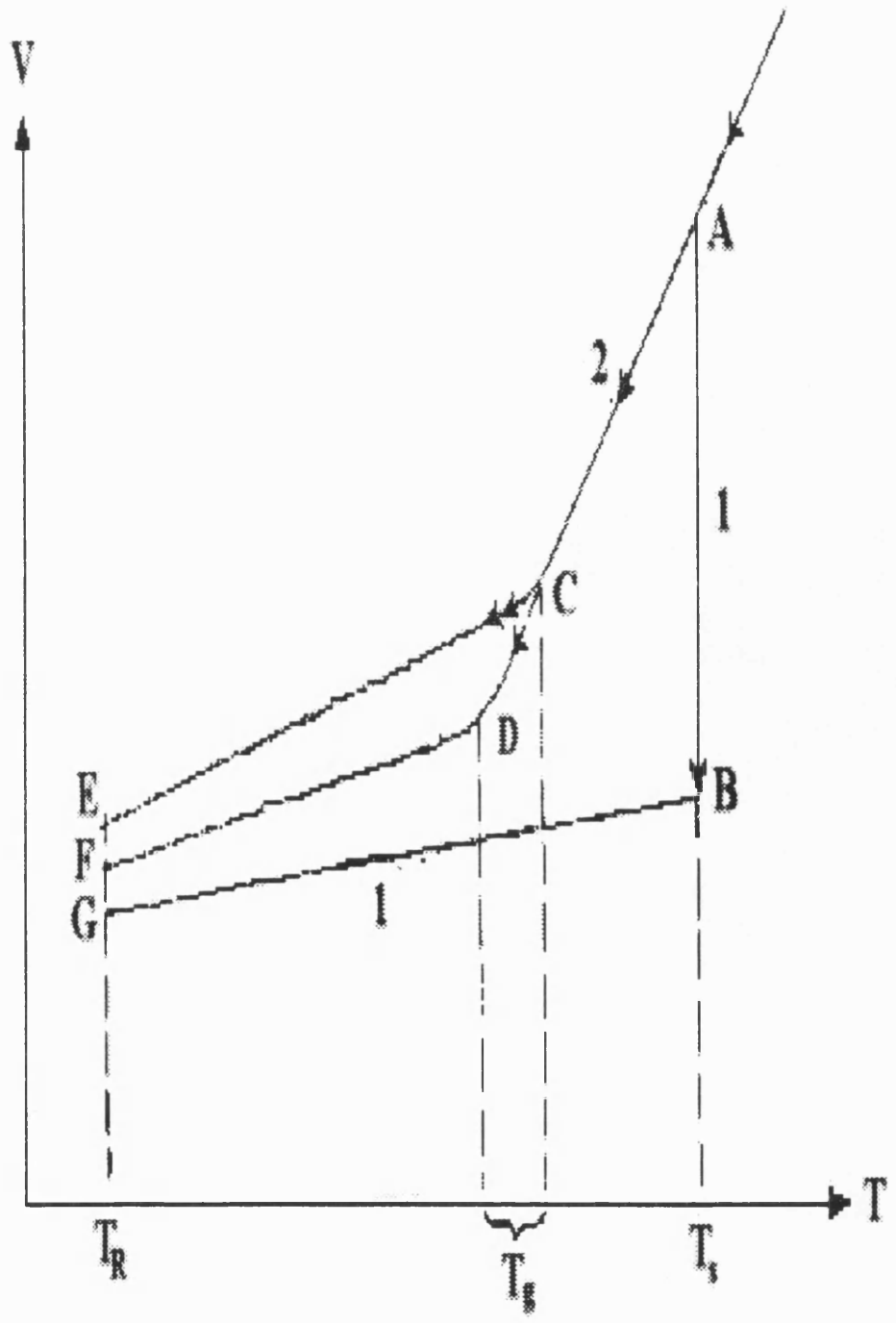

Figure 4.2. Change in volume of a melt during (1) crystallisation (2) glass formation (after Pfaender 1983).

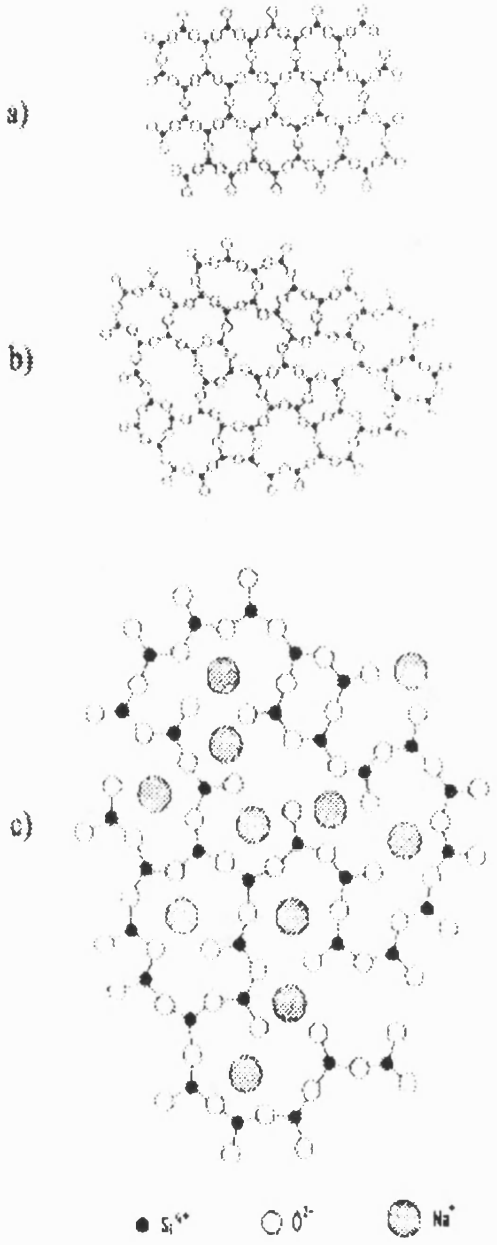

Figure 4.3. Network of SiO_4 tetrahedra a) in crystal, b) in fuse silica, c) in sodium silicate glass (two-dimensional display, the 4th oxygen bond of the tetrahedron is perpendicular to the plane of the picture).

with the number of components so it can also be said it influenced by the composition.

4.3. RANDOM NETWORK THEORY AND GLASS FORMATION

The first successful attempt to envisage the atomic arrangement in glass was made by Zachariasen (1932). A model was proposed on the basis of a random three dimensional network. The theory of this model was firstly based on oxide glasses because of the broad knowledge was available on them at the time and also their commercial importance.

Zachariasen (1932) considered the relative glass-forming ability of oxides and concluded that the ultimate condition for glass formation is that a substance can form extended three-dimensional networks lacking periodicity and symmetry with an energy content comparable with that of the corresponding crystal network. From this condition, he derived four rules for oxide structure that point out which oxides tend to form glasses. The rules are:

1- No oxygen atom may be linked to more than two glass-forming.

2- The co-ordination number of the glass-forming atoms is small.

3- The oxygen polyhedra share corners with each other, not edges or faces.

4- The polyhedra are linked in a three-dimensional network.

These rules were remarkably successful in predicting new glass-forming oxides as well as including such oxides known at the time of their formulation. From these considerations Zachariasen concluded that the following oxides should be glass formers: B_2O_3, SiO_2, GeO_2, P_2O_5, As_2O_5, P_2O_3, As_2O_3, Sb_2O_3, V_2O_5, Sb_2O_5, Nb_2O_5, and Ta_2O_5. Warren and Biscoe (1938) confirmed, using X-ray diffraction, the atomic structures of some of the proposed glass-forming oxides such as SiO_2, GeO_2, B_2O_3 and P_2O_5.

General experience in the field of glass-forming oxides has shown that the most suitable components of the oxides are characterised by relatively small and highly charge cations such as B^{3+}(Boron), Si^{4+} (silicon) and P^{5+}(phosphorus). This stems from the fact that the high charge on the cation in the centre will attract the large

oxygen ions which as a result will only offer a small space for such a small positive cations between them. The basic unit of structure of these oxides is a triangle or tetrahedron built up by the cations surrounded by either three (in the case of B^{3+}) or four (in the case of Si^{4+} and P^{5+}) oxygen negative ions (O^{2-}).

In pure oxides, the structural units are joined together at their corners only and each oxygen atom is shared by two cations. This arrangement is a common feature of the corresponding crystalline materials. If a glass is made up of the oxides of different elements, as is often done in order to obtain a lower melting temperature, only one of the oxides need be a glass-forming oxide. The cation of the other oxides take up positions in the large cavities of the structure. Since the whole must remain electrically neutral, the number of negative oxygen ions must of course also be increased. This is done by breaking the connection between neighbouring oxygen tetrahedra at a number of spots, a bridging oxygen ion of two neighbouring groups being replaced in each case by two non-bridging oxygen atoms. The structure which results in this way is shown in Figure 4.3c, plane diagram being given for the sake of simplicity. By varying quantities and combinations of these ions it is possible to obtain many thousands of different glasses with very divergent properties (Stevels 1946).

4.4. STRUCTURE OF PHOSPHATES

As defined above phosphates consist of PO_4 groups. These groups can be connected to each other by sharing oxygen atoms in three different ways. First, the PO_4 group can share three oxygen atoms with neighbouring PO_4 groups at a "branching point". Second, the PO_4 group can share two oxygen atoms with neighbouring PO_4 groups: a "middle PO_4 group", leaving one negative charge on the unshared oxygen atom. Third, the PO_4 group can share one oxygen in an "end PO_4 group", leaving two negative charges on the two unshared oxygen atoms (Figure 4.4a).

By combining end group, middle group, and branching points in all possible ways, a large number of hypothetical phosphate formulas can be derived. In the case of a single unconnected PO_4 group, there is just one arrangement, that of the orthophos-

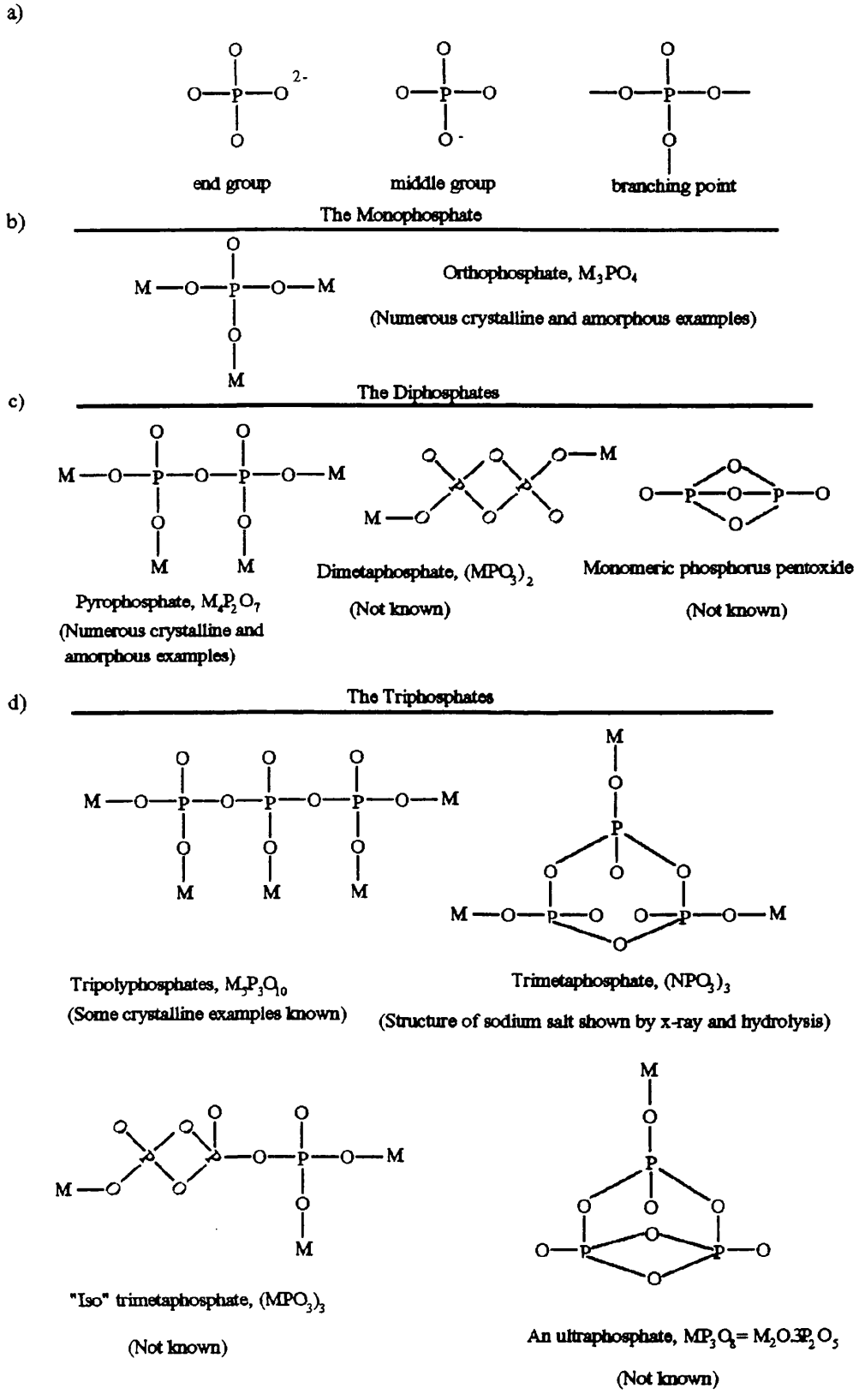

Figure 4.4. Different structures of phosphates (after Van Wazer 1964).

phate shown in Figure 4.4b. For two PO_4 groups, there are three possible arrangements, which are depicted in Figure 4.4c; one of these is the pyrophosphate. In the case of three PO_4 groups, there are four ways in which they can be connected (Figure 4.4d). The linear structure, called the tripolyphosphate anion, is well known and so is the simple ring structure called trimetaphosphate anion. With more PO_4 groups a large number of possible structures can be obtained which are in the region of tetra, such as tetrametaphosphate $(MPO_3)_4$ and tetrapolyphosphate $M_6P_4O_{13}$.

For a chain of phosphate the formula is $M_{n+2}P_nO_{3n+1}$ where n is the number of phosphorus atoms. When n=0 the formula vanishes, but when n=1, the formula converts to that for the orthophosphate, M_3PO_4. For n=2, the pyrophosphate formula $M_4P_2O_7$ is obtained; for n=3 the tripolyphosphate formula, $M_5P_3O_{10}$, etc. With a large number of phosphorus atoms (n goes to infinity) the formula gives a highly polymerised metaphosphate, $M_{n+2}P_nO_{3n+1}=(MPO_3)_n$. The formula for ring shape phosphates is $M_nP_nO_{3n}$ (Figure 4.4d), which shows that such a structure can only exist at the metaphosphate composition.

4.5. STRUCTURE OF BINARY PHOSPHATE GLASSES

To understand the ways in which binary phosphate glasses, such as the rare earth phosphate glasses under study, are structured it is useful to know the structure of pure P_2O_5 glass former. Pure P_2O_5 glass is extremely hygroscopic, volatile, and colourless glass (Galeener and Mikkelsen 1979). This hygroscopic nature has limited the number of studies and made it difficult to have a good insight at its structure. Bobovich (1962) made the first structural studies of P_2O_5 glass, but these did not offer results compatible with the Raman spectrum of the glass measured by Galeener and Mikhelsen (1979). The latter study has shown that the structure of pure P_2O_5 glass consists of a three-dimensional network of corner sharing PO_4 tetrahedra (Figure 4.1). Each tetrahedra has three bridging and one nonbridging oxygen atoms consistent with the random network theory of Zachariasen (1932).

In contrast to the difficulty in preparing and handling the pure P_2O_5 glass, binary phosphate glasses ($xM_2O_3.yP_2O_5$), when the metal oxide is greater than 30mole %,

are easily prepared and handled. Numerous studies have been made of their structure and properties over the past five decades after the pioneering work of Zachariasen (1932), using X-ray diffraction, X-ray absorption spectroscopy (XAS), extended X-ray absorption fine structure (EXAFS), and Raman and IR spectroscopies. Books such as those by Van Wazer (1964) and Corbridge (1974) give extensive details concerning phosphorus and its compounds. Bues and Gehrk (1956) and Fawcett et al. (1976) used Raman spectroscopy to study a variety of phosphate glasses, in particular $La(PO_3)_3$ and $Ba(PO_3)_2$, and found these glasses to be built up from linked PO_4 tetrahedral. X-ray diffraction of some binary phosphate glasses such as the one on calcium phosphate glasses by Biscoe et al. (1941) has shown that each phosphorus atom is covalently and tetrahedrally bonded to four oxygen atoms which lie at the corners of a tetrahedron with an approximate angle of 140° for the P-O-P bond. The PO_4 tetrahedra are linked together to form the three dimensional network of the glass structure. The total number of oxygen atoms in a phosphate glass is always greater than twice the number of phosphorus atoms, and therefore for all compositions there is an appreciable number of oxygen atoms which are bonded only to one phosphorus as well as those that are bonded to two phosphorus atoms (Brady 1958, Milberg and Daly 1963).

In binary phosphates ($xM_2O.yP_2O_5$), the ratio between the metal oxide to phosphorus pentoxide is defined as $R=M_2O/P_2O_5$. For a monovalent ion modifier, R=0 corresponds to the phosphorus pentoxide and R=3 corresponds to the orthophosphate. In between these two limits the polyphosphate region can be defined as such $1 \leq R < 3$, and the metaphosphate composition as R=1. Ultraphosphate composition corresponds to $0 < R < 1$ (Van Wazer 1964). Therefore, the structure of phosphate glasses can be changed from a continuous cross-linked PO_4 tetrahedra three-dimensional network into a polymer type of PO_4 chain with a distribution of chain length, depending on the the phosphate content.

In metaphosphate glasses prepared from P_2O_5 oxide and alkali or alkaline earth oxide each phosphorus-oxygen tetrahedron is linked to two other tetrahedra, and one oxygen ion per tetrahedron is associated with a metal ion. Such glasses with the metaphosphate composition consist of long chains of PO_4 tetrahedra (Van Wazer

and Campanella 1950) linked to adjacent tetrahedra by bridging oxygen atoms; these are considered the most stable of the phosphate glasses (Van Wazer 1958, Sales et al. 1986, Mierzejewski et al. 1988). An x-ray study by Brady (1958) has shown that these metaphosphate glasses do consist of long chains of tetrahedra and increase of the amount of metal oxide produces rings of phosphate tetrahedra. The long-chain phosphate molecules in these glass are entwined in much the same way as long thin organic molecules are in polymers (Doremus 1973). The exact arrangement of the chain in metaphosphate glasses was not known until Milberg and Daly (1963) studied the x-ray scattering pattern of the $Na_2O.P_2O_5$ fibre; they have illustrated two chain configurations, namely, the straight phosphorus oxygen chain and the zig-zag chain (Figure 4.5). In the straight chain model, all the phosphorus atoms lie on the chain axis. The chain is made up of identical PO_4 tetrahedra sharing oxygen atoms at two opposite corners so that there are two non-bridging oxygen atoms on each tetrahedron. In the zig-zag chain model, all the phosphorus atoms and the bridging oxygen atoms lie on a plane passing through the chain axis with the identical PO_4 tetrahedra arranged in a zig-zag manner. The infrared spectra of vitreous metaphosphate are consistent with the number of modes available for a zig-zag chain rather than for a straight one. Evidence that such chains are probably present in vitreous metaphosphate $NaPO_3$ comes from the resemblance of its Raman spectrum to that of crystalline Maddrell's salts $NaPO_3$II which contains such chains of infinite length.

Investigation of the structure of lead phosphate glasses by Sales et al. (1986) has shown that when the the metal cation concentration is increased, non-bridging oxygen bonds are created to preserve charge balance and the PO_4 tetrahedra network breaks up. If enough metal cation is added to the glass, each fourfold coordinated phosphorus has one doubly bonded and singly bonded oxygen and two bridging oxygens to neighbouring PO_4 tetrahedra (Figure 4.6a). The chains are interconnected via somewhat weaker bonds (ionic bonds) to the metal cations. With still higher metal-to-phosphorus ratios, the average length of the phosphorus chains becomes shorter (Sales 1990) until the glass network consists primarily of isolated pyrophosphate dimers embedded in a 'sea' of metal cations (Figure 4.6b).

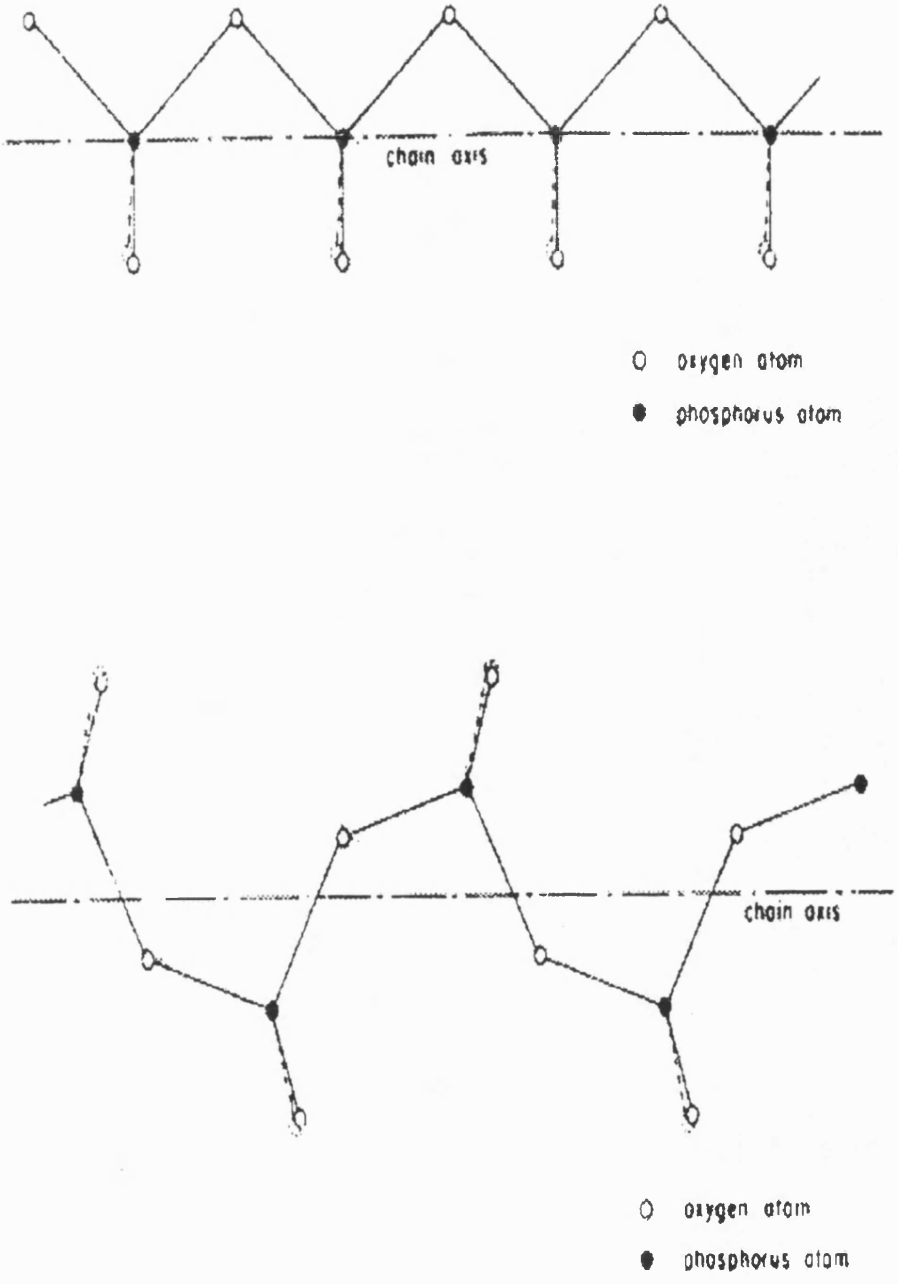

Figure 4.5. The straight chain phosphate model (above), and the zigzag chain phosphate model (after Milberg and Daly 1963).

a)

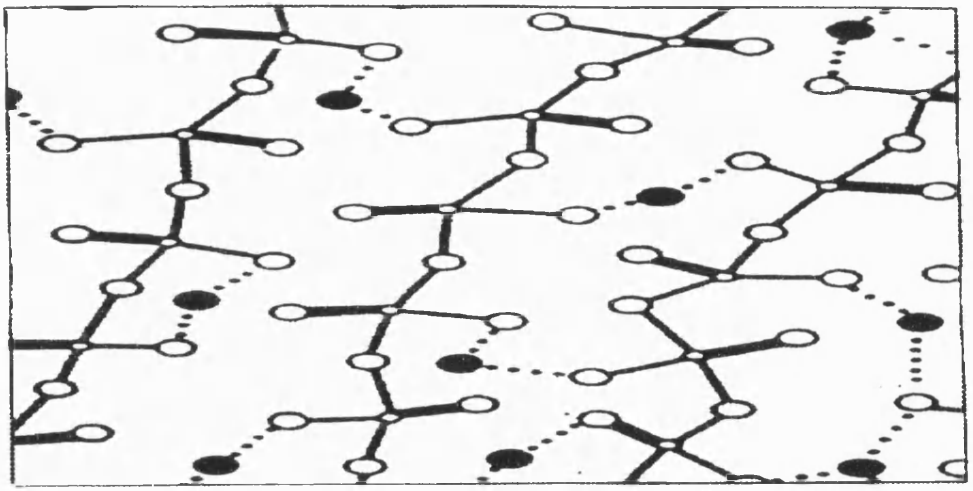

b)

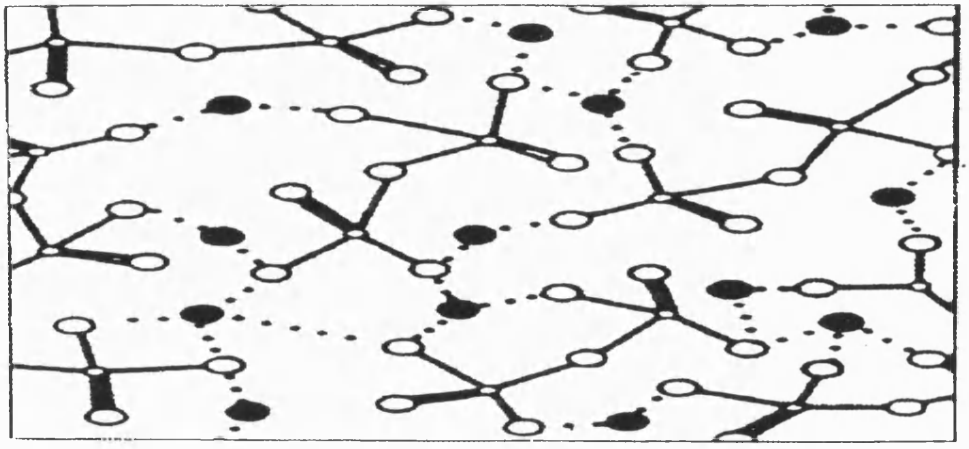

Figure 4.6. Schematic illustrations of the structures of a) lead metaphosphate glass, b) lead pyrophosphate glass (after Sales 1990).

4.6. STRUCTURAL STUDIES ON RARE EARTH METAPHOSPHATE GLASSES

Earlier atomic structural investigations of phosphate glasses were mainly focused on monovalent or divalent network modifiers (Kordes 1939, Biscoe et al. 1941, Westman 1960), and those formed from alkali oxides (Martin 1991). More recently there have been several structural studies of phosphate glasses with rare earth ions modifiers. One of the first structural studies of phosphate glasses containing the rare earth ions of Pr^{3+} and Dy^{3+}, using infrared and Raman spectroscopy was made by Sun and Risen (1986). That work suggested that these glasses have the metaphosphate composition with a dominant $(PO_3)_n$ chain. Morgan et al. (1987) have measured the Raman spectra of binary CeO_2-P_2O_5 and Pr_2O_3-P_2O_5 glasses and concluded that the rare-earth ions enter into the glass in modifying sites. They found that these praseodymium and cerium phosphate glasses are characteristic binary phosphate glasses comprised of PO_4 tetrahedra in which each phosphorus atom surrounded by four oxygen atom, one double bonded to the central phosphorus, the other three two of them connected to neibouring tetrahedra and the third connected weakly to the rare earth ions. Mierzejewski et al. (1988) have measured the Raman spectra of samarium metaphosphate glasses and found that this glass is also built up from phosphorus-oxygen tetrahedral units with covalent bonding dominating within and between the PO_4 tetrahedra. The samarium ions occupy sites between the non-bridging oxygen atoms and provide weaker ionic bonds between the strongly covalently bond chains. Using modern techniques, such as x-ray absorption fine structure (EXAFS), high performance liquid chromatography (HPLC), Mossbauer absorption and Raman scattering, it is possible to provide detailed information about the local environment around particular atoms in phosphate glasses. Martin (1991) has written a review on using these techniques for structural investigations of phosphate glasses. A recent direct structural study by Bowron et al. (1995) has employed the complementary probes EXAFS and x-ray as a probe to study the local structure of the rare earth metaphosphate glasses and has established several structural details. The EXAFS results on the metaphosphate systems modified by the rare earth oxides of Tb_2O_3, Pr_6O_{11}, Nd_2O_3, Eu_2O_3, Gd_2O_3, and Ho_2O_3 have demonstrated that the rare earth ions are incorporated into the phosphate net-

work in high coordination states typically surrounded by between six and eight oxygen atoms. This suggests that the network has a high degree of crosslinkage between the PO_4 units, mediated by the incorporated rare earth ions. This high level of crosslinkage could play a significant part in the observed increased resistance to hygroscopic attack displayed by these glasses over other phosphate systems.

Ultrasonic measurements can shad some light on glass structure connectivity using the definition of fractal dimensionality $4C_{44}/B$, where C_{44} is the longitudinal modulus and B is the bulk modulus. The fractal dimensionality of the rare earth metaphosphate glasses have been determined by Senin (1994). The values range between 2.14 to 2.79 indicating that the connectivity of these glasses tends towards having a three dimensional disordered network, suggesting the existence of crosslinks between PO_4 chains.

However, these studies on the rare earth metaphosphate glasses are not complete, and do not provide a clear picture of the structure and vibrational properties of these glasses. Therefore, the present work focuses on systematic study of the structure and optical properties of rare earth metaphosphate glasses and pentaphosphate crystals at different conditions of temperatures and pressures using Raman and fluorescence spectroscopy.

4.7. MANUFACTURING PROCEDURE FOR THE RARE EARTH METAPHOSPHATE GLASSES AND PENTAPHOSPHATE CRYSTALS

In this section a brief explanation of the process of manufacturing and concentration analysis of the rare earth metaphosphate glasses is given together with the crystal growth of the rare earth pentaphosphate crystals. The glasses were made here by our colleague Senin (1994). The crystals were made by W. Hönle and E. Schönherr from the Max-Planck-Institut für Festkörperforschung in Germany as part of a collaboration with our Physics Department.

Rare earth phosphate $(R_2O_3)_x(P_2O_5)_{1-x}$ glasses, in which the mole fraction x is close to 0.25, where R represents one of the rare earth elements Ce, Pr, Sm, Nd, Eu, Gd, Tb, Dy, and Er or La or Y have all been made. The glass samples were made from laboratory reagent 99.9% purity grades of dry phosphorus pentoxide P_2O_5 and rare

earth oxide R_2O_3. In general the preparation method for each glass is similar. Nevertheless, there are subtle differences in the manufacture due to the fact that some heavier oxides have higher melting temperatures. The melting temperature of these glasses is normally in the range 1300-1800°C - the exact temperature depending on the type of rare earth oxide used. The approximate melting temperature for each of these glasses was less than 1600 °C, except for the terbium and the holmium metaphosphate glasses which were higher (1600-1800 °C). The mixed oxides were reacted in quantities of about 50g by heating for about 1h at 500°C in a closed alumina crucible in an electric furnace. The mixture was then melted in a second furnace and held for 1h at the melting temperature appropriate for that glass (in the range 1400-1800°C). After stirring, the melt was cast into a preheated (500°C) steel split mould to make up a glass cylinder of 10mm long and 14mm in diameter. Following casting, the glass was immediately transferred to an annealing furnace at 500°C and kept there for 24h to relieve any residual stresses which would have embrittled the glass. After this the furnace was switched off and the glasses were left to cool down to room temperature, at a cooling rate of 0.5°C/min. The glass colours were dependent on the rare earth element incorporated and they showed a wide range (samarium yellow, europium pink, terbium colourless, neodymium pink, lanthanum colourless, and holmium dark salmon pink and yellow under the sun light). Samples were polished to have flat and parallel faces to within 10-3 radian and had a thickness of about 5mm, which is well suited for optical measurements.

The compositions of the rare earth metaphosphate glass samples were determined by quantitative analysis using a JEOL JXA-8600M electron probe microanalyser (EPMA) fitted with wavelength dispersive spectrometers (WDS). Pure standard samples containing rare earth elements were needed for concentration determination (the standards were EuS, $NdAl_2$, $Tb_3Fe_5O_{12}$, and Ho_3F). The microanalyser was fitted with four double-crystal spectrometers, which could be used to analyse the x-ray spectrum of the elements present in the glass. Using this technique, the electron beam could be directed at a relatively small area without destroying the sample. The chemical compositions of the glass samples are given in Table 4.1. The results of this analysis led to an interesting observation. Although the starting charges were varied from 5 to 25 mole % of R_2O_3, the compositions of the end product gla-

Table 4.1. Nominal and the analysed compositions of the manufactured rare earth metaphosphate glasses (after Senin 1994).

Sample	Nominal Composition	Analysed Composition
Samarium phosphate glass	$(Sm_2O_3)_{5.0}$ $(P_2O_5)_{95.0}$	$(Sm_2O_3)_{19.0}$ $(P_2O_5)_{81.0}$
	$(Sm_2O_3)_{10.0}$ $(P_2O_5)_{90.0}$	$(Sm_2O_3)_{19.5}$ $(P_2O_5)_{80.5}$
	$(Sm_2O_3)_{15.0}$ $(P_2O_5)_{85.0}$	$(Sm_2O_3)_{21.2}$ $(P_2O_5)_{78.8}$
	$(Sm_2O_3)_{20.0}$ $(P_2O_5)_{80.0}$	$(Sm_2O_3)_{22.4}$ $(P_2O_5)_{77.6}$
	$(Sm_2O_3)_{25.0}$ $(P_2O_5)_{75.0}$	$(Sm_2O_3)_{24.8}$ $(P_2O_5)_{75.2}$
Neodymium phosphate glass	$(Nd_2O_3)_{5.0}$ $(P_2O_5)_{95.0}$	$(Nd_2O_3)_{19.1}$ $(P_2O_5)_{80.9}$
	$(Nd_2O_3)_{10.0}$ $(P_2O_5)_{90.0}$	$(Nd_2O_3)_{19.4}$ $(P_2O_5)_{80.6}$
	$(Nd_2O_3)_{15.0}$ $(P_2O_5)_{85.0}$	$(Nd_2O_3)_{19.6}$ $(P_2O_5)_{80.4}$
	$(Nd_2O_3)_{20.0}$ $(P_2O_5)_{80.0}$	$(Nd_2O_3)_{23.4}$ $(P_2O_5)_{76.6}$
	$(Nd_2O_3)_{25.0}$ $(P_2O_5)_{75.0}$	$(Nd_2O_3)_{25.4}$ $(P_2O_5)_{74.6}$
Europium phosphate glass	$(Eu_2O_3)_{5.0}$ $(P_2O_5)_{95.0}$	$(Eu_2O_3)_{18.6}$ $(P_2O_5)_{81.4}$
	$(Eu_2O_3)_{10.0}$ $(P_2O_5)_{90.0}$	$(Eu_2O_3)_{20.0}$ $(P_2O_5)_{80.0}$
	$(Eu_2O_3)_{15.0}$ $(P_2O_5)_{85.0}$	$(Eu_2O_3)_{20.8}$ $(P_2O_5)_{79..2}$
	$(Eu_2O_3)_{20.0}$ $(P_2O_5)_{80.0}$	$(Eu_2O_3)_{21.8}$ $(P_2O_5)_{78.2}$
	$(Eu_2O_3)_{25.0}$ $(P_2O_5)_{75.0}$	$(Eu_2O_3)_{25.2}$ $(P_2O_5)_{74.8}$
Terbium phosphate glass	$(Tb_2O_3)_{5.0}$ $(P_2O_5)_{95.0}$	$(Tb_2O_3)_{26.3}$ $(P_2O_5)_{73.7}$
	$(Tb_2O_3)_{10.0}$ $(P_2O_5)_{90.0}$	$(Tb_2O_3)_{26.3}$ $(P_2O_5)_{73.7}$
	$(Tb_2O_3)_{15.0}$ $(P_2O_5)_{85.0}$	$(Tb_2O_3)_{22.6}$ $(P_2O_5)_{77.4}$
	$(Tb_2O_3)_{20.0}$ $(P_2O_5)_{80.0}$	$(Tb_2O_3)_{24.7}$ $(P_2O_5)_{73.3}$
	$(Tb_2O_3)_{25.0}$ $(P_2O_5)_{75.0}$	$(Tb_2O_3)_{27.1}$ $(P_2O_5)_{72.9}$
Holmium phosphate glass	$(Ho_2O_3)_{5.0}$ $(P_2O_5)_{95.0}$	$(Ho_2O_3)_{20.8}$ $(P_2O_5)_{79.2}$
	$(Ho_2O_3)_{7.5}$ $(P_2O_5)_{92.5}$	$(Ho_2O_3)_{22.0}$ $(P_2O_5)_{88.0}$
	$(Ho_2O_3)_{10.0}$ $(P_2O_5)_{90.0}$	$(Ho_2O_3)_{23.1}$ $(P_2O_5)_{76.9}$
Lanthanum phosphate glass	$(La_2O_3)_{10.0}$ $(P_2O_5)_{90.0}$	$(La_2O_3)_{22.2}$ $(P_2O_5)_{77.8}$
	$(La_2O_3)_{15.0}$ $(P_2O_5)_{85.0}$	$(La_2O_3)_{26.3}$ $(P_2O_5)_{73.7}$
	$(La_2O_3)_{20.0}$ $(P_2O_5)_{80.0}$	$(La_2O_3)_{26.5}$ $(P_2O_5)_{73.5}$
	$(La_2O_3)_{25.0}$ $(P_2O_5)_{75.0}$	$(La_2O_3)_{26.6}$ $(P_2O_5)_{73.3}$

sses each turned out to be similar, quite close to $(R_2O_3)_{0.25}(P_2O_5)_{0.75}$ - which corresponds to the metaphosphate $R(PO_3)_3$. This suggests that the metaphosphate is much the most stable composition in the phosphate glass systems modified by a high concentration of rare earth.

The rare earth pentaphosphate crystals have the formula RP_5O_{14},where R represents the rare earth element. They were grown from a H_3PO_4-R_2O_3 solution in a vitreous graphite crucible (Danielmeyer et al. 1972). The rare earth oxide powder was (R_2O_3) added to about 200g 85%H_3PO_4 acid in a weight proportion of $7.81x10^{-3}$. The crucible was covered with a vitreous graphite plate. The mixture was slowly heated to 500°C at a constant rate of 8.3°C/h in air. At 500°C rhombically shaped crystals of RP_5O_{14} appeared within 700hrs on the crucible walls. When small crystals of about 1mm in length were used as seed, large crystals up to 7mm in length and 2mm in thickness could be obtained. The seed crystals were inserted in the hot solution after the reach of 500°C. The crystals were isolated by decanting the hot acid.

CHAPTER FIVE

THE EFFECTS OF TEMPERATURE AND PRESSURE ON THE FLUORESCENCE SPECTRA OF EUROPIUM METAPHOSPHATE GLASS AND EUROPIUM PENTAPHOSPHATE CRYSTAL

5.1. INTRODUCTION

Fluorescence spectral measurement of glasses and crystals can provide information about energy levels, valency, and local symmetry of ions incorporated in their matrices. For glasses the short range environment around the incorporated ion approximates the environment which exists in crystals of the same composition (Prins 1965). Therefore, analysis of the fluorescence spectrum of europium metaphosphate glassis assisted by a study the fluorescence spectrum of europium pentaphosphate crystal (EuP_5O_{14}), which is also based on the structural phosphate unit (PO_4 tetrahedra).

Glasses containing Eu^{3+} ions are amongst those which can exhibit enduring photo-induced property changes, a particularly interesting and useful feature. Persistent, but erasable, modifications of refractive index have been induced in Eu^{3+} and Pr^{3+}-doped multicomponent oxide glasses subsequent to resonant excitation of certain 4f-4f transitions (Durville et al. 1986, Behrens et al. 1986, 1989, 1990, French et al. 1991). Permanent refractive index grating formation has been observed in a rare earth phosphate glass of composition $(Eu_2O_3)_{0.125}(La_2O_3)_{0.125}(P_2O_5)_{0.75}$ at 300K following excitation of the $^5D_2$ state of Eu^{3+}, using four wave mixing; a transient grating effect was also found in $(Eu_2O_3)_{0.167}(P_2O_5)_{0.835}$ (Broer et al. 1992). It has been suggested that a light-induced reordering of the ligand ions surrounding the rare earth ion, mediated by high energy phonons created during the nonradiative relaxation of the excited state, may be responsible for the permanent change in refractive index. A double-minimum potential well model including two possible configurations in the local environment of the Eu^{3+} ions in which the phonons induce transi-

tions between the two wells was used to account for the effects (Behrens et al. 1989). These observations have prompted the present study of the optical spectra of europium metaphosphate glasses.

Ultrasonic studies have shown that the europium phosphate glass exhibit anomalous elastic behaviour as a function of temperature and pressure. The hydrostatic pressure derivatives $(\partial C_{11}/\partial P)_{T,P=0}$ and $(\partial C_{44}/\partial P)_{T,P=0}$ are negative: the long-wavelength acoustic modes soften under pressure. This glass becomes easier to squeeze when subjected to high pressure (Farok et al.1994). In marked contrast, lanthanum phosphate glasses show normal elastic response to pressure (Sidek et al. 1988). The question arises: what is the origin of such anomalous elastic behaviour under pressure which is shown by the europium phosphate glass? The complete difference between the elastic behaviours of europium and lanthanum phosphate glasses under pressure, and as a function of temperature, is not likely to be due to gross structural dissimilarities. This conclusion is based upon the similarities of their Raman spectra which will be analysed in chapter 9. There have been several possible explanations (Mierzejewski et al. 1988, Sidek et al. 1993) for the physical origins of the anomalous negative values obtained for the hydrostatic pressure derivatives. One suggestion was that pressure varying, volume sensitive, mixed valence of the europium ion could produce the differences between the ultrasonic properties of the europium and lanthanum phosphate glasses. Europium can enter a host in either its divalent ($4f^7$) or trivalent ($4f^6$) state, making it necessary to ascertain its valence state. This has been achieved here by measuring the optical absorption and fluorescence and comparing them with the spectra reported for divalent (Freed and Katcoff 1948) and trivalent europium ions in various hosts.

Europium pentaphosphate crystal has a monoclinic structure with four EuP_5O_{14} molecules per unit cell. The x-ray diffraction of this crystal by Beucher (1970) shows that the unit cell has the dimensions: a=12.95Å b=8.930Å c=8.751Å and β=90.45°. Spectral measurements made by Brecher (1974) showed that this crystal possesses intense fluorescence and interesting optical properties. The present spectral study of this crystal differs from that by Brecher in two respects. First, it has been achieved using an argon ion laser as an excitation source for the fluores-

cence spectrum, while the previous study was made using xenon arc lamp for the excitation purpose. Secondly, in the present study the crystal temperature was lowered to 10K, whereas previously it was down to 77K.

In this chapter the absorption and the fluorescence spectra of europium ion incorporated into the phosphate glass will be presented. The fluorescence measurements were taken at different temperatures (in the range 300-10K) and different pressures (1bar-50Kbar). Temperature and pressure effects, on the fluorescence spectrum of monocrystalline europium pentaphosphate crystal (EuP_5O_{14}) were also measured in the same ranges. The aims are to find the energy levels and the valence of the europium ion in these glasses and crystal and also to identify the local symmetry around the ion. To investigate the existence of any valency variation and phase transition under pressure, the diamond anvil pressure cell was used to generate pressures up to 50Kbar on the europium phosphate glass and the europium pentaphosphate crystal. It is necessary to note that there is a considerable difference between the acquired pressure data on the glass, using the ultrasonic technique and the ones by the DAC technique. The former provides information about the macroscopic properties of the glass; ultrasound waves have long wavelengths which measure large scale effects. The latter gives microscopic information related to the effect of local environment on the fluorescence of the rare earth ion in the glass.

5.2. RARE EARTH ION ENERGY LEVELS AND LASER INDUCED FLUORESCENCE LINE NARROWING

Before proceeding to the experimental results of the rare earth phosphate glasses and pentaphosphate crystals, it is necessary to describe the energy level scheme of the free rare earth ions and the effect of crystal field on such ions when incorporated in glassy or crystalline materials. Free ions possess spherical symmetry with each energy level having (2J + 1) fold degenerate. Placing an ion in a crystal leads to the destruction of the spherical symmetry and each level splits under the influence of the electric field produced by the environment. The electric crystal field produces a 'Stark Effect' which splits all levels in to a maximum of (2J + 1) components for an even number of electrons and (J + 1/2) components for an odd number. The number and spacing of the energy level components depends on the type of symmetry

and intensity of the crystal field. In most cases the total splitting of an energy level is of the order of a few hundred cm^{-1}, in general small compared to the spacing between adjacent multiplet components (Rice and DeShazer 1969).

For rare earth ions incorporated in glasses and crystals, it is reasonable to believe that the crystal field of the surrounding ions has no great effect on them. This is due to the shielding effect of the outer electrons, the outermost electrons of these ions form a complete rare gas shell, which is the xenon shell with two 5s and six 5p electrons. This shell is optically inactive and next inside the xenon shell is the 4f shell, which is filled successively in passing from one element to the next. Trivalent cerium, Ce^{3+}, has one 4f electron, and trivalent ytterbium, Yb^{3+}, has 13. As long as the 4f shell is not completely filled with 14 electrons, a number of 4f levels are unoccupied, and electrons already present in the 4f shell can be raised by light absorption into these empty levels. The sharp lines observed in rare earth absorption and fluorescence spectra are ascribed to these transitions, and the sharpness of the lines is explained by the fact the electrons making the transition lie inside the xenon shell and thus interact only weakly with outside ions. The energy level scheme for the free trivalent rare earth ions has been calculated by Dieke and Crosswhite (1963). The energy level arrangements for each of all free rare earth ions is shown in Figure 5.1.

Rare earth ions usually exist in solids in either the trivalent or the divalent state. A divalent rare earth ion is formed when the atom gives up its outermost 6s electrons. When a trivalent ion is formed, the atom loses its 5d electron if it has one; otherwise, one of the 4f electrons is lost. Absorption and fluorescence spectral measurements of Re^{3+} ion in glasses and crystals allow the determination of the energy levels of these ions. In general, the spectrum of the crystals show extremely fine lines, even at high temperatures, indicating a weak interaction between the Re^{3+} ions while the spectrum of the glasses show broader bands due to the randomness of the structure.

To study the optical transitions between energy levels of ions incorporated in glasses and crystals, the laser induced fluorescent line narrowing (FLN) technique has been proved to be a useful tool and especially in studying spectral diffusion in

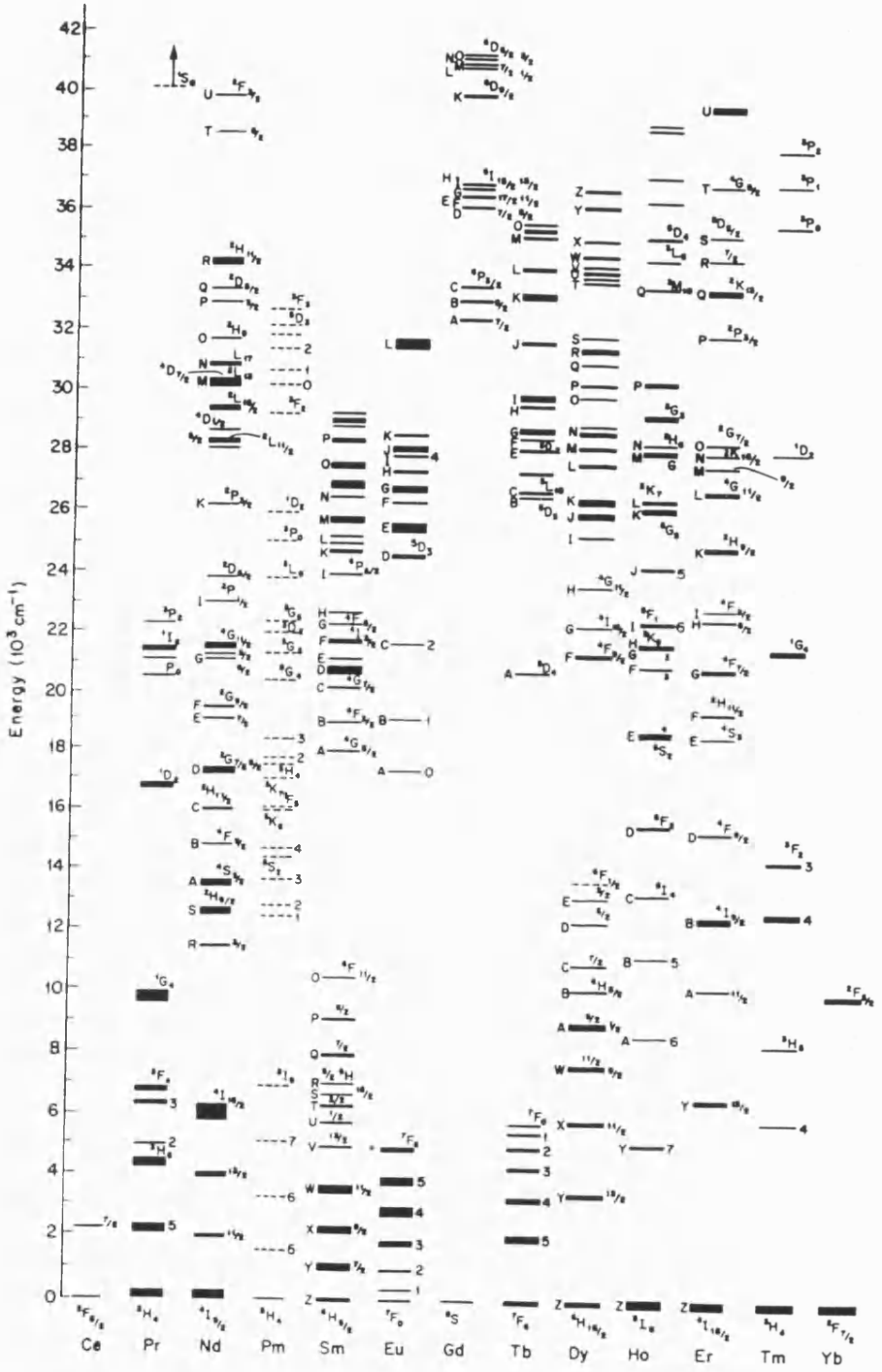

Figure 5.1. The observed multiplet energy levels of the rare earth ions in $LaCl_3$ (after Dieke 1969).

glasses. This technique, which was first applied by Szabo in ruby (1970, 1971), takes advantage of the narrow line width of a laser source to excite a selected narrow energy band within the spectral profile of an inhomogeneously broadened system. If the energy transfer processes leading to diffusion of the excitation throughout the spectral line are slow compared with the fluorescent lifetime of the emitting levels, then only the ions that are within the narrow range that is excited will participate in the emission. Thus, the fluorescence can be observed under resolution limited by the width of the exciting laser or by the homogeneous width of the absorption, whichever is greater (Riseberg 1972).

The preferred ions for FLN studies will have intrinsically sharp pure electronic absorption and luminescent transitions, easily accessible with conventional laser systems. Trivalent rare earth ions have the attraction of possessing a large number of sharp pure-electronic transitions. Further, since the optically active 4f electrons are shielded by the outer 5s and 5p shells of electrons, these rare earth ions are not very sensitive to the electrostatic crystal fields of the neighbouring ions and the inhomogeneous broadening in glasses is often not excessive. It is not surprising, therefore, attention has been intensely directed to investigate glasses doped with rare earth ions (Imbusch 1987).

Despite the absence of long range symmetry, the immediate vicinity of all rare earth ions does not vary significantly from one site to another and all sites have a definite microsymmetry. Hence, the optical properties of rare earths in glasses may be analysed in a manner similar to that of impurities in crystals, the principle difference being that the disorder will introduce pertubative effects into these properties e.g. inhomogeneous broadening (Reisfeld 1973).

The site symmetry of a rare earth ion in glassy material or crystalline can be deduced by the methods of group theory from the number of fluorescence lines in spectrum into which the free ion levels are split. Bethe (1929) determined the number of levels produced by crystal field splitting from a given level of a free ion. Runciman (1956) classified the 32 crystallographic point groups into four headings: cubic, hexagonal (including the hexagonal and rhombohederal systems), tetragonal, lower symmetry (including orthorhombic, monoclinic and triclinic). Therefore,

fluorescence studies can be used to relate the local symmetry of the rare earth ions in the crystalline and glass matrices to the Runciman classification.

5.3. LOW TEMPERATURE EFFECTS ON THE FLUORESCENCE SPECTRUM OF EUROPIUM METAPHOSPHATE GLASS

The optical absorption spectrum of europium ion, introduced into phosphate glass, was measured using a standard commercial double-beam instrument. Figure 5.2 shows the absorption spectrum in the range (200nm-620nm) of a glass having the composition $(Eu_2O_3)_{0.186}(P_2O_5)_{0.814}$ at room temperature. The absorption band peaks are compared in Table 5.1 with known data for the Eu^{3+} ion (Capobianco et al. 1990). The band peaks reported for Eu^{3+} ion (column 2) correspond to transitions from the $^7F_0$ ground state and the thermally populated $^7F_1$ to the excited states belonging to the $4f^6$ configuration (column 3). The agreement between the spectral wavelengths (columns 1 and 2) establishes that the bands observed for the $(Eu_2O_3)_{0.186}(P_2O_5)_{0.814}$ glass are typical of Eu^{3+} ion. The absorption bands are sharp; this is usual for those observed for Eu^{3+} and other rare earth trivalent ions, a characteristic of the small influence of the crystal field on the deep 4f states (McClure and Kiss 1963). Below 400nm there is strong increase in the background absorption due to the existence of very dense energy levels in this spectral region (DeShazer and Dieke 1963). This severely limits the resolution of the absorption bands below about 300nm.

The fluorescence spectrum of europium phosphate glass was measured using the optical system, described in section 9.4, by utilising the 5145Å green line of the argon ion laser as an excitation source. The laser power used was varied from 50 to 200mW depending on the resultant fluorescence intensity in the specified spectral region. The scattered fluorescence at 90° to the laser beam was collected and focused into the triple grating monochromator with slitwidths set to 150μ resulting in 0.45Å resolution. Figures 5.3a and b show the fluorescence spectrum of $(Eu_2O_3)_{0.186}(P_2O_5)_{0.814}$, measured at 300K, overlapped on that obtained at 10K; both spectra are similar but the 10K spectrum is thermally broadened. The fluorescence peaks measured at 10K are compared in Table 5.2 with fluorescence lines of Eu^{3+}

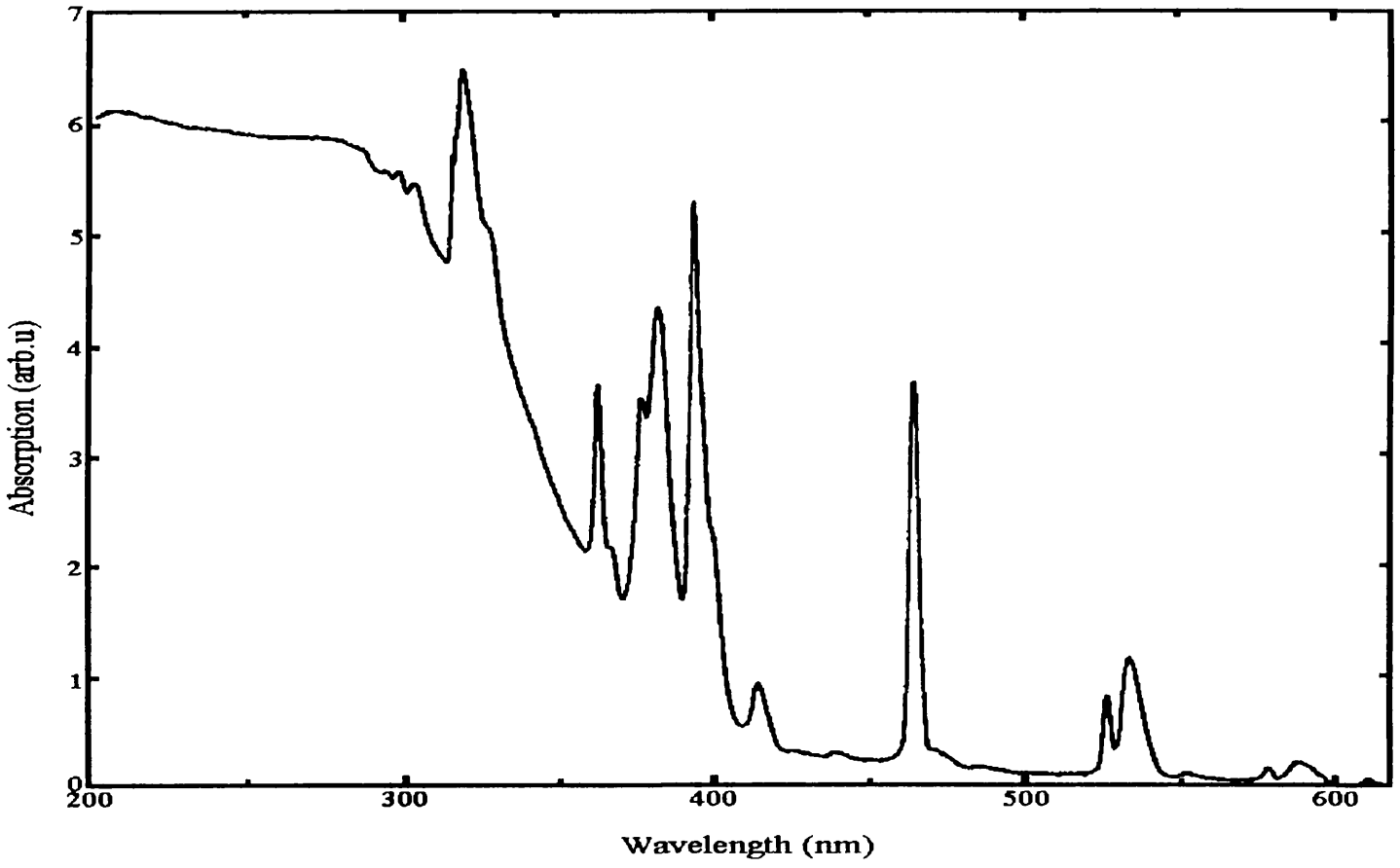

Figure 5.2. Absorption spectrum of $(Eu_2O_3)_{0.186}(P_2O_5)_{0.814}$ glass measured at room temperature.

Table 5.1. Measured wavelengths of the absorption bands at room temperature of $(Eu_2O_3)_{0.186}(P_2O_5)_{0.814}$ glass compared with the wavelengths of the absorption bands of Eu^{3+} ion given by Capobianco et al. (1990). The transitions which are responsible for these absorption are quoted from DeShazer and Dieke (1963).

Wavelength (nm) $(Eu_2O_3)_{0.186}(P_2O_5)_{0.814}$ glass	Wavelength (nm)	Transition
610	-	$^5D_0 \leftarrow {}^7F_2$
588	-	$^5D_0 \leftarrow {}^7F_1$
578	577.5	$^5D_0 \leftarrow {}^7F_0$
534	531.9	$^5D_1 \leftarrow {}^7F_1$
527	526.0	$^5D_1 \leftarrow {}^7F_0$
465	464.5	$^5D_2 \leftarrow {}^7F_0$
415	414.5	$^5D_3 \leftarrow {}^7F_0$
400	399.5	$^5L_6 \leftarrow {}^7F_1$
394	393.4	$^5L_6 \leftarrow {}^7F_0$
382	381.9	$^5L_7 \leftarrow {}^7F_1$
377	378.9	$^5G_2 \leftarrow {}^7F_1$
368	375.2	$^5G_4 \leftarrow {}^7F_0$
363	362.0	$^5D_4 \leftarrow {}^7F_0$
328	-	-
320	-	-

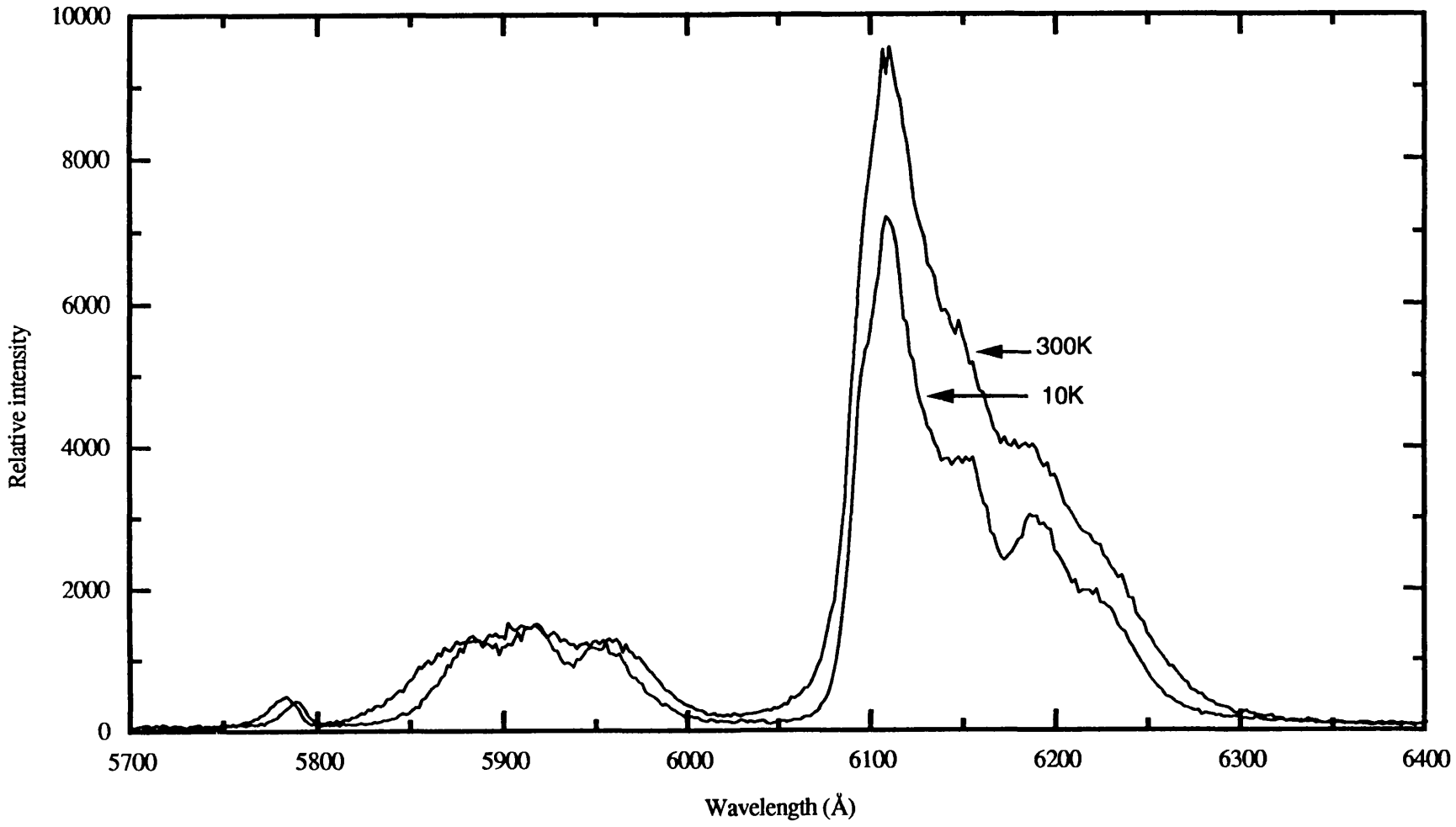

Figure 5.3a. Fluorescence spectrum of a $(Eu_2O_3)_{0.186}(P_2O_5)_{0.814}$ glass at 10 and 300K excited using the green 5145Å argon ion laser line.

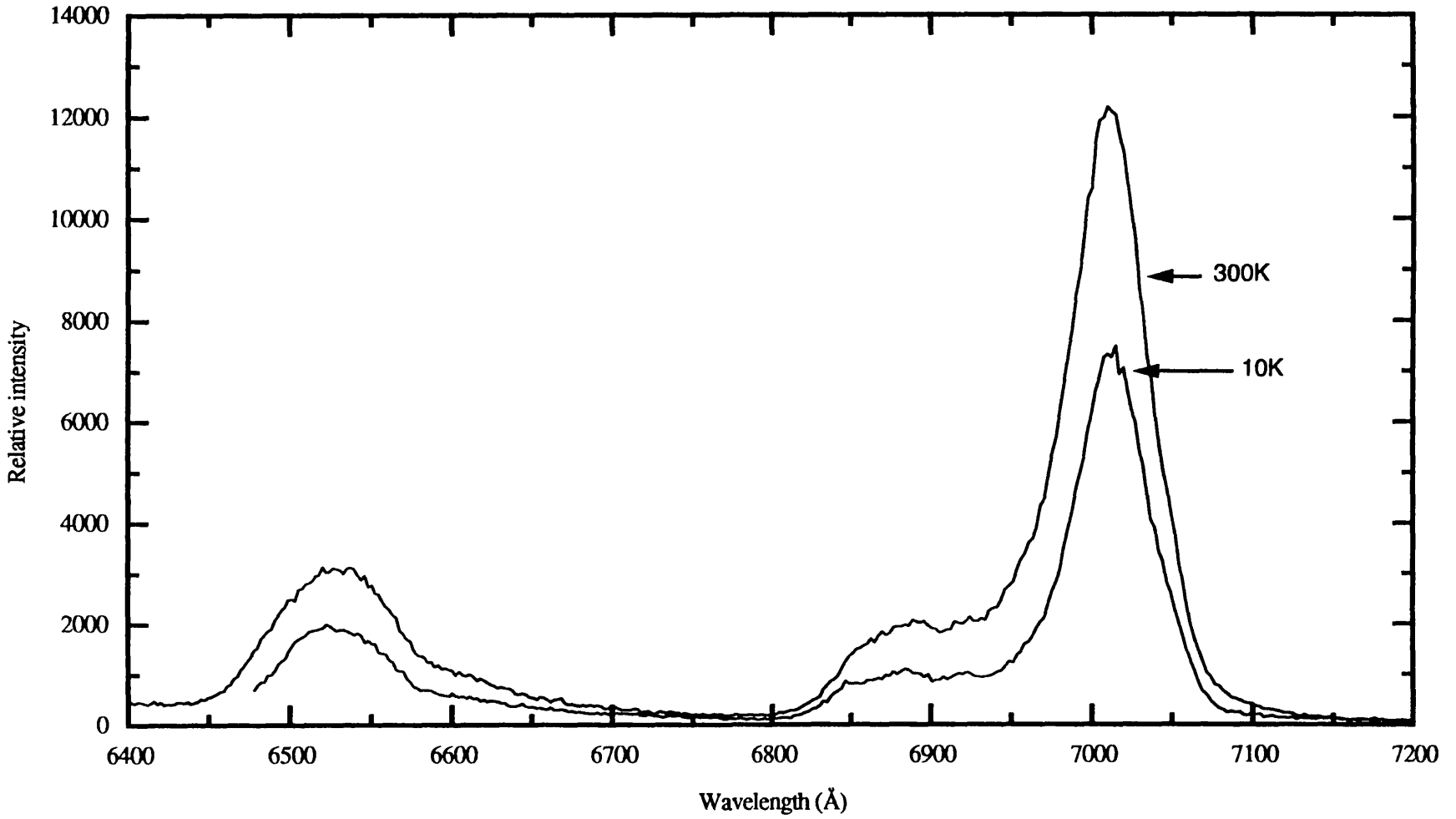

Figure 5.3b. Fluorescence spectrum of a $(Eu_2O_3)_{0.186}(P_2O_5)_{0.814}$ glass at 10 and 300K excited using the green 5145Å argon ion laser line.

Table 5.2. Measured wavelengths of the fluorescence band peaks of $(Eu_2O_3)_{0.186}(P_2O_5)_{0.814}$ glass at temperature of 10K compared with the wavelengths of the fluorescence lines of Eu^{3+} ion given by (Brecher 1974). The transitions which are responsible for these fluorescence are quoted from the same reference.

Wavelength (Å) $(Eu_2O_3)_{0.186}(P_2O_5)_{0.814}$ glass	Wavelength (Å)	Transition
5788	5784	$^5D_0 \rightarrow {}^7F_0$
5883	5876	$^5D_0 \rightarrow {}^7F_1$
5914	5918	
5951	5947	
6110	6116	$^5D_0 \rightarrow {}^7F_2$
6147	6124	
6185	6166	
	6176	
	6208	
6521	6485	$^5D_0 \rightarrow {}^7F_3$
	6488	
	6494	
	6506	
	6510	
	6533	
	6546	
7013	6872	$^5D_0 \rightarrow {}^7F_4$
	6899	
	6907	
	6923	
	6935	
	6985	
	6988	
	7002	
	7018	

ion given by Brecher (1974). The close similarity between the two sets of data confirms that this glass contains trivalent europium ions.

A central aim has been to find out if these glasses contain Eu^{2+} in addition to Eu^{3+}. This can be done by comparing the fluorescence spectrum with that of a material containing a known europium valence state (Table 5.2). For example, the fluorescence of europium doped $CaSO_4$ consists of a broad band at 3850Å with full width at half maximum of 200Å and another group of three sharp lines at 5970, 6250, and 7000Å; the emission in the first group is attributed to Eu^{2+} and the remainder to Eu^{3+} (Bapat 1977). To find a band in the region of 3850Å in the glass, it was necessary to excite it using an ultra-violet line. To do this, the experiments were made using the 2600Å line in a fluorometer in a 90° configuration. An ultra-violet absorbing filter (Ealing OY10) was used to block all the ultra-violet below 3000Å from passing on to the grating so as to prevent any interference between the resulting spectrum of the glass and the excitation line. The fluorescence obtained at 45° from the surface of the $(Eu_2O_3)_{0.186}(P_2O_5)_{0.814}$ glass excited using the 2600Å ultra-violet line is shown in Figure 5.4. Two distinct spectral regions can be seen. The first one comprises two sharp bands around 6000Å, which comparison with the spectral data of Bapat (1977) shows can definitively be attributed to the Eu^{3+} ion fluorescence, although they are not resolved into their components since the resolution of the grating is too low and also the ultra-violet exciting line is broad (unlike the laser line). The second spectral region comprises overlapped bands from 3500Å to 5500Å; however these are not due to Eu^{2+} ions. This overlapped band originates from the absorption bands (Figure 5.2) of the Eu^{3+} acting as fluorescence bands. This band is not obtainable in the 90° configuration; in this configuration, when the Eu^{3+} bands are excited, any fluorescence obtained from the absorption bands in the range 3500 to 5500Å is low in intensity and is reabsorbed by Eu^{3+} ions. It is important to note that, as a result of the allowed transition $4f^7 \rightarrow 4f^6 5d$ (KishanKumar et al. 1989), the absorption bands of the Eu^{2+} ions around 232.7, 322 and 288.5nm (Runciman 1958) are two orders of magnitude stronger than those of the Eu^{3+} ions, yet they are not shown in the absorption spectrum (Figure 5.2): it can be deduced that the content of Eu^{2+} ions is minimal.

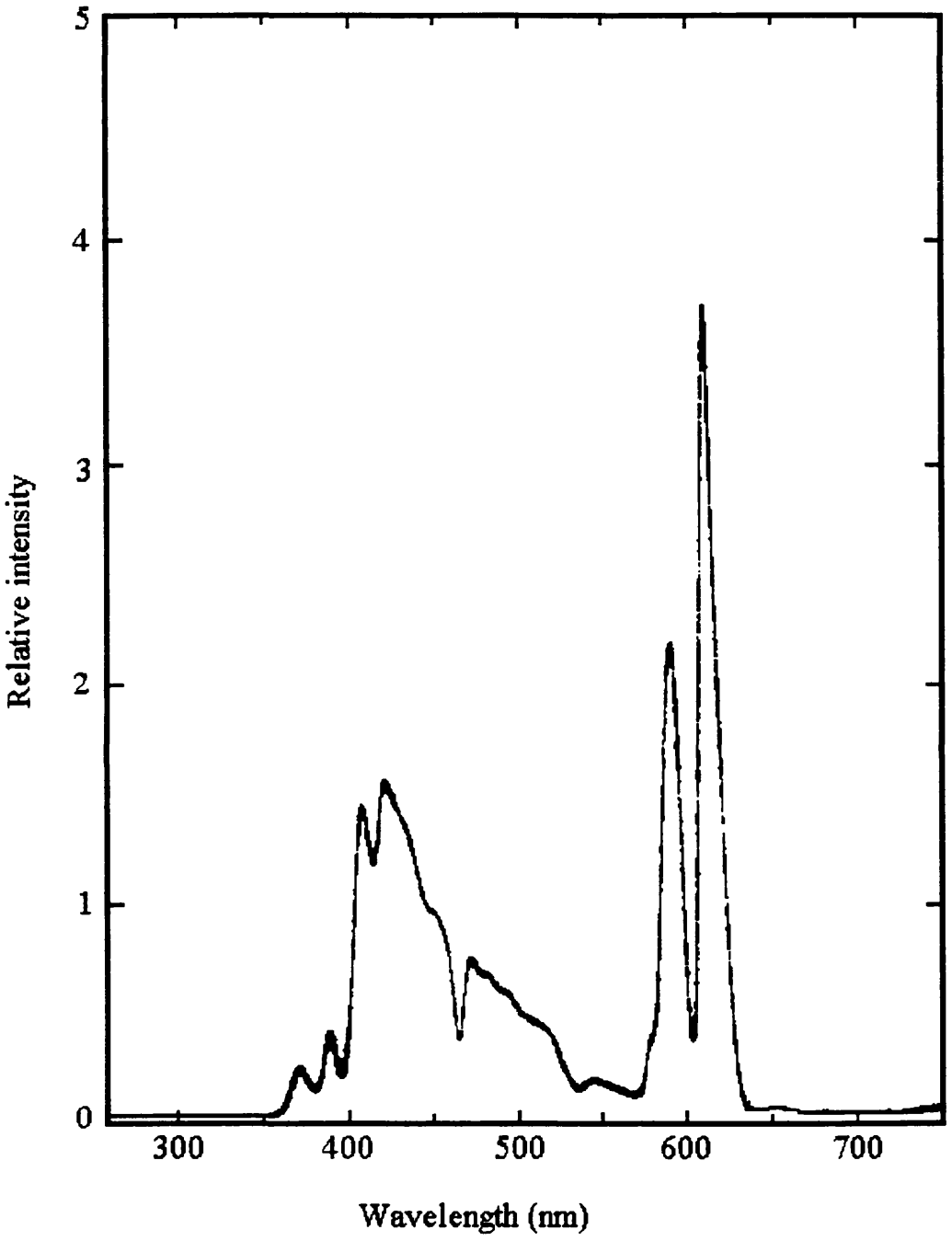

Figure 5.4. The fluoresence spectrum of a $(Eu_2O_3)_{0.186}(P_2O_5)_{0.814}$ glass at room temperature excited using the ultraviolet 260nm line. The fluorescence has been collected at 45^0 configuration from the surface of the glass.

The first peak in the fluorescence spectrum of the $(Eu_2O_3)_{0.186}(P_2O_5)_{0.814}$ glass at 10K (Figure 5.3a) is attributed to the transition $^5D_0 \rightarrow {}^7F_0$ in Eu^{3+} ion. This transition is a singlet because the $^7F_0$ level is nondegenerate (J=0). Trial fits to this peak has been made using a Gaussian fitting software (Origin version 4). A good fit could only be achieved using two Gaussian peaks (Figure 5.5) rather than one (Figure 5.6). The wavelengths obtained from this two Gaussian fit are 5780.73 and 5789.16Å, corresponding to a small energy difference of $\Delta E = 0.00312eV$. The $^5D_0 \rightarrow {}^7F_1$ transition of this glass at 10K has been fitted in the same way. However this transition consists of three peaks (Table 5.2 and Figure 5.3a). In this case six Gaussian distributions are needed (Figure 5.7), rather than three (Figure 5.8), to provide a good fit. The wavelength values of the peaks of the six fitted Gaussians are 5871.97, 5887.53, 5906.49, 5918.54, 5941.34 and 5959.98Å. The difference in wavelengths between the first two of these peaks corresponds to an energy difference of $\Delta E = 0.0055eV$; that between the third and the fourth Gaussians results in an energy difference of $\Delta E = 0.0042eV$ and between the fifth and the sixth Gaussians to $\Delta E = 0.0065eV$. The same procedure has been applied to the transition $^5D_0 \rightarrow {}^7F_2$, which consists of five peaks. Now the best fit has been obtained with ten Gaussian distributions. The presence of two peaks instead of one in the transition $^5D_0 \rightarrow {}^7F_0$ (in spite of it being a singlet) and six rather than three for $^5D_0 \rightarrow {}^7F_1$ and ten peaks instead of five for $^5D_0 \rightarrow {}^7F_2$ suggests the Eu ions are sited in two different low symmetry environments at least, which are shifted from each other by an energy difference of approximately $\Delta E = 0.00312eV$, taken because the fit to the singlet transition (J=0) is the most reliable. Trials to fit the $^5D_0 \rightarrow {}^7F_0$ transition to more than two Gaussian (3,4,5 peaks) and the $^5D_0 \rightarrow {}^7F_1$ transition to more than six (9,12 peaks) resulted, in some cases, in better fits. But these fits based upon choosing Gaussian components with linewidth of less than 10Å; such linewidths are rather sharp to be used for fluorescence bands of glasses which are normally broad.

5.4. LOW TEMPERATURE EFFECTS ON THE FLUORESCENCE SPECTRUM OF EUROPIUM PENTAPHOSPHATE EuP_5O_{14} CRYSTAL

The fluorescence spectrum of a europium pentaphosphate crystal having the formula EuP_5O_{14} was measured at 300 and 12K temperatures in the wavelength range 5700-7200Å. The spectral measurements were obtained using the 4880Å argon ion

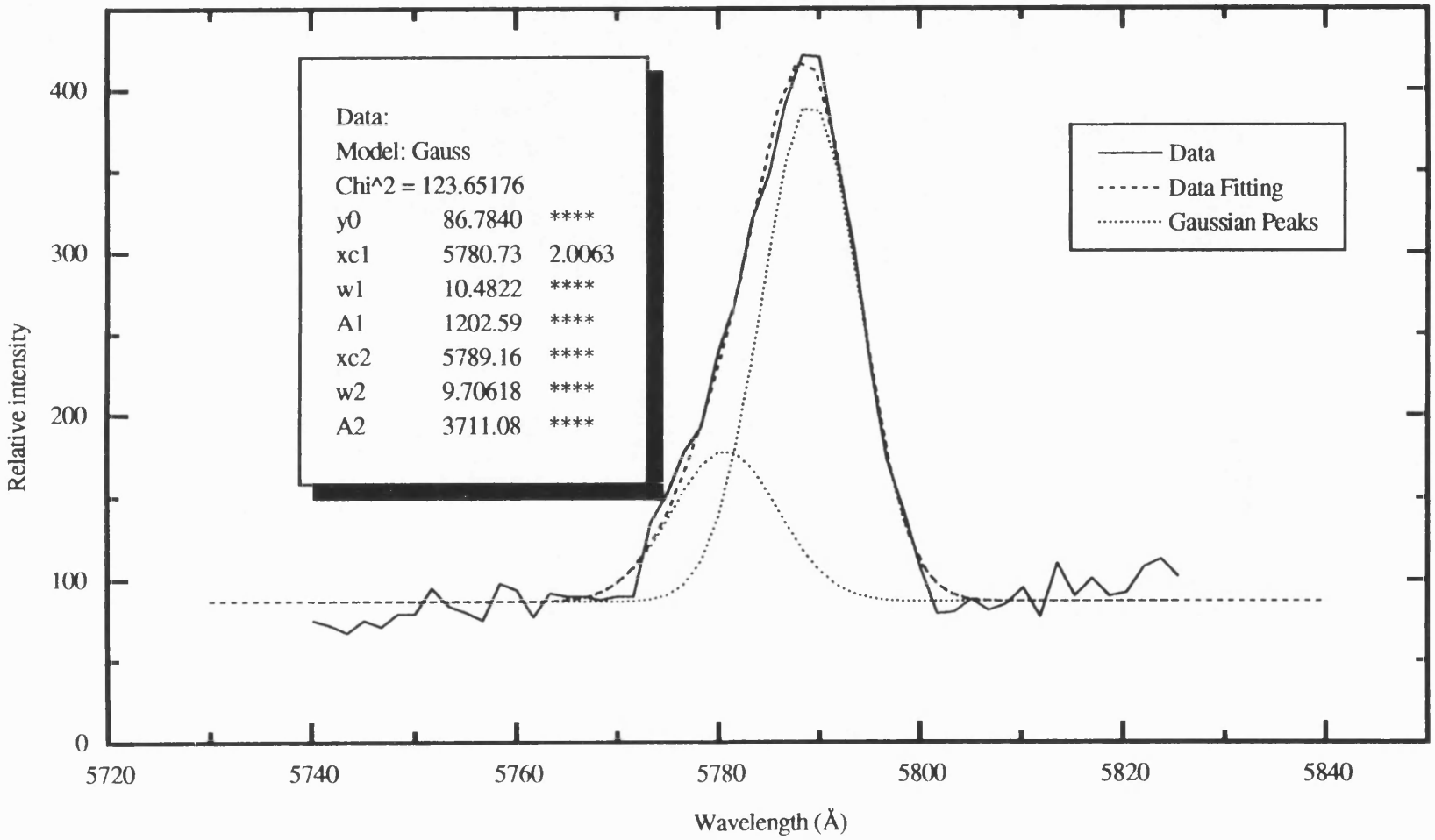

Figure 5.5. The $^5D_0 \rightarrow {}^7F_0$ transition of $(Eu_2O_3)_{0.186}(P_2O_5)_{0.814}$ glass at 10K fitted by two Gaussian distributions ($(\chi^2=123.6$).

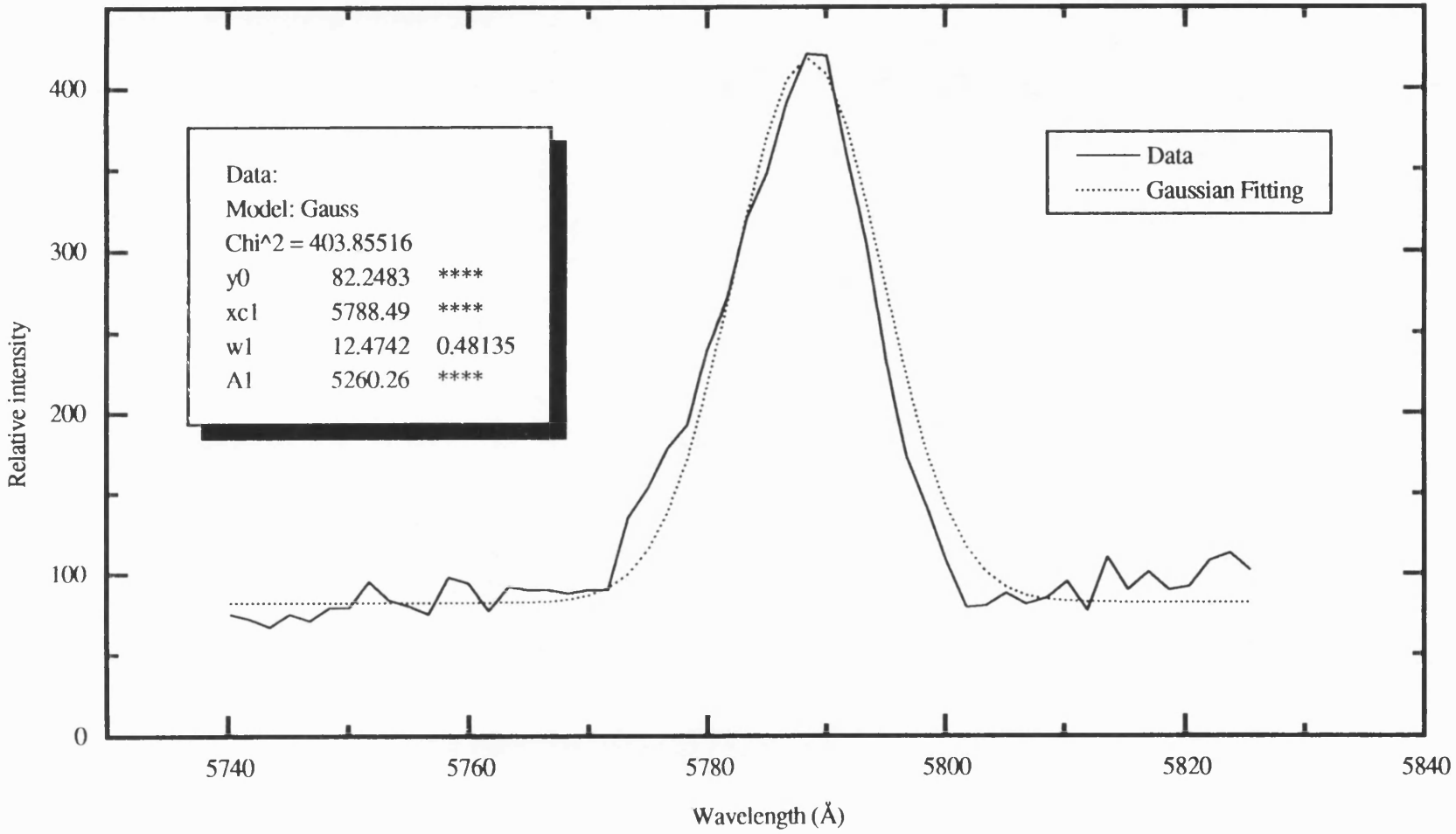

Figure 5.6 . The $^5D_0 \rightarrow {}^7F_0$ transition of $(Eu_2O_3)_{0.186}(P_2O_5)_{0.814}$ glass at 10K fitted by a single Gaussian distribution (χ^2= 403.8).

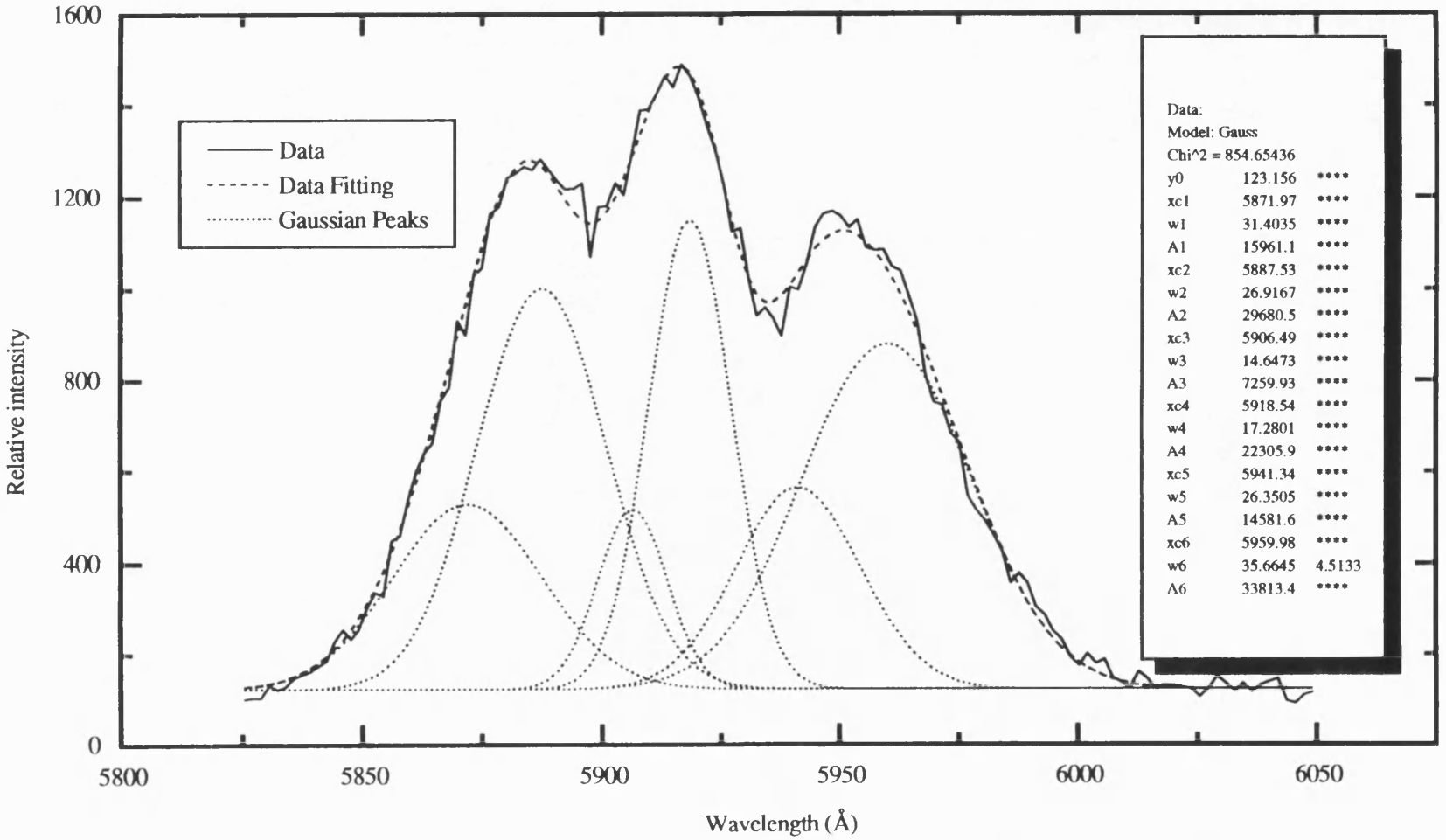

Figure 5.7. The $^5D_0 \rightarrow {}^7F_1$ transition of $(Eu_2O_3)_{0.186}(P_2O_5)_{0.814}$ glass at 10K fitted by six Gaussian distributions ((χ^2= 854.6).

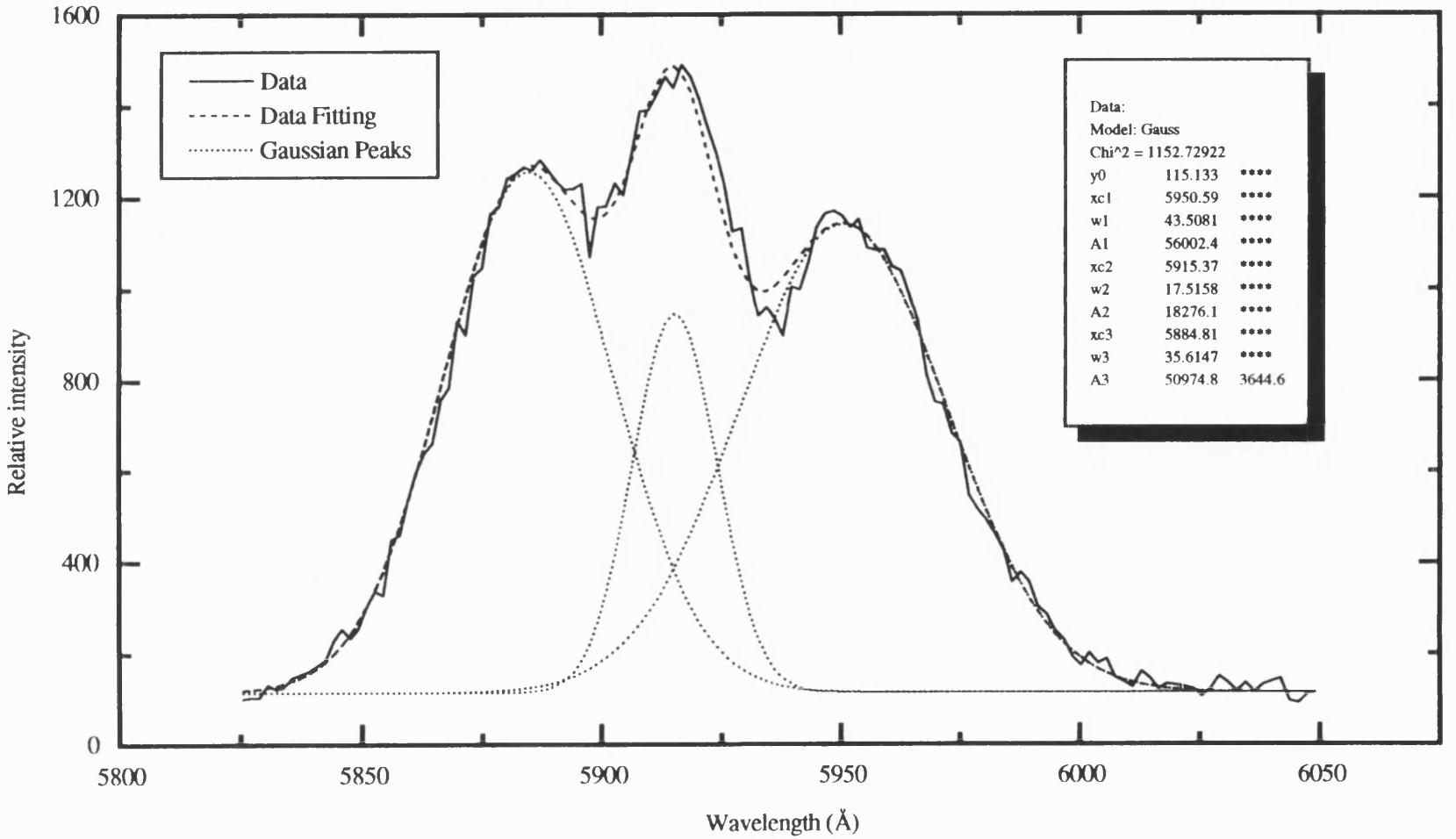

Figure 5.8 . The $^5D_0 \rightarrow {}^7F_1$ transition of $(Eu_2O_3)_{0.186}(P_2O_5)_{0.814}$ glass at 10K fitted by three Gaussian distributions (χ^2=1152.7).

laser line. The fluorescence spectrum at 300K was obtained using $2cm^{-1}$ per second scanning steps, 200μ slit widths and 30mW laser power. Due to sharp fluorescence lines of the spectrum found for the crystal at 12K, the experimental conditions were changed to $1cm^{-1}$ per second scanning steps, 100μ slit widths and 250mW laser power. Figures 5.9a and b show the normalised fluorescence spectrum of the EuP_5O_{14} crystal recorded at 300K overlapped on the spectrum measured at 12K. The spectrum measured at 300K shows that the fluorescence lines are sharp and well defined; at 12K but they are even sharper (less than 1Å linewidth in some of the fluorescence lines). The sharpness of the fluorescence lines is consistent with a weak interaction between the Eu ions and the surroundings, in spite of high Eu ion concentration (this behaviour is normally attributed to the shielding effect of the 4f electrons in rare earths). The fluorescence spectrum (Figure 5.9a,b) consists of five well separated main bands with each band resolved into a group of sharp fluorescence lines. The locations of the fluorescence lines are listed in Table 5.3 for both temperatures, together with some of their half linewidths, and compared with the listing reported by Brecher (1974). The comparison shows that these lines are typical of the fluorescence of trivalent europium ion (Eu^{3+}).

To identify the local symmetry around the Eu^{3+} ion in the EuP_5O_{14} crystal the same procedure used for the spectrum of europium phosphate glass can be employed here. It can be seen from the spectrum at 12K (Figure 5.9a,b) that the transition from $^5D_o \rightarrow {}^7F_o$ is a singlet (1 fluorescence line), the $^5D_o \rightarrow {}^7F_1$ is a triplet (3 lines), the $^5D_o \rightarrow {}^7F_2$ is a quintuplet (5 lines), the $^5D_o \rightarrow {}^7F_3$ is a septet (7 lines) and the $^5D_o \rightarrow {}^7F_4$ is a nonet (9 lines). It is evident that these line splittings in each transition can not be attributed to high symmetries (cubic, hexagonal, and tetragonal) as these need low numbers of line splittings than that found in the fluorescence of this crystal. If a low symmetry is proposed for the Eu^{3+} ion in this crystal, the term splitting for integral J= 0,1,2,3,4,5,6 would be 1,3,5,7,9 respectively (Runciman 1956). Therefore, transitions from the ^5D_o (J=0) to any of the levels of the ^7F_J manifold, where J= 0,1,2,3,4,5,6 would result in splitting of 1,3,5,7,9 respectively. Counting the number of the fluorescence lines in each of the fluorescence bands of the 12K spectrum (Figure 5.9a,b) reveals that the local symmetry of the europium ion in this crystal fits the low symmetry option (C_s , C_v).

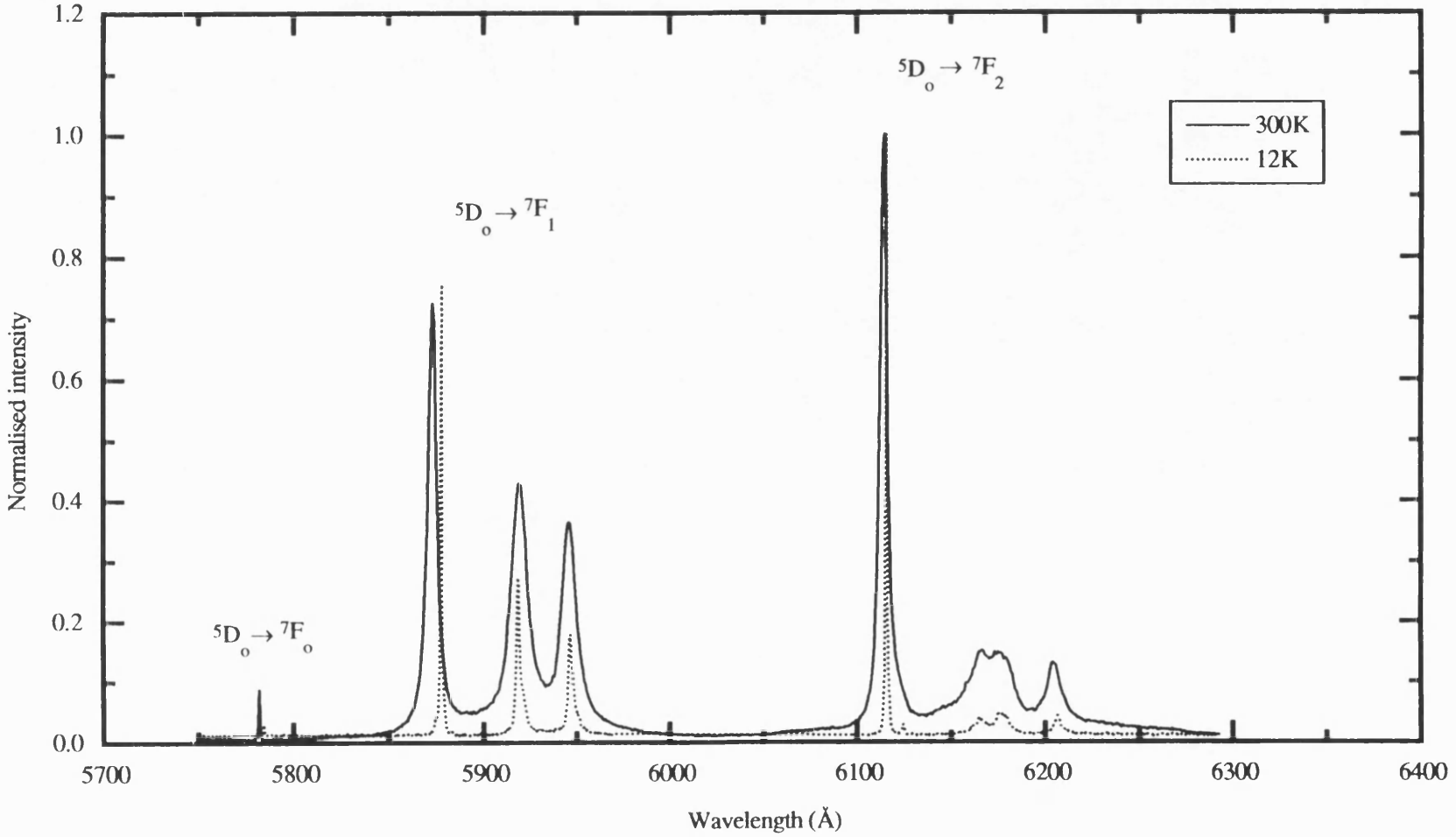

Figure 5.9a. The fluorescence spectrum of monocrystalline EuP_5O_{14} excited by the 4880Å argon ion laser line. Less laser power used to excite this part than the one in the next figure.

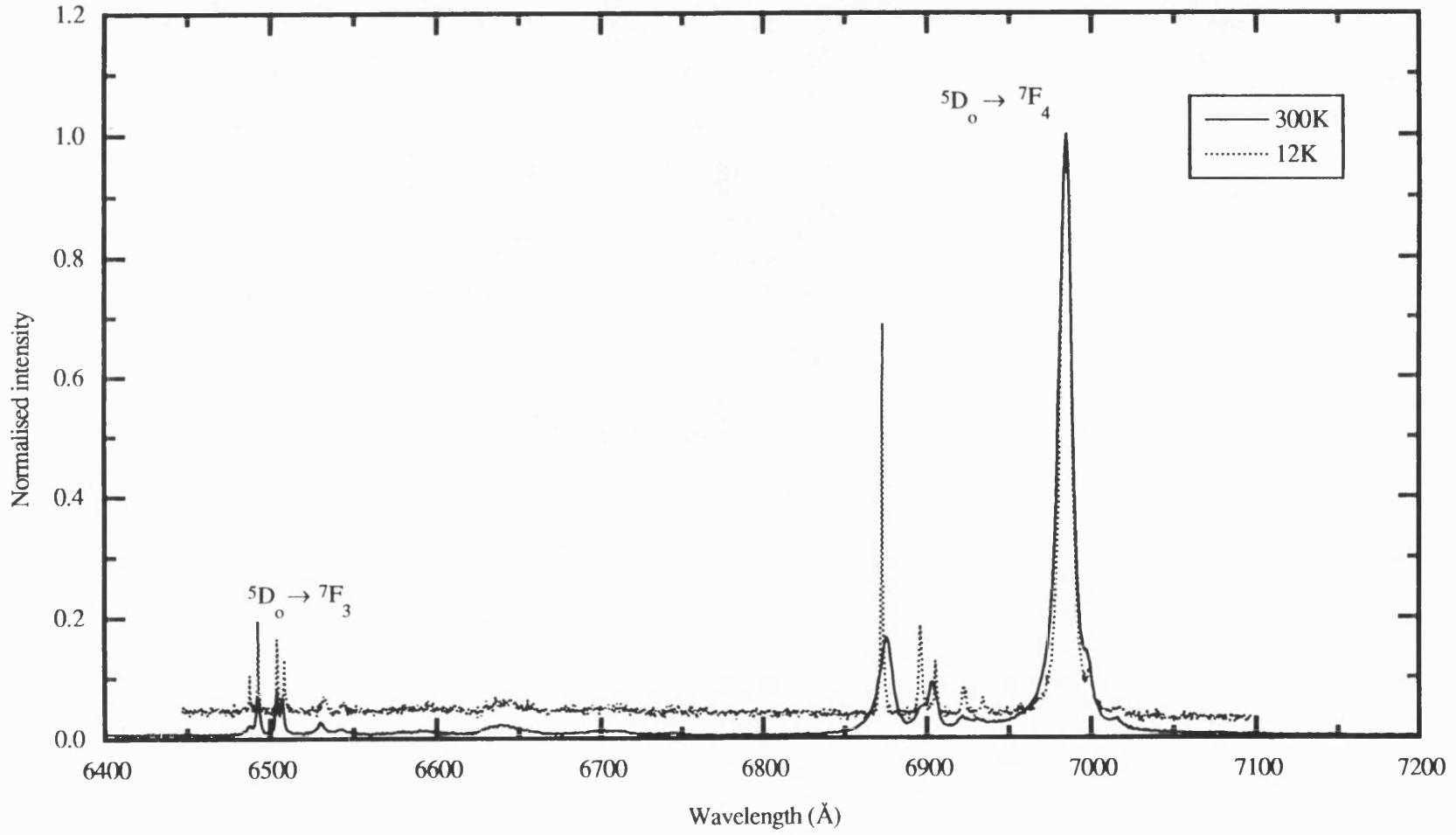

Figure 5.9b. The continuation of the fluorescence spectrum of monocrystalline EuP_5O_{14} excited by the 4880Å argon ion laser line. Higher laser power was used to excite this part than the one in the previous figure.

Table 5.3. Measured wavelengths of the fluorescence band peaks of EuP_5O_{14} crystal at temperature of 12 and 300K compared with the wavelengths of the fluorescence lines of Eu^{3+} ion in pentaphosphate crystal (EuP_5O_{14}) measured at 100K by Brecher (1974). The transitions which are responsible for these fluorescence lines are quoted from the same reference.

Wavelength (Å) (EuP_5O_{14}) crystal (300K)	Line width at Half maximum (Å) (300K)	Wavelength (Å) (EuP_5O_{14}) crystal (12K)	Line width at Half maximum (Å) (12K)	Wavelength (Å)	Transition
5782.0	1	5784.3	0.5	5784.0	$^5D_0 \rightarrow {}^7F_0$
5873.0	5.5	5877.8	0.85	5876.0	$^5D_0 \rightarrow {}^7F_1$
5918.9	10	5918.5	2	5918.0	
5945.6	9	5946.7	2.75	5947.0	
6114.3	4.25	6115.4	1	6116.0	$^5D_0 \rightarrow {}^7F_2$
-	-	6124.4	-	6124.0	
6166.3	-	6164.8	-	6166.0	
6174.7	-	6175.1	-	6176.0	
6203.8	-	6206.5	-	6208.0	
-	-	-	-	6485.0	$^5D_0 \rightarrow {}^7F_3$
6488.0	-	6487.6	0.75	6488.0	
6492.2	2.25	6492.6	0.75	6494.0	
6504.0	2.25	6504.0	1	6506.0	
6507.4	3	6508.7	1	6510.0	
6530.3	-	6532.1	-	6533.0	
6543.2	-	6542.7		6546.0	
6593.2	-	-	-	-	
6640.5	-	6642.3	-	-	
6875.2	8.75	6872.8	1	6872.0	$^5D_0 \rightarrow {}^7F_4$
6897.0	-	6896.0	2	6899.0	
6902.7	-	6905.1	1.5	6907.0	
6921.8	-	6922.3	-	6923.0	
-	-	6933.8	-	6935.0	
6984.7	-	6984.2	-	6985.0	
-	-	-	-	6988.0	
6997.4	10	6998.3	8	7002.0	
7016.0	-	7018.0	-	7018.0	

Comparison between the fluorescence spectrum of the $(Eu_2O_3)_{0.186}(P_2O_5)_{0.814}$ glass and the europium pentaphosphate crystal (EuP_5O_{14}) can be used to identify similarities and differences between the two spectra. In Figure 5.10a,b an overlap between the spectrum of the glass and the crystal, in the same wavelength range at 12K, has been made. The two spectra share nearly the same overall profile, yet the spectrum of the glass shows greater broadening, which is due to the randomness of the glass structure. In addition, some of the fluorescence lines of the glass spectrum are enhanced relative to their most intense lines. This is can be related to relaxation in the selection rules of transitions compared with the crystal fluorescence. For example, the lines locate at higher wavelengths (higher than 6125Å in the $^5D_o \rightarrow {}^7F_2$ band of the crystal). The opposite effect can be detected in the $^5D_o \rightarrow {}^7F_1$ (less than 5900Å) and the $^5D_o \rightarrow {}^7F_4$ band as some of the lines (less than 6900Å) in the glass have lower intensity than the ones in the crystal. The $^7F_1$ multiplet is thermally populated due to its closeness to the ground state ($^7F_0$); therefore at 12K it will be depopulated, this causes a reduction in the intensity of the $^5D_o \rightarrow {}^7F_1$ transition. The reduction of the intensity of the $^5D_o \rightarrow {}^7F_4$ transition can be attributed to reduction in the fluorescence of the $^5D_1 \rightarrow {}^7F_6$ transition, which has nearly the same wavelength and is less active at low temperatures. Another point, which can be noticed in the comparison of the spectrum of the glass with the spectrum of the crystal of the europium phosphate (Fig. 5.10a,b), is the shift of the spectrum of the glass towards higher wavelengths. This shift may be taken as a sign of higher stress on the Eu ion by the oxygen atoms of phosphate tetrahedra in the disordered glass compared with the crystal. EXAFs measurements made by Bowron et al. (1994, 1995) on europium metaphosphate glass have shown a variation in the distance between the europium ion and the surrounding oxygen ions (Eu-O), which implies that some oxygen atoms are closer to the Eu ion than others; this difference in Eu-O distance constitutes a strain and implies that the mean stress on the Eu ion may be enhanced.

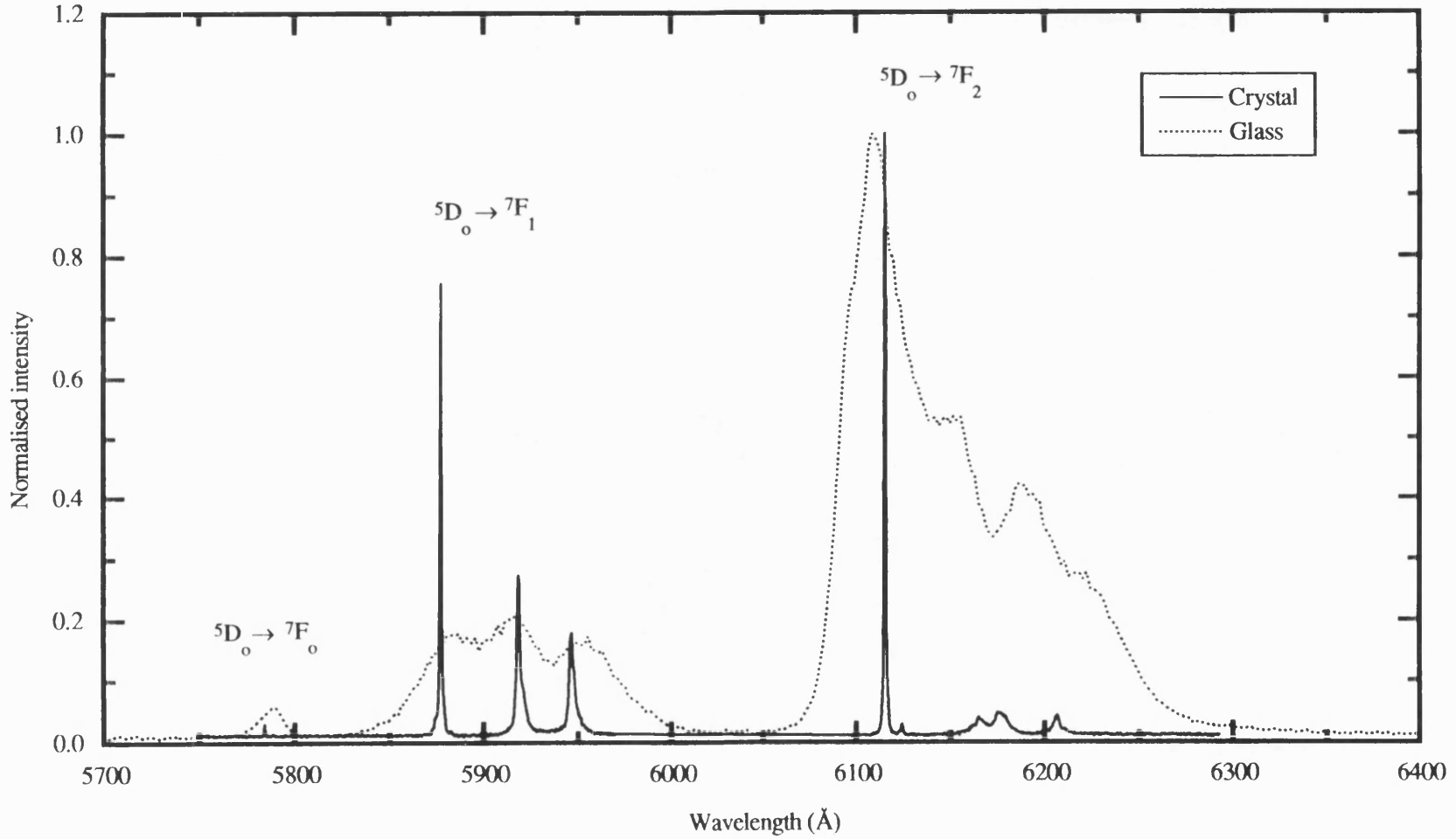

Figure 5.10a. Comparison between the fluorescence spectra of the EuP_5O_{14} crystal and $(Eu_2O_3)_{0.186}(P_2O_5)_{0.814}$ glass in the first three bands measured at 12K.

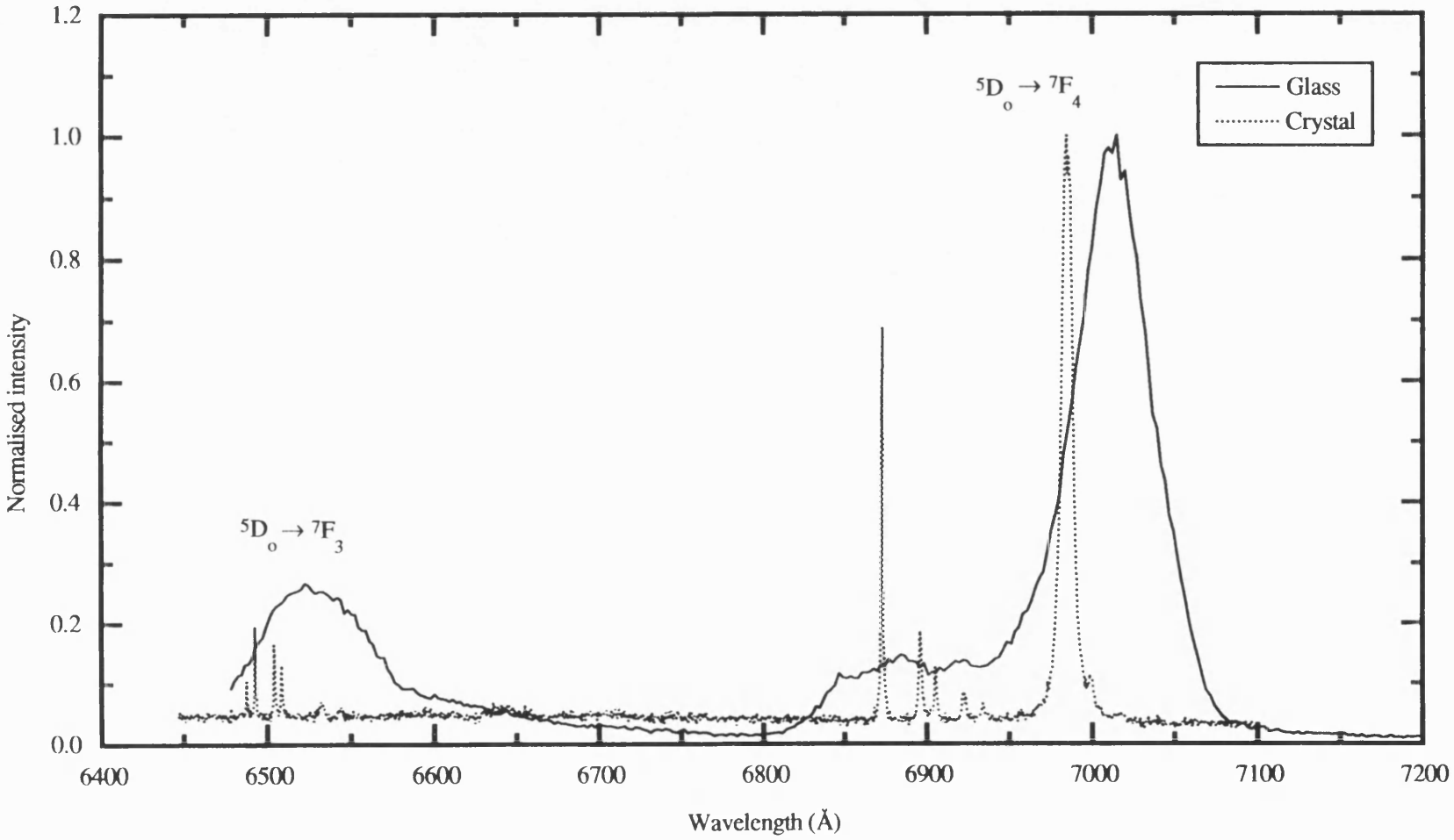

Figure 5.10b. Comparison between the fluorescence spectra of the EuP_5O_{14} crystal and $(Eu_2O_3)_{0.186}(P_2O_5)_{0.814}$ glass in the second two bands measured at 12K.

5.5. PRESSURE EFFECTS ON THE FLUORESCENCE SPECTRA OF EUROPIUM METAPHOSPHATE GLASS AND EUROPIUM PENTAPHOSPHATE CRYSTAL

The effects of pressure on the laser induced fluorescence spectra of the $(Eu_2O_3)_{0.186}(P_2O_5)_{0.814}$ glass and the europium pentaphosphate crystal (EuP_5O_{14}) were measured at room temperature using the diamond anvil cell (DAC). The linear shift in the ruby fluorescence lines was used to calibrate and measure the pressure generated in the DAC. The full procedure of the sample loading and pressure generating in the DAC has been detailed in chapter 2. The fluorescence measurement were examined and recorded in pressure steps of 5-10Kbar in the range 1bar-50Kbar using the assembled optical system which has been illustrated in Figure 3.5. The fluorescence spectrum of $(Eu_2O_3)_{0.186}(P_2O_5)_{0.814}$ glass sample was induced by the 4880Å argon ion laser line set in the power range 100-200mW, and measured by the single grating monochromator using the 150μ slitwidths and 1.66Å/s scan speed. In the case of the europium pentaphosphate crystal sample (EuP_5O_{14}), the fluorescence measurements under high pressures were obtained using the 4880Å laser line (set at 300mW), 200μ slit widths, and scanning speed of $1cm^{-1}$ every 4 seconds.

Figure 5.11 shows the fluorescence spectrum of the europium phosphate glass, having the composition $(Eu_2O_3)_{0.186}(P_2O_5)_{0.814}$, obtained under 50kbar pressure overlapped on the spectrum measured under atmospheric pressure. The fluorescence spectrum does not show noticeable changes with pressure increase in the range covered; it is typical of Eu^{3+} ion with no measureable shifts in the peak positions of the fluorescence bands under pressure or any sign of phase transition. These results suggest that the valency of the europium ion in this glass remains 3+ under pressure, up to the maximum 50kbar obtained.

The fluorescence spectrum of the europium pentaphosphate crystal (EuP_5O_{14}) measured under 52Kbar pressure and overlapped on the spectrum measured at atmospheric pressure, is shown in Figure 5.12. The fluorescence line positions extracted from the spectrum, measured at 52Kbar and 1bar, are listed in Table 5.4. The spectrum shows measurable shifts in some of the fluorescence lines towards longer wavelengths with increasing pressure. The effect of pressure on the wave

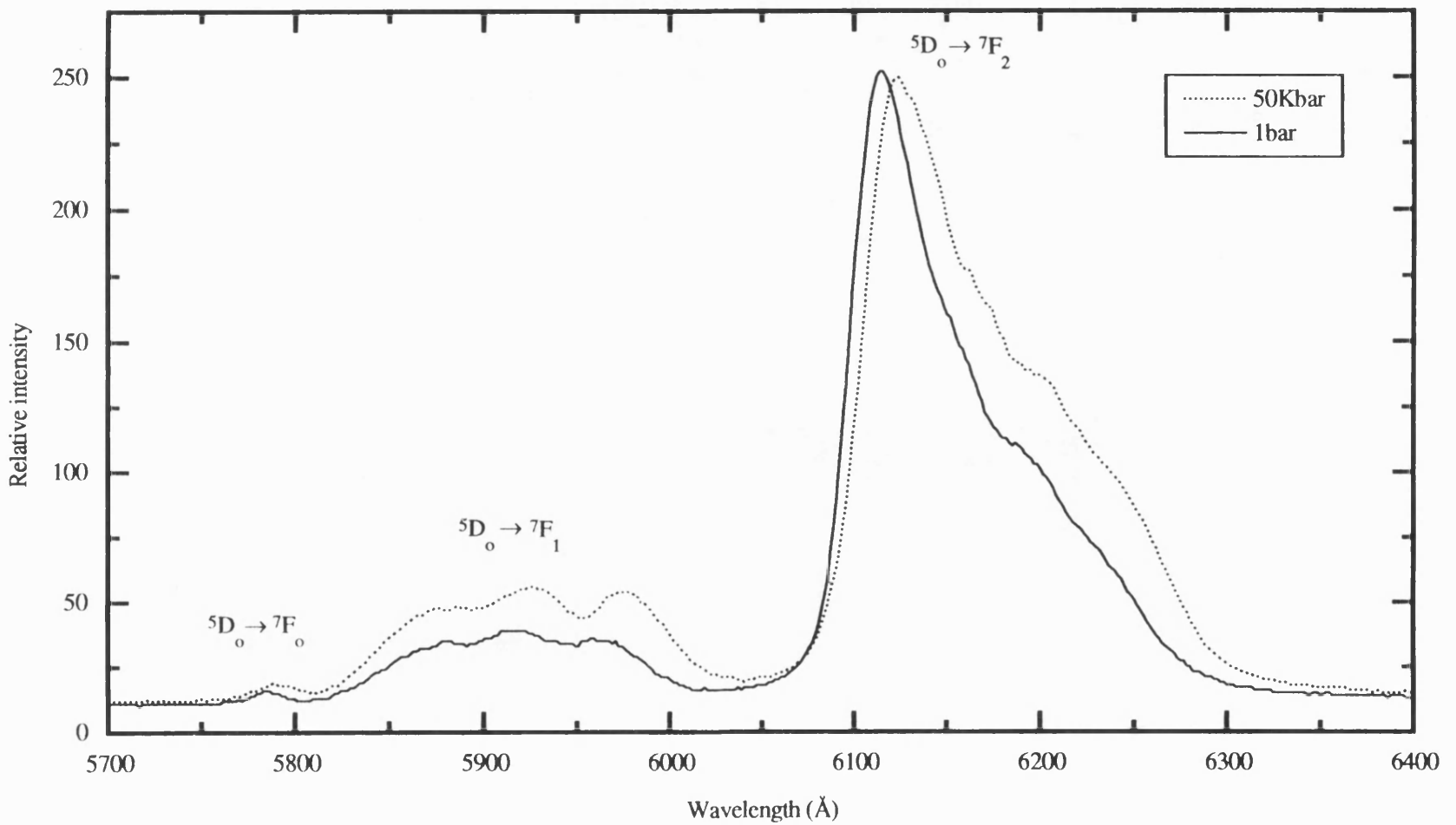

Figure 5.11. The effect of pressure on the fluorescence spectrum of the $(Eu_2O_3)_{0.186}(P_2O_5)_{0.814}$ in the short wavelength region measured at 292K.

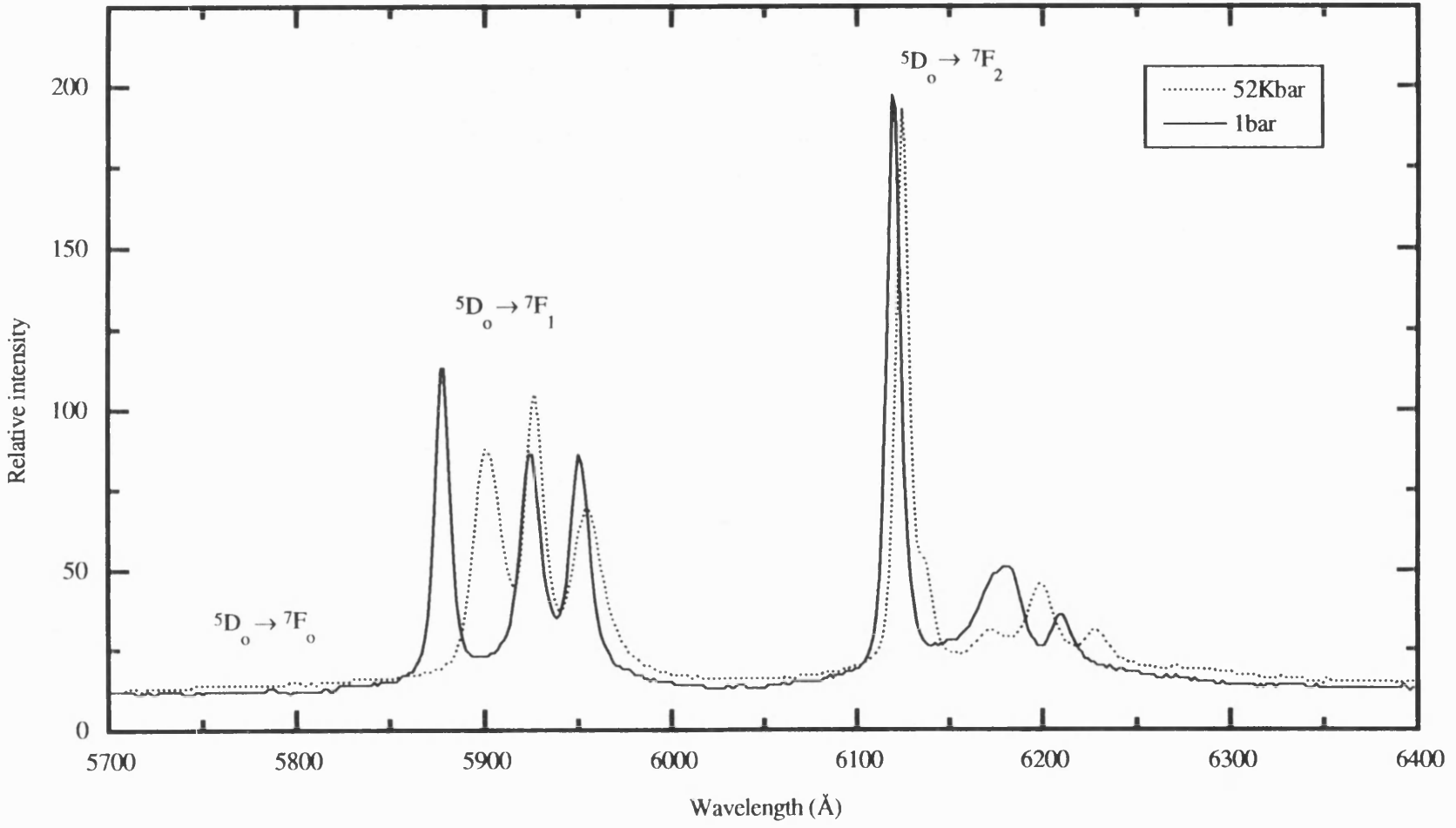

Figure 5.12. The effect of pressure on the fluorescence spectrum of the EuP_5O_{14} crystal in the short wavelength region at 292K.

length of the three fluorescence lines originating from the $^5D_o \rightarrow {}^7F_1$ transition is shown in Figure 5.13. Linear fittings were applied to the pressure dependences of these lines and the pressure derivatives ($d\lambda/dP$) determined from the experimental data are 0.43, 0.08, and 0.06Å/Kbar (Table 5.4). The fluorescence line originating from the $^5D_o \rightarrow {}^7F_o$ transition can not be seen in the spectrum of crystal for two reasons: (i) the crystal sample size is too small (100μ) to give a sufficient fluorescence signal, (ii) this fluorescence line is polarised in specific direction which will be affected by the crystal sample orientation in the DAC. Apart from the fluorescence line shifts with pressure no other dramatic changes were observed in the spectrum. Therefore it can be concluded that this crystal has no phase transition under pressure in the range covered, and also the valency of the europium ion remains trivalent with increasing pressure (no valency change).

Table 5.4. The pressure effect on some of the fluorescence lines of EuP_5O_{14} crystal at temperature of 300K.

Wavelength (Å) 1bar	Wavelength (Å) 52Kbar	Transition
5877.0	5900.3	$^5D_0 \rightarrow {}^7F_1$
5924.0	5927.0	
5950.3	5955.0	
6118.9	6123.9	$^5D_0 \rightarrow {}^7F_2$
-	6135.6	
6175.0	6172.3	
6180.7	6199.0	
6211.0	6227.4	

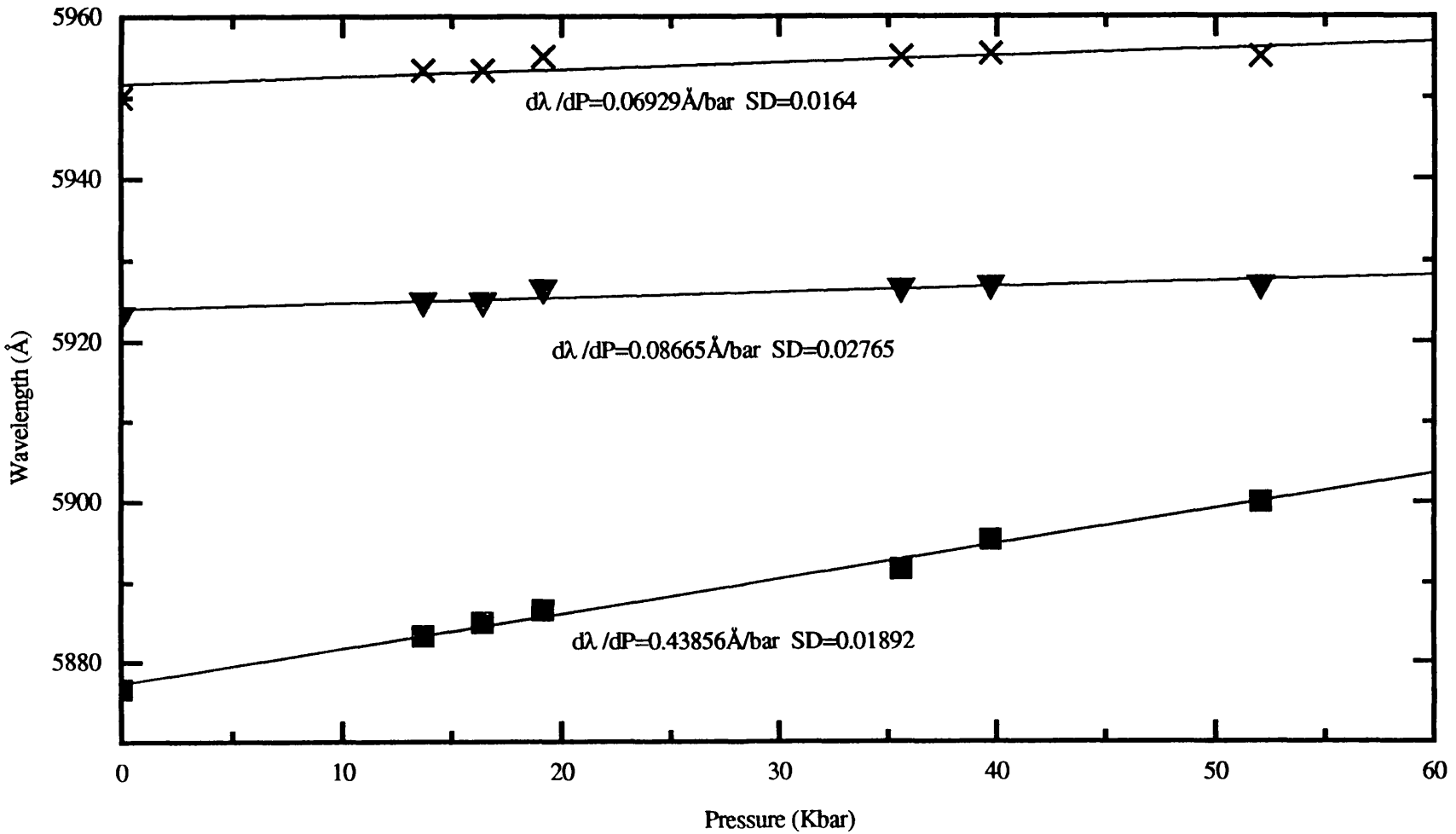

Figure 5.13. The effect of pressure on the wavelengths of the fluorescence lines of the $^5D_0 \rightarrow {}^7F_1$ transition for the EuP_5O_{14} crystal. Linear fittings were applied and the pressure derivatives are indicated on each line.

CHAPTER SIX

LOW TEMPERATURE AND HIGH PRESSURE FLUORESCENCE SPECTRA OF SAMARIUM METAPHOSPHATE GLASS AND PENTAPHOSPHATE CRYSTAL

6.1. INTRODUCTION

In general rare earth ions incorporated in glasses tend to show similar optical absorption and fluorescence spectra to those of rare-earth ions in inorganic crystals-perhaps of low symmetry - except for inhomogeneous line broadening due to a multiplicity of rare-earth sites in a glass (Reisfeld and Eckstein 1972, Reisfeld et al. 1971). Hence to develop an understanding of the changes in the glass fluorescence, the results are compared with those determined as functions of temperature and pressure for fluorescence of a single crystal of samarium pentaphosphate SmP_5O_{14}, which also is constructed from linked phosphate groups. Rare earth pentaphosphates crystal have three types of structure, that of SmP_5O_{14} being monoclinic (pseudo-orthorhombic $\beta \approx 90°$) with four SmP_5O_{14} molecules per unit cell having the unit cell dimensions of a=12.99Å, b=8.944Å, c=8.757Å, and β=90.41° (Beucher 1970). The rare earth pentaphosphate compounds are themselves a class of luminescent crystalline materials with interesting optical properties, which have possible uses in optical communication systems (Danielmeyer and Weber 1972, Weber et al. 1972). Both the $(Sm_2O_3)_{0.248}(P_2O_5)_{0.752}$ glass and crystalline SmP_5O_{14} are strongly fluorescent, the crystal rather more so than the glass.

A rare-earth ion incorporated in glass or crystal matrix is subjected to the crystal field of the surrounding ions and the Stark effect produces a set of levels for each single level of the free ion. Using group-theoretical methods, Bethe (1929) determined the number of levels produced by crystal field splitting from a given level of a free ion. Runciman (1956) classified the 32 crystallographic point groups into four headings: cubic, hexagonal (including the hexagonal and rhombohederal systems),

tetragonal, lower symmetry (including orthorhombic, monoclinic and triclinic). The present intention is to use fluorescence studies to relate the local symmetry of the Sm^{3+} ion in the crystalline and glass matrices to the Runciman classification. Therefore, laser-induced fluorescence has been employed first to probe the emission properties of the Sm^{3+} ions in the ordered SmP_5O_{14} crystal; then results can be extended to explore the local environment of the Sm^{3+} ions in a metaphosphate glass of composition $(Sm_2O_3)_{0.248}(P_2O_5)_{0.752}$. Since an amorphous solid does not have the ordered structure normally found in crystals, the environment of a fluorescent ion is not sufficiently well defined to enable a simple characterisation of its optical properties. In glassy host media, the emission observed from rare-earth ions consists of a superposition of contributions from individual ions distributed among the entire ensemble of local environments. The resulting statistical distribution of Stark components brings about a significant degree of inhomogeneous broadening of the absorption and emission lines, limiting attempts at interpretation. By contrast sharp lines characterise the crystal fluorescence; these have been used in an examination of the local structure in the light of crystal field effects surrounding the samarium ions in the crystal and the criteria developed have then been carried over to evaluation of the local structure of the glass. Cooling the glass of composition $(Sm_2O_3)_{0.248}(P_2O_5)_{0.752}$ and crystalline SmP_5O_{14} from room to low temperature is found to alter their fluorescence spectra in systematic fashions. Possible causes are examined. Since the changes seem to be associated with structural instability, the effects of high pressure on the fluorescence spectra have also been determined.

Ultrasonic studies have shown that the samarium phosphate glass, like europium phosphate glass, exhibits anomalous elastic behaviour as a function of temperature and pressure. The hydrostatic pressure derivatives $(\partial C_{11}/\partial P)_{T,P=0}$ and $(\partial C_{44}/\partial P)_{T,P=0}$ are negative: the long-wavelength acoustic modes soften under pressure (Mierzejewski et al. 1988). This glass become easier to squeeze when subjected to high pressure. Therefore, fluorescence spectral measurements of the samarium phosphate glass and crystal under high pressure using the DAC were recorded to search for any indication of spectral variation with pressure which may explain the anomalous behaviour of this glass.

6.2. LOW TEMPERATURE EFFECTS ON THE FLUORESCENCE SPECTRUM OF SAMARIUM METAPHOSPHATE GLASS

To understand the fluorescence spectrum of a glass, it is essential to know their absorpotion spectrum. This is necessary to determine the appropriate wavelengths which are needed to induce the fluorescence spectrum and also to identify the higher energy levels of the spectrum. Absorption measurements were carried out on the samarium phosphate glass samples in a standard commercial double-beam instrument. The fluorescence measurements were accomplished (in range 10-300K temperature) using the experimental set-up described in section 9.4. The fluorescence spectrum of a samarium metaphosphate glass, having the composition $(Sm_2O_3)_{0.19}(P_2O_5)_{0.81}$, was excited using the 4765, 4880, and 5145Å lines of the argon ion laser. Typical power for each laser line at the sample was varied from 50mW to 200mW according to the strength of the fluorescence in the spectral region specified. The slitwidths of the monochromator were set at 150μ to obtain a resolution of $1.5cm^{-1}$.

The optical absorption spectrum of vitreous $(Sm_2O_3)_{0.19}(P_2O_5)_{0.81}$ measured between 315nm and 700nm at room temperature is shown in Figure 6.1. They are similar to the absorption spectra measured by Reisfeld and Boehm (1972) on samarium phosphate glasses prepared from different starting materials (Sm_2O_3 and $NaH_2PO_4.H_2O$). Both sets of spectra are typical of Sm^{3+} ions, showing no sign of absorption bands which characterise Sm^{2+} ions [determined for Sm^{2+} in fluoroberyllate glasses, which exhibit a broad absorption band centred at about 500nm (Petrovskii et al. 1966), and for Sm^{2+} in a crystalline CaF_2 host lattice for which the absorption bands are at about 636nm and 424.8nm (Kaiser et al. 1961)].

The fluorescence spectra of $(Sm_2O_3)_{0.19}(P_2O_5)_{0.81}$ glass measured at 300K and 10K are shown overlapped in Figure 6.2a,b; those determined for $(Sm_2O_3)_{0.224}(P_2O_5)_{0.776}$ and $(Sm_2O_3)_{0.248}(P_2O_5)_{0.752}$ glasses are closely similar. The line profiles show the typical characteristics of laser induced, non-resonant fluorescent line narrowing (Riseberg 1972). The shoulders at 300K, which become secondary peaks at 10K, can be attributed to the spectral diffusion effect, which results from variation of the optical transition frequency within the glass from sites which have different sur

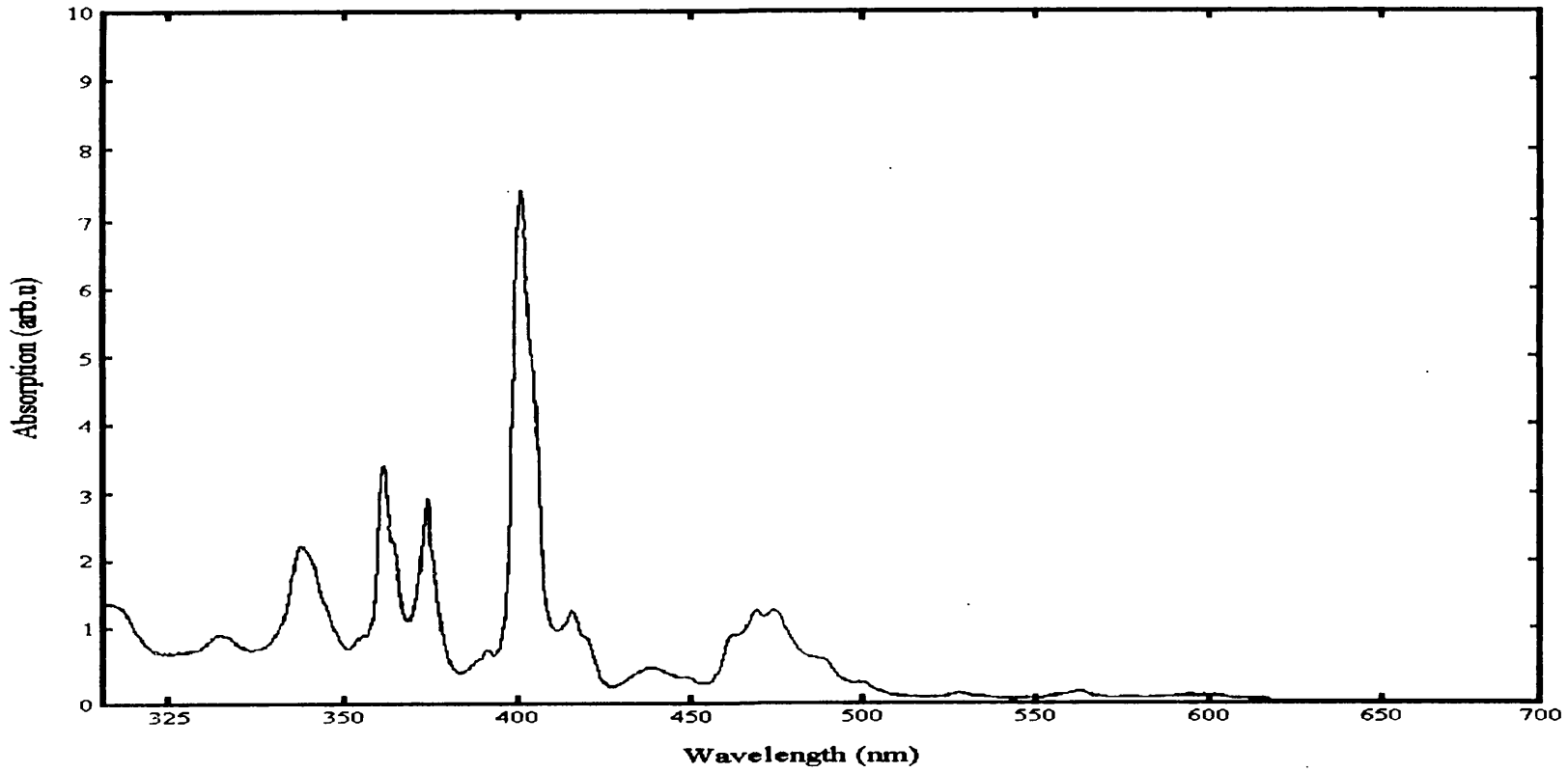

Figure 6.1. The absorption spectrum of $(Sm_2O_3)_{0.19}(P_2O_5)_{0.81}$ glass measured at room temperature.

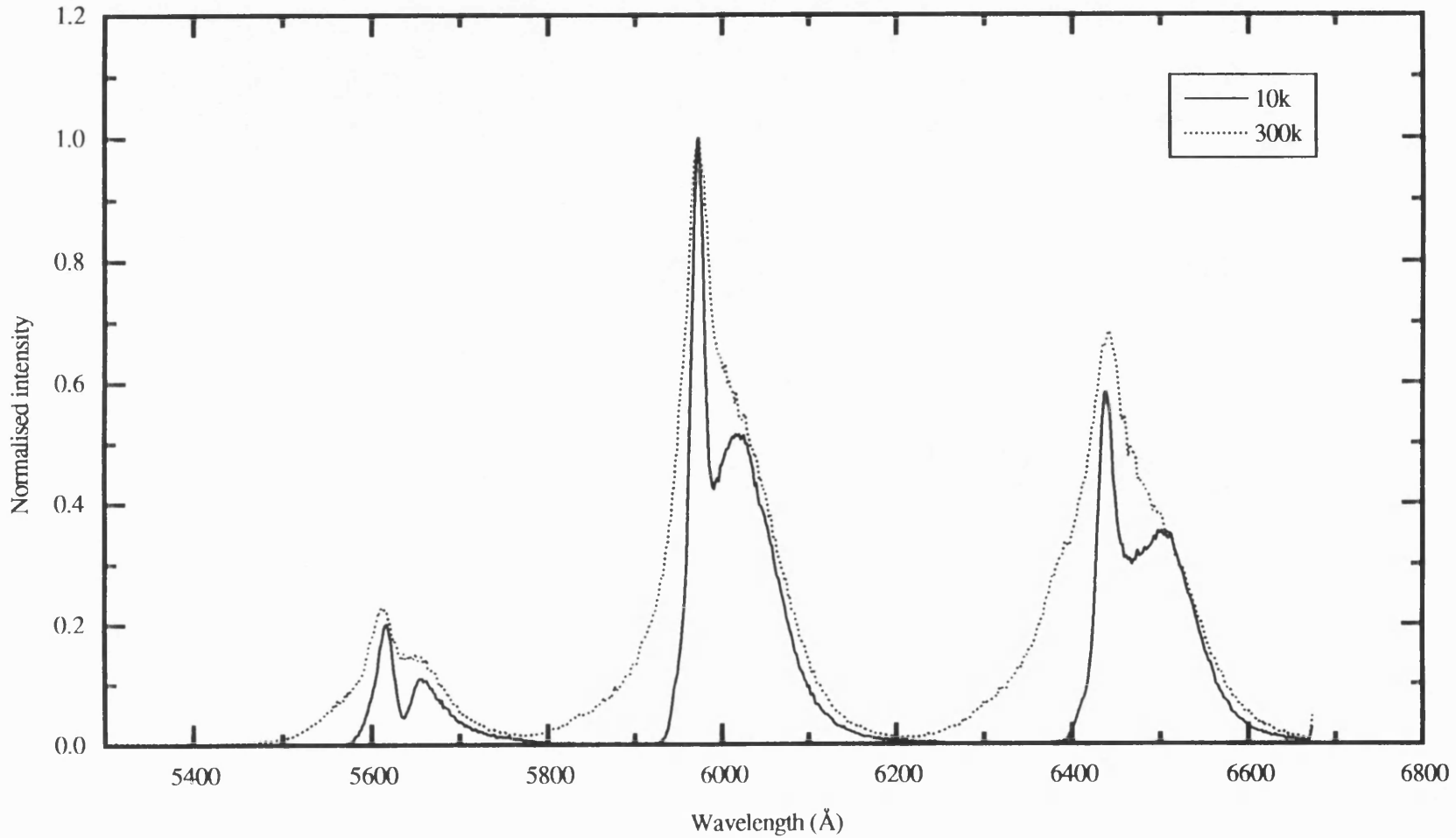

Figure 6.2a. The fluorescence spectrum of $(Sm_2O_3)_{0.19}(P_2O_5)_{0.81}$ glass excited by the blue 4765Å argon ion laser line.

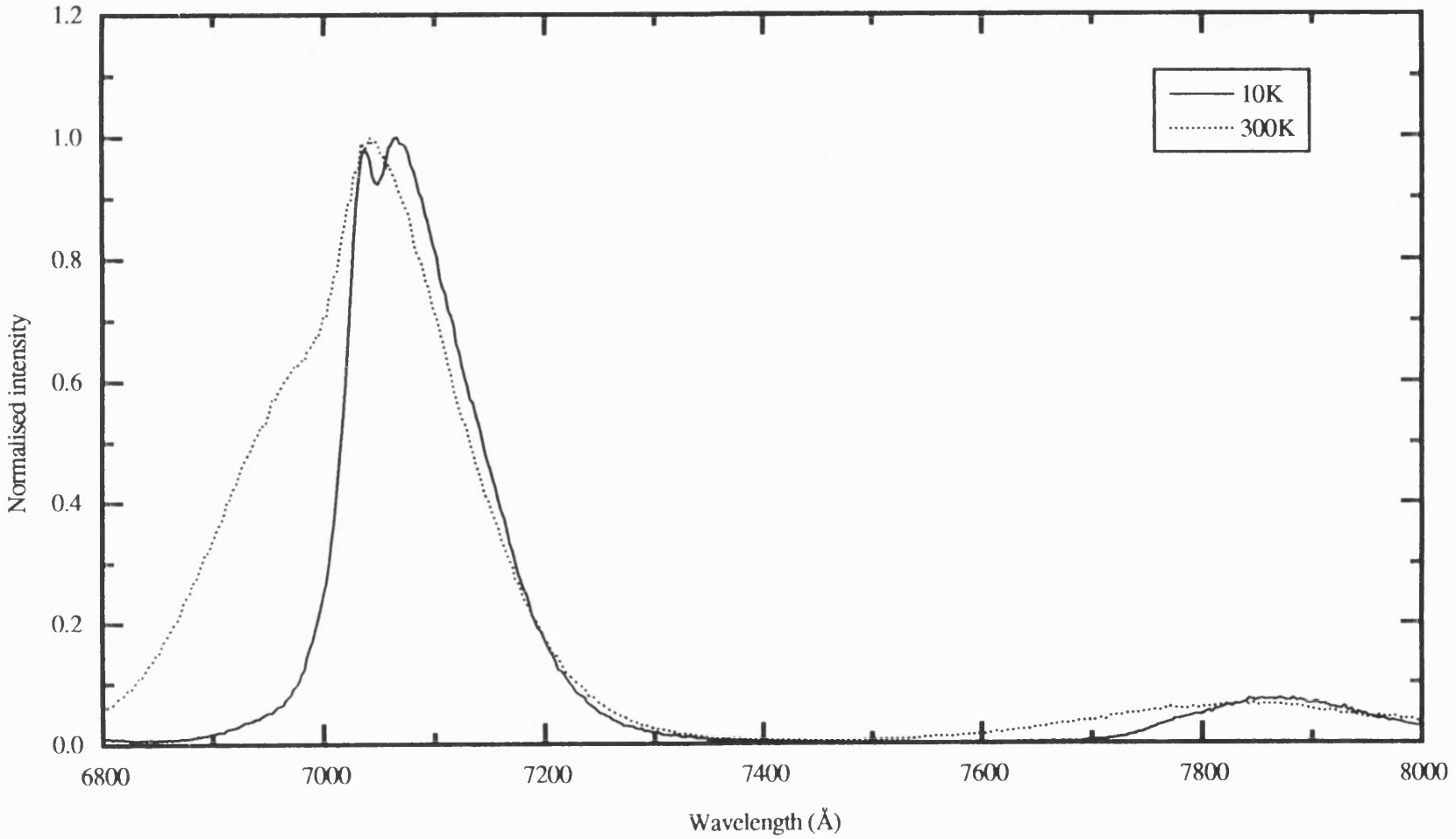

Figure 6.2b. The continuation of the fluorescence spectrum of $(Sm_2O_3)_{0.19}(P_2O_5)_{0.81}$ glass excited by the 4765Å argon ion laser line.

roundings (Imbusch 1987). The most intense lines are located at absolute wavelengths shown in Table 6.1; these do not shift within experimental error either with samarium ion concentration or with temperature between 300K and 10K. The line widths decrease strongly as the temperature is lowered (the line half-widths measured at 10K are listed in Table 6.1). The line positions are those expected of Sm^{3+}. Trivalent samarium emits fluorescence in the visible and near infrared region in various host materials. This fluorescence is due to transitions between the energy levels in the $4f^5$ electron configuration (Reisfeld and Boehm 1972, Reisfeld et al. 1974). The ground multiplet for Sm^{3+} is ^6H_j where j=5/2,7/2,9/2,11/2,13/2,15/2, the approximate energy level positions measured from $^6H_{5/2}$ (=0cm^{-1}) are: $^6H_{7/2}$=1200cm^{-1}, $^6H_{9/2}$=2400cm^{-1}, $^6H_{11/2}$=3500cm^{-1}, $^6H_{13/2}$=4800cm^{-1}, $^6H_{15/2}$=6600cm^{-1}. Higher energy levels are located at $^4G_{5/2}$=17800cm^{-1}, $^4F_{3/2}$=18700cm^{-1}, and $^4G_{7/2}$=19900cm^{-1} (Dieke and Crosswhite 1963). Reisfeld and Boehm (1972) attribute the spectra of their samarium phosphate glass to the Sm^{3+} ion. The fluorescence peaks originate from transitions from $^4G_{5/2}$ to the components of the ground multiplet ^6H_j giving the corresponding wavelengths listed in the third column in Table 6.1. The wavelengths of the peaks observed here in the fluorescence spectra (Fig. 6.2a,b) are closely similar to these.

In general, the fluorescence spectrum of the $(Sm_2O_3)_{0.19}(P_2O_5)_{0.81}$ glass shows that each fluorescence band has two major peaks (10K spectrum of Figure 6.2a,b), which reflect the presence of two main sites for the samarium ion. Therefore, each fluorescence band in 10K spectrum of the glass was fitted with two Gaussian distribution functions to obtain the width and the location of the peaks (peak locations and widths are listed in Table 6.1). The energy difference between the two sites was calculated from the results of the fitting. For the first band (the $^4G_{5/2} \rightarrow ^6H_{5/2}$ transition) the locations of the two peaks correspond to an energy difference of ΔE= 0.0196eV, the second band peak locations ($^4G_{5/2} \rightarrow ^6H_{7/2}$ transition) correspond to an energy difference of ΔE= 0.0166eV, the third band peak locations ($^4G_{5/2} \rightarrow ^6H_{9/2}$ transition) correspond to an energy difference of ΔE= 0.0168eV, and the fourth band peak locations ($^4G_{5/2} \rightarrow ^6H_{11/2}$ transition) corresponding to an energy difference of ΔE= 0.0128eV. The average energy difference is approximately ΔE= 0.0164eV. This suggests that the Sm ions are sited in at least two different low-

Table 6.1. Measured wavelengths of the fluorescence lines of $(Sm_2O_3)_{0.19}(P_2O_5)_{0.81}$ glass compared with the wavelengths of the fluorescence lines of Sm^{3+} ion given by Reisfeld et al. (1974)*, Reisfeld and Boehm (1972). The transitions which are responsible for these fluorescence are quoted from Dieke and Crosswhite (1963)**.

Wavelength (Å) at 10K $(Sm_2O_3)_{0.19}(P_2O_5)_{0.81}$ glass	Half width (Å) at 10K	Wavelength (Å)*	Transition**
5613.7	19.6	5620	$^4G_{5/2} \rightarrow {}^6H_{5/2}$
5663.9	59.9		
5971.9	14.0	5970	$^4G_{5/2} \rightarrow {}^6H_{7/2}$
6020.3	81.9		
6438.5	18.2	6450	$^4G_{5/2} \rightarrow {}^6H_{9/2}$
6495.5	88.3		
7048.2	58.2	7070	$^4G_{5/2} \rightarrow {}^6H_{11/2}$
7100.0	118.6		
7870.0	-	8300	$^4G_{5/2} \rightarrow {}^6H_{13/2}$
8162.5	-	9000	$^4G_{5/2} \rightarrow {}^6H_{15/2}$
8483.8			
8667.3			
8788.4			

Table 6.2. The oscillator strengths associated with sleeted absorption lines of Sm^{2+} and Sm^{3+} ions (Kaiser et al. 1961).

Valency	Absorption line (nm)	Oscillator strength f x 10^3
Sm^{2+}	636.0	1.8
	424.8	3.1
Sm^{3+}	400.2	0.33

symmetry environments, which are shifted from each other by an energy difference of approximately $\Delta E = 0.0164eV$. On comparing the average value of the energy difference for the samarium metaphosphate glass with the one for the europium metaphosphate glass ($\Delta E = 0.00312eV$, see chapter 5) it can be concluded that the two sites of the samarium ion are further apart than the two sites of the europium ion in the metaphosphate glasses.

The fluorescence spectra of Sm^{2+} ions in various host materials comprise two parts. The first part consists of sharp lines arising from transitions between levels of the 4f configuration, that is from an excited $^5D_0$ level to components of the ground multiplet ^7F_j. The second part is a broad band connected with f-d transitions (Pissarenko and Bykovskii 1968). Dieke and Sarup (1962) examined the fluorescence of Sm^{2+} ion in a $LaCl_3$ crystal and arranged the lines in two sequences, one coming from a state A and the other one from a state B about $1330cm^{-1}$ above A. Both sequences have lower states, which are denoted z,y,x,w,...etc., in common. The corresponding energy levels are shown in figure 5 of their paper. The lower states are the components of the ground multiplet ^7F_j and the higher states correspond to $^5D_0$ and $^5D_1$. The transitions from $^5D_0$ to the ^7F_j components (where j equals 0,1,2,3,4,5) result in the following mean wavelengths 6921, 7062, 7331, 7713, 8204Å respectively, the last (j =5) being unmeasured. The transitions from $^5D_1$ to the ^7F_j components result in the following wavelengths 6336, 6454, 6678, 6994, 7394 and 7881Å respectively. Therefore most of these Sm^{2+} fluorescence lines fall into the spectral range occupied by the broad fluorescence which peaks at 7045Å for the samarium phosphate glasses (Figure 6.2b) making it difficult to ascertain for certain whether the glasses contain divalent samarium ions as well as trivalent ones.

However the oscillator strengths for the Sm^{2+} absorption transitions are of the order of 10 times (or more) larger than those for the Sm^{3+} transitions in a sample containing 20% Sm^{2+} ions and 80% Sm^{3+} ions (Kaiser et al. 1961). Therefore, were Sm^{2+} ions to be present in the samarium phosphate glasses, there would be very intense absorption bands at about 6360Å and 4248Å compared with the Sm^{3+} ion bands. However the measured absorption band at about 400nm which is a characteristic of

the Sm^{3+} (Reisfeld and Boehm 1972, Kaiser et al. 1961) is quite intense compared with the measured absorption at 6360Å and 4248Å (Figure 6.1). The oscillator strengths, given in Table 6.2, indicate that the maximum proportion of Sm^{2+} is about 0.03%, the majority being Sm^{3+} ions. Another feature providing evidence that the broad fluorescence peaking at 7045Å corresponds to Sm^{3+} ion is its width which is approximately only half that reported for the fluorescence line of Sm^{2+} ion (Kaiser et al. 1961, Pissarenko and Bykovskii 1968).

6.3. LOW TEMPERATURE EFFECTS ON THE FLUORESCENCE SPECTRUM OF SAMARIUM PENTAPHOSPHATE CRYSTAL SmP_5O_{14}

The fluorescence spectrum of the samarium pentaphosphate crystal (SmP_5O_{14}) was measured at 12 and 300K using the optical system illustrated in section 9.4. The spectrum was excited using the 4765Å blue line of the argon ion laser. The exciting laser power was varied between 50 to 200mW depending on the resultant fluorescence intensity in the specified spectral region. The input and exit slit widths of the triple monochromator were set to 100μ.

The fluorescence spectrum of the SmP_5O_{14} crystal measured at 12K and 300K at atmospheric pressure are shown overlapped in Figure 6.3a,b. The positions of the fluorescence peaks at both temperatures are listed in Table 6.3. On cooling the crystal down to 12K, there was no measurable shift in the fluorescence lines. The fluorescence spectrum splits into five groups of well separated bands: the first at around 5600Å, the second one around 6000Å, the third around 6500Å, the fourth one at around 7000Å, the fifth one at around 7700Å. This spectral structure is consistent with a 3+ valence state (as listed by Reisfeld 1972) for the samarium ions: the bands can be attributed to transitions from the $^4G_{5/2}$ level to the lower levels of ^6H_J where J=5/2, 7/2, 9/2, 11/2, and 13/2 (Table 6.3). The fine structure revealed in these bands is due to the crystal field interaction on the free-ion energy levels of Sm^{3+} (Thomas and Nampoori 1990). A striking and interesting feature of all the five bands is the disappearance of some of their shorter wavelength lines at low temperature.

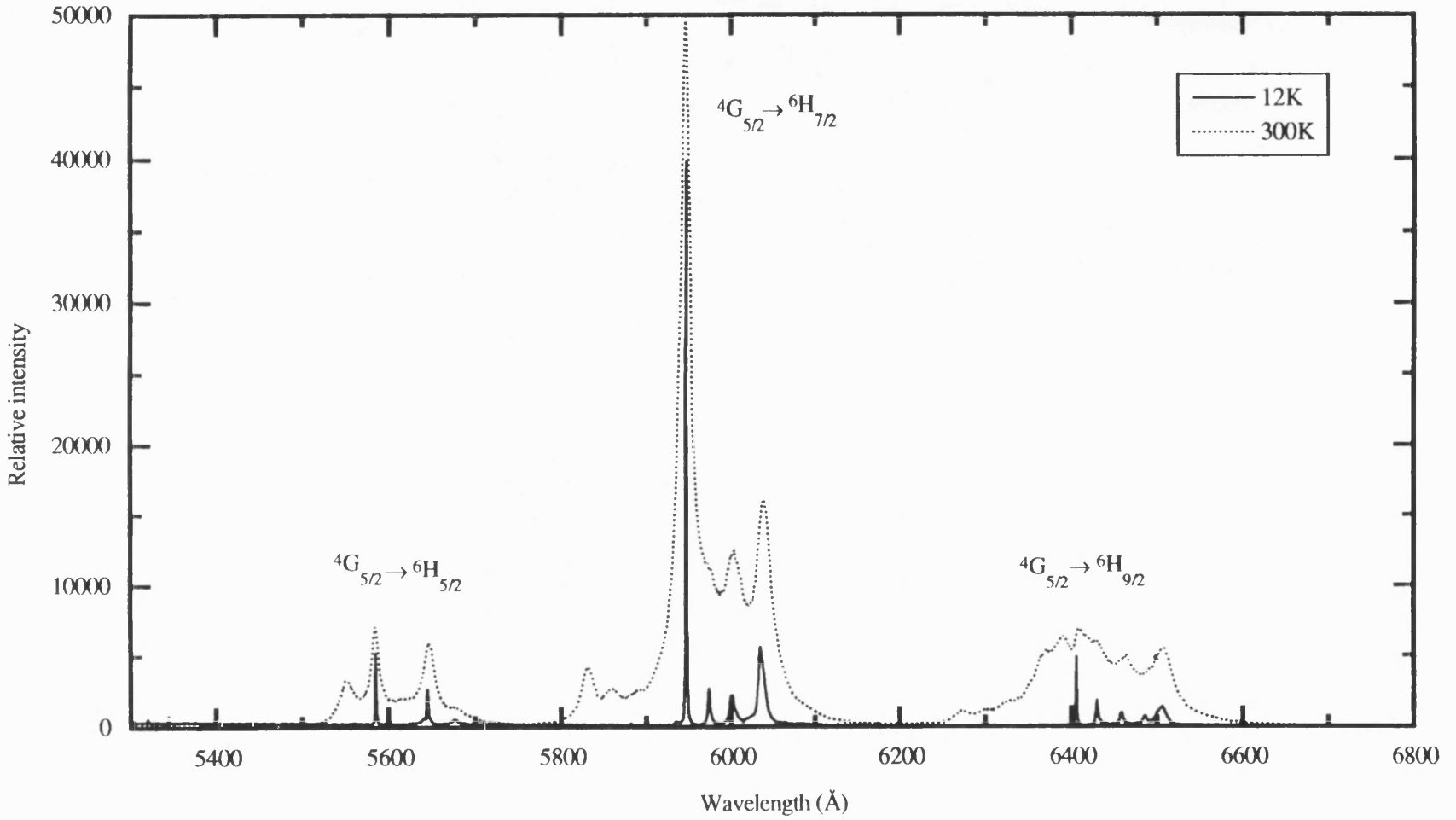

Figure 6.3a. The fluorescence spectrum of monocrystalline SmP_5O_{14} ecxited by the 4765Å argon ion laser line. Less laser power used to excite this part than the one in the next figure.

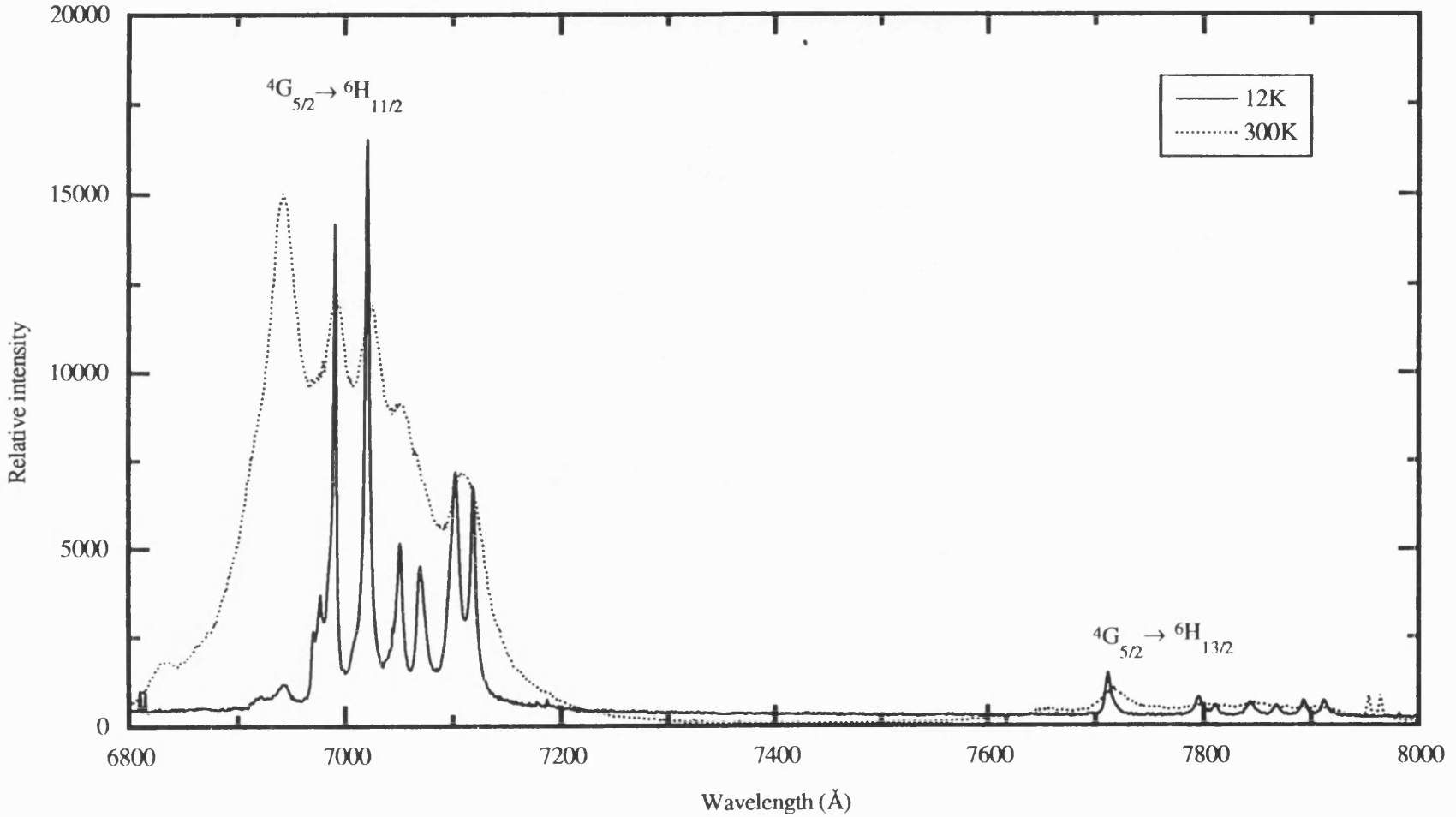

Figure 6.3b. The continuation of the fluorescence spectrum of monocrystalline smP_5O_{14} excited the 4765Å argon ion laser line. Higher laser power was used to excite this part than the one in the previous figure.

Table 6.3. The measured fluorescence peak wavelengths (Å) of the SmP_5O_{14} crystal at 12K (column 2), 292K (column 3).

Transition assignments	Fluorescence line wavelengths of SmP_5O_{14} at 12K.	Fluorescence line wavelengths of SmP_5O_{14} at 292K.
$^4F_{3/2}$	disappeared	5256.5
↓		5260.3
$^6H_{5/2}$		5314.3
		5342.7
$^4G_{5/2}$	-	5550.6
↓	5584.7	5584.1
$^6H_{5/2}$	5641.4 (s)	-
	5645.2	5646.5
	5676.0 (w)	5674.7
$^4G_{5/2}$	-	5831.5
↓	-	5858.9
$^6H_{7/2}$	-	5888.5
	5934.0 (s)	-
	5947.4 (vs)	5946.0
	5973.7	5971.5
	6000.9	6003.8
	6026.2 (s)	-
	6035.0	6038.0
$^4G_{5/2}$	-	6271.1
↓	-	6388.1
$^6H_{9/2}$	6406.1	6408.6
	6430.0	-
	6459.1	6464.1
	6486.7	-
	6506.1	6507.0

Continuation of Table 6.3.

$^4G_{5/2}$	-	6829.6
↓	-	6866.2
$^6H_{11/2}$	6921.0	6866.2
	6943.0	6942.5
	6970.0	-
	6977.3	-
	6991.0	6992.0
	7021.49	7025.4
	7051.1	7051.1
	7070.1	-
	7102.2	7107.3
	7118.4	-
$^4G_{5/2}$	-	7658.1
↓	7711.3	7717.2
$^6H_{13/2}$	7795.4	7799.1
	7811.2	-
	7843.1	7846.8
	7867.8	-
	7892.6	-
	7911.3	-

Inspection of the fluorescence spectrum (Figure 6.3a,b) and the assignments given in Table 6.3, together with systematic absences of lines at low temperature (12K), can provide a useful link with the local environment of the Sm^{3+} ions. At room temperature the transition from the $^4G_{5/2}$ level to the $^6H_{5/2}$ shows four peaks (dotted line). Four peaks can also be seen in the low temperature (12K) spectrum (solid line). The transition from $^4G_{5/2}$ level to the $^6H_{7/2}$ level shows seven peaks at room temperature but only six peaks at 12K. The third transition to the $^6H_{9/2}$ level shows about nine peaks at room temperature and six peaks at 12K. The fourth transition to the $^6H_{11/2}$ level shows what seem to be eight peaks at room temperature and ten peaks at 12K. The fifth transition to the $^6H_{13/2}$ level indicate that there are probably seven peaks at room temperature and that number also at 12K.

Taking into consideration the term-splitting for the half-integral J of the trivalent samarium ion terms in the Runciman classification (1956), there are two options for the local symmetry. The first one is cubic and the second one comprises all the other groups (hexagonal, tetragonal, and low symmetry). For the option of the cubic symmetry the splitting of the terms of the Sm^{3+} ion would be $^4G_{5/2}$ =2, $^6H_{5/2}$ =2, $^6H_{7/2}$ =3, $^6H_{9/2}$ =3, $^6H_{11/2}$ =4, $^6H_{13/2}$ =5, so the expected fluorescence line number would be 4 in the first band, 6 in the second band, 6 in the third band, 8 in the fourth band, and 10 in the fifth band. For the second option, considering all the other symmetries, the splitting would be $^4G_{5/2}$ =3, $^6H_{5/2}$ =3, $^6H_{7/2}$ =4, $^6H_{9/2}$ =5, $^6H_{11/2}$ =6, $^6H_{13/2}$ =7, and the expected fluorescence line number in each band would be 9 in the first band, 12 in the second band, 15 in the third band, 18 in the fourth band, and 21 in the fifth band. A count of the number of lines in each of the bands shown in Figure 6.3a,b is in accord with this option: the local symmetry must be so close to being cubic in SmP_5O_{14} crystal that it is not possible to separate the lines, which in principle should be possible because the symmetry is not strictly cubic. An interpretation of the fluorescent spectral lines for the SmP_5O_{14} crystal that the local symmetry around the Sm^{3+} ion is pseudocubic is in accord with the shape of the coordination polyhedron of the eight oxygen atoms surrounding a Sm^{3+} ion shown in Figure 6.4, which can be thought of as a distorted cube. The symmetry of the real coordination polyhedra is clearly lower than that of the ideal antiprism which has D_{4d} symmetry. So in the real structure the local site symmetry is something like C_{4v} or

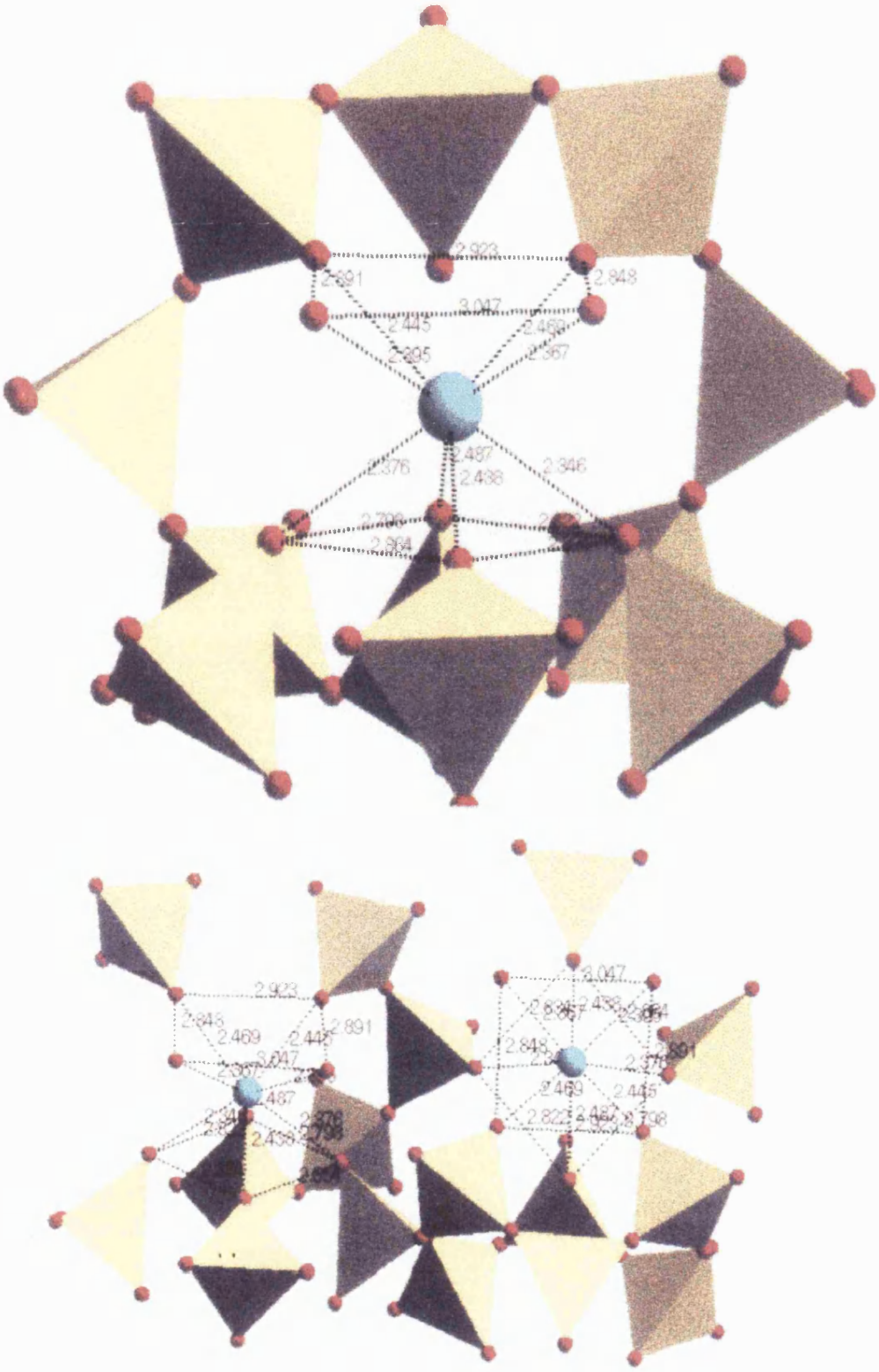

Figure 6.4. The pseudocubic local symmetry around the samarium ion (blue) in SmP_5O_{14} crystal. The red spheres are the oxygen atoms of the PO_4 tetrahedra (yellow).

C_{2V} or even C_{1h}. Now the disappearance of some lines at the short wavelengths in each band, as the temperature is lowered, needs to be accounted for. One explanation would be the existence of an almost symmetry-non-breaking transition in this crystal from the pseudocubic local symmetry around the Sm^{3+} ion to another more regular cubic local symmetry with a slightly different crystal field; this would lead to the observed rearrangement of some line positions in each band while keeping others in almost the same locations. The local change in symmetry is such as to transform the distorted antiprism into a more regular antiprism, which would require only a small rearrangement of the tetrahedral units.

This is not the only possible explanation of the line disappearance at low temperatures. Another might have been transitions from the $^4F_{3/2}$ level, which is located at 18860cm^{-1} in the free ion (that is higher than the $^4G_{5/2}$ level) down to the multiplets that comprise the ^6H_j (Martin 1978). However calculations, which need not be detailed here, made of the fluorescence spectral line positions, which would occur in this case, show that they are on the higher, rather than the lower wavelength side, of each of the five bands. Furthermore the $^4F_{3/2}$ level is a singlet in an environment of cubic symmetry; so a transition from it to the $^6H_{5/2}$ (which is a doublet in cubic symmetry) would give only two lines in the vicinity of 5302Å. This has been tested experimentally. Due to the low level of the signal, to obtain the fluorescence in this region, it proved necessary to use wider slitwidths (both 200μ) and higher laser power (200mW) instead of the values of 100μ and 100mW employed to determine the spectrum shown in Figure 6.3(a,b). Figure 6.5 shows this particular part of the fluorescence spectrum at 300K; it consists of at least four observable lines (listed in Table 6.3), which have much lower intensities than those shown in Figure 6.3(a,b); these lines do not exist at 12K. Transitions from the $^4F_{3/2}$ level cannot correspond to the fluorescence lines which disappear at low temperature because (i) those vanishing lines are much stronger at room temperature than can be expected of transitions from $^4F_{3/2}$ and (ii) secondly their locations on the longer wavelength side of each band is not consistent with the observation that the disappearing lines are on the shorter wavelength side.

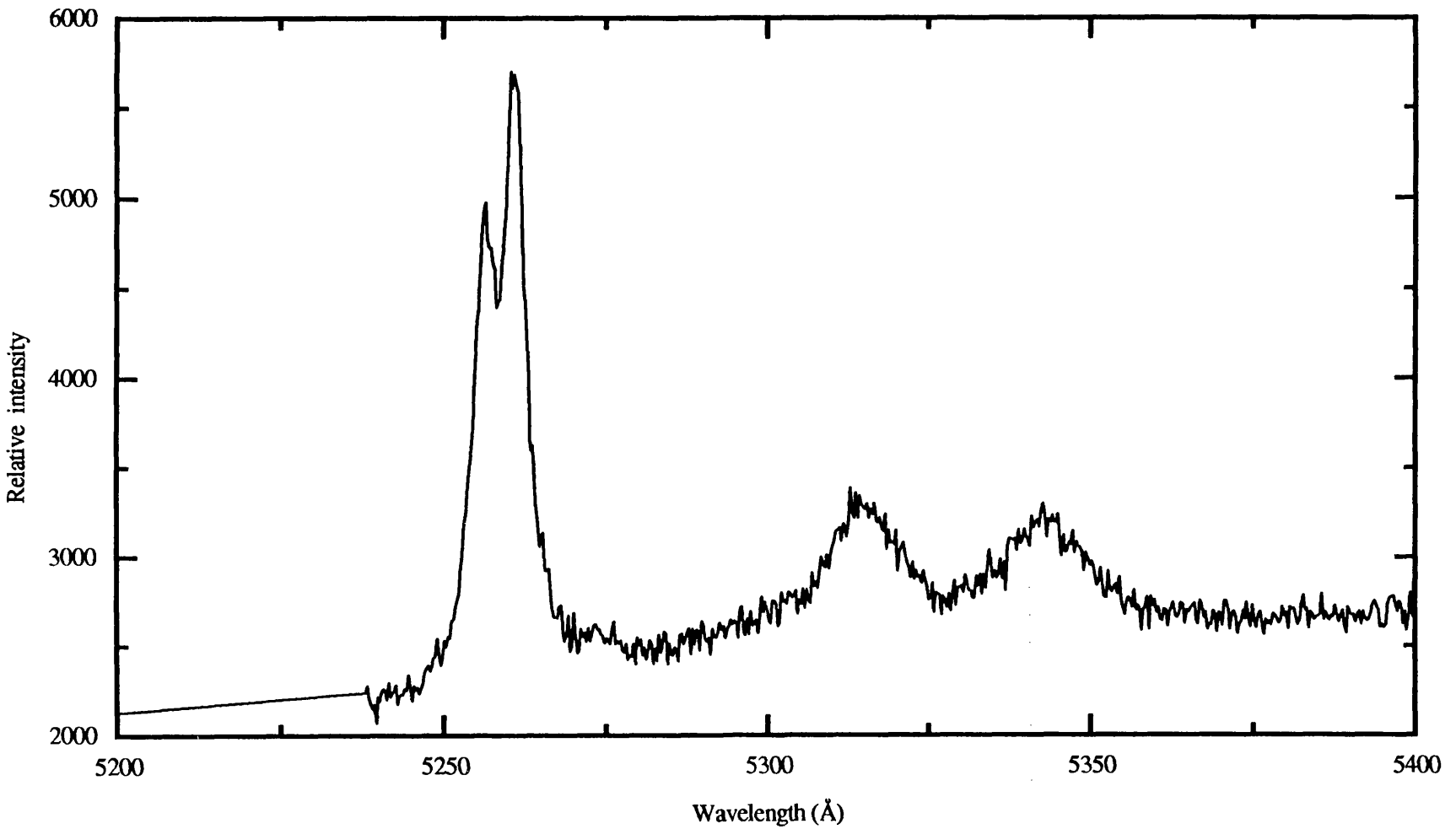

Figure 6.5. Low wavelength region fluorescence of monocrystalline smP_5O_{14} at 300K temperature (determined using 200μ slitswidths in the monochromator).

In principle, anti-Stokes Raman spectra induced from the fluorescent lines could be the source of the peaks seen on the shorter wavelength side of the bands at room temperature: anti-Stokes lines would disappear at low temperature. For example, if the strongest fluorescence line at 5947.4Å were to be an excitation source of an intrinsic Raman spectrum, it would then be responsible for the peaks on the short wavelength side of the first two bands. To test this possibility, Raman spectrum measurements have been made; this has become a study in itself and full details will be given in chapter 9. Suffice to say here that those studies have made it clear that, although the lines which disappear at low temperature do fit some positions which would be expected for anti-Stokes lines of the crystal, at room temperature they are much too strong and wide for them to be Raman lines induced by an intrinsic fluorescent source.

6.4. COMPARISON BETWEEN THE FLUORESCENCE SPECTRUM OF SAMARIUM METAPHOSPHATE GLASS AND PENTAPHOSPHATE CRYSTAL

By comparing the fluorescence of the samarium metaphosphate glass, with that of the pentaphosphate crystal useful insight can be gained about the local symmetries of Sm^{3+} ions in the glass. The fluorescence of the samarium metaphosphate glass $[(Sm_2O_3)_{0.19}(P_2O_5)_{0.81}]$ at 300K (dotted line) is overlapped on the spectrum at 10K (solid line) in Figure 6.2(a,b). As it does for the SmP_5O_{14} crystal (Figure 6.3(a,b) and Table 6.3), the fluorescence of the glass falls naturally into five bands, although, due to the existence of nonuniform, non-identical ligand fields caused by slightly different values of rare-earth oxygen distances (Reisfeld 1972), they are now much broadened and do not show the individual lines. Thus the fluorescence of the glass originates in the same Sm^{3+} transitions as in the crystal, namely those listed in Table 6.3. For the glass at both room temperature and 10K the intensity of the $^4G_{5/2} \rightarrow {}^6H_{9/2}$ band is not much higher than that of the $^4G_{5/2} \rightarrow {}^6H_{7/2}$ band (Figure 6.2a,b). By contrast for the crystal the intensities of these two fluorescence bands are very different in intensity (Figure 6.3a), probably due to the operation of selection rules for the crystal. Comparison between the spectra of the glass and the crystal both at room temperature and 12K show that the whole spectrum of the glass is shifted to-

wards longer wavelength. A comparison between fluorescence lines in the first three bands for the crystal and the glass at 12K shows the shifts clearly (Figure 6.6). In the first band the shift is about 33Å, in the second is about 24Å, and in the third band is about 33Å. The shift occurs even in the longer wavelength band region but its measurement is not reliable there due to the low level signal, the breadth of the bands and also because the high energy levels are more susceptible to crystal field effects. This shift towards the longer wavelength for the glass is an indication of a stronger ligand field around the Sm^{3+} ion in the glass than in the crystal.

EXAFS structural studies carried out recently on a range of rare earth metaphosphate $R(PO_3)_3$ glasses modified using the rare earth oxides Nd_2O_3, Eu_2O_3, Gd_2O_3, Tb_2O_3, Ho_2O_3 and Pr_6O_{11} have established that the glass skeleton is made up from linked PO_4 tetrahedra (Bowron et al. 1995, 1996). One of the four oxygen atoms in a PO_4 tetrahedron is doubly bonded to the phosphorus and may not take part in the network bonding. The rare earth ions occupy sites with an average coordination number of surrounding oxygen atoms in the range $6 \leq N \leq 8$. This is a common range for oxygen coordination in rare earth oxides and is consistent with a cubic or "pseudo-cubic" local environment for the R^{3+} ions. There is no evidence from EXAFS for rare-earth ions being adjacent to each other in the metaphosphate glasses, an important feature in relation to their magnetic or optical properties. Further structural indications can be obtained from the fractal dimensionality $4C_{44}/B$ (Bergman and Kantor 1984, Bogue and Sladek 1990). Ultrasonic pulse echo measurements have shown that the elastic stiffnesses of the glass of composition $(Sm_2O_3)_{0.248}(P_2O_5)_{0.752}$ studied here are C_{44} and bulk modulus B equal to 22.3GPa and 39.1GPa respectively giving a fractal dimensionality of 2.3 (Senin 1994) indicating that the connectivity of this glass falls between a two and three dimensional character. In the Reisfeld and Eckstein (1972) model, a rare earth ion in a phosphate glass is considered to occupy the centre of a distorted cube comprised of four phosphate tetrahedrons. An edge of the cube is formed by two oxygens belonging to a single tetrahedron. The coordination number of the rare earth ion in such an arrangement is eight oxygens. This model is consistent with the EXAFS structural

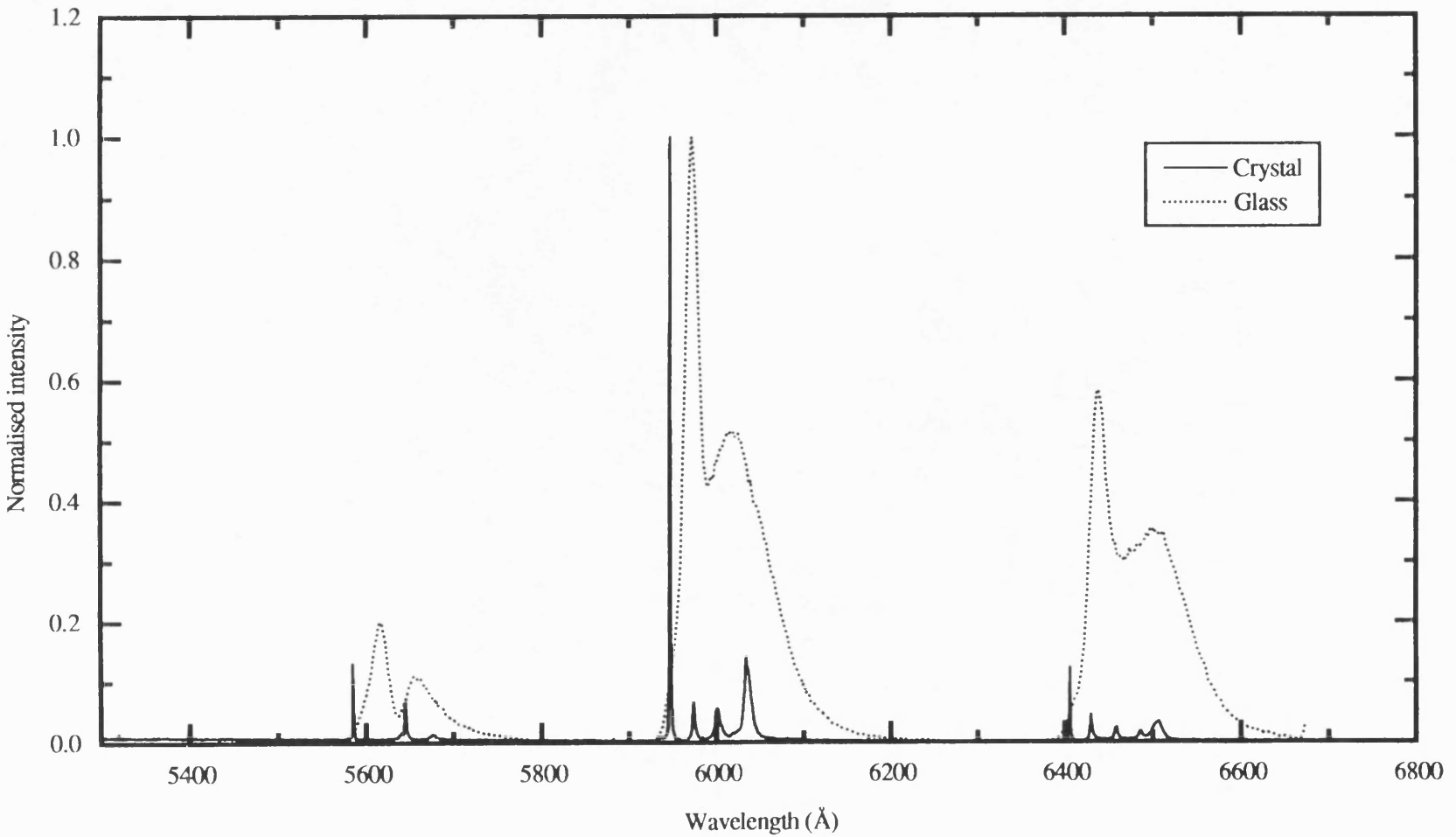

Figure 6.6. Comparison between the fluorescence spectra at 12K of the SmP_5O_{14} crystal and the $(Sm_2O_3)_{0.19}(P_2O_5)_{0.81}$ glass in the first three bands.

studies of other metaphosphate glasses. So picturing the rare-earth ion in these glasses as being at the centre of a distorted cube is useful practise.

When the glass is cooled down to 10K, one obvious feature is the disappearance of the tail on the short wavelength side for each of the five fluorescence bands (solid line in Figure 6.2(a,b)). This appears to be a counterpart of the disappearance of the shorter wavelength lines in the crystal fluorescence as the temperature is reduced (Figure 6.3a,b), which was attributed earlier to a nearly symmetry non-breaking phase transition of the cubic local structure. It is tempting to suggest that the glass undergoes a similar change in the local environment of the Sm^{3+} to that postulated for the crystal. Such a transition in the SmP_5O_{14} crystal or in the metaphosphate glass from pseudocubic local symmetry to another more regular cubic local symmetry with a slightly different crystal field, would require a slight structural rearrangement of the linked PO_4 tetrahedra; this would be likely to involve mode softening. In fact vitreous samarium metaphosphate shows anomalous elastic behaviour as a function of temperature and pressure (Mierzejewski et al. 1988, Carini et al. 1990, Senin et al. 1993). The hydrostatic pressure derivatives $(\partial C_{11}/\partial P)_{T,P=0}$ and $(\partial C_{44}/\partial P)_{T,P=0}$ of the elastic stiffness tensor components are negative: the long-wavelength acoustic modes soften under pressure. The hydrostatic pressure derivative $(\partial B^s/\partial P)_{T,P=0}$ of the adiabatic bulk modulus is negative; the glass becomes easier to squeeze when subjected to high pressure (Mierzejewski et al. 1988). Production of this markedly anomalous elastic behaviour of the samarium phosphate glasses requires a strong stress wave interaction. Previously it was inferred that one possible source of this behaviour could be pressure varying, volume sensitive, mixed valence of the samarium ion. The present study of fluorescence of the samarium phosphate glasses has been carried out to examine this possibility. Since divalent samarium ion is found to be absent or at most in very small concentration, there cannot be enough intermediate valence samarium present to produce the large elastic anomalies which are observed. The physical origin of this acoustic mode softening was suggested to be nonlinear acoustic contributions from bending vibrations of the bridging oxygen atoms, which correspond to transverse motion against small force constants, or rotations of the coupled PO_4 tetrahedra (Bergman et al. 1984, Bogue and Sladek 1990, Carini et al. 1990). This is consis-

tent with the suggestion the fluorescence line disappearances at low temperature in the metaphosphate glass may result from a slight structural change involving a rearrangement of the linked PO_4 tetrahedra possibly driven by a soft acoustic mode.

6.5. HIGH PRESSURE EFFECTS ON THE FLUORESCENCE SPECTRA OF SAMARIUM METAPHOSPHATE GLASS AND PENTAPHOSPHATE CRYSTAL

To record the fluorescence spectra of the samarium metaphosphate glass and the pentaphosphate crystal under high pressures at room temperature, the assembled optical system, described in chapter 3, was used. The single grating monochromator with 1200lines/mm was employed with its slitwidths set at 200μ in the case of the glass and 100μ for the crystal. The fluorescence spectra of the $(Sm_2O_3)_{0.248}(P_2O_5)_{0.752}$ glass and SmP_5O_{14} crystal were induced using the 4765Å argon ion laser line with the laser power varied between 100mW and 300mW as needed according to the strength of the fluorescence signal. The pressure was generated by the diamond anvil cell (DAC). The gasket in the DAC was made of hard stainless steel, 0.3mm thick, with a 0.35mm diameter hole drilled in its centre. A glass sample of about 100μ was placed in the gasket hole. It was accompanied by a chip of ruby of about 50μ in size for pressure measurement; both were surrounded by a 4:1 methanol-ethanol liquid mixture which comprised the hydrostatic pressure medium (Piermarini et al. 1973). The pressure level in the DAC was determined by measuring the shift of the ruby 6942Å fluorescence line and using the calibration equation $\partial\lambda/\partial P$= 0.365Å/kbar (Piermarini and Block 1975). The fluorescence spectra were recorded at various pressures between 1bar and 50kbar in steps of about 5 kbar. To ensure high resolution and accurate measurement of the ruby calibration line, the slitwidths of the monochromator were set at 50μ, which then enables accurate determination of the pressure exerted in the DAC. The error in the pressure measurement was ±1kbar and the experimental error in wavelength measurement of the spectra of the crystal and glass was ±2Å. The procedure used for loading the DAC with the samples and the method of generating high pressure have been described in details in chapter 2. Figure 6.7 shows the fluorescence spectrum of the samarium metaphosphate glass, having the composition

$(Sm_2O_3)_{0.248}(P_2O_5)_{0.752}$, under atmospheric pressure (solid line) overlapped onto that obtained at 50kbar (dotted line). Within the range of the applied pressure no significant changes in the fluorescence spectrum were observed; the same profile, width and band positions of the broad fluorescence peaks. The whole fluorescence spectrum of the glass at 50Kbar was shifted vertically due to the high level of noise present cause by high level of light scattering in the DAC pressure chamber. The small peaks in the vicinity of 6700Å are caused by the ruby fluorescence lines (Figure 6.7).

The effect of pressure on the wavelengths of the laser induced fluorescence lines of the SmP_5O_{14} crystal can be seen in Figure 6.8 which shows the fluorescence spectrum obtained under a pressure of 50kbar superimposed on that determined at atmospheric pressure. The positions of the fluorescence lines of the crystal under pressure of 50kbar and room temperature are given in Table 6.4. The wavelength λ of the lines increases approximately linearly with pressure; as an example, the effect of pressure on the lines in the $^4G_{5/2} \rightarrow {}^6H_{7/2}$ transition band is shown in Figure 6.9. Under pressure all lines shift towards longer wavelengths; the pressure derivatives ($d\lambda/dP$) determined from the experimental data are listed in Table 6.3. Bands sited at wavelengths more than 6800Å have low intensity and overlap with ruby chip fluorescences so it was not possible to measure their pressure shifts in the DAC. An experimental feature shown by SmP_5O_{14} is polarisation of some of the fluorescence lines in the bands, when the crystal is oriented at different angles. The relative intensities of some of the lines (5550Å, 6038Å, and 6408Å) at 50kbar increase is due to a change of the orientation of the sample during application of pressure; these lines are directionally polarised. The most pronounced polarisation effects observed were a moderate increase in intensity of the lines at 5550Å (first band), 6038Å (second band), 6408Å (third band) while the remainder keep their original intensities in all other orientations. Within the range of the applied pressure neither the fluorescence spectrum of the samarium pentaphosphate crystal nor that of the samarium phosphate glass show any essential changes.

These results add further support to the idea that the samarum ion valency is 3+ in the pentaphosphate crystal and metaphosphate glass and does not change with pressure.

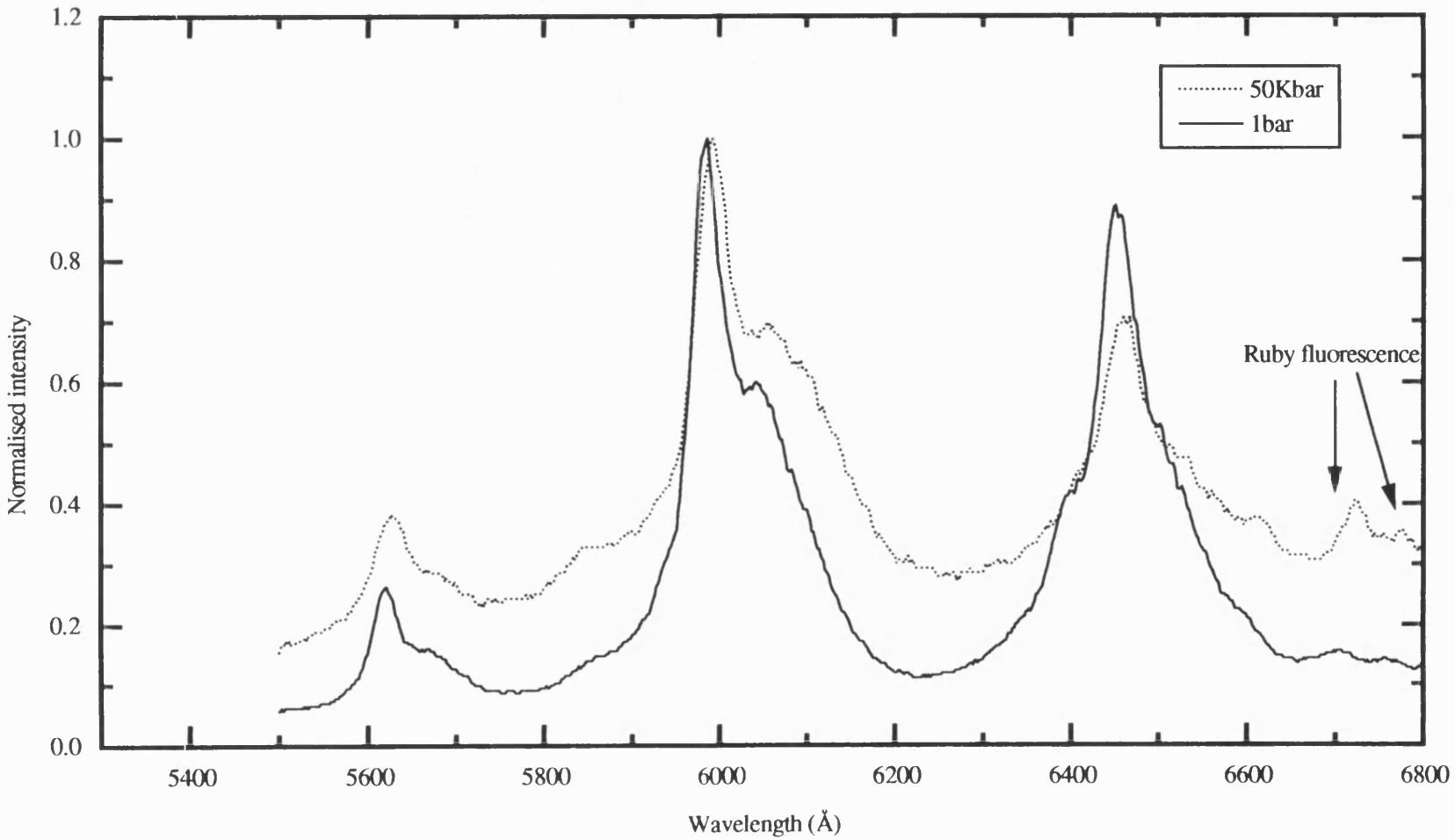

Figure 6.7. The effect of pressure on the fluorescence spectrum of the $(Sm_2O_3)_{0.19}(P_2O_5)_{0.81}$ glass measured at 292K in the short wavelength region.

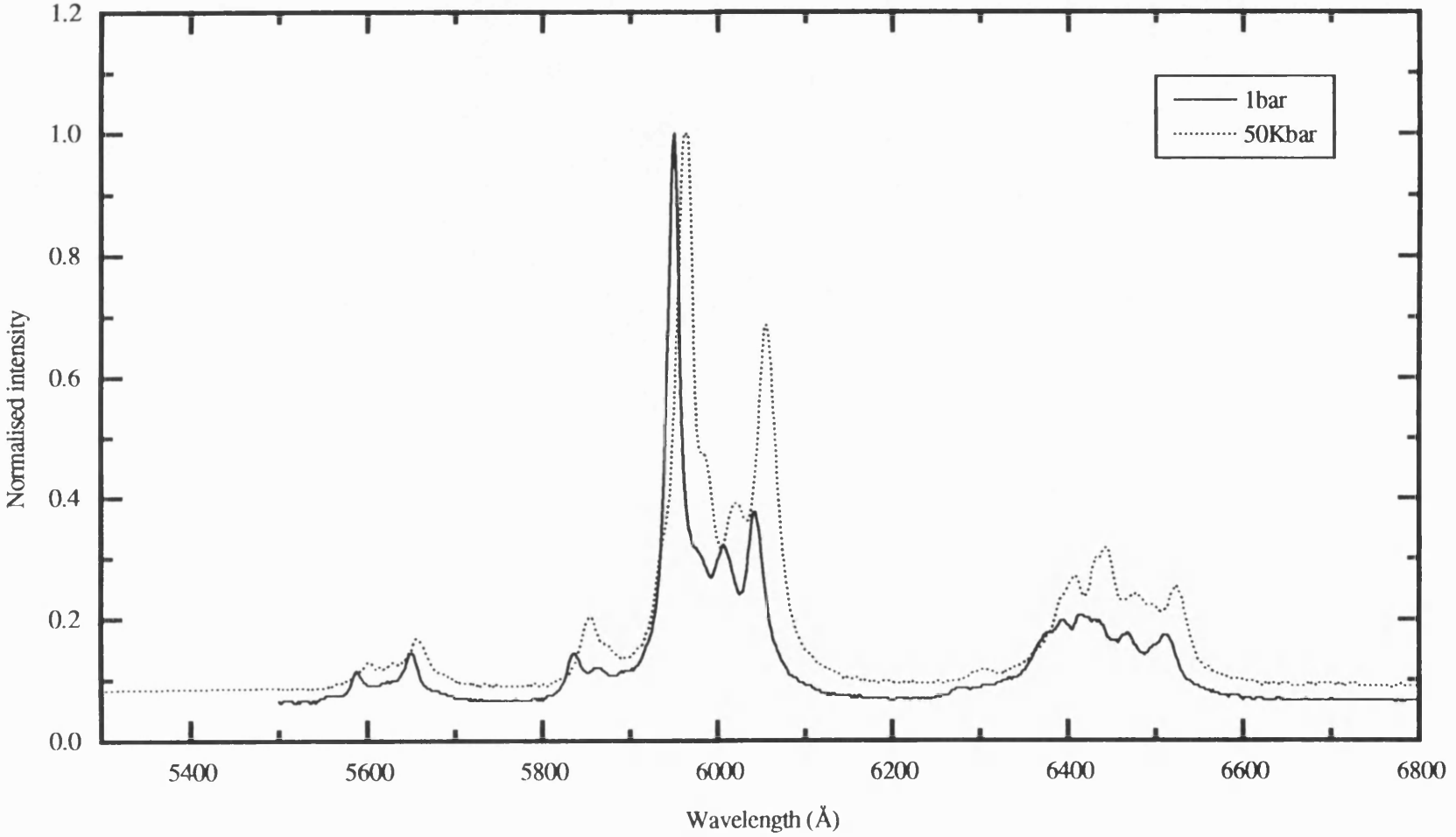

Figure 6.8. The effect of pressure on the fluorescence spectrum of monocrystalline SmP_5O_{14} in the short wavelength region at 292K.

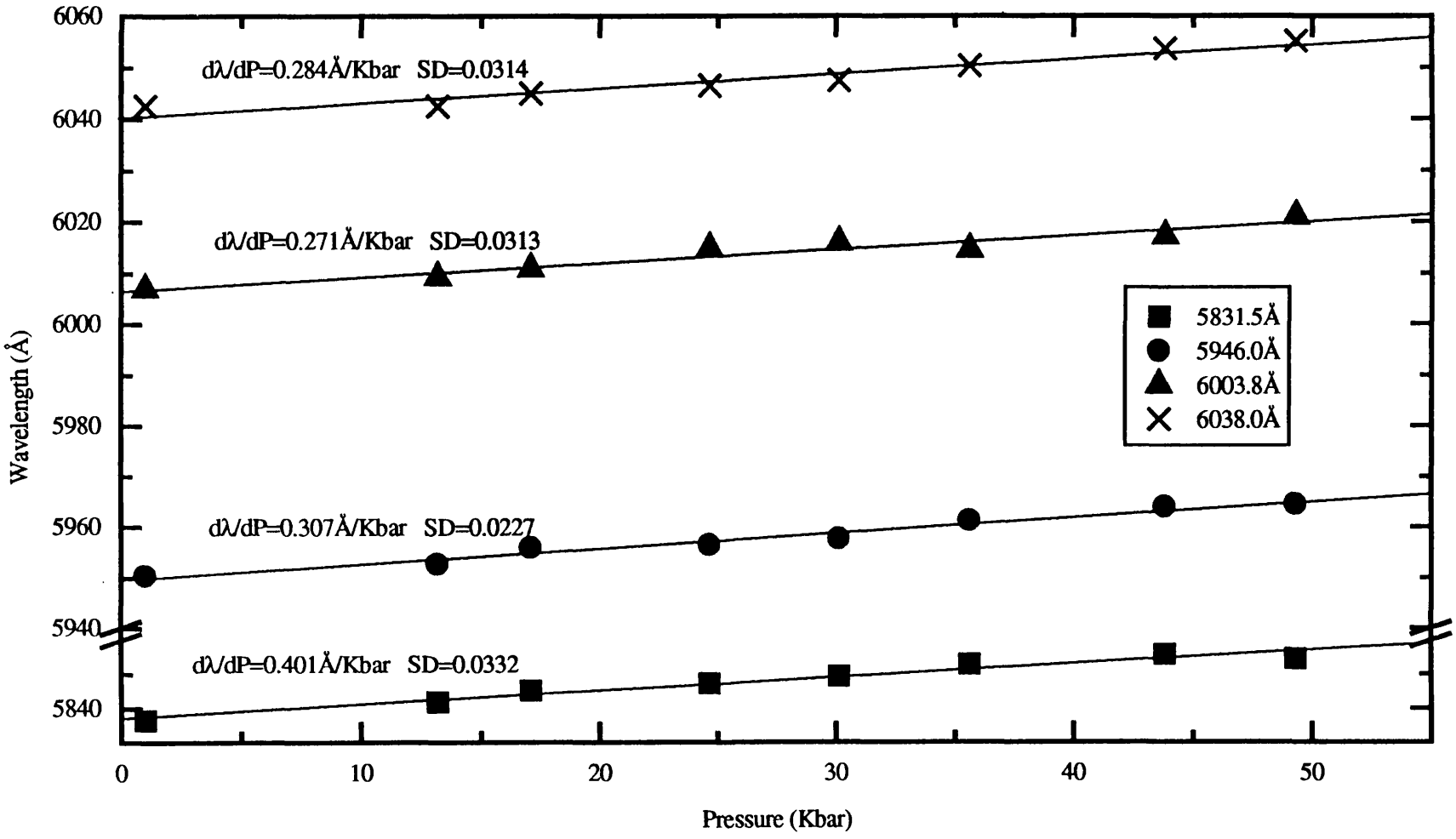

Figure 6.9. The effect of pressure on the wavelength of the fluoresence lines in the $^4G_{5/2} \rightarrow {}^6H_{7/2}$ transition band for the SmP_5O_{14} crystal at 292K. Linear fittings were applied and the pressure derivatives are indicated on each line.

Table 6.4. The effect of pressure on the wavelengths of some of the fluorescence lines of the spectrum of the samarium pentaphosphate crystal measured at room temperature.

Fluorescence line wavelengths (Å) of SmP_5O_{14} crystal under atmospheric pressure.	Fluorescence line wavelengths (Å) of SmP_5O_{14} crystal at 50kbar pressure	Pressure derivatives [$d\lambda/dp$ (Å/kbar)] of some of the fluorescence lines of the SmP_5O_{14} crystal
5256.5	—	—
5260.3	—	—
5314.3	—	—
5342.7	—	—
5550.6	—	—
5584.1	5601.5	0.316
—	—	—
5646.5	5656.4	0.155
5674.7	—	—
5831.5	5854.5	0.401
5858.9	—	—
5888.5	—	—
—	—	—
5946.0	5964.4	0.307
5971.5	5984.4	—
6003.8	6021.0	0.271
—	—	—
6038.0	6055.9	0.284

CHAPTER SEVEN

LOW TEMPERATURE AND HIGH PRESSURE EFFECTS ON THE FLUORESCENCE SPECTRA OF TERBIUM METAPHOSPHATE GLASS AND PENTAPHOSPHATE CRYSTAL

7.1. INTRODUCTION

In the previous two chapters, absorption and fluorescence measurements were used to investigate and identify the valency and the local symmetry of the europium and samarium ions in the metaphosphate glasses and pentaphosphate crystals. Here the same procedure and arguments will be used in an examination of fluorescence of terbium metaphosphate glass and pentaphosphate crystal made in part to look for any general similarities or differences among the rare earth phosphate matrices. The fluorescence spectra of terbium metaphosphate glass having the composition $(Tb_2O_3)_{22.6}(P_2O_5)_{77.4}$, and TbP_5O_{14} crystal have been measured and compared, in the temperature range 12-300K, to provide direct information on the terbium ion valency and local symmetry. An important observation is that the fluorescence spectra of these glasses and crystals are much stronger than the rest of the rare earth metaphosphate glass and pentaphosphate crystal samples studied here (specially at low temperatures) which may make them good candidates as lasing materials. Further, the fluorescence spectrum of the $(Tb_2O_3)_{22.6}(P_2O_5)_{77.4}$ glass has been measured under high pressures, using the diamond anvil cell, to search for phase transition and any valency change under pressures.

X-ray measurements on the structure of TbP_5O_{14} crystal have shown that the lattice is either monoclinic (pseudo-orthorhombic) having the dimensions a=12.91Å b=8.887Å c=8.728Å β =90.49° or body-centred monoclinic with all three axes nearly equal a=12.91Å b=12.80Å c=12.48Å and β =91.31° (Beucher 1970). The unit cell of crystal contains 4 molecules of TbP_5O_{14}.

7.2. ROOM TEMPERATURE ABSORPTION AND LOW TEMPERATURE FLUORESCENCE SPECTRA OF TERBIUM METAPHOSPHATE GLASS

To obtain an intense fluorescence spectrum of the terbium metaphosphate glass, it is essential to measure the absorption spectrum first to find out which of the laser lines coincide with one of its absorption bands. The absorption spectrum was recorded in the range 200-750nm, at room temperature, using a standard commercial double-beam instrument (Perkin-Elmer). Figure 7.1 shows the absorption spectrum of a terbium metaphosphate glass sample, having the composition $(Tb_2O_3)_{22.6}(P_2O_5)_{77.4}$. The absorption band peaks are listed in Table 7.1, along with known data for the Tb^{3+} ion (Carnall et al. 1968). Trivalent terbium ion (Tb^{3+}) has a ground state of $^7F_6$, which results from its $4f^8$ electronic configuration. According to the energy level scheme of Dieke and Crosswhite (1963), absorption bands of Tb^{3+} ion can arise from transitions between the ground $^7F_6$ state and higher states of the f orbital such as $^5D_4$ $^5D_3$,$^5G_6$, $^5L_{10}$,$^5G_5$ etc. (Figure 5.1). A comparison between the absorption bands of the terbium metaphosphate glass (column 1) and reported ones of Tb^{3+} ion (column 2) shows a good agreement between both sets which establishes that the bands observed for $(Tb_2O_3)_{22.6}(P_2O_5)_{77.4}$ glass are typical of trivalent terbium ion (Table 7.1). Below 350nm the spectrum shows a broad absorption band which is continuous down to 200nm. This is believed to be a combination of the high energy bands of the terbium (as this region comprises dense energy levels $^5D_1$, $^5D_0$,$^5H_7$, $^5H_6$,$^5H_5$, $^5H_4$, $^5F_5$, $^5H_3$, $^5I_8$, $^5F_4$) and the intrinsic absorption of the glass matrix (Figure 5.1).

The fluorescence spectrum of the terbium metaphosphate glass, having the composition $(Tb_2O_3)_{22.6}(P_2O_5)_{77.4}$, was measured in the temperature range 12-300K using the optical system described in chapter 9. The spectrum was excited using the 4880Å laser line of the argon ion and the lasing power was varied (within 30mW) according to the strength of the fluorescence in the wavelength range studied. Due to the intense and relatively broad fluorescence bands of this glass, the slitwidths of the triple monochromator were set at 100μ and the scanning speed at $4cm^{-1}$/second. Figures 7.2(a and b) show the normalised fluorescence spectrum of the $(Tb_2O_3)_{22.6}(P_2O_5)_{77.4}$ glass measured at 300K overlapped on the spectrum measured at 12K in the wavelength range of 5200-7000Å. At both temperatures the spectrum

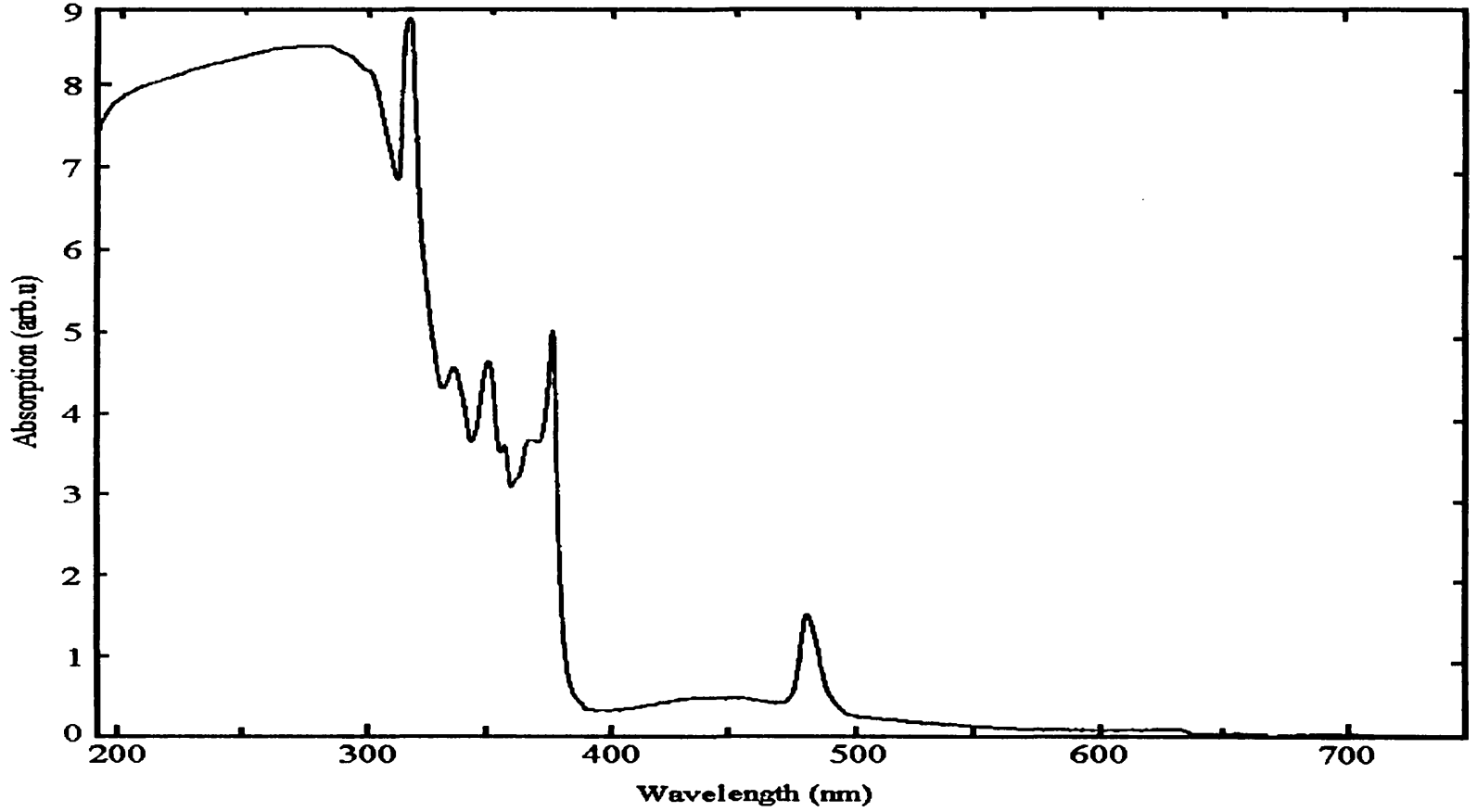

Figure 7.1. The absorption spectrum of $(Tb_2O_3)_{22.6}(P_2O_5)_{77.4}$ glass measured at room temperature.

Table 7.1. Measured wavelengths of the absorption bands at room temperature of $(Tb_2O_3)_{22.6}$ $(P_2O_5)_{77.4}$ glass compared with the wavelengths of the absorption bands of Tb^{3+} ion (Carnall et al. 1968). The transitions, which are responsible for these absorption, are quoted from the same reference.

Wavelength (nm) $(Tb_2O_3)_{22.6}$ $(P_2O_5)_{77.4}$ glass	Wavelength (nm) Tb^{3+} ion	Transition
480.28	500 - 471	$^5D_4 \leftarrow {}^7F_6$
376.05 364.78	386 - 362	$^5D_3, {}^5G_6, {}^5L_{10} \leftarrow {}^7F_6$
356.33	362 - 345	$^5G_5, {}^5D_2, {}^5G_4, {}^5L_9 \leftarrow {}^7F_6$
349.29	345- 331	$^5G_3, {}^5L_8, {}^5L_7, {}^5L_6, {}^5G_2 \leftarrow {}^7F_6$
336.62	328 - 323	$^5D_1 \leftarrow {}^7F_6$
316.90	323- 312	$^5D_0, {}^5H_7 \leftarrow {}^7F_6$
300-200	307 - 298	$^5H_6 \leftarrow {}^7F_6$
300-200	297 - 293	$^5H_5 \leftarrow {}^7F_6$
300-200	290 -279	$^5H_4, {}^5F_5, {}^5H_3, {}^5I_8, {}^5F_4 \leftarrow {}^7F_6$

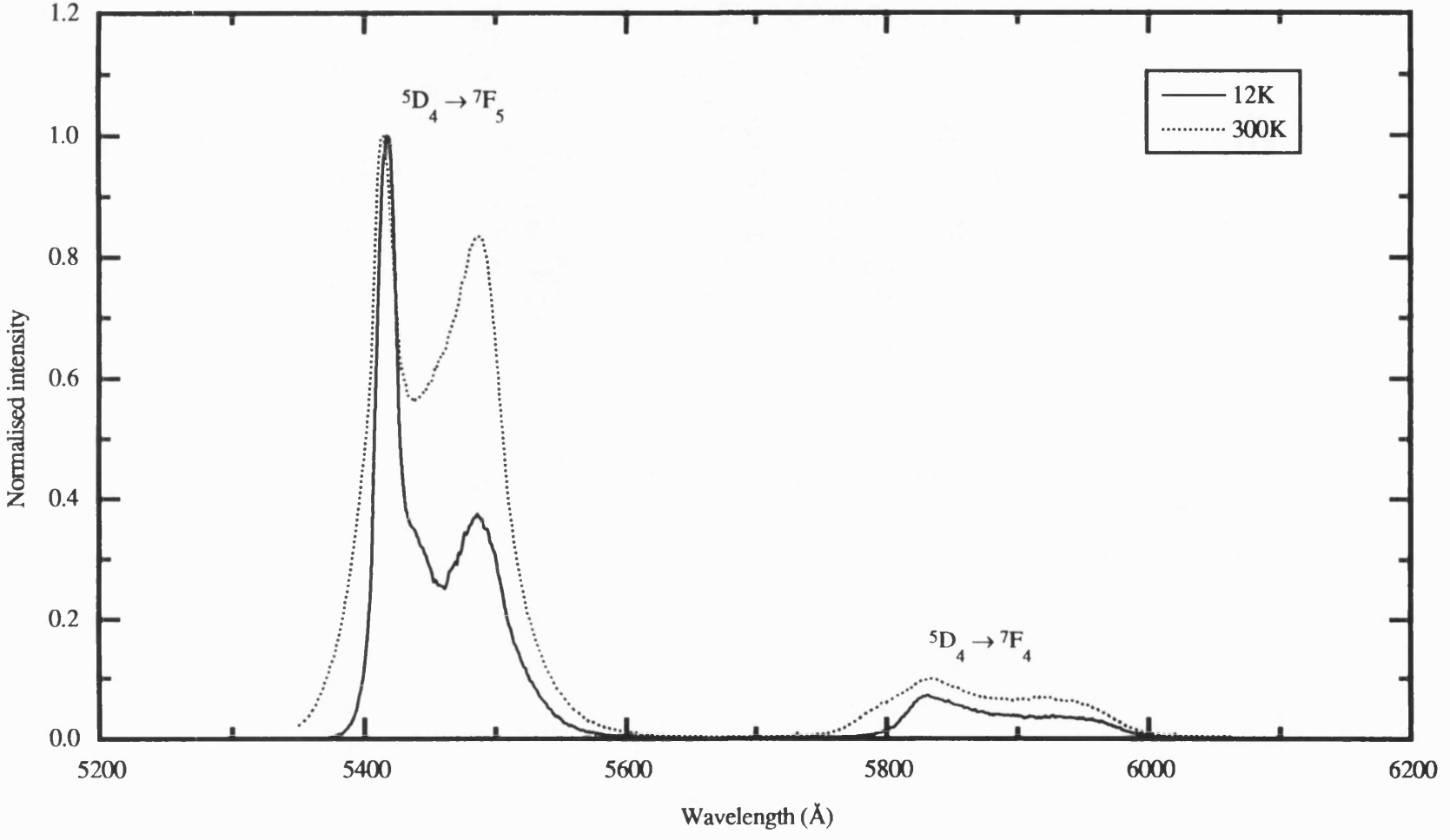

Figure 7.2a. The fluorescence spectrum of $(Tb_2O_3)_{22.6}(P_2O_5)_{77.4}$ glass excited by the blue 4880Å argon ion laser line.

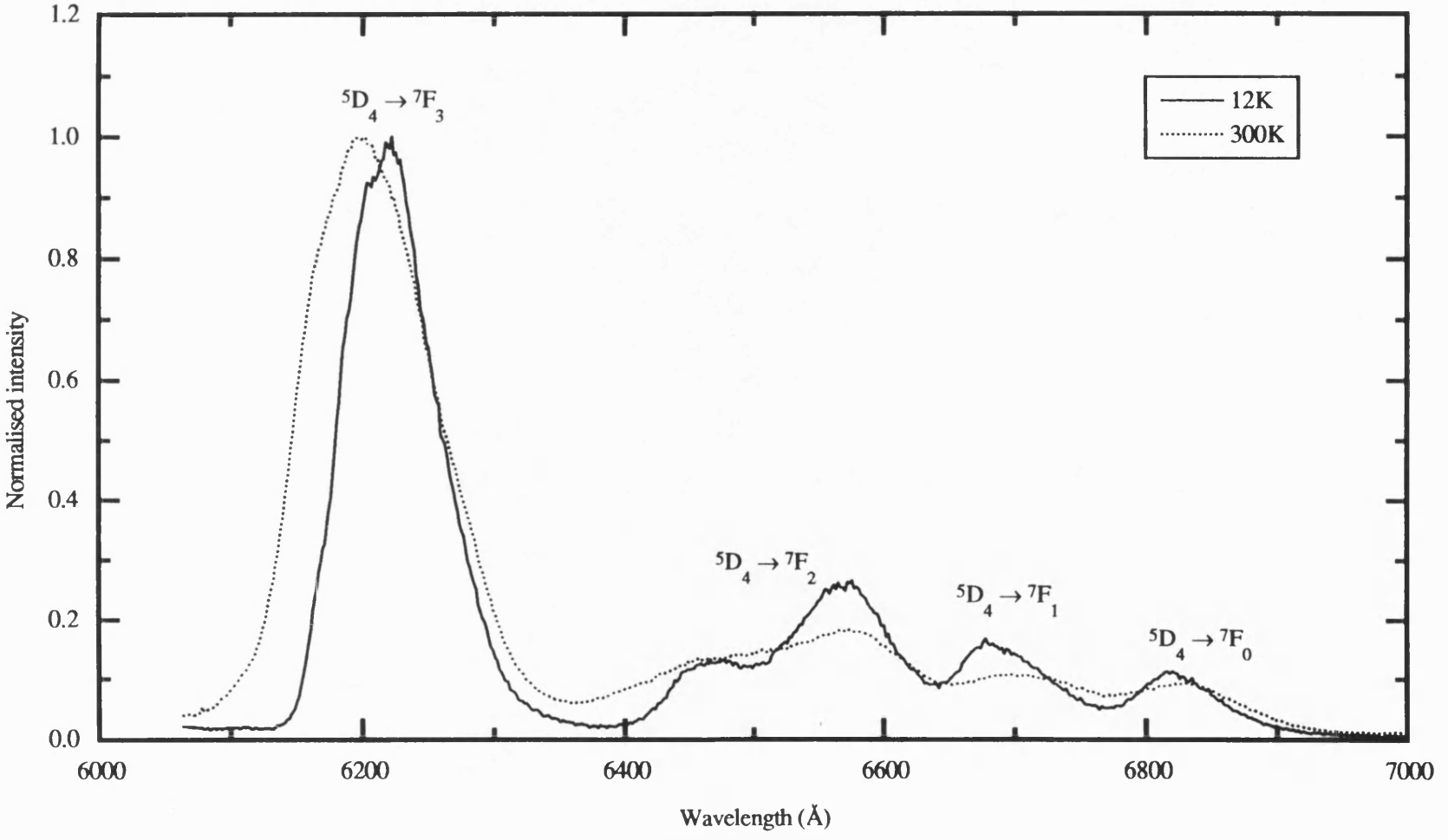

Figure 7.2b. The continuation of the fluorescence spectrum of the $(Tb_2O_3)_{22.6}(P_2O_5)_{77.4}$ glass excited by the blue 4880Å argon ion laser line.

shows the same profile, but in the spectrum obtained at 300K the bands are broader due to thermal broadening. In order to measure fluorescence bands positioned at wavelengths shorter and around the 4880Å region, the 4579Å laser line was used as an excitation source. Figure 7.3 shows the fluorescence band obtained, measured at 300K, which has two distinct peaks at around 4879Å and 4938Å. Therefore, the overall spectrum of the glass has seven well-separated bands (Figures 7.2a,b and 7.3). Fluorescence bands of trivalent terbium ion can be attributed to transitions from the $^5D_4$ and $^5D_3$ excited states to the lower ^7F_j states (Figure 5.1), where J= 6,5,4,3,2,1,0 (Dieke and Crosswhite 1963). Therefore, the spectrum of Tb^{3+} ion is expected to have seven fluorescence bands resulting from transitions between the $^5D_4$ high state and the multiplets of the $^7F_{6,5,4,3,2,1,0}$ states when any of the argon ion laser blue lines is used. Fluorescence bands originating from transitions between the $^5D_3$ excited state and the manifold of the ^7F_j states are not possible to excite here since the wavelength corresponding to the $^5D_3$ excited state is 3800Å, which is out of the wavelength range of the argon ion laser lines (the lowest wavelength available is the 4579Å laser line). Hence, to establish the valency of the Tb ion in the metaphosphate glass, the experimental fluorescence bands measured at 12K (Figure 7.2a,b) have been listed in Table 7.2 and compared with reported fluorescence bands of Tb^{3+} ion in borate glass (Reisfeld 1972). The close similarity between the numbers and the wavelengths of the experimental fluorescence bands (column 1) and the reported data (column 2) verifies that valency of the Tb ions in $(Tb_2O_3)_{22.6}(P_2O_5)_{77.4}$ glass is trivalent. The transitions responsible for the fluorescence bands of the glass are labelled on each band in Figures 7.2 and 7.3. and listed in Table 7.2.

Fluorescence bands and Raman bands occasionally interfer in the spectral region closer to the laser line used as excitation source. Therefore to detect such interference another laser line was used to excite the spectrum of terbium metaphosphate glass to look for shifts and band changes. Figure 7.4 shows the first part of the spectrum (between 5145Å and 5600Å) excite by the 5145Å laser line and measured at 12 and 300K. The spectrum at 300K shows an intense band having two peaks, one located at around 5417Å and the other at 5486Å, and another two weak bands at 5339Å and 5235Å. The fluorescence peaks at 5417Å and 5486Å can be attrib-

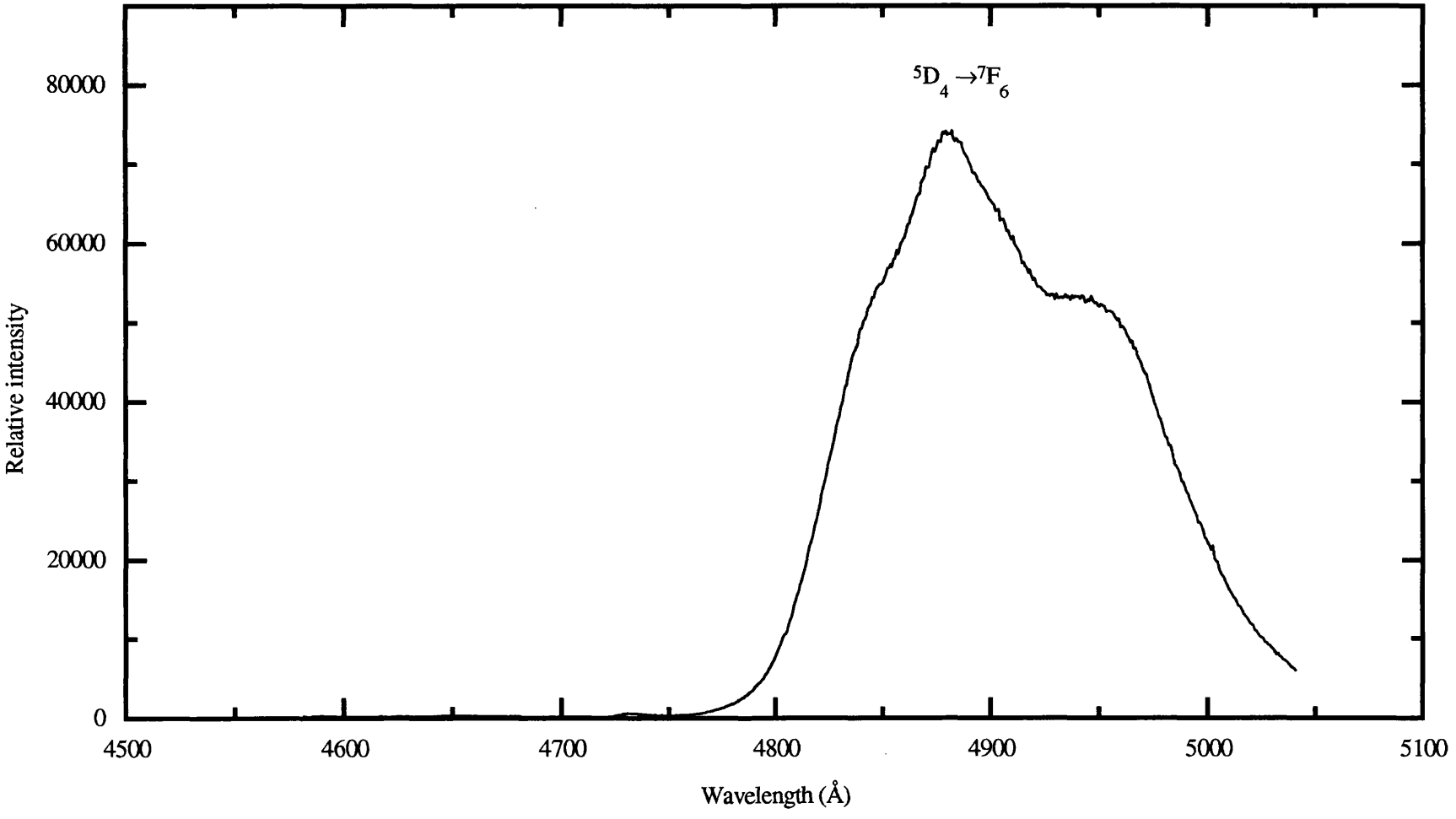

Figure 7.3. The fluorescence spectrum of $(Tb_2O_3)_{22.6}$ $(P_2O_5)_{77.4}$ glass measured at 300K and excited by the 4579Å laser line.

Table 7.2. Measured wavelengths of the fluorescence band peaks at 12K of $(Tb_2O_3)_{22.6}(P_2O_5)_{77.4}$ glass (excited by the 4880Å laser line) compared with the wavelengths of the fluorescence lines of Tb^{3+} ion in borate glass (Reisfeld 1972). The transitions which are responsible for these absorption are quoted from the same reference. The sign * refers to the fluorescence bands excited using the 4579Å argon ion laser line.

Wavelength (Å) $(Tb_2O_3)_{22.6}(P_2O_5)_{77.4}$ glass	Wavelength (Å) Tb^{3+} ion in borate glass	Transition
4880.9* 4938.53*	4860	$^5D_4 \rightarrow {}^7F_6$
5417.4 5486.3	5410	$^5D_4 \rightarrow {}^7F_5$
5831.9 5942.8	5850	$^5D_4 \rightarrow {}^7F_4$
6222.3	6240	$^5D_4 \rightarrow {}^7F_3$
6472.0 6569.0		$^5D_4 \rightarrow {}^7F_2$
6679.5		$^5D_4 \rightarrow {}^7F_1$
6819.8		$^5D_4 \rightarrow {}^7F_0$

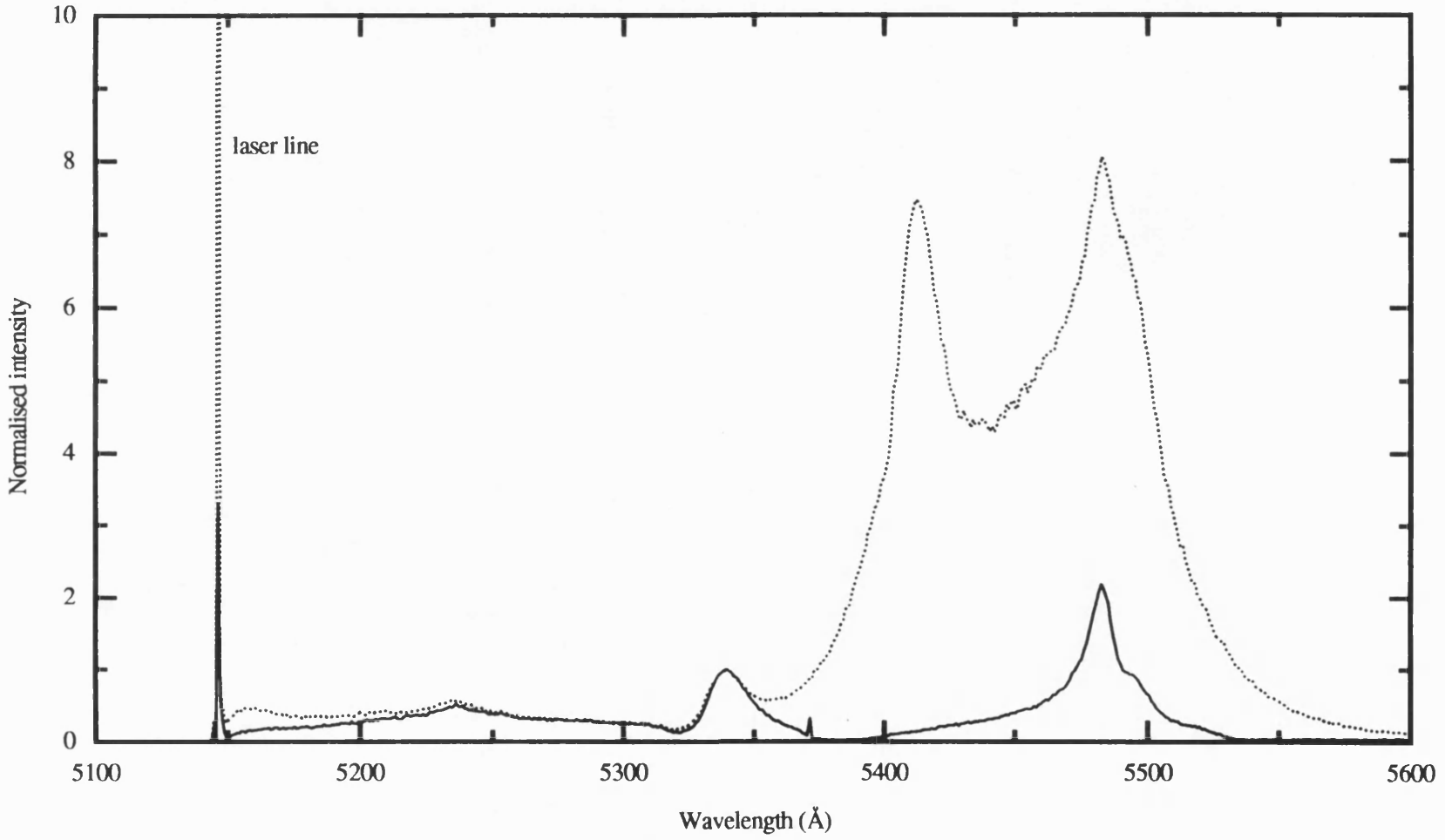

Figure 7.4. The fluorescence spectrum of $(Tb_2O_3)_{22.6}(P_2O_5)_{77.4}$ glass measured at 12K (full line) and 300K (dotted line) excited using the 5145Å laser line.

uted to the transition $^5D_4 \rightarrow {}^7F_5$ since they have the same wavelengths and profiles (although they are broader due to using wider slitwidths, 200μ) as the ones excited by the 4880Å laser line (Figure 7.2a). At 12K, the 5417Å and 5486Å fluorescence peaks ($^5D_4 \rightarrow {}^7F_5$ transition) disappear and instead a weak band can be seen at around 5483Å which must have been embedded under this fluorescence band. Careful inspection of the overall profile and locations of the bands shown in the 12K spectrum shows that these bands are typical of rare earth metaphosphate glass Raman bands (see chapter 9 for full explanation of these Raman bands). In fact when the 12K spectral data are converted to frequency shift in unit cm^{-1} and redrawn, as in Figure 7.5, the main Raman bands located at around 338, 707, 1196, and 1230cm^{-1} are shown up. At room temperature, the 5145Å laser line falls on the edge of 480.2nm absorption band (Figure 7.1). Therefore fluoresence bands can be excited with high intensity. But at 12K the 480.2nm absorption band would become sharper and the 5145Å laser line will be outside this band, which in turn causes no absorption and eventually no fluoresence. Therefore, the disappearance of the fluorescence band related to the $^5D_4 \rightarrow {}^7F_5$ transition at 12K (Figure 7.4) can be attributed to sharpening of the absorption band at 480.2nm.

The main purpose of lowering the temperature of the terbium phosphate glass to 12K was to reduce the thermal broadening of the fluorescence bands in order to observe the fluorescence components of each band (the splitting). Unfortunately, even at 12K the fluorescence bands retained their overall shape and did not show any clear splitting; this made it difficult to identify the local symmetry of the Tb ion in the metaphosphate glass matrix. However, two important effects due to temperature reduction can be noticed in the spectrum. First, the fluorescence bands sharpen more on the higher frequency side of each band (dotted lines in Figure 7.2a,b). Secondly, the intensity of some of the fluorescence bands varies; the intensity variation can not be seen in the spectrum as they are normalised, but the measurements showed an increase of about 3 times in the $^5D_4 \rightarrow {}^7F_5$ transition (Figure 7.2a), and a decrease of about 10 times in the intensity of the $^5D_4 \rightarrow {}^7F_3$ transition (Figure 7.2b).

Due to difficulties in measuring the room temperature Stokes Raman bands of the terbium metaphosphate glass trials were made to record the anti-Stokes Raman

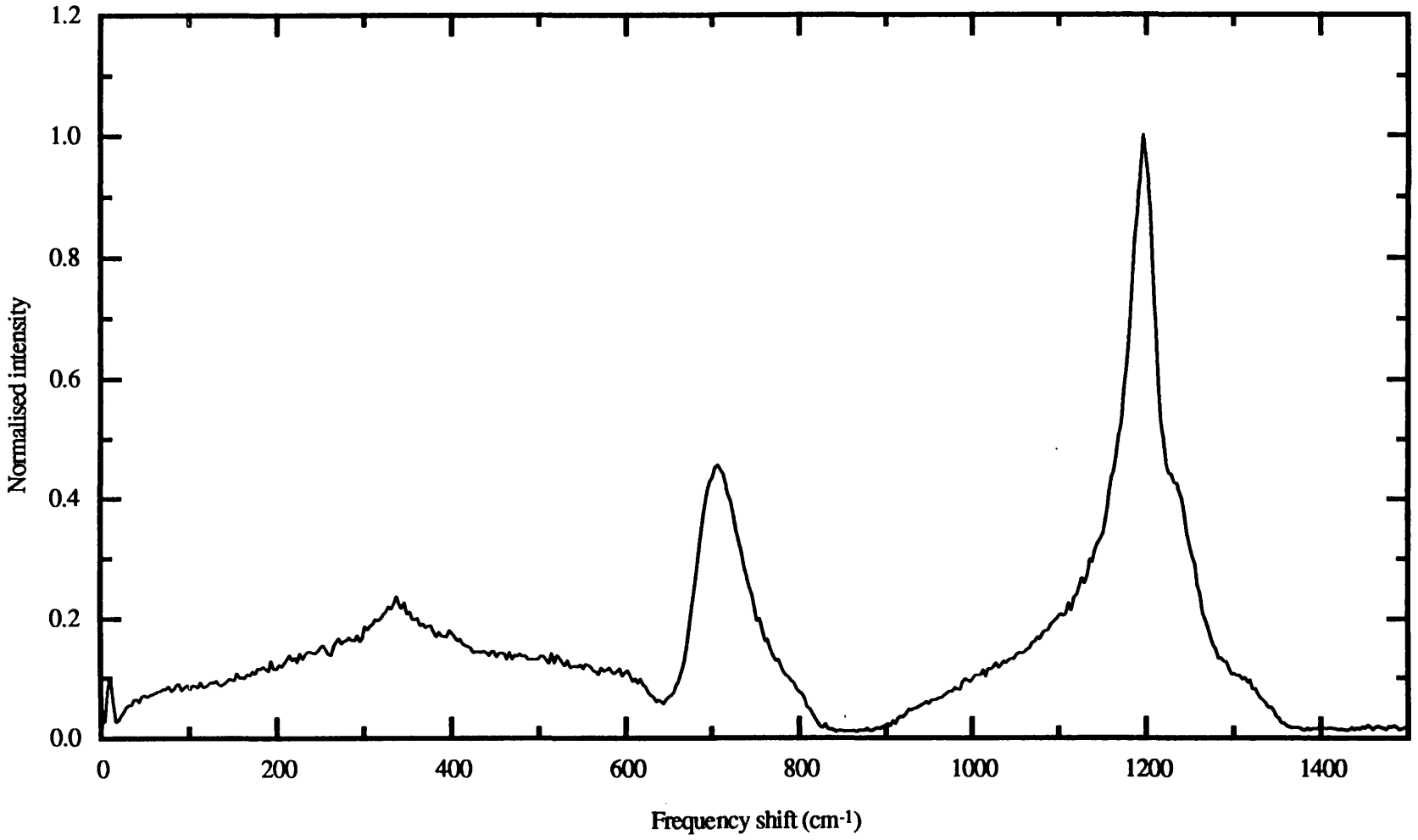

Figure 7.5. The fluorescence spectrum of $(Tb_2O_3)_{22.6}(P_2O_5)_{77.4}$ glass measured at 12K excited by the 5145Å argon ion laser line. The bands are typical of Raman bands of the rare earth metaphosphate glasses.

bands instead. To our surprise, the measurements showed an intense fluorescence tail on this frequency side (above the laser line frequency) and no sign of the Raman bands. Therefore, detailed spectral measurements were made in the high frequency region to investigate this phenomenon. The fluorescence spectrum of glass was recorded on both sides of the 4880Å laser line, at different temperatures, under the same conditions used above to obtain a reliable comparison. Figure 7.6 shows the wavelength region related to the $^5D_4 \rightarrow {}^7F_6$ transition measured at 12, 100, and 300K. It is evident from the figure that there is a fluorescence tail on the high frequency side of the laser line which extends about 100Å towards lower wavelength (higher frequency) beyond the laser line. The intensity of this tail (as well as the intensity of rest of the band on the lower frequency side) decrease with temperature reduction in a coherent manner. It can be speculated that this tail on the higher frequency side could be caused by phonon-assisted fluorescence; hence the 4f electrons of the Tb ion would be assisted in climbing to higher levels within the band of $^5D_4$ excited states (higher than the energy of the laser line, which falls in the middle of the broad $^5D_4$ band) by absorbing phonons. The Raman spectra of rare earth metaphosphate glasses show the highest energy phonon at around 1200cm^{-1}, a medium one at around 700 cm^{-1} and a weak one at around 300 cm^{-1} (see Figure 7.5 and chapter 9). Therefore, it is possible that some of the laser photons could gain further energy by absorbing Raman phonons created by light scattering inside the glass.

7.3. THE EFFECT OF TEMPERATURE ON THE FLUORESCENCE SPECTRUM OF TERBIUM PENTAPHOSPHATE CRYSTAL

The fluorescence spectrum of a sample of a terbium pentaphosphate crystal (TbP_5O_{14}) was excited using the 4880Å blue line of argon ion laser. The spectrum was recorded at selected temperatures (300, 200, 100, 50 and 12K) using the optical system described in section 9.4. Due to the intense and sharp fluorescence lines of the spectrum, the input and exit slitwidths of the monochromator were set to 30μ (high resolution). In addition, a very slow scanning speed of 0.125cm^{-1}/second was used for the 12K fluorescence measurements while 1cm^{-1}/second scanning speed was employed for the higher temperature measurements, to preserve the natural line

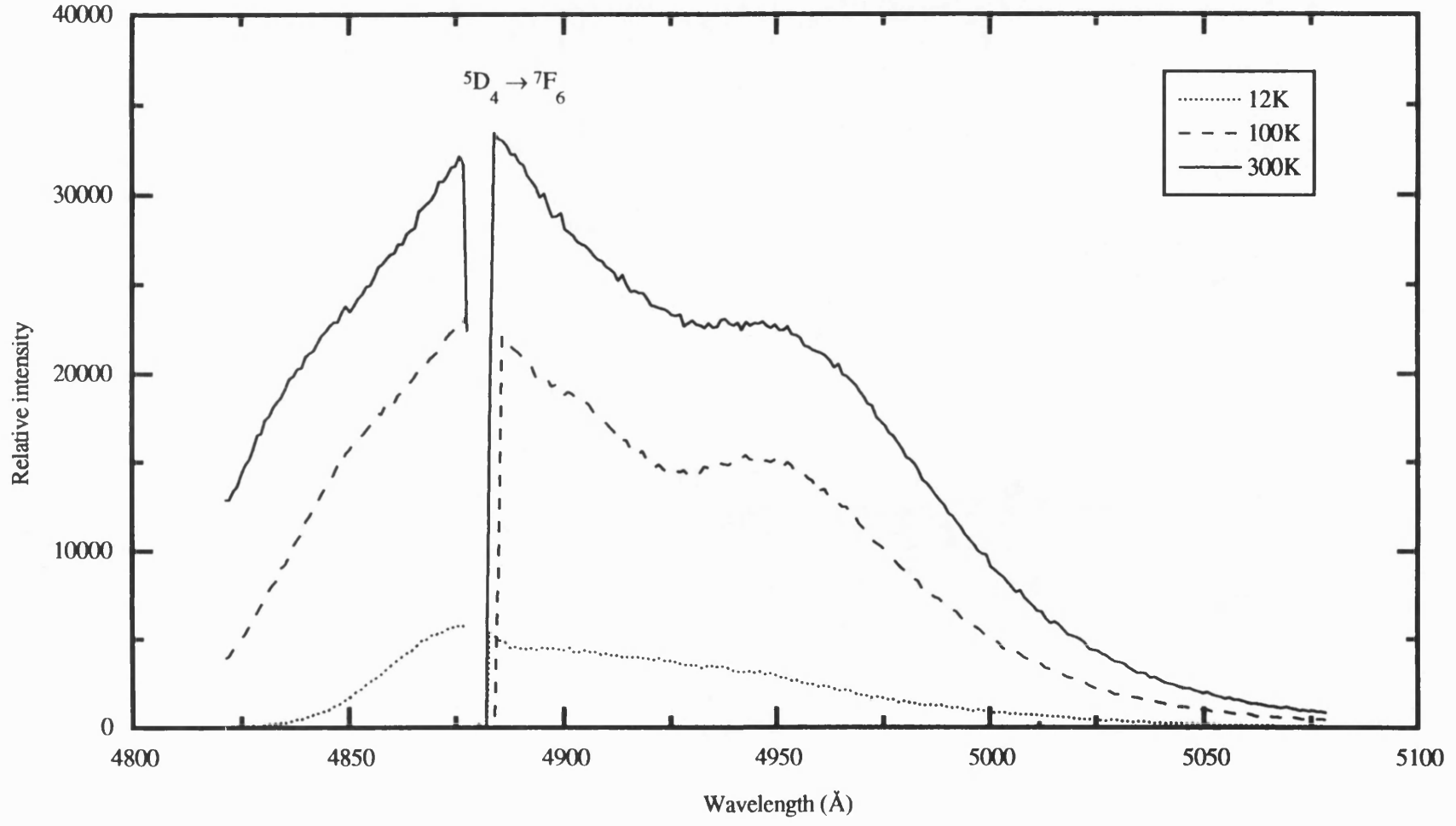

Figure 7.6. The $^5D_4 \rightarrow {}^7F_6$ fluorescence band of the $(Tb_2O_3)_{22.6}(P_2O_5)_{77.4}$ glass excited by the 4880Å argon ion laser line at different temperatures. The fluorescence tails on the shorter wavelengths are related to assisted fluorescence by phonons.

widths of the sharp fluorescence lines. Depending upon the intensity of the fluorescence, the laser power was varied in the vicinity of 30mW (quite low compared with the power used for the other rare earth metaphosphate glasses and pentaphosphate crystals).

The normalised fluorescence spectra of the TbP_5O_{14} crystal measured at 12K and 300K, are shown overlapped in Figures 7.7-7.11, in the wavelength range 4880-7000Å. The spectrum is composed of seven well-separated fluorescence bands at around: (i) 4900Å (Figure 7.7), (ii) 5450Å (Figure 7.8), (iii) 5850Å (Figure 7.9), (iv) 6200Å (Figure 7.10), (v) 6500Å, (vi) 6700Å, (vii) 6800Å (the last three bands are in Figure 7.11). The positions of the fluorescence peaks in each band extracted from the 12K spectrum are listed in Table 7.3. The spectral structure of the fluorescence bands and their positions are consistent with a 3+ valence state for the terbium ions: the bands can be attributed to transitions from the $^5D_4$ excited state to the seven levels of ^7F_J ground state, where J= 6, 5, 4, 3, 2, 1, and 0. The fine structure revealed in each of the fluorescence bands can be related to the crystal field effect on the energy levels of Tb^{3+} ion. An interesting feature of all the seven bands is the disappearance of some of their shorter wavelength lines at low temperature. On cooling the crystal down to 12K, there was no measurable shift in the fluorescence lines but two distinctive features were observed in comparison with the spectrum taken at 300K. First, an extraordinary sharpening of the fluorescence lines occurred in each of the seven bands (Figures 7.7-7.11). Line widths at half maximum of some of the sharpest fluorescence lines in each band were measured (Table 7.3) and line widths as low as 0.2Å were obtained. Secondly, there was an enormous intensity increase in some of the lines; these intensity increases are not clear in the figures as they were normalised, but they were measured to be around 25 times in the $^5D_4 \rightarrow {}^7F_6$ transition and 1.5 times in the $^5D_4 \rightarrow {}^7F_3$ transition.

To search for any phonon-assisted fluorescence similar to the one observed in the spectrum of the terbium metaphosphate glass, the fluorescence band related to the $^5D_4 \rightarrow {}^7F_6$ transition (Figure 7.7) was thoroughly re-examined on both side of the laser line at different temperatures. Figure 7.12 shows this fluorescence band measured at 12, 100, and 300K on both sides of the 4880Å laser line, using the same conditions for comparison purposes (the relative intensity scale is a true one). It is

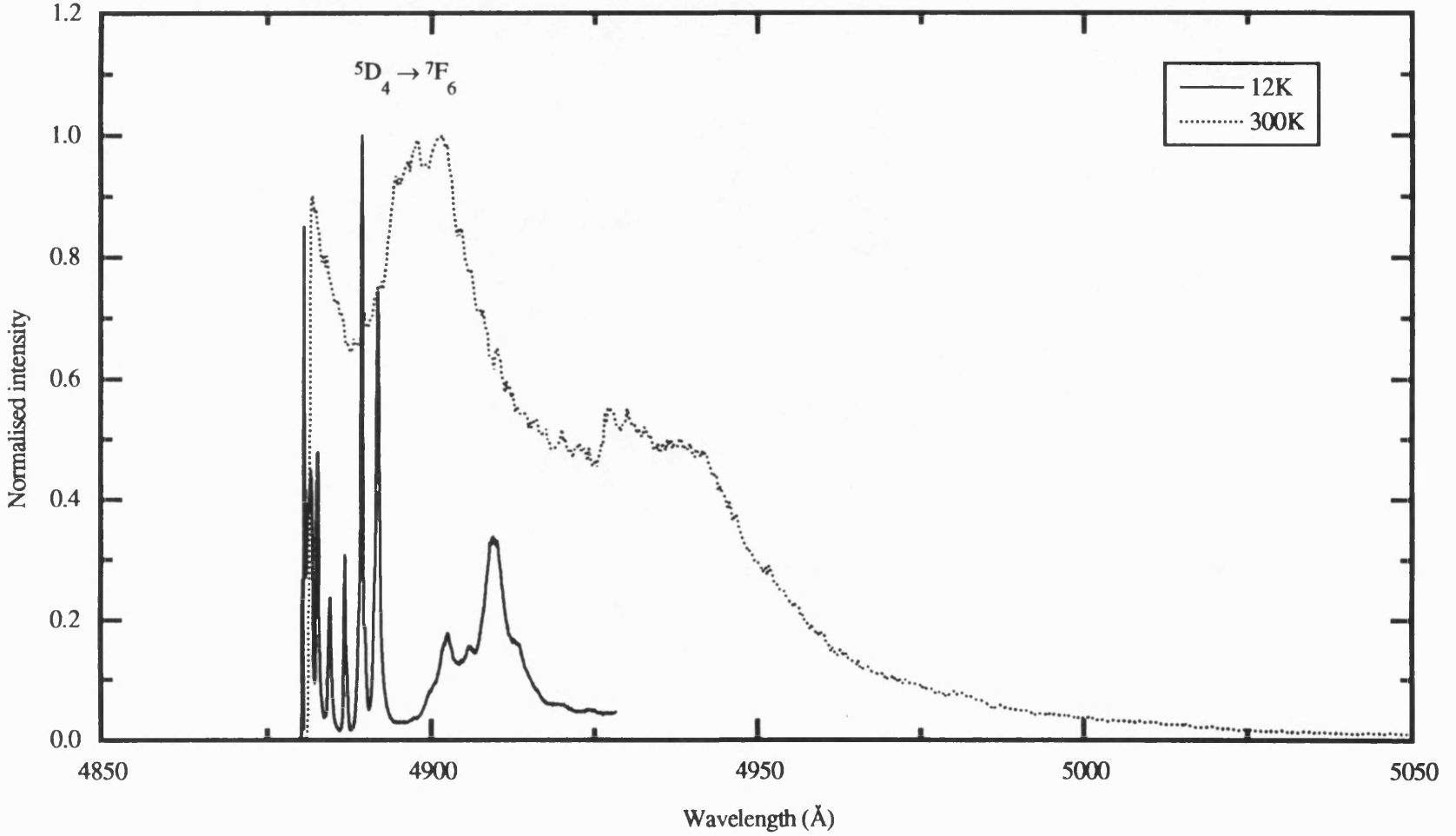

Figure 7.7. The first part of the fluorescence spectrum of monocrystalline TbP_5O_{14} excited by the blue 4880Å argon ion laser line.

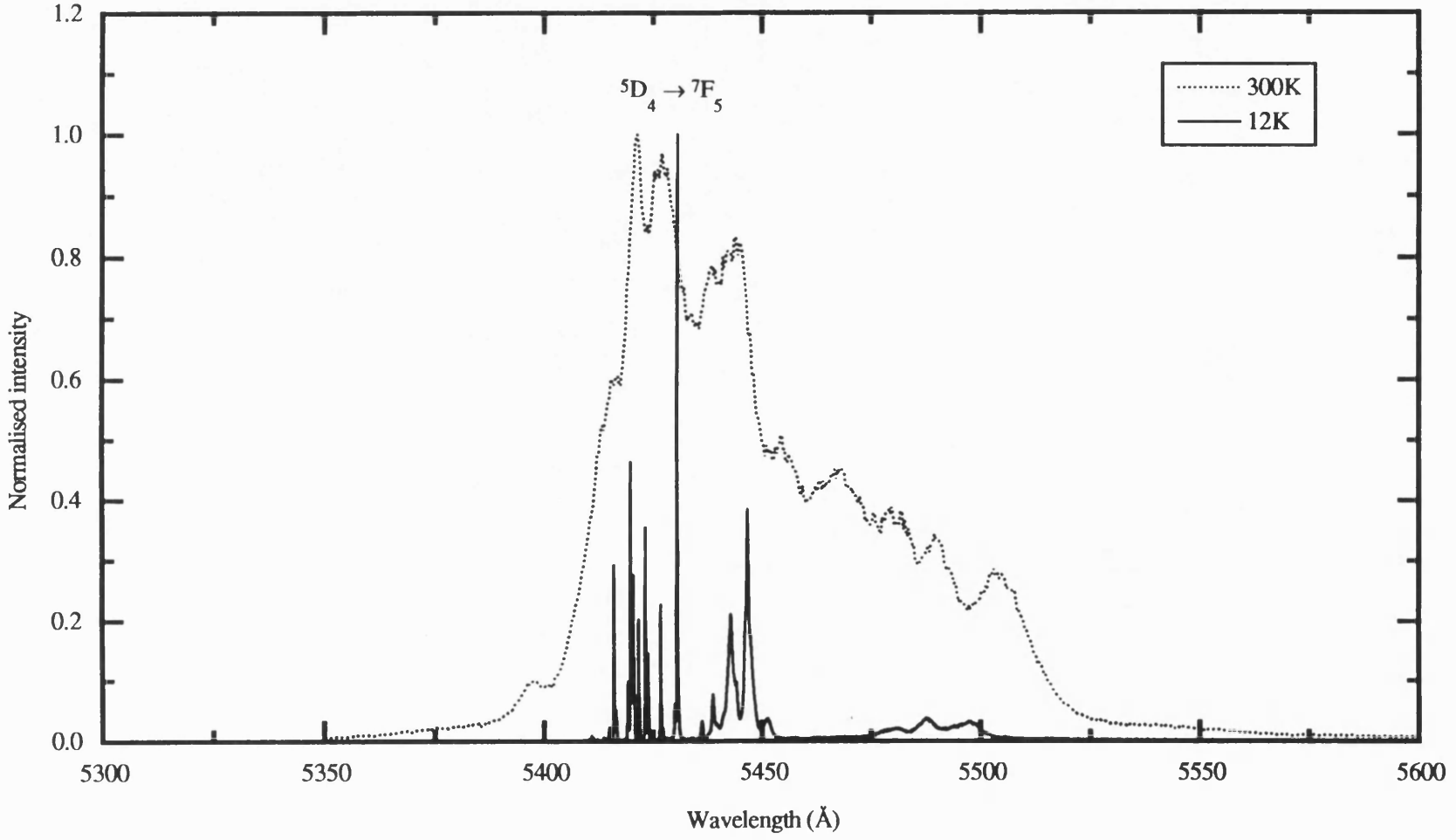

Figure 7.8. The second part of the fluorescence spectrum of monocrystalline TbP_5O_{14} excited by the blue 4880Å argon ion laser line.

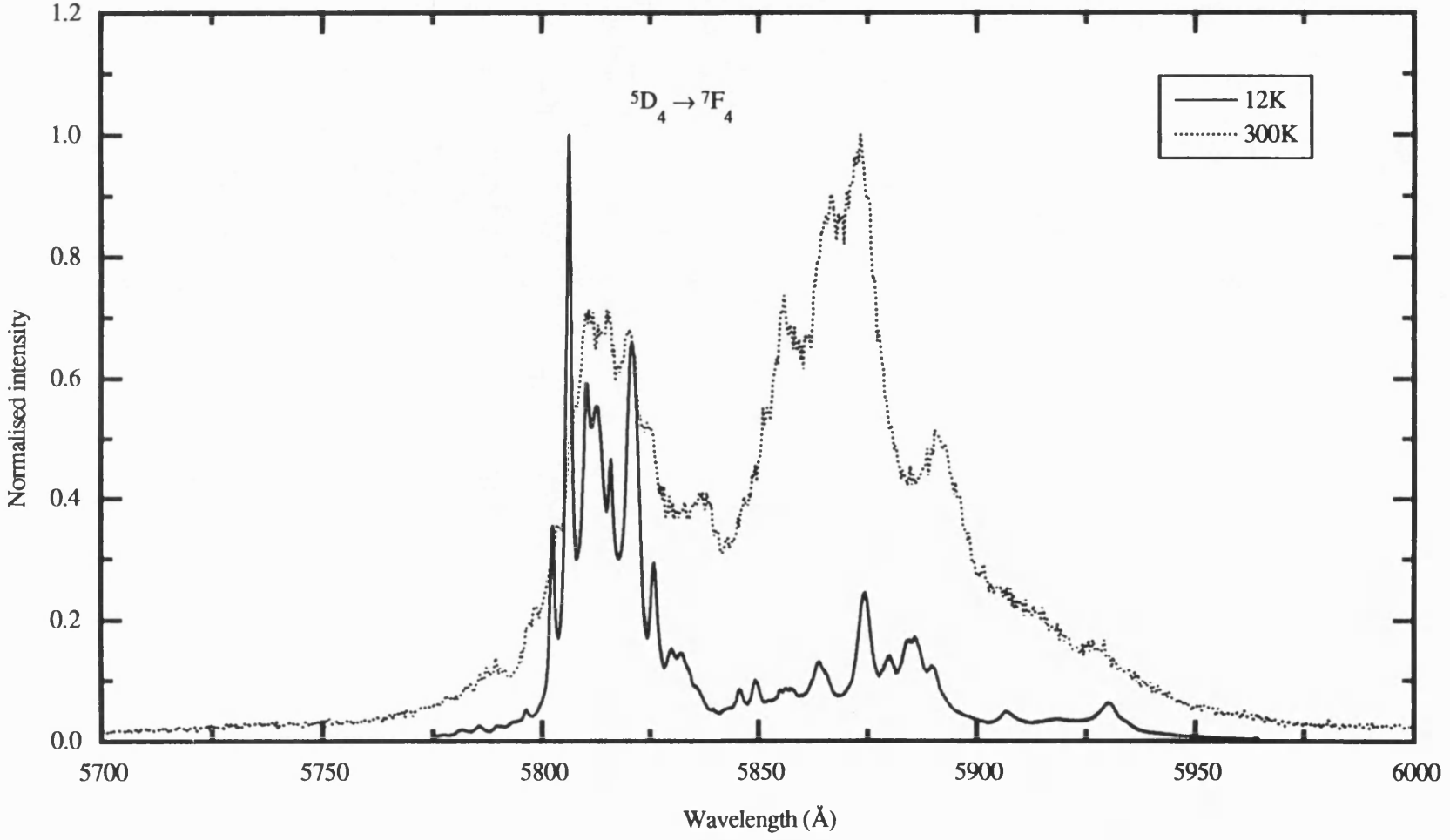

Figure 7.9. The third part of the fluorescence spectrum of monocrystalline TbP_5O_{14} excited by the blue 4880Å argon ion laser line.

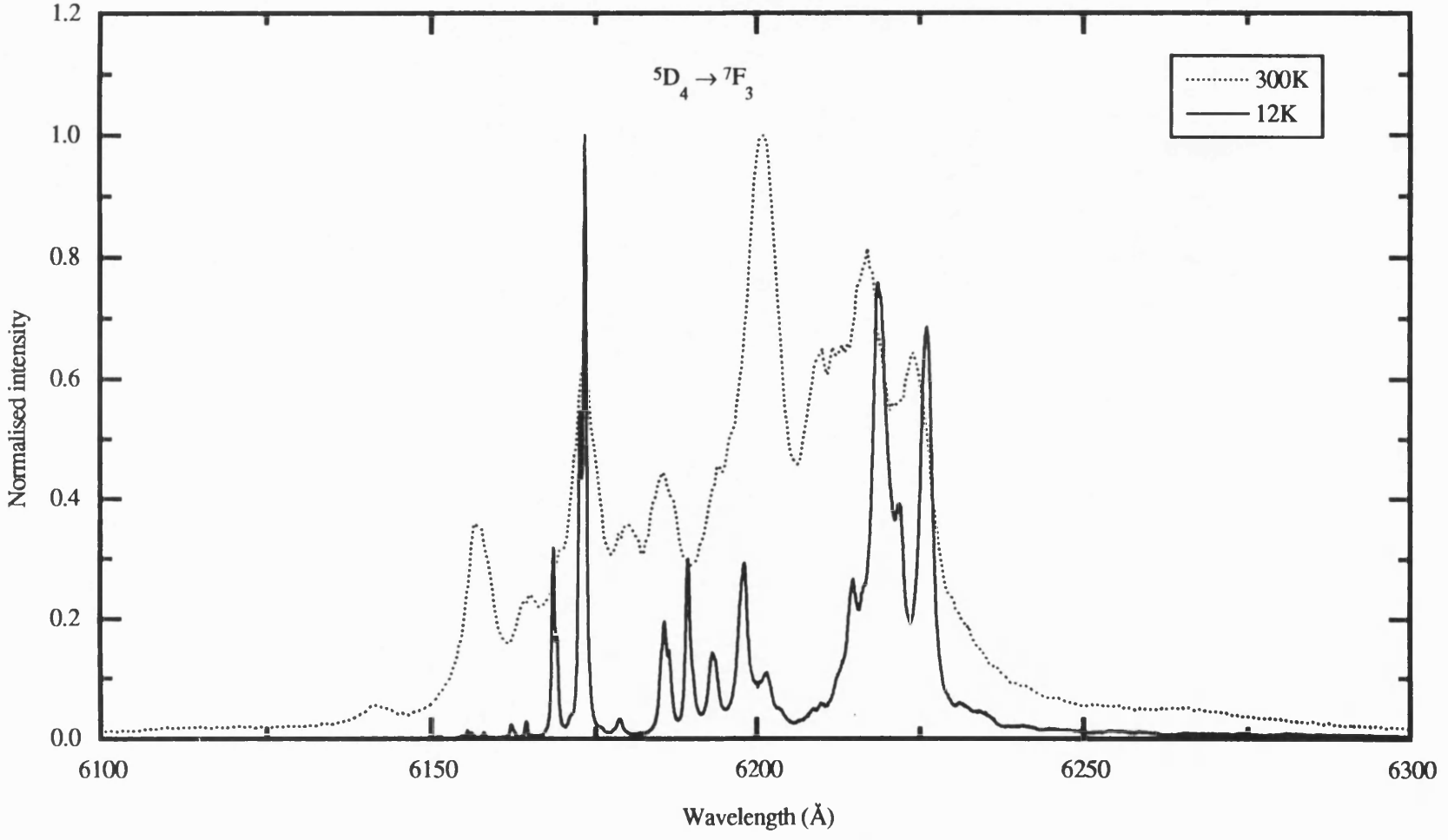

Figure 7.10. The fourth part of the fluorescence spectrum of monocrystalline TbP_5O_{14} excited by the blue 4880Å argon ion laser line.

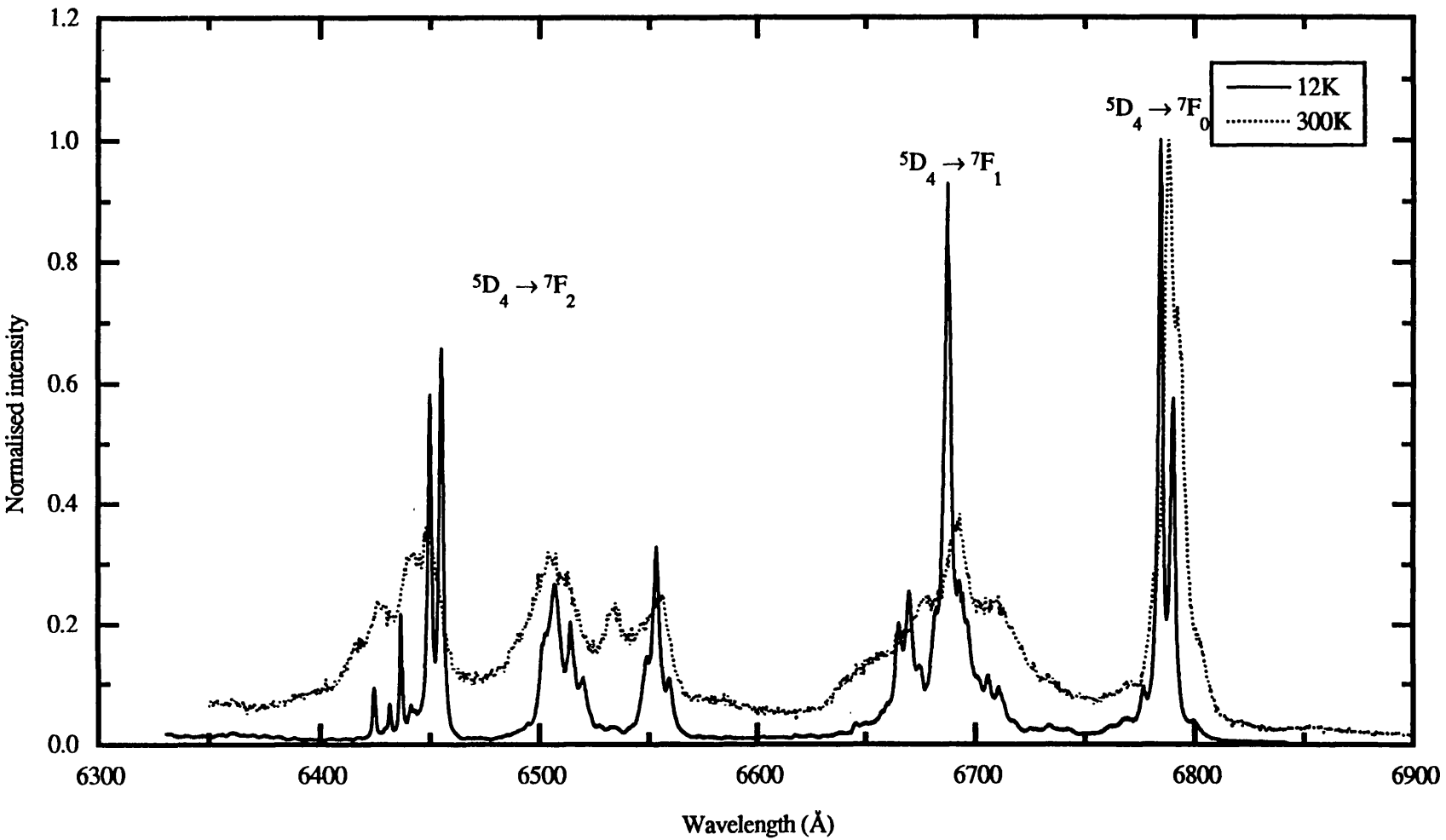

Figure 7.11. The fifth part of the fluorescence spectrum of monocrystalline TbP_5O_{14} excited by the blue 4880Å argon ion laser line.

Table 7.3. Measured wavelengths of the fluorescence line peaks of TbP_5O_{14} crystal excited using the 4880Å, at 12K. The sign * refer to fluorescence lines on the low wavelength side of the laser line and numbers in brackets are linewidths.

Trans-ition	$^5D_4 \rightarrow {}^7F_6$	$^5D_4 \rightarrow {}^7F_5$	$^5D_4 \rightarrow {}^7F_4$	$^5D_4 \rightarrow {}^7F_3$	$^5D_4 \rightarrow {}^7F_2$	$^5D_4 \rightarrow {}^7F_1$	$^5D_4 \rightarrow {}^7F_0$
Wave-	4869.55*	5411.03	5781.47	6151.24	6424.56	6645.23	6761.38
length	4870.92*	5412.39	5785.02	6154.65	6431.59	6665.5	6768.36
(Å)	4871.98*	5413.81	5789.54	6155.45	6436.87(1.67)	6669.89	6776.5
TbP_5O_{14}	4872.34*	5415.20	5793.02	6156.0	6441.37	6674.39	6784.49(2.5)
crystal	4873.17*	5416.16	5796.38	6157.91	6442.77	6682.87	6790.3
	4873.47*	5416.56	5802.44	6162.04	6449.94	6687.34(4)	6799.77
	4874.18*	5419.31	5806.35(1.7)	6164.32	6455.36(2.46)	6692.43	
	4874.54*	5419.94	5810.44	6168.50	6494.24	6694.0	
	4875.90*	5420.56	5812.51	6169.03	6502.90	6696.46	
	4877.69*	5421.81	5815.85	6172.64	6507.08	6700.33	
	4878.52*	5423.36	5820.84	6173.41(0.5)	6514.23	6705.5	
	4880.31	5423.98	5825.85	6175.60	6519.91	6710.67	
	4880.54	5426.81	5829.67	6178.65	6528.32	6716.7	
	4881.11	5427.18	5831.92	6185.67	6534.66	6733.04	
	4881.59	5429.98	5845.47	6186.39	6542.46		
	4882.66	5430.57(0.2)	5849.4	6189.36	6549.16		
	4884.57	5436.25	5856.85	6193.1	6553.56		
	4886.77	5438.77	5863.72	6198.04	6559.25		
	4889.34(0.35)	5439.51	5874.31	6201.55			
	4889.85	5441.43	5879.97	6203.57			
	4891.79	5442.84	5883.99	6208.57			
	4902.56	5443.99	5885.72	6209.73			
	4905.98	5446.14	5889.71	6213.59			
	4909.50	5446.73	5906.80	6214.79			
		5447.43	5930.09	6216.63			
		5451.22		6218.61			
		5480.65		6221.75			
		5487.6		6226.06			
		5497.18		6231.59			
		5498.54		6234.4			
		5505.39		6241.66			
				6361.93			

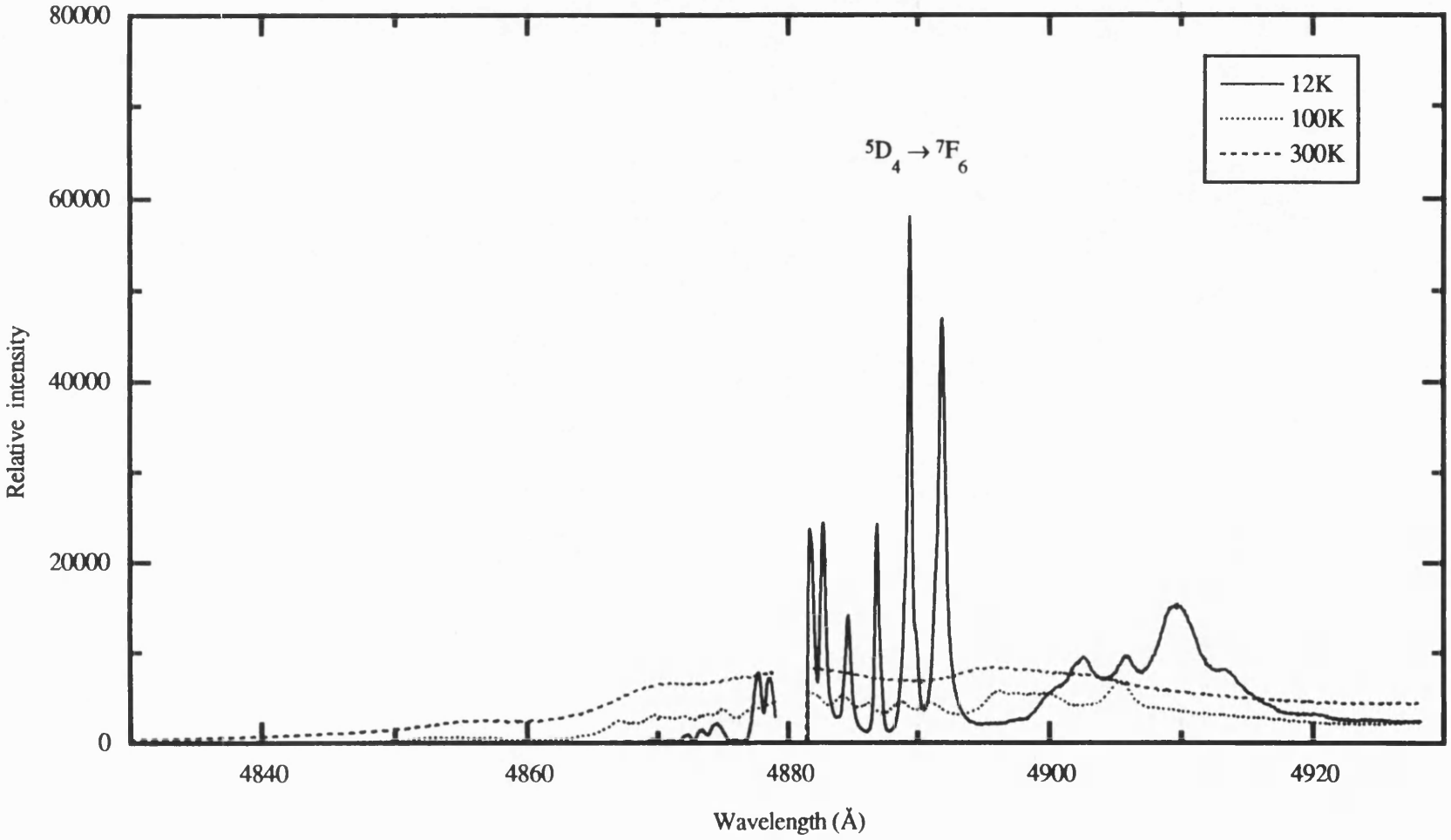

Figure 7.12. The $^5D_4 \rightarrow {}^7F_6$ fluorescence band of monocrystalline TbP_5O_{14} excited by the blue 4880Å argon ion laser line at differnt temperatures. The band has tails on the shorter wavelengths side related to fluorescence assisted by phonons.

evident that this fluorescence band in the crystal also has a tail which extends beyond the wavelength of the laser line towards lower wavelengths (higher frequencies). At 12K, this $^5D_4 \rightarrow {}^7F_6$ band shows a strong intensity increase and a marked sharpening of its fluorescence components. As speculated above for the terbium metaphosphate glass, it is possible that the high frequency fluorescence tail in the crystal spectrum (Figure 7.12) could be caused by the absorption of Raman phonons (created by laser scattering) by the 4f electrons of the Tb^{3+} ions excited to the $^5D_4$ state. Therefore, it would be possible for the 4f electrons in the $^5D_4$ state to be excited to higher energy levels with the extra energy gained from the phonons.

Examination of the fluorescence spectrum of the crystal given in Figures 7.7-7.11, and the assignments of the bands listed in Table 7.3, together with systematic sharpening of lines at low temperature (12K), can provide useful information about the local environment of the Tb^{3+} ions. In the 300K spectrum of the crystal the fluorescence bands are broad and not resolved sufficiently to reveal their components (dotted lines in Figures 7.7-7.11); therefore it is necessary to use the 12K spectrum, in which the fluorescence bands are well resolved into their components, to identify the local symmetry of the Tb^{3+} ion. According to the Runciman classification (1956), the term-splitting for the integral J of the trivalent terbium ion can have one of four options for the local symmetry (cubic, hexagonal, tetragonal and low symmetry). For the option of the cubic symmetry the splitting of the terms of the Tb^{3+} ion for J= 0, 1, 2, 3, 4, 5, 6 would be 1, 1, 2, 3, 4, 4, 6 respectively. For the hexagonal case the splitting would be 1, 2, 3, 5, 6, 7, 9. For tetragonal symmetry the splitting would be 1, 2, 4, 5, 7, 8, 10. For low symmetry the splitting would be 1, 3, 5, 7, 9, 11, 13. Therefore, the number of lines into which the band splits for transitions from the $^5D_4$ state to the multiplet of the ^7F_J levels can be calculated; Table 7.4 summarises all the options for the band splitting (the expected fluorescence lines) depending on the local symmetry of the terbium ion. A count of the number of fluorescence lines in each band, listed in Table 7.3, reveals the following: the $^5D_4 \rightarrow {}^7F_6$ band has 24 fluorescence lines, $^5D_4 \rightarrow {}^7F_5$ band has 31, $^5D_4 \rightarrow {}^7F_4$ has 25, $^5D_4 \rightarrow {}^7F_3$ has 32, $^5D_4 \rightarrow {}^7F_2$ has 18, $^5D_4 \rightarrow {}^7F_1$ has 14, $^5D_4 \rightarrow {}^7F_0$ has 6. These splitting numbers exclude the option of low symmetry for the Tb^{3+} ion which produces larger numbers of lines than are available from the experimental results. Also the cubic

Table 7.4. The band splittings resulted from the integral J term splittings of the Tb^{3+} ion for different symmetries.

Symmetry Type	Transition	Band splitting
Cubic	$^5D_4 \rightarrow {}^7F_6$	24
	$^5D_4 \rightarrow {}^7F_5$	16
	$^5D_4 \rightarrow {}^7F_4$	16
	$^5D_4 \rightarrow {}^7F_3$	12
	$^5D_4 \rightarrow {}^7F_2$	8
	$^5D_4 \rightarrow {}^7F_1$	4
	$^5D_4 \rightarrow {}^7F_0$	4
Hexagonal	$^5D_4 \rightarrow {}^7F_6$	54
	$^5D_4 \rightarrow {}^7F_5$	42
	$^5D_4 \rightarrow {}^7F_4$	36
	$^5D_4 \rightarrow {}^7F_3$	30
	$^5D_4 \rightarrow {}^7F_2$	18
	$^5D_4 \rightarrow {}^7F_1$	12
	$^5D_4 \rightarrow {}^7F_0$	6
Tetragonal	$^5D_4 \rightarrow {}^7F_6$	70
	$^5D_4 \rightarrow {}^7F_5$	56
	$^5D_4 \rightarrow {}^7F_4$	49
	$^5D_4 \rightarrow {}^7F_3$	35
	$^5D_4 \rightarrow {}^7F_2$	28
	$^5D_4 \rightarrow {}^7F_1$	14
	$^5D_4 \rightarrow {}^7F_0$	7
Low symmetry	$^5D_4 \rightarrow {}^7F_6$	117
	$^5D_4 \rightarrow {}^7F_5$	99
	$^5D_4 \rightarrow {}^7F_4$	81
	$^5D_4 \rightarrow {}^7F_3$	63
	$^5D_4 \rightarrow {}^7F_2$	45
	$^5D_4 \rightarrow {}^7F_1$	27
	$^5D_4 \rightarrow {}^7F_0$	9

symmetry option can be waived as it does not fit the observed number of lines, except that resulting from the split of the $^5D_4 \rightarrow {}^7F_6$ transition. This transition can not be relied upon since there is the possibility that it would be affected by fluorescence originating from transition between the $^5D_3$ state and the $^7F_0$ state, which accidently falls in the same wavelength range. The energy gap between the $^5D_3$ and the $^7F_0$ falls in the range of the 4880Å laser line wavelength; therefore any electron dropping down from the $^5D_4$ state to the $^7F_0$ state can be re-excited by the 4880Å laser line to the higher energy $^5D_3$ state before going down to lower levels. Then the $^5D_3 \rightarrow {}^7F_0$ transition is a possible effect as the $^5D_3$ level itself is a fluorescence level which leads to the options of hexagonal and tetragonal symmetries. Hence hexagonal and tetragonal symmetries are the remaining available ones for the Tb^{3+} ion local symmetry in this crystal. The numbers of lines corresponding to the $^5D_4 \rightarrow {}^7F_{5,4,2,0}$ transitions approximately fit hexagonal symmetry, but those for the transitions $^5D_4 \rightarrow {}^7F_{3,1}$ fit tetragonal symmetry. Therefore, overall both symmetries (hexagonal and tetragonal) can be considered to be an option for the local symmetry of the Tb^{3+} ion in this crystal. For small distortions both these local symmetries are close to pseudocubic. An interpretation of the fluorescent spectral lines of the TbP_5O_{14} crystal that the local symmetry around the Tb^{3+} ion is pseudocubic is in accord with the shape of the co-ordination polyhedron of the eight oxygen atoms surrounding a Tb^{3+} ion shown in Figure 6.4, which can be thought of as a distorted cube.

7.4. COMPARISON BETWEEN THE FLUORESCENCE SPECTRA OF THE TERBIUM METAPHOSPHATE GLASS AND TERBIUM PENTAPHOSPHATE CRYSTAL

Similarities and differences between the fluorescence spectra of the $(Tb_2O_3)_{22.6}(P_2O_5)_{77.4}$ glass and the terbium pentaphosphate crystal (TbP_5O_{14}) are now explored. This comparison should identify the local symmetry of Tb^{3+} ions and disclose any phase transition in these matrices. As it does for the TbP_5O_{14} crystal (Figures 7.7-7.11), the spectrum of the glass falls into seven well-separated bands (Figures 7.2a,b and 7.3); both spectra share nearly the same overall profile, although the spectrum of the glass shows greater broadening due to the randomness of the glass structure. Figures 7.13-7.15 show overlaps between the spectra of the glass and crystal made in the first three fluorescence bands measured at 12K. Some

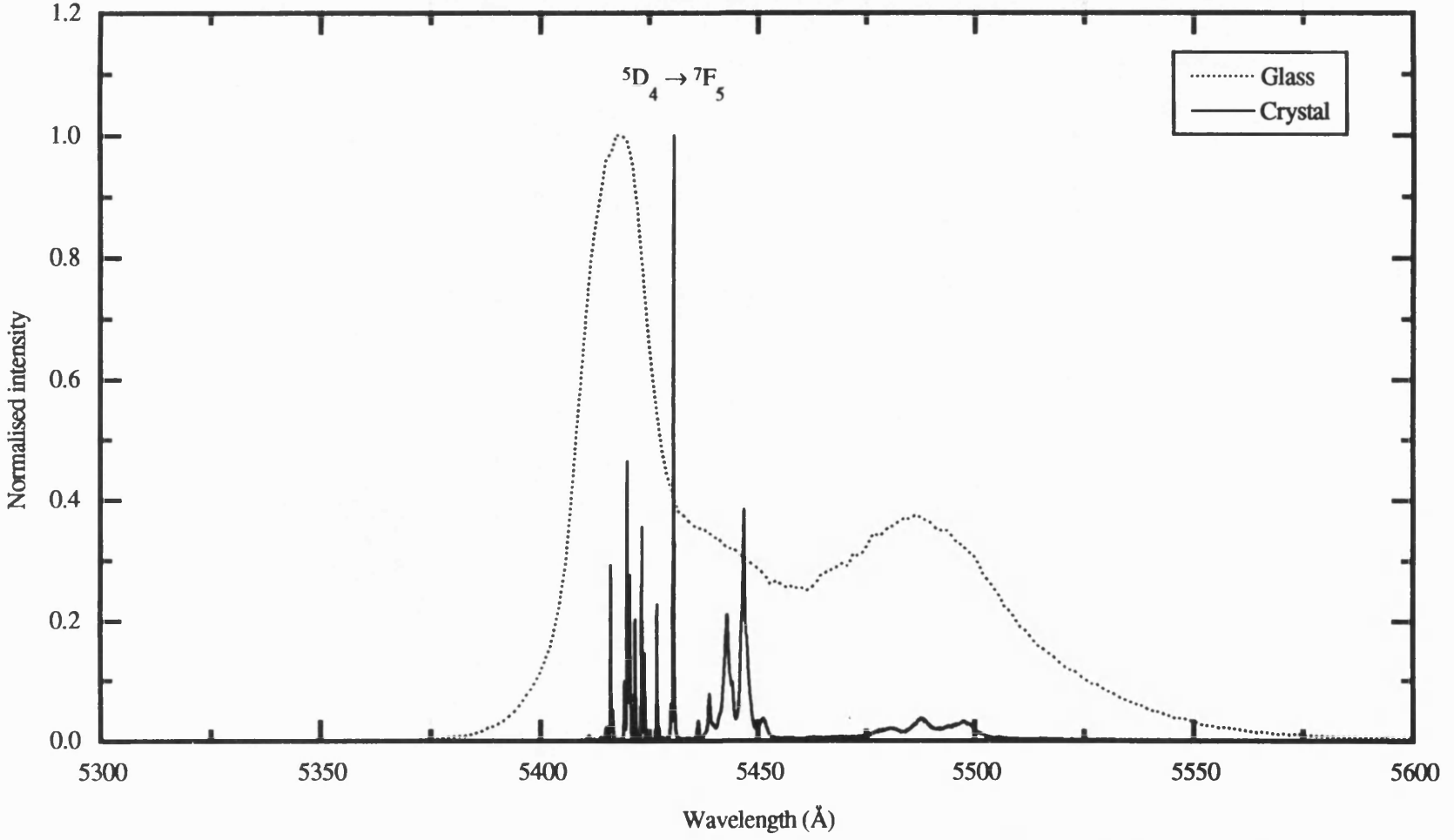

Figure 7.13. A comparison between the fluorescence spectra of the $(Tb_2O_3)_{22.6}(P_2O_5)_{77.4}$ glass and the TbP_5O_{14} crystal in the $^5D_4 \rightarrow {}^7F_5$ band.

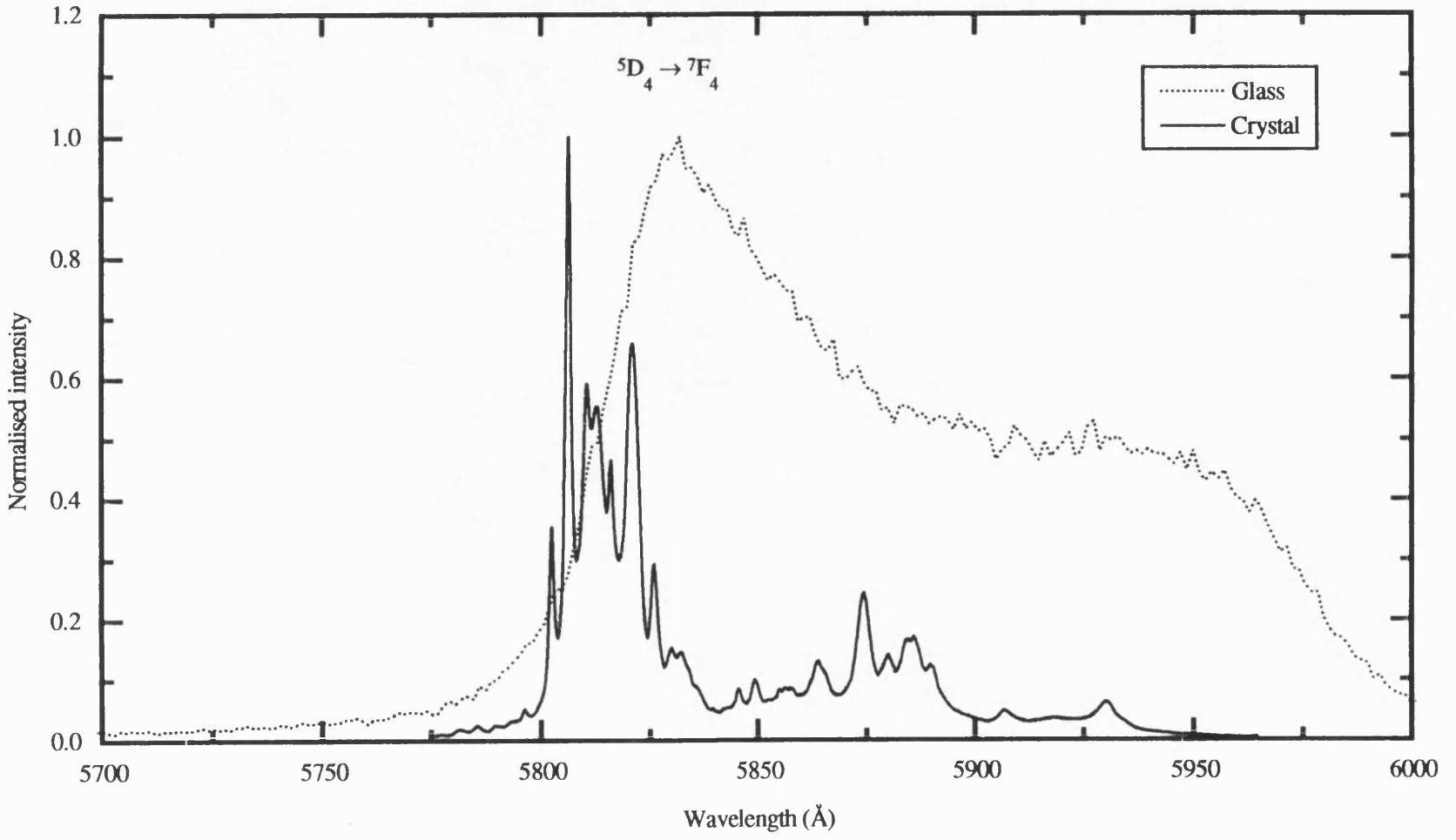

Figure 7.14. A comparison between the fluorescence spectra of the $(Tb_2O_3)_{22.6}(P_2O_5)_{77.4}$ glass and the TbP_5O_{14} crystal in the $^5D_4 \rightarrow {}^7F_4$ band.

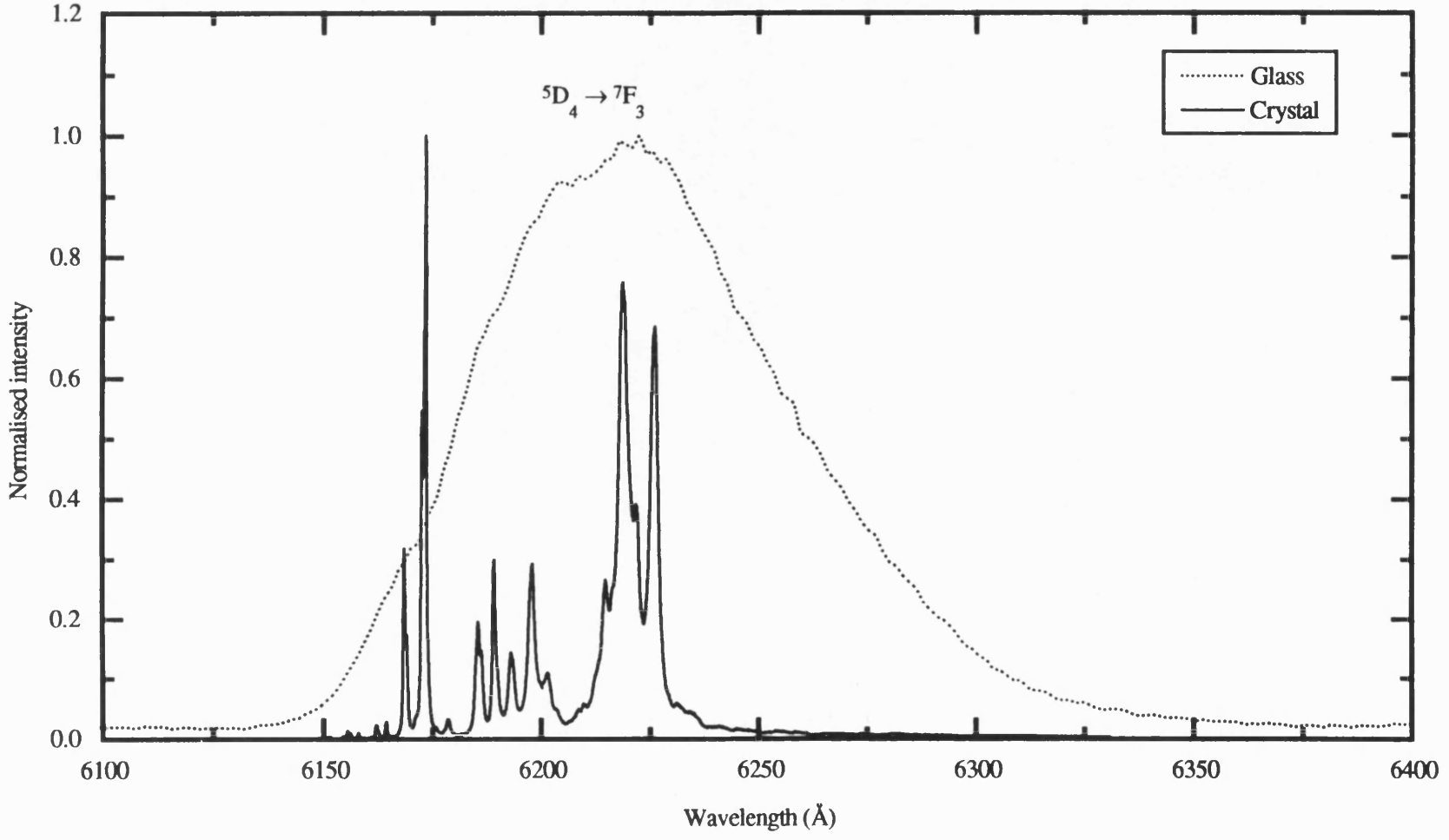

Figure 7.15. A comparison between the fluorescence spectra of the $(Tb_2O_3)_{22.6}(P_2O_5)_{77.4}$ glass and the TbP_5O_{14} crystal in the $^5D_4 \rightarrow {}^7F_3$ band.

of the fluorescence lines of the crystal spectrum are enhanced relative to their most intense lines in comparison with the ones in the glass spectrum, for example, the line located at 5430.5Å in the $^5D_4 \rightarrow {}^7F_5$ band of the crystal (Figure 7.13 solid line), that located at 5806.3Å in the $^5D_4 \rightarrow {}^7F_4$ band (Figure 7.14 solid line) and that situated at 6173.4Å in the $^5D_4 \rightarrow {}^7F_3$ band (Figure 7.15 solid line). This enhancement may be related to the polarisation effect caused by slight changes in the orientation of the phosphate units around the Tb ion in the crystal matrix with temperature reduction. A fascinating finding in the fluorescence spectra of the glass and crystal is the observation of intense fluorescence especially at low temperatures; the fluorescence spectrum of the terbium pentaphosphate crystal shows a higher fluorescence intensity than the glass even with using a very low power laser and narrow slitwidths.

To gain further insight about the temperature effects on the glass and crystal spectra, it is worthwhile to look back on the spectra individually. It is apparent from the spectrum of the terbium pentaphosphate crystal measured at 300K (dotted line in Figures 7.7-7.11) that each fluorescence band consists of larger number of interfered fluorescence lines in comparison with the lesser number of fluorescence lines observed in the spectrum measured at 12K (solid line). According to the symmetry options listed in Table 7.4 the local symmetry for the Tb^{3+} ion in the crystal is low at 300K and high (hexagonal or tetragonal) at 12K. Therefore it can be suggested that the local symmetry of the Tb^{3+} ion experiences a change, from a low value to hexagonal or tetragonal, with temperature reduction. Further, it is evident from the spectra of the crystal that there are variations in the intensity of the fluorescence lines (redistribution of energy among the lines) with temperature reduction; some lines get stronger and other weaker within the same band. These intensity variations can be ascribed to the change in the local symmetry of the Tb^{3+} ion, from low to high symmetry, which results in different polarisation effect on the fluorescence lines due to change of orientation in the PO_4 tetrahedra surrounding the terbium ions.

For the fluorescence spectrum of the terbium metaphosphate glass the effect of temperature reduction can be summarised as three features: (i) narrowing in the widths of the seven fluorescence bands (dotted line in Figures 7.2a and b) and es-

pecially on the short wavelength side of the $^5D_4 \rightarrow {}^7F_3$ transition (Figure 7.2b), (ii) the relative intensity of the $^5D_4 \rightarrow {}^7F_1$ and $^5D_4 \rightarrow {}^7F_2$ transitions increase slightly with respect to the intensity of the $^5D_4 \rightarrow {}^7F_0$ transition with temperature reduction (Figure 7.2b), (iii) a decrease in the intensity of the 5486.3Å peak relative to the intensity of the 5417.4Å peak in the $^5D_4 \rightarrow {}^7F_5$ transition (Figure 7.2a). To understand some of these features it is better to compare the effects of temperature on the spectrum of the glass with that on the spectrum of the crystal. First, the observed sharpness of the low wavelength side of the $^5D_4 \rightarrow {}^7F_3$ transition (Figure 7.2b) is similar to the intensity reduction on the low wavelength side of this transition (Figure 7.10) recorded for the crystal. Second, the relative intensity increases in the $^5D_4 \rightarrow {}^7F_1$ and $^5D_4 \rightarrow {}^7F_2$ transitions with respect to the intensity of the $^5D_4 \rightarrow {}^7F_0$ transition with temperature reduction in the glass spectrum (Figure 7.2b) can be seen too in the spectrum of the crystal (Figure 7.11). Third, it is evident that the decrease in the intensity of the 5486.3Å peak relative to the intensity of the 5417.4Å peak in glass spectrum (Figure 7.2a) is similar to the intensity decrease found in the lines around 5480Å relative to the intensity of the lines at around 5425Å (Figure 7.8) for the crystal. Therefore, these variations with temperature decrease in the spectrum of the terbium metaphosphate glass can be considered as a counterpart of the variations found in the fluorescence spectrum of the crystal. Since the local symmetry of the Tb^{3+} ion in the pentaphosphate crystal experience a change with temperature reduction, it could be suggested that the local symmetry of the Tb^{3+} ion in the metaphosphate glass is similar to the one in the crystal and experiences the same local symmetry change with temperature reduction. The EXAFS measurements made for the $(Tb_2O_3)_{0.26}(P_2O_5)_{0.74}$ glass showed that the phosphorus-oxygen distance in a tetrahedra is 1.58±0.05Å, the oxygen-oxygen distance is 2.56Å and that separating the terbium-oxygen is 2.34±0.05Å with an average co-ordination number of 7±1 for oxygen atoms surrounding the Tb^{3+} ion (Bowron et al. 1995); the structural parameters in other rare earth metaphosphate glasses are similar (Bowron et al. 1996). Therefore, picturing the terbium ion in metaphosphate glass as being at the centre of a distorted cube is in accord with the EXAFS results. The change of symmetry in the TbP_5O_{14} crystal or in the metaphosphate glass from low local symmetry to hexagonal or tetragonal local symmetry, would

require a slight structural rearrangement of the linked PO_4 tetrahedra; this would be likely to involve mode softening. The low frequency Raman spectra of the rare earth pentaphosphate crystals, measured and analysed in chapter 9, has shown the existence of mode softening in the lowest frequency Raman lines. This mode softening shows the effect of the phase transition in these rare earth pentaphosphate crystals which may be associated with the ferroelasticity found in these crystals.

7.5. HIGH PRESSURE EFFECTS ON THE FLUORESCENCE SPECTRUM OF TERBIUM METAPHOSPHATE GLASS

The effects of high pressure on the room temperature fluorescence spectrum of a sample of $(Tb_2O_3)_{22.6}$ $(P_2O_5)_{77.4}$ glass were measured using the diamond anvil cell. The optical system assembled for high pressure measurements described in chapter 3 was used with the 4880Å argon laser line for this purpose with the monochromator slitwidths set at 100μ and a laser power of 100-250mW. The fluorescence spectrum was recorded in pressure steps of approximately 5-10Kbar. Figures 7.16 and 7.17 show the fluorescence spectrum obtained under a pressure of 52Kbar superimposed on the spectrum measured at atmospheric pressure (both spectra were normalised for comparison purposes). The two most intense bands at 5501.3Å and 6203.2Å are shifted (about 10Å) towards higher wavelengths under pressure to 5511.5Å and 6214.97Å respectively. The shifts in the rest of the fluorescence bands of the spectrum can not be measured due to their low intensities and broad peaks. The shoulder of the 5501.3Å band at 5607.5Å shows an intensity increase at 52Kbar. This increase is probably due to the shift in the 5501.3Å band to 6203.2Å which has led to a closer overlap between this band and the soulder at 5501.3Å. Overall, the spectrum of the glass did not show great changes with pressure up to 52Kbar; the same spectral profile which is typical of the Tb^{3+} ion fluorescence bands was retained through out. These pressure measurements suggest that the is no phase transition in the glass and the valency of the Tb remains trivalent up to the higher pressure measured.

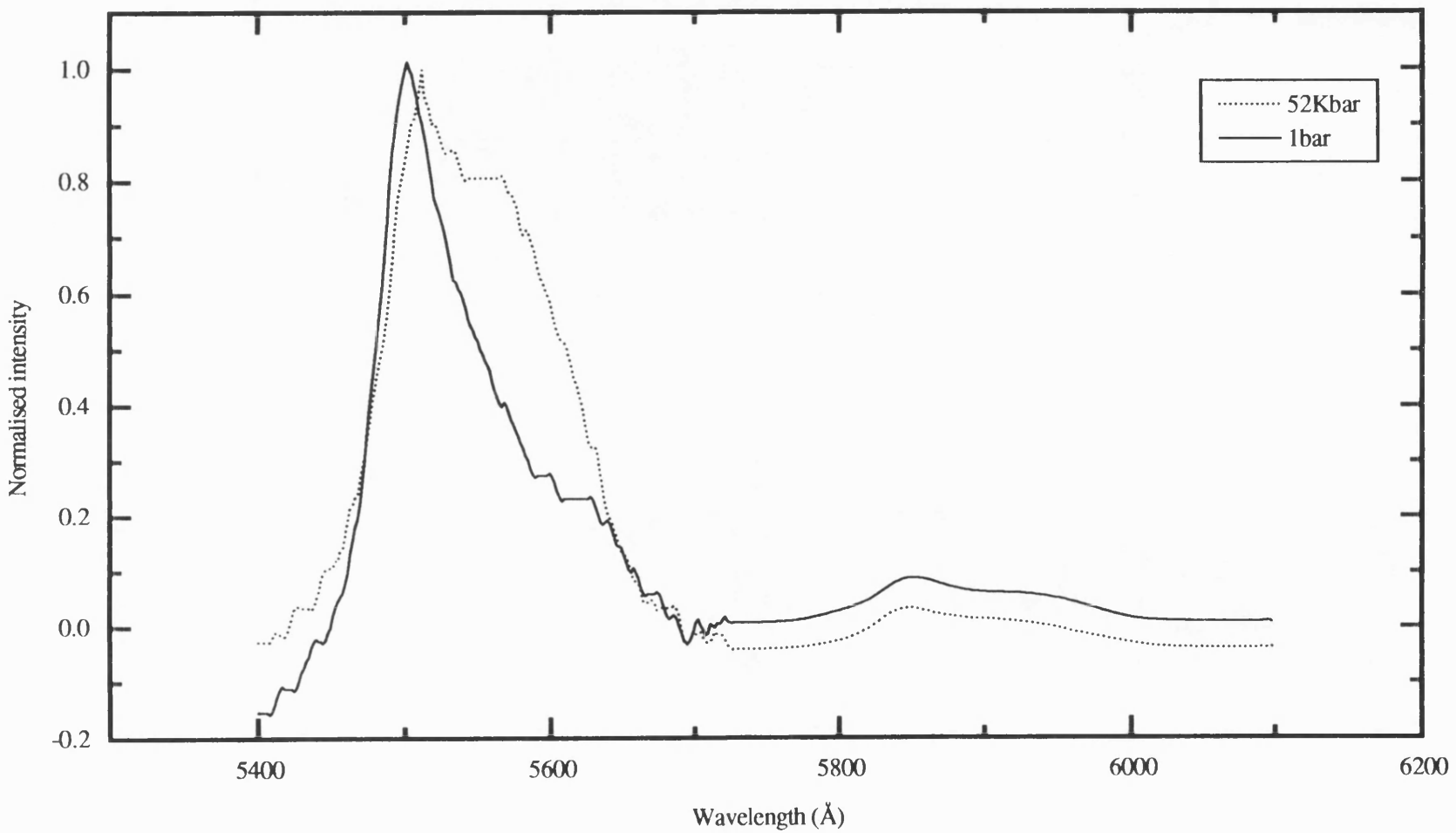

Figure 7.16. The effect of pressure on the fluorescence spectrum of $(Tb_2O_3)_{22.6}(P_2O_5)_{77.4}$ glass at 292K excited using the blue 4880Å argon ion laser line.

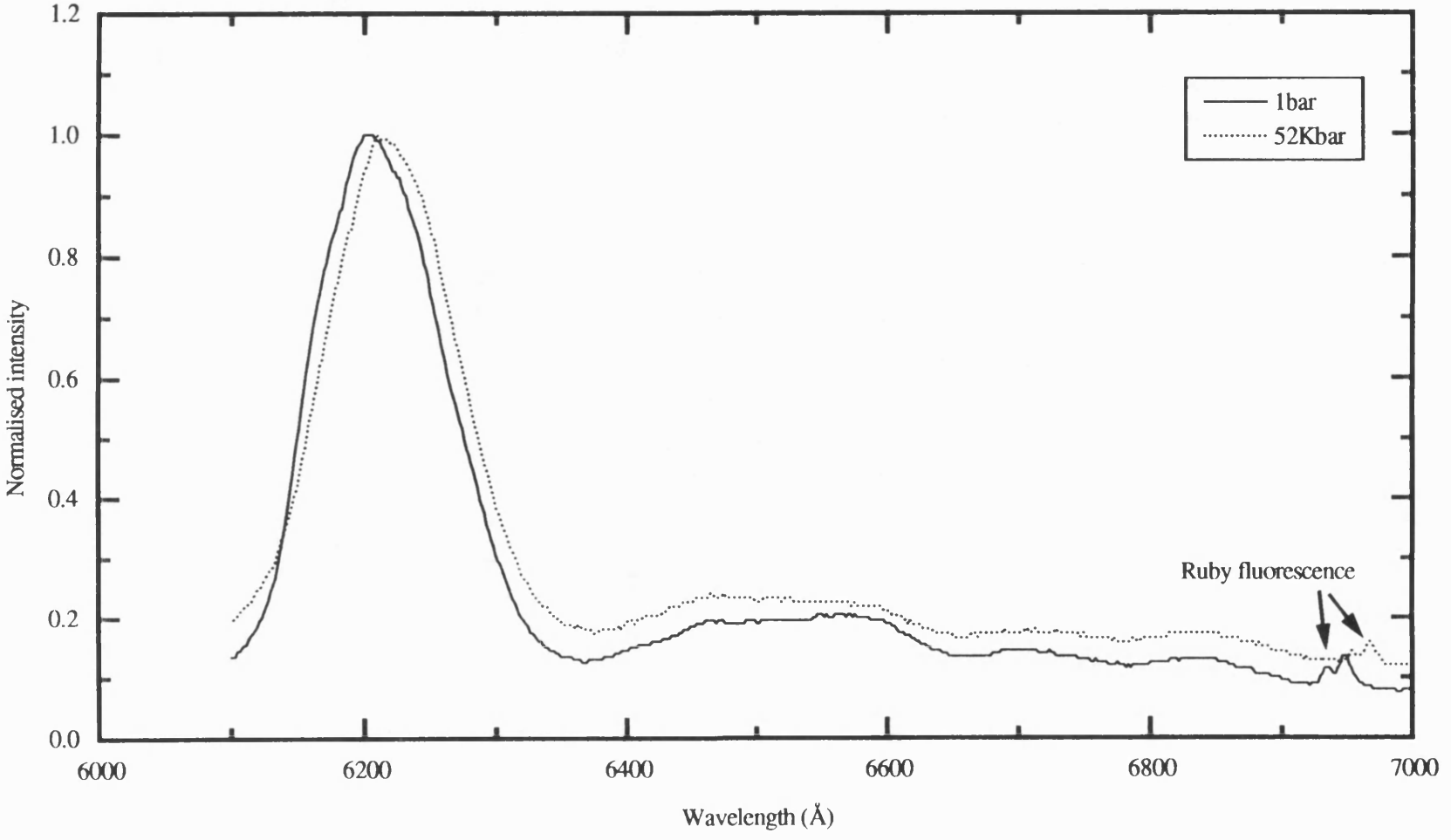

Figure 7.17. The effect of pressure on the fluorescence spectrum of $(Tb_2O_3)_{22.6}(P_2O_5)_{77.4}$ glass at 292K excited using the blue 4880Å argon ion laser line.

CHAPTER EIGHT

AN 'ALEXANDRITE' EFFECT AND OPTICAL PROPERTIES OF HOLMIUM METAPHOSPHATE GLASS

8.1. INTRODUCTION

The type of the incident radiation, and the physiological response of the human eye to a particular region of the visible spectrum, can influence the perceived colour of a material. We have observed that holmium metaphosphate glass changes its apparent colour when it is viewed under different light sources. A striking colour change, when this material was moved from incandescent light to daylight at a window, drew our attention to this optical effect unusual in a glass or in a Ho^{3+} doped material. The existence of alexandrite effects have been reported before in glasses containing Nd^{3+} ions (Ctyroký 1940); a review can be found in the book on coloured glasses by Weyl (1951). Similar behaviour, giving the effect its name, characterises the crystalline alexandrite (Cr^{3+} doped Al_2BeO_4), a variety of chrysoberyl, valued as a unique gemstone which appears green in daylight but reddish-purple in incandescent light (Farrell and Newnham 1963, White et al. 1967). The dopant ion Cr^{3+} can occupy two crystallographically inequivalent Al^{3+} sites, one has mirror symmetry (C_s) and the other a centre of inversion (C_i) (Farrell et al. 1963). The optical spectrum of alexandrite is bimodal with absorption maxima occurring in the violet-blue and yellow-orange regions and with "windows" of comparably low absorption in the red and green regions. Since daylight is equally rich in all wavelengths in the visible region, alexandrite transmits equal proportions of red and green light. However alexandrite appears to be green because the eye is most sensitive to green light. Under incandescent light, which is richer in low-energy wavelengths, alexandrite transmits more red light swamping out the green so that the gem is perceived as red. The operation of Cr^{3+} doped alexandrite as a tunable laser at room temperature (Walling et al. 1979) has led to the development of the first commercial solid state laser with wide tunability. The lasing action of alexandrite is primarily associated with the Cr^{3+} dopant ion at the mirror (C_s) site. In addition the change in the fluo-

rescence characteristics has promoted use of the fluorescence decay of alexandrite for temperature sensing applications.

The objective here has been to examine the alexandrite effect of holmium metaphosphate glass and attempt to account for it in terms of its optical absorption spectrum. Since rare earth metaphosphate glasses can fluoresce, often strongly, the fluorescence spectra has also been determined to find out if that property could affect the colour appearance to any extent. There have been no previous studies of the optical properties of holmium metaphosphate glass so these data provide useful insight into the physical properties of this vitreous material, including the optical excitation spectrum and valent state of the holmium ions.

8.2. ABSORPTION SPECTRUM OF HOLMIUM METAPHOSPHATE GLASS

The optical absorption spectrum of holmium metaphosphate glasses was measured using a standard commercial double-beam instrument. Figure 8.1 shows the absorption spectrum in the range (200nm-750nm) at room temperature of a glass having the composition $(Ho_2O_3)_{0.22}(P_2O_5)_{0.78}$. The absorption bands are quite sharp, a usual feature for rare earth trivalent ions owing to the weak influence of the local field on the deep 4f states (McClure and Kiss 1963). Below 300nm there is strong increase in the background absorption due to the existence of very dense energy levels in this spectral region (Caspers and Rast 1970, Weber and Matsinger 1972) and also because of the intrinsic absorption of the phosphate glass. This severely limits the resolution of the absorption bands below about 300nm.

The energy levels of the Ho^{3+} ion determine the character of the optical absorption spectrum. The absorption band peaks are compared in Table 8.1 with data for the Ho^{3+} ion doped LaF_3 crystal (Caspers and Rast 1970). Optical spectra of rare-earth ions arise mainly from electric and magnetic-dipole transitions between states of the ground f^n electronic configuration. The lowest configuration of trivalent holmium is $4f^{10}$. According to Hund's rules, the ground state of Ho^{3+} is $^5I_8$ (Caspers and Rast 1970). The band peaks reported for Ho^{3+} ion correspond to transitions from the

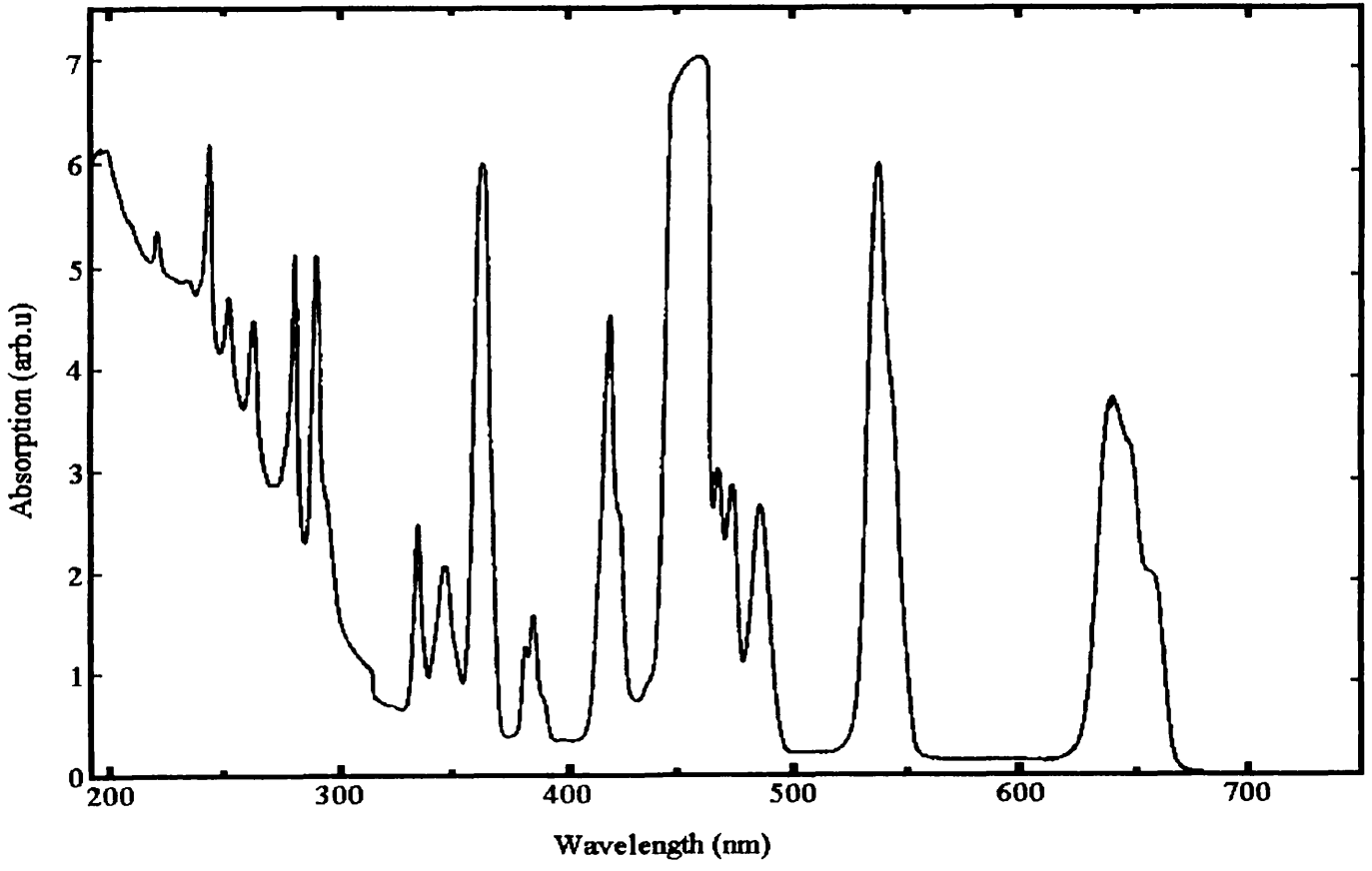

Figure 8.1. Absorption spectrum of $(Ho_2O_3)_{0.22}(P_2O_5)_{0.78}$ glass measured at room temperature.

Table 8.1. The absorption bands of holmium metaphosphate $(Ho_2O_3)_{0.22}(P_2O_5)_{0.78}$ glass at room temperature compared with the transitions between the 4f electron states of Ho^{3+} ion in LaF_3 crystal recorded by Caspers and Rast (1970).

Transition	Experimental wavelength (nm) $(Ho_2O_3)_{0.22}(P_2O_5)_{0.78}$ glass
-	219.7
	233.8
	242.2
	250.7
$^5I_8 \rightarrow {}^3I_7$	261.9
$^5I_8 \rightarrow {}^3H_4, {}^3F_2$	278.8
$^5I_8 \rightarrow {}^3L_8, {}^3M_{10}, {}^5D_4, {}^3F_3$	290.1
$^5I_8 \rightarrow {}^3K_6, {}^3F_4, {}^3D_2$	335.2
$^5I_8 \rightarrow {}^5G_3, {}^3L_9$	346.5
$^5I_8 \rightarrow {}^3H_6, {}^3H_5$	360.5
$^5I_8 \rightarrow {}^5G_4, {}^3K_7$	381.7
	385.9
	388.7
$^5I_8 \rightarrow {}^5G_5, {}^5G_6, I_1$	416.9
	422.5
	436.6
	445.1
$^5I_8 \rightarrow {}^3K_8$	461.9
$^5I_8 \rightarrow {}^5F_3, {}^5F_2$	467.6
	473.2
	484.5
$^5I_8 \rightarrow {}^5S_2, {}^5F_4$	536.6
$^5I_8 \rightarrow {}^5F_5$	640.8
	647.8
	656.3

ground state $^5I_8$ to the excited states belonging to the $4f^{10}$ configuration (column 1). The accord between the measured spectral wavelengths (column 2) and the transition related to Ho^{3+} ion (column 1) establishes that the bands observed for the glass $(Ho_2O_3)_{0.22}(P_2O_5)_{0.78}$ are characteristic to Ho^{3+} ion, and are due to electronic excitations from the ground state to higher energy levels of the 4f-electrons. The spectral wavelengths and their notations provide the electronic energy level structure needed for the development of optical devices.

8.3. LASER INDUCED FLUORESCENCE OF HOLMIUM METAPHOSPHATE GLASS

The room temperature fluorescence of the glasses was excited by the argon laser set at a power of 100mw and tuned at the blue line at 4579Å. The back scattered fluorescence from the glass was collected and focussed into the single grating Rank-Hilger monochrometer facilitated with a $1200mm^{-1}$ grating and slitwidths set to 150μ (Chapter 2). The experimental resolution of the wavelength was ±2Å. The fluorescence of the holmium metaphosphate glass is much weaker than those observed previously for the corresponding glasses modified with Eu^{3+} (chapter 5), Sm^{3+} (chapter 6), and Tb^{3+} (chapter 7) ions. Figure 8.2 shows the fluorescence spectrum measured at room temperature of a holmium metaphosphate glass of composition $(Ho_2O_3)_{0.22}(P_2O_5)_{0.78}$. The measured fluorescence peaks are compared in Table 8.2 with the transitions of fluorescence lines of Ho^{3+} ion in a crystalline LaF_3 host made by Caspers and Rast (1970). The close similarity between the two sets of data confirm that the holmium ions in this glass are in the trivalent state.

8.4. THE ORIGIN OF COLOUR CHANGES IN HOLMIUM METAPHOSPHATE GLASS

A straightforward but instructive method has been used to examine the physical origin of the colour change. Knowledge of the spectra of the light sources to be used was a prerequisite; the characteristics of the fluorescent lamps used are given in Table 8.3. One of the lamps is the Thorn halophosphate lamp (TWW) with a

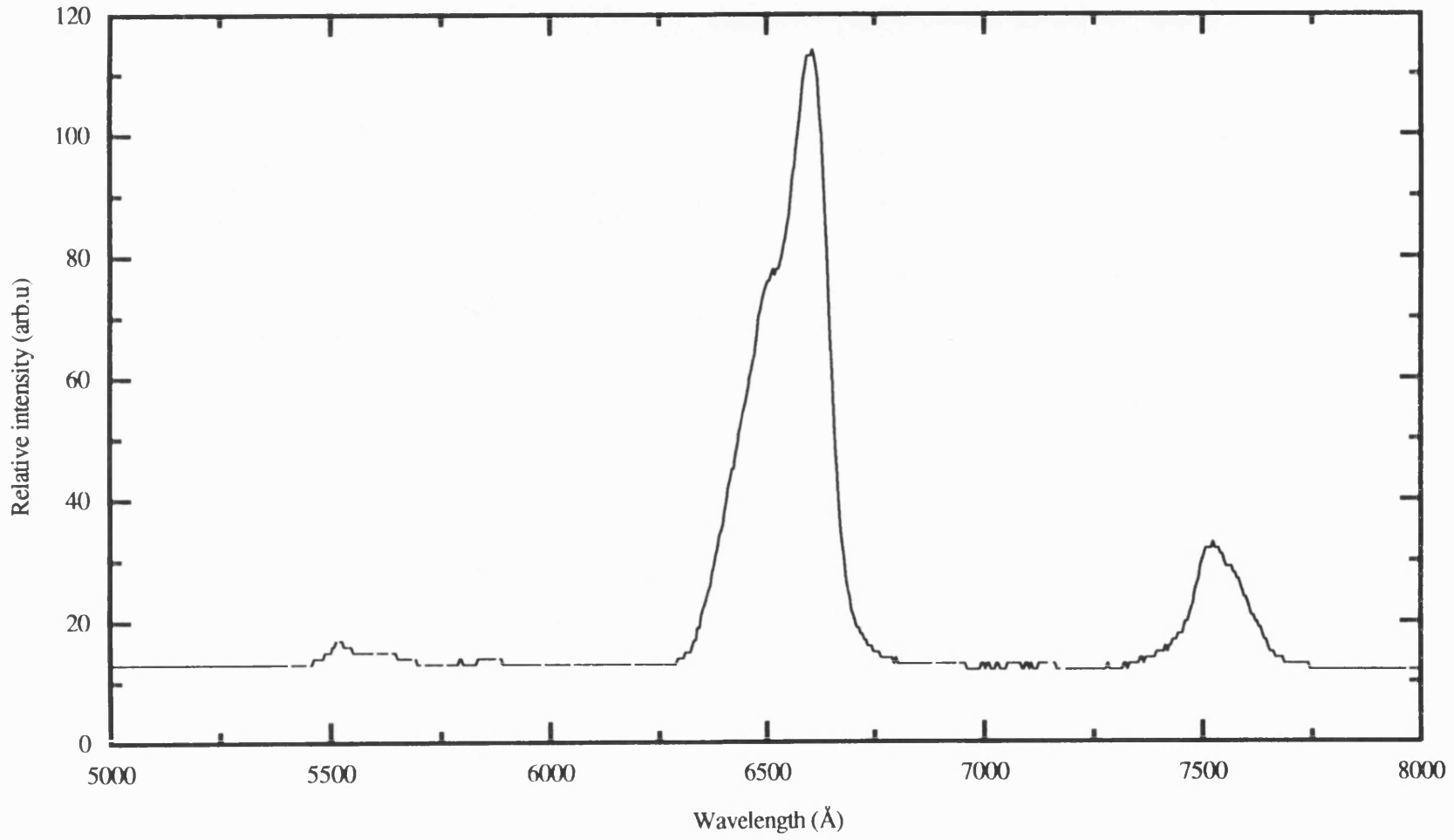

Figure 8.2. Fluorescence spectrum at room temperature of holmium metaphosphate $(Ho_2O_3)_{0.22}(P_2O_5)_{0.78}$ glass excited with an argon ion laser set at 100mW power and tuned at 4579Å blue line.

Table 8.2. Fluorescence lines of holmium metaphosphate $(Ho_2O_3)_{0.22}(P_2O_5)_{0.78}$ glass obtained at room temperature using the 4579Å blue line of an argon ion laser at 100mw power. The transitions between the 4f electron states of Ho^{3+} ion have been taken from Caspers and Rast (1970) for comparison with the experimental data.

Transition	fluorescence line (Å)
$^5I_8 \leftarrow {}^5I_4$	7526
$^5I_8 \leftarrow {}^5F_5$	6600 6515
$^5I_8 \leftarrow {}^5S_2, {}^5F_4$	5631 5526

Table 8.3. Characteristics of the fluorescent lamps used to investigate the alexandrite effect.

Symbol used	TWW	P84
Manufacturer	Thorn	Philips
Colour	Warmwhite	Colour 84 (Neutral White)
Correlated colour temperature	2900K	4000K
CIE chromaticy coordinates *	x = 0.440 y = 0.403	x = 0.380 y = 0.377

* Commission Internationale de l'Eclairage 1931 Cambridge, Cambridge University Press.

"warmwhite colour". The second lamp is the Philips triphosphorus lamp colour 84, which has a "neutral white colour".

Figures 8.3 and 8.4 show the experimentally determined emission line spectra of the P84 and TWW lamps respectively overlapped on the transmission spectra emerging from the glass using these lamps as light sources. The absorption spectrum exhibits four main absorption areas in the visible range: around 418nm (blue), 455nm (blue-green) (with some smaller lines towards longer wavelengths), 539±2nm (yellow-green), 644±3nm (red). In particular the regions from 497±1nm to 526±3nm (green) and from 554±2nm to 626±3nm (yellow to orange) are "windows" of comparably low absorption (Figure 8.1). Neither of the lamps have any emission lines in the green window (497-526nm) of the glass (Figure 8.3). The most marked feature seen in the response to the P84 lamp (Figure 8.3) is the absorption of the yellow band at about 545±10nm by the glass. This band of the lamp is close to the absorption band of the Ho^{3+} ion at 536.6±14nm. The rest of the emission lines of the lamp pass through the glass relatively intact with a much smaller overall absorption; there is some absorption of the weak bands around 650nm because there is a moderately strong absorption band in the vicinity of 640±20nm (Figure 8.1). The remaining lines can be grouped into two bands: (i) one in the deep yellow-orange between about 580 to 600nm, ie more toward the red, (ii) the other between about 605 to 630nm in the red. This red band, produced by the lamp, is much stronger than the yellow-orange band (Figure 8.3). In particular these comparisons show that under the P84 light source the colour perceived by the eye is largely due to the high emission intensity from the lamp of this red band at about 611nm to 613nm mixed with a moderate emission of the deep yellow-orange band (Figure 8.3) in combination with the fact that both bands lie in the yellow-orange absorption window (554-626nm) of the glass (Figure 8.1); the other parts of the lamp spectrum are absorbed.

The comparison between the emission spectrum of the Thorn halophosphate lamp and the transmission spectrum of the glass with this lamp as light source (Figure 8.4) shows a similar absorption of the yellow line at about 545nm by the glass. There is an extended tail in the lamp emission spectrum beyond 630nm but this is absorbed in the glass due to the moderately strong absorption band in the vicinity of

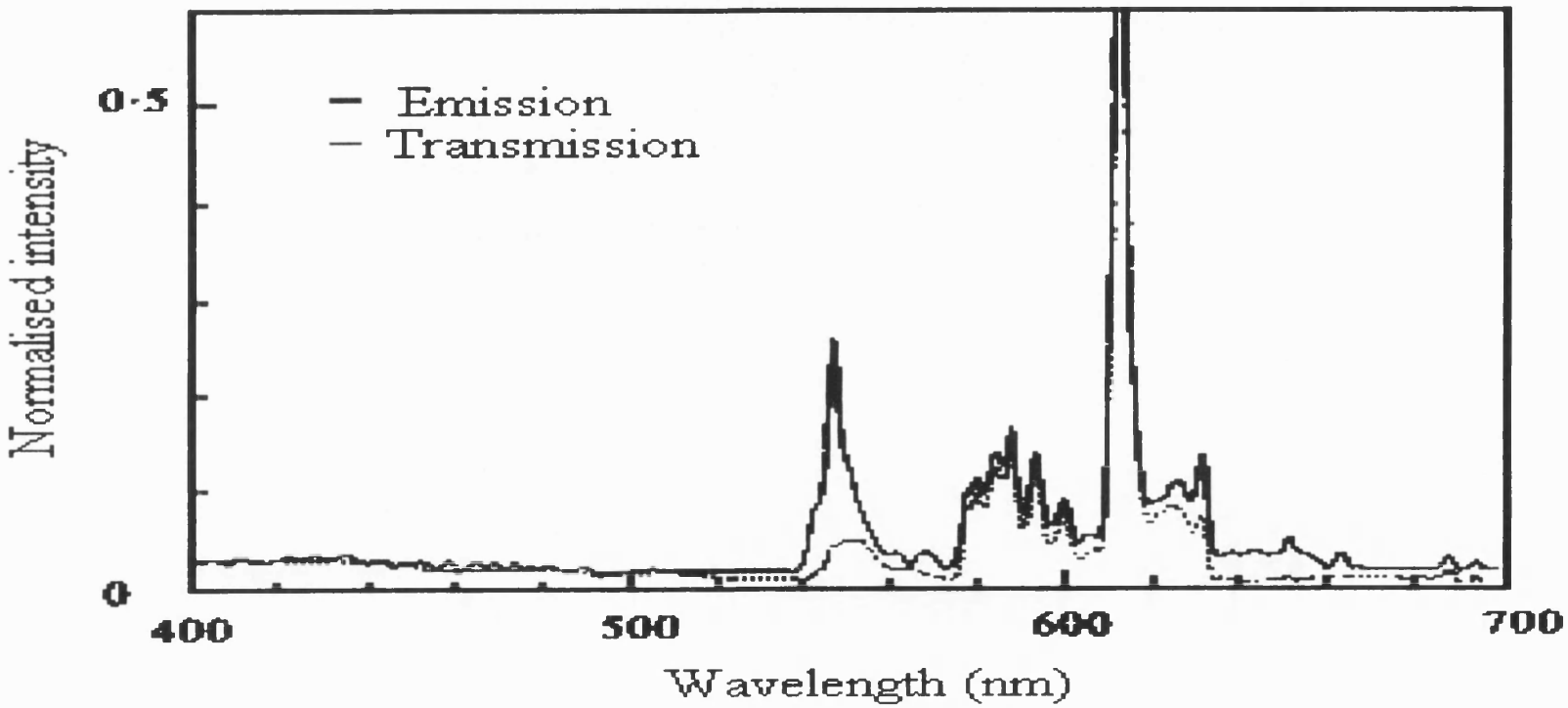

Figure 8.3. Emission spectrum of Philips triphosphorus lamp colour 84 (neutral white) and the transmission spectrum of holmium metaphosphate glass using this lamp as the source.

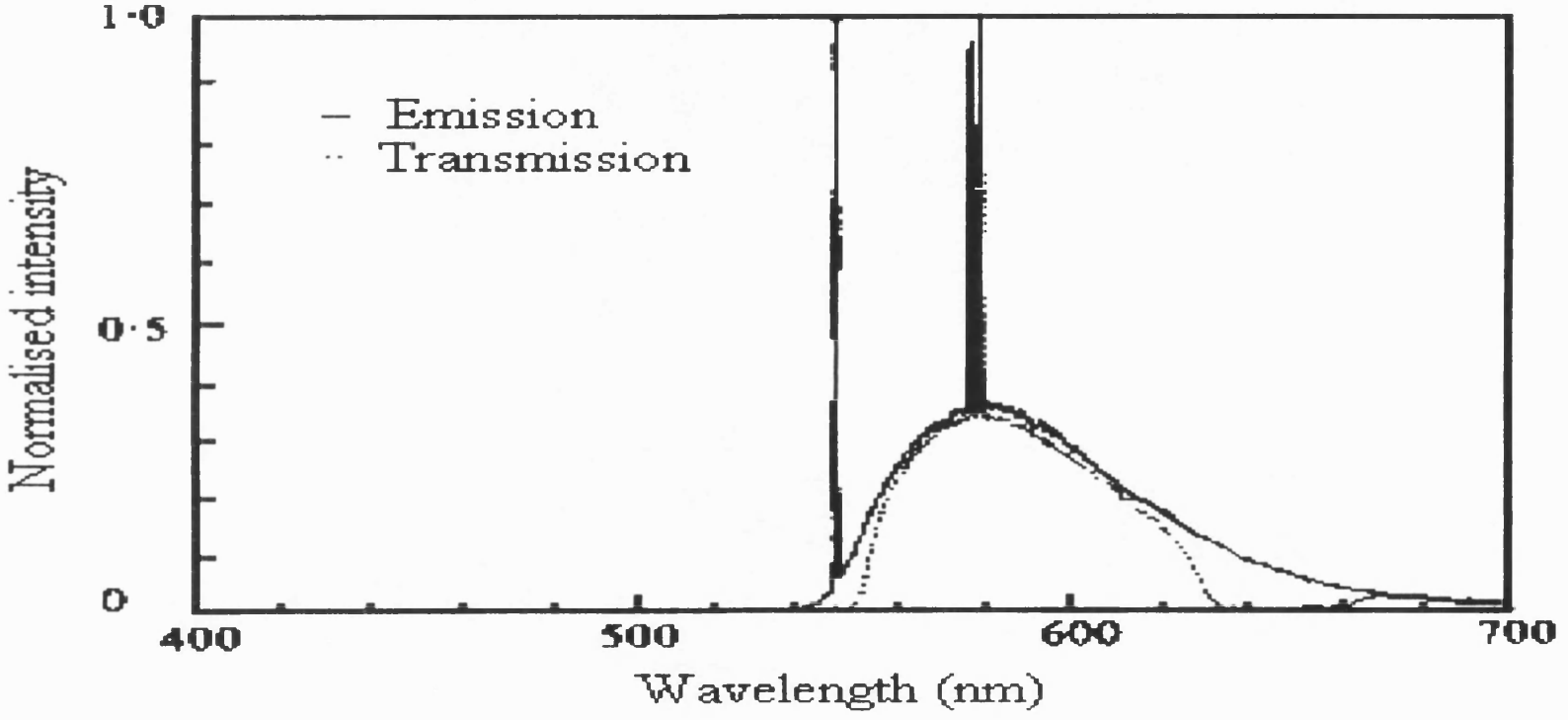

Figure 8.4. Emission spectrum of Thorn halophosphate lamp (colour 'warm white') and the transmission spectrum of holmium metaphosphate glass using this lamp as the source.

640±20nm (Figure 8.1). However the colour of the glass viewed with this light source is not quiet so red being more orange than it appears with the other source. This is caused by the strong double peaks produced by the TWW lamp at about 570nm, which add more orange to the colour perceived by the eye.

Overall the perceived colour of the glass when viewed under these fluorescence lamps is in the orange-red. Since daylight is equally rich in all wavelengths in the visible region, the appearance of the glass under sun light is yellow. This can be ascribed to the two windows in the optical absorption spectrum of the glass in the yellow-orange between 554nm to 626nm and the green from 497nm to 526nm (Figure 8.1), which pass effectively all the wavelengths in these ranges; the rest of the sun light is absorbed in varying proportion. As a result the colour of the glass perceived by the eye due to transmission of sunlight through the glass is determined by admixture of some green through the narrower green band window together with substantially more yellow through the wider window in the yellow-orange; this leads to a yellow colour, although the eye is more sensitive to the green.

The possibility that the red colour of the glass might be the result of fluorescence at 660nm does not arise because of the weakness of the fluorescence even when excited with a 100mw laser power with a relatively wide opening slits of the monochromator. Such a weak fluorescence cannot affect the colour appearance to any notable extent. The colour changes of holmium metaphosphate glass when viewed under different light sources are of a similar nature to those in alexandrite itself.

CHAPTER NINE

EXPERIMENTAL STUDIES OF RAMAN SPECTRA OF RARE EARTH METAPHOSPHATE GLASSES AND THEIR COMPARISON WITH THOSE OF PENTAPHOSPHATE CRYSTALS OVER THE TEMPERATURE RANGE OF 10-300K

9.1. INTRODUCTION

Due to the weak Raman intensity spectra of glasses, at one time infrared (IR) spectra played the most important role in studying the local vibrational states of the constituent components of glasses. But since the development of laser in 1960s, laser Raman spectroscopy has been used extensively as a major tool for such studies. Laser Raman spectroscopy has become even more powerful in studying vibrational states in glasses now that high sensitivity detection techniques with photon counting have been developed.

Raman spectra in crystals can usually be interpreted using group theory, but the Raman spectra in glasses can not, due to the absence of long-range order in their structures. One useful approach to interpretation of the Raman spectra of glasses is to make a comparison with the Raman spectra of a crystal having similar composition. The key to an understanding of the experimental Raman spectra of glasses is the breakdown of the wave-vector selection rule of crystalline Raman scattering. This leads to a continuous first-order vibrational spectrum of glasses instead of the discrete Raman spectrum of crystals. Two properties of glass are responsible for this fundamental difference. Firstly, in glass, the coupling between the atomic displacement and the fluctuation of the dielectric susceptibility is itself a random quantity because of the irregular atomic bonding. This aspect of the disorder is referred to as "electrical disorder". Secondly, with the exception of very low frequencies, vibrational modes of glass are not plane waves. The disorder which manifests itself by the distortion of the vibrational modes is termed "mechanical disorder", (Jäckle 1981).

In glasses the cation (modifier) play a big role in the physical and chemical properties. Studying the Raman spectrum can provide some information about the effect of the cation (its site, size, concentration and charge) on the backbone network (the glass former). Also, the Raman spectra can be used to establish the nature of the links between the structural units of the glasses and the local geometry around their cations. It is expected that the local geometry and the forces around each cation are similar in the glassy and crystalline states. This expectation is supported by the observed Raman spectra of some glasses and their crystalline analogues (Rouse et al. 1978). It is believed that glasses have short-range structure similar to their crystal counterparts.

The central objective of the present chapter can be thought of as two fold. The first aim has been to determine the vibrational motions of structural units of phosphates (PO_4 units), which exists in the rare earth phosphate glasses, using Raman spectroscopy. This vibrational motion determination enables us to picture the type of connection present between the PO_4 units, which can help in visualising the local environment around the rare earth ions of these glasses. The second objective has been to measure the effect of temperature and the rare earth ion on the Raman modes of these glasses.

During the process of vibrational mode determination of the rare earth phosphate glasses, it has proved useful to study the Raman spectra of rare earth pentaphosphate crystals (ReP_5O_{14} where Re is the rare earth ion). Instructive similarities between Raman spectra of glasses and crystals having the same structural units (the PO_4 unit) have been found. Therefore, the Raman spectra of these crystals were measured at room and low temperatures. The low frequency modes of these crystals showed some shifts with decreasing temperature (mode softening). Therefore, some attention was directed to measure in detail the effect of temperature on these low frequency modes.

9.2. RAMAN SCATTERING: DEFINITION:

When an intensive monochromatic radiation of wavenumber ω_0 is incident on gas, liquid or solid, most of it is transmitted without change, but, in addition, some scattering of the radiation occurs. If the frequency content of the scattered radiation is analysed, there will be observed to be present, not only the wavenumber ω_0 associated with the incident radiation, but also, in general, pairs of new wavenumbers of the type $\omega = \omega_0 \pm \omega_m$. The unchanged wavenumber of the scattered light is called the Rayleigh scattering. In molecular systems, the wavenumbers ω_m are found to lie principally in the ranges associated with transitions between rotational, vibrational and electronic levels. The scattered radiation usually has polarisation characteristics different from those of the incident radiation, and both the intensity and the polarisation of the scattered radiation depend on the direction of observation. Such scattering of radiation with change of frequency is called Raman Scattering (Long 1977).

In the spectrum of the scattered radiation, the new wavenumbers are termed Raman lines, modes or bands, and collectively are said to constitute a Raman spectrum. Raman bands at wavenumbers less than the incident wave number (which means of the type $\omega_0-\omega_m$) are referred to as Stokes bands, and those at wavenumbers greater than the incident wave number (which means of the type $\omega_0+\omega_m$) as anti-Stokes bands. The anti-Stokes bands are usually weaker than the Stokes one due to the low population of the higher vibrational states which are responsible for it (Gilson and Hendra 1970).

9.3. RAMAN SPECTRAL INVESTIGATIONS OF PHOSPHATE GLASSES AND CRYSTALS

There have been a number of studies on the vibrational spectroscopy of binary phosphate glasses, see for example Rouse et al. (1978), Nelson and Exarhos (1979), and the review of Martin (1991). Most of these studies have focused mainly on glasses in which the network modifier (cation) is a monovalent and divalent metal. The present work has been devoted to study the Raman spectra of rare earth phosphate glasses, in which the rare earth ion has a valence of +3.

A short review is now given of the previous examinations of the Raman spectra of phosphate glasses and crystals, made by other workers, to serve later as a guide to interpret the results of the Raman spectra obtained on the rare earth phosphate glasses and crystals. For the sake of clarity this review has been split into two sub-sections according to the frequency shift region: high and low frequency Raman modes.

a) High Frequency Raman Modes

The work reported by Galeener and Mikkelsen (1979) on the Raman spectra of pure P_2O_5 glass at 530°C and also of gaseous P_4O_{10} can be of use to specify some of the vibrational motions of structural units of phosphates. According to their experimental Raman spectrum the P_2O_5 glass has an intense band at about 1390cm^{-1} which they attributed to the strong P=O stretching mode (Figure 9.1) and a second band at about 640cm^{-1} was attributed to the symmetric stretching of the bridging oxygen atoms.

Previous studies of Raman spectra of binary phosphate glasses show three major bands. In alkali metal phosphate glasses, the bands occur at about 670, 1160, and 1260cm^{-1} and they have been assigned to vibrations of the polyphosphate backbone network (Bobovich 1962). The strong, sharp, polarised band occurring at about 1160cm^{-1} in the alkali metal metaphosphate glasses has been signed to the symmetric out-of-chain stretching vibration of the PO_2 while the band at about 1260cm^{-1} assigned to the antisymmetric out-of-chain stretching vibration of the PO_2 unit. The weak band observed at about 670cm^{-1} has been attributed to the in-chain symmetric stretching vibration of the P-O-P unit (Bues and Gehrke 1956, Jost 1963).

Rouse et al. (1978) discovered that the frequencies of the symmetric vibration bands corresponding to (PO_2) and (P-O-P) vary as the compositions of phosphates are varied. They also found that both of these bands are cation-dependent and decrease in frequency through the alkali metal metaphosphate series in the order of Li>Na>K>Rb>Cs. While the antisymmetric (PO_2) vibration band shifts in frequency by a tiny amount through the same series.

Parent et al. (1987) studied the Raman spectra of phosphate glasses with different composition ratios R (see chapter 4). They have found that when the glass has the

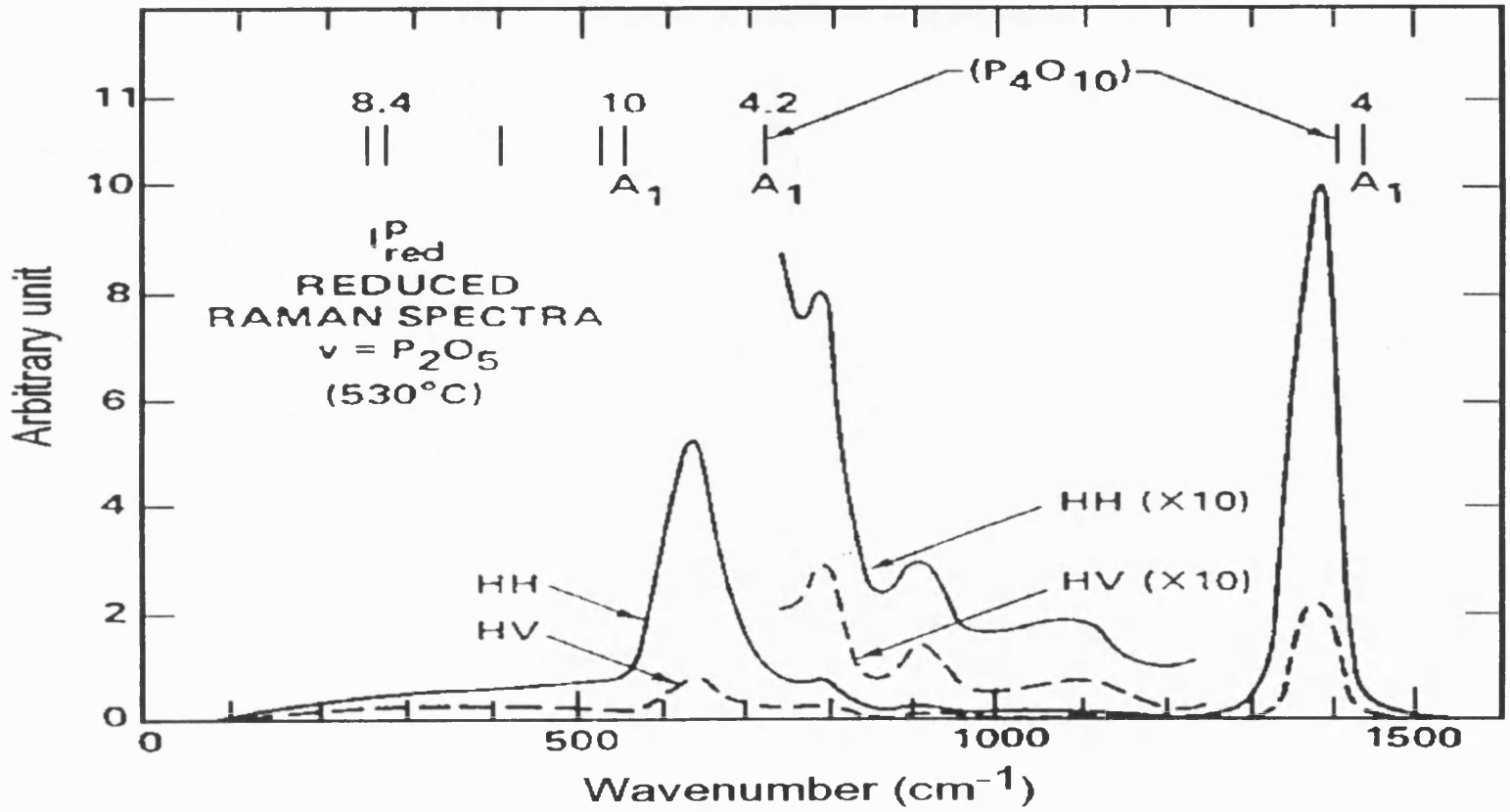

Figure 9.1. The Raman spectra of pure P_2O_5 glass compared with the observed Raman lines in gaseous P_4O_{14} (after Galeener and Mikkelsen 1979).

ratio R>1, a new band arises around 1040cm^{-1} in addition to the three main bands mentioned above. This band has been assigned to a PO_3 vibration (Fawcett et al. 1976). They also found that when R<1 the intensity of the lines located at 1234-1270cm^{-1} increases progressively as R decreases. This increase has been interpreted as a consequence of the emergence of a new band attributed to P=O vibration which is superimposed to the antisymmetric PO_2 vibration band. The emergence of the band due to P=O mode vibration has been related to the appearance of branching points and so is evidence for the existence of cross-linked metaphosphate chains for glasses with R<1. Their findings can be summarised as that when R=1 the glasses are built up from quasi-infinite metaphosphate chains, and when R>1 these chains shorten, so that the proportion of terminal PO_3 groups increases. On the other hand the observed broadening of the P-O-P band at 700cm^{-1} has been interpreted as a larger distribution of bond lengths and bond angles.

In many studies of metaphosphate glasses, Raman spectroscopy has proved to be a useful tool to obtain information about the interaction between the cation and the PO_2 group. A simple vibrational model which assumes that the cation has a negligible effect on the in-chain P-O-P vibration has been used by Rouse et al. (1978) to explain the Raman spectral results. The work of Nelson and Exarhos (1979) on metal ion modified metaphosphate glasses has confirmed that the frequency and intensity of the in-chain P-O-P symmetric vibration is almost the same for all ion modifiers. They suggested that the metal cations have only a weak interaction with the bridging oxygens of the polyphosphate chain. Therefore, P-O-P symmetric vibration at about 700cm^{-1} has been used as an internal standard to measure the cation effect on the intensity of the out-of-chain PO_2 symmetric vibration. Jost (1963) and Guitel and Tordjman (1976) reported for alkali metal metaphosphate crystals that the O-P-O bond angle (φ) is increased when the cation size is increased. The increase in φ causes a decrease in the frequency of the PO_2 vibration. This has been interpreted as a natural consequence of the increase in PO_2 bond angle and decrease in the metal-oxygen force constant (Rouse et al. 1978), resulting from substitution of a larger cation for a smaller one. Nelson and Exarhos (1979) have also confirmed the effect of the cation size on the frequency of the out-of-chain, symmetric vibration of the PO_2 band in the Raman spectra of Al, Mg, and Na metaphosphate

glasses. They have found that the larger the cation size ($Al^{3+} < Mg^{2+} < Na^{1+}$) the lower the frequency of the PO_2 vibrational band, reflecting larger bond angle φ.

Raman bands occurring below $500cm^{-1}$ in metaphosphate glasses are difficult to assign with certainty owing to the strong dependence upon chain conformation. In general, they have been assigned to bending and torsional vibrations. The weak bands in glassy $NaPO_3$ and $Mg(PO_3)_2$ at 360 and $300cm^{-1}$ have been assigned to PO_2 bending and in-chain O-P-O bending motions, respectively (Bues and Gehrke 1956).

As the structure of crystalline materials can be obtained from crystallographic studies their Raman spectra can be of assistance in interpreting the spectra of the corresponding glasses. For example a comparison between the Raman spectra of crystalline and glassy phosphate samples was used to show that the Raman spectra of the alkali metal metaphosphate glasses form an envelope of the spectra of the corresponding crystalline material. This observation gave a strong indication that the short range structure of the glass is similar to that of the corresponding crystal (Exarhos and Risen 1971, 1972), except that the fixed sites in the crystal are replaced by a distribution of many types of different but similar sites in the glass. This is consistent with the random network model for the glass structure, in which the local order of the crystal is maintained in the glass, but the long range order is absent (Zachariasen 1932). On this basis, it is reasonable to consider the local vibrations in glasses in terms of the local geometry of their corresponding crystals.

As is the case in other phosphates, the basic unit of the rare earth pentaphosphate crystal structure is the PO_4 tetrahedron. The structure of rare earth pentaphosphate crystals (ReP_5O_{14}) is comprised of cross-linked PO_4 tetrahedra sharing three oxygen atoms and forming rings (Hong and Pierce 1974). Such rings give rise to Raman bands that are produced by the P=O vibration band which occur at high frequency (higher than $1250cm^{-1}$) in the lanthanum pentaphosphate crystal (LaP_5O_{14}). Another Raman band which characterises the Raman spectrum of rare earth pentaphosphate crystals (related to rings) is the band in the vicinity of $700cm^{-1}$ (Parent et al. 1987). Thus the presence of these two Raman bands can be used as an indication of existence of rings of PO_4 tetrahedra.

On the other hand, rare earth metaphosphate crystals having the formula ReP_3O_9 are believed to comprise of helical ribbons, $(PO_3)_n$, formed by corner-sharing of PO_4 tetrahedra (Hong 1974). Such ribbons (or chains of PO_4 tetrahedra) produce Raman bands in the vicinity of 680 and 1190cm^{-1} in the Raman spectrum of the lanthanum metaphosphate crystal (LaP_3O_9) (Parent et al. 1987). Again these two Raman bands can be taken as a sign of the existence of chains of PO_4 tetrahedra in a phosphate material.

b) Low Frequency Raman Modes

By low frequency Raman modes is meant the vibrational states occurring typically below 100cm^{-1} frequency shift from the laser exciting line of the Raman spectrum. In this part of the spectrum the most marked differences between vibrational states of glasses and crystals can be noted, and it is in this part of the frequency spectrum where the most marked differences occur. Although these states have been extensively studied, there is no generally agreed microscopic description even for vitreous silica, the most studied glass. These vibrational states contribute to the heat capacity C(T) in the low temperature range 2-20K (Buchenau 1986).

The Raman spectrum in the low frequency region consists of two parts; the low-frequency tail of the first order vibrational spectrum and a broad quasielastic line which extends beyond the Brillouin lines (Jäckle 1981). Taking these two points into consideration with others, this part of the spectrum can be thought of as a combination of intrinsic Raman activated by vibrational modes, such as rocking, localised (cage-like) heavy metal or acoustic Raman modes (Miller et al. 1988) in addition to an enhancement due to some thermal and scattering effects. The causes of the thermal and scattering effects have been attributed to the following points:

1. An increase in the Bose-Einstein thermal phonon population $n(\omega) = 1/[\exp(\hbar\omega/K_BT) - 1]$, where ω is the Raman shift, $\hbar = h/2\pi$ is Planck's constant, K_B is Boltzmann's constant and T is the temperature.

2. An increase in the Raman scattering proportional to $(\omega_o - \omega)^4$, where ω_o is the frequency of the laser line.

3. The elastically scattered radiation wing, due to Rayleigh scattered light.

In the low frequency Raman spectra of glasses the most prominent peak occurs at around $50cm^{-1}$. This peak is referred to as the " boson peak" and it has been attributed to an increase in the thermal population with decreasing phonon frequency at room temperature (Almeida 1988). Thus the low frequency region is determined by two spectral contributions which are characteristic of vitreous materials: the light scattering excess and the "boson peak". The light scattering excess (LSE) can clearly be observed for frequencies below $10cm^{-1}$, while the boson peak can be observed above $20cm^{-1}$.

Theoretically, the Raman scattering intensity in an amorphous system (Shuker and Gammon 1970) is given by

$$I(\omega) = C(\omega).g(\omega).\frac{n(\omega)+1}{\omega} \qquad 9.1$$

where $[n(\omega)+1]$ is the Bose-Einstein population factor for Stokes components, $1/\omega$ is the harmonic propagator, $g(\omega)$ the density of vibrational states and $C(\omega)$ is the coupling constant. To reflect the density of states modulated by the coupling constant, the Raman scattering intensity can be reduced by the harmonic propagator and the population factor as below:

$$I_R = \frac{I_{exp.}\,\omega}{n(\omega)+1} = C(\omega).g(\omega) \qquad 9.2$$

In the low temperature region, where the vibrational modes are acoustic, the density of states is expected to be Debye-like and hence to have an ω^2 -behaviour. Thus in this frequency range, the power of the coupling constant for light scattering from acoustic modes may be determined from Raman measurements.

Studies of low frequency Raman spectra of rare earth pentaphosphate crystals as a function of temperature can yield valuable information concerning the structural changes associated with phase transitions. Rare earth pentaphosphate crystals, ReP_5O_{14} (Re = La - Tb), have the space group C^5_{2h} at room temperature with four chemical formulas, and 80 atoms in the primitive cell. These crystals undergo a second order ferroelastic transition with symmetry change mmm→2/m (or $D^7_{2h} \rightarrow C^5_{2h}$) in the range 398K (for LaP_5O_{14}) to 447K (for TbP_5O_{14}) (Schulz et al. 1974, Budin 1975, Weber 1975, Kobayashi et al. 1976). Several observations of soft acoustic and optic modes have been reported in these compounds (Errandonea and Sapriel 1979). Soft modes usually manifest themselves as a frequency shift in some of the low frequency Raman modes towards lower values, approaching zero frequency as the temperature increases in the direction of the phase transition temperature. This soft mode behaviour is characteristic of a displacement of ions in the lattice at the phase transition.

9.4. OPTICAL SYSTEM USED FOR RAMAN SPECTRAL MEASUREMENTS

The optical system, and its components, used to measure the Raman spectra of the rare earth phosphate glasses and crystals is generally described in this section. The Raman spectra were obtained using an experimental set-up in the Physics Department of the University of Edinburgh, in collaboration with ourselves. The experimental set-up used can be found in any textbook dealing with experimental Raman spectroscopy, for example the one by Gilson and Hendra (1970), with little difference in the specification of the equipment. Therefore, a brief description of the set-up need only be given here.

Since all the phosphate samples were sufficiently transparent, the Raman spectra could be taken in the 90° scattering configuration. The excitation was provided by one of the lasing lines of a CW argon ion laser (Coherent Radiation model 52). The laser beam was passed through a small monochromator to block any plasma lines, generated inside the laser tube, so that only one single laser line was allowed to pass through. The incident laser beam was focused down on the sample with a focusing lens to obtain a maximum excitation. The scattered light from the sample was then

gathered at right angles to the laser beam and passed through a polarisation scrambler. This scattered light was focused on the entrance slit of a triple grating monochromator (Coderg model RS100) with each grating having 1200line/mm. The analysed scattered light then fell onto a detection system which consisted of a cooled RCA 31034A (at -20°C) phototube sensitive in the region between 2000-9000Å. The output of the phototube was amplified by a preamplifier in pulse form and sent to a discriminator (model 1121 from Princeton Supplied Research) and from there to a photon counter. The outputs of the photon counter and the unit control of the monochromator were connected to a computer. Software was used to control the scanning steps and the measurements of the system.

The low temperature measurements of the Raman spectra of the rare earth phosphate glasses and crystals under study were achieved by putting the sample in a cryostat (model Cryophysics) capable of reaching a temperature as low as 10K. The sample temperature was kept constant to an accuracy of ±1°C. Sample heating by the laser beam was negligible: only miniscule changes in the spectra were observed when the laser power was reduced.

9.5. THE EXPERIMENTAL RAMAN SPECTRA OF THE RARE EARTH PHOSPHATE GLASSES AND CRYSTALS

The experimental results of the Raman spectra (Stokes bands only) determined for the rare earth phosphate glasses and pentaphosphate crystals will be given in next seven sections. The first four present the Raman spectra of the europium, samarium, neodymium, and lanthanum metaphosphate glasses. The rest give the Raman spectral results of Sm, Eu, and Nd pentaphosphate crystals.

The slit widths of the triple monochromator determine the instrumental linewidth of the measured Raman spectra. Three different slit widths were used (400, 200, and 150μ) in the measurements, depending on the sample and the frequency region required; in the visible region these three slitwidths produce instrumental linewidths of 4, 2, and 1.4cm^{-1}, respectively.

9.6. EXPERIMENTAL RAMAN SPECTRA OF NEODYMIUM PHOSPHATE GLASS

The Raman spectra of two samples of neodymium phosphate glass were examined over the temperature range of 10-300K. The spectral measurements were obtained using the 4880Å argon ion laser line, 200mW laser power, $5cm^{-1}$ for every two second scanning steps, and 400μ slit widths. Figures 9.2 and 9.3 show the normalised spectra, at different temperatures, for these two samples of compositions $(Nd_2O_3)_{0.194}(P_2O_5)_{0.806}$ and $(Nd_2O_3)_{0.196}(P_2O_5)_{0.804}$ respectively. The spectrum of the first sample $[(Nd_2O_3)_{0.194}(P_2O_5)_{0.806}]$ shows that it consists of six main bands situated at 60, 330, 690, 1200, 1250, and $1320cm^{-1}$ from the laser line (Figure 9.2). An apparent decrease in the intensity of some of the Raman bands of this sample was observed relative to the Raman band at $1200cm^{-1}$, when the temperature lowered from 300 to 10K. The measured Raman spectrum of the second glass sample $[(Nd_2O_3)_{0.196}(P_2O_5)_{0.804}]$ reveals the same six main bands, but at slightly different locations, being at 60, 320, 695, 1195, 1240, and $1315cm^{-1}$ (Figure 9.3). The Raman bands of this spectrum also show an intensity decrease, relative to the main band at $1195cm^{-1}$, when the temperature lowered to 10K. To visualise the small differences between the Raman spectra of these two neodymium metaphosphate glass samples, the two spectra have been overlapped. Figures 9.4 show this comparison between the Raman spectra at 300K and Figure 9.5 shows the comparison at 10K. An obvious shift and intensity reduction of the band in the vicinity $1250cm^{-1}$ can be observed at both temperatures. In addition, a narrowing on the low frequency side, only, of the band at $700cm^{-1}$ can be noticed, but no measurable shift can be calculated in this band within the experimental error. The Raman band at $330cm^{-1}$ has shifted to $320cm^{-1}$. These pronounced differences in the Raman spectra of the two glass samples cannot be attributed to the minute difference of the rare earth ion concentrations which is too small to cause such spectral variations. It is possible that these differences between the Raman spectra could be due to traces of residual microscopic stresses in these glasses with resultant microscopic structural differences. The residual stresses can be ascribed to the difficulties in controlling the glass formation parameters (such as the temperature of the furnace, the melting point of the rare earth oxides, the rate of phosphate evaporation etc.) in the time of

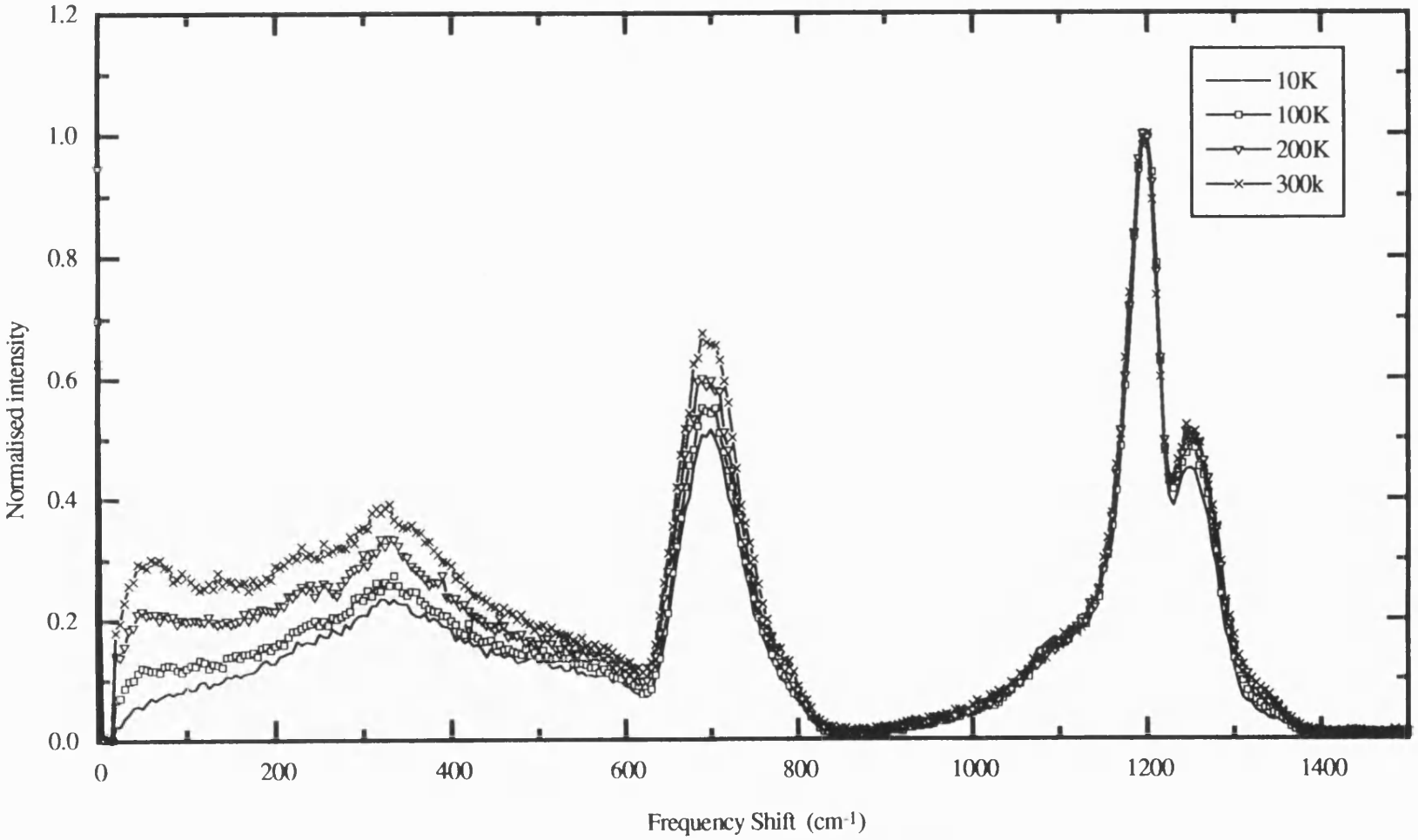

Figure 9.2. The Raman spectrum of $(Nd_2O_3)_{0.194}(P_2O_5)_{0.806}$ glass at different temperatures.

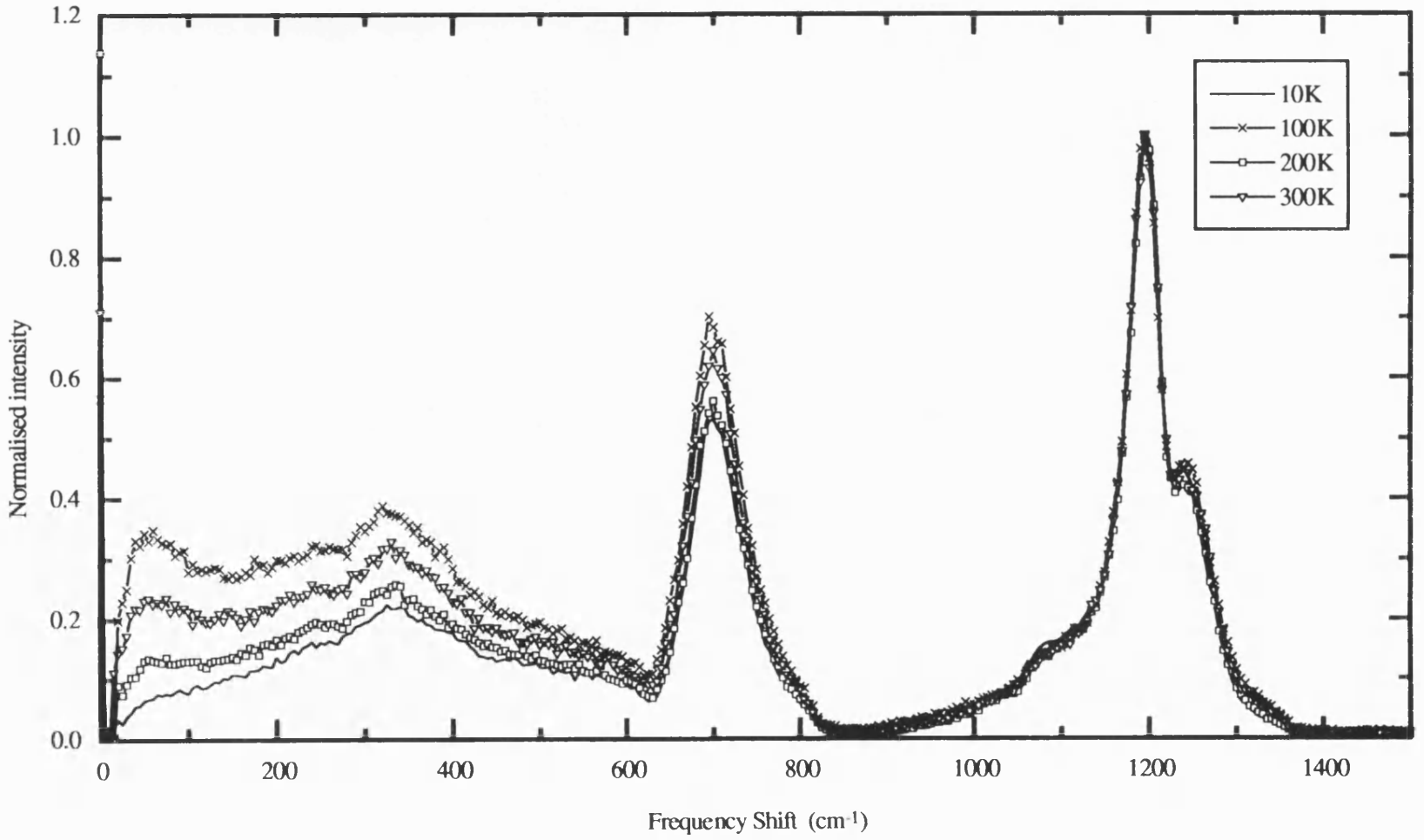

Figure 9.3. The Raman spectrum of $(Nd_2O_3)_{0.196}(P_2O_5)_{0.804}$ glass at different temperatures.

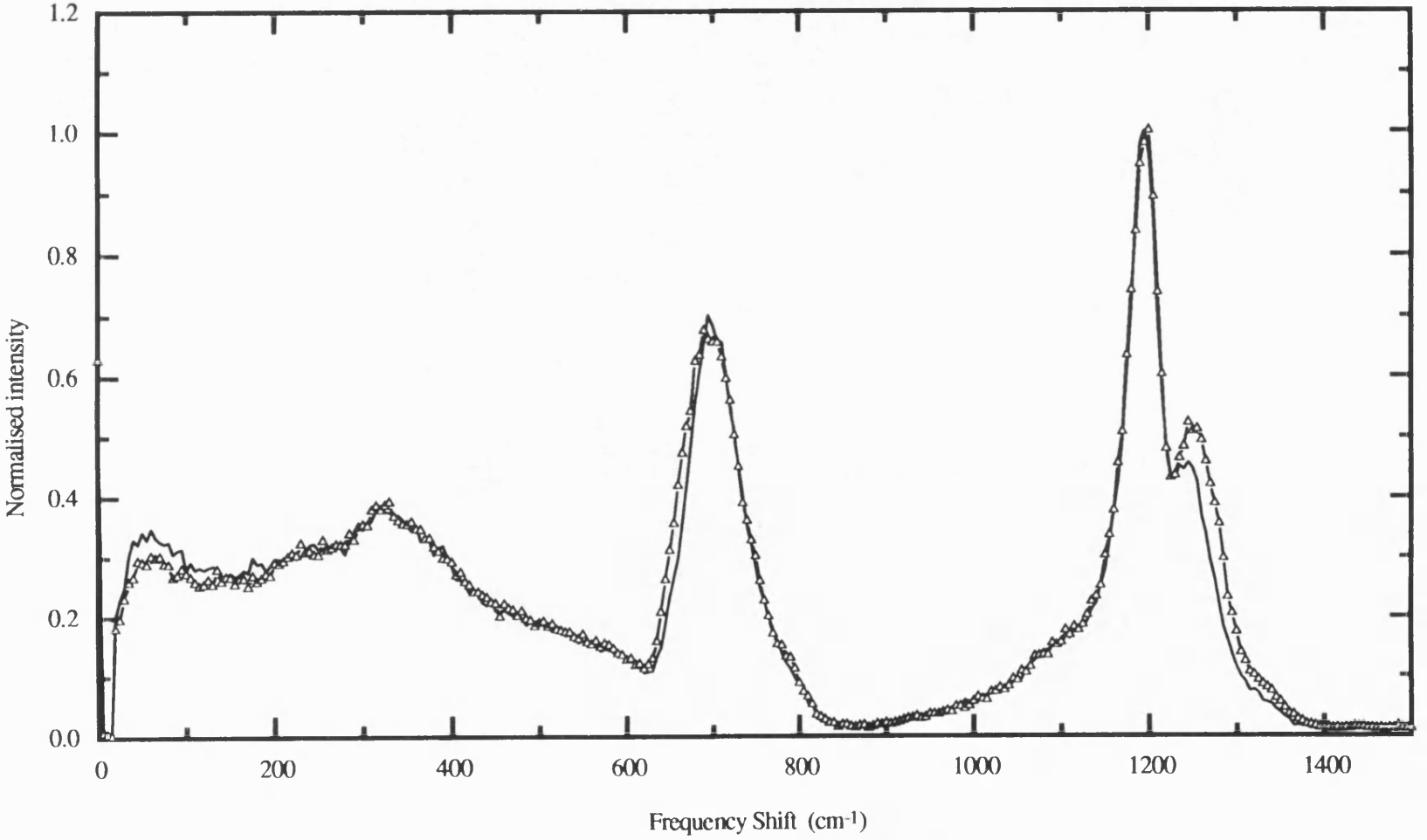

Figure 9.4. A comparison between the Raman spectra of $(Nd_2O_3)_{0.194}(P_2O_5)_{0.806}$ glass (triangle) and the $(Nd_2O_3)_{0.196}(P_2O_5)_{0.804}$ glass (line) at 300K.

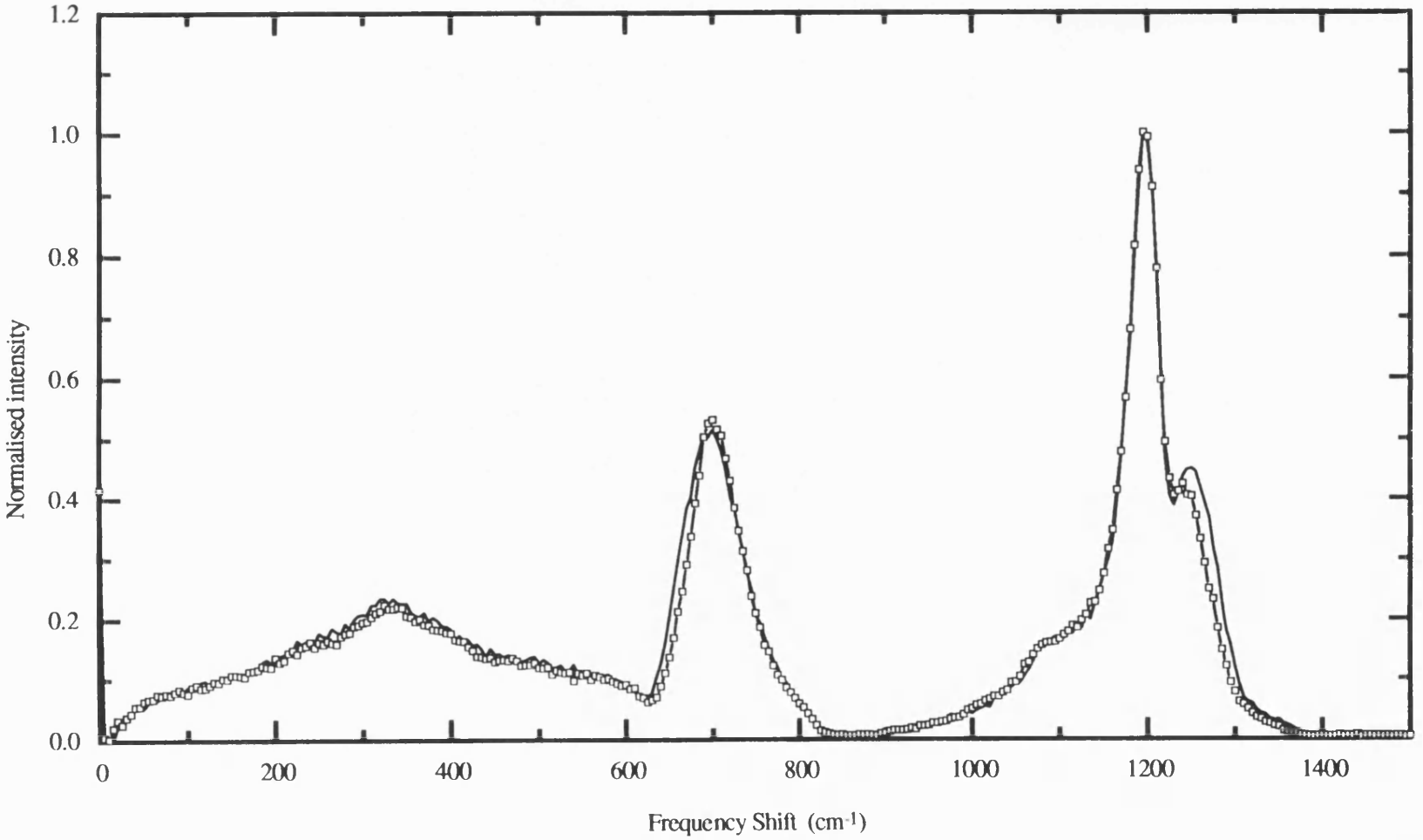

Figure 9.5. A comparison between the Raman spectra of $(Nd_2O_3)_{0.194}(P_2O_5)_{0.806}$ glass (square) and the $(Nd_2O_3)_{0.196}(P_2O_5)_{0.804}$ glass (line) at 10K.

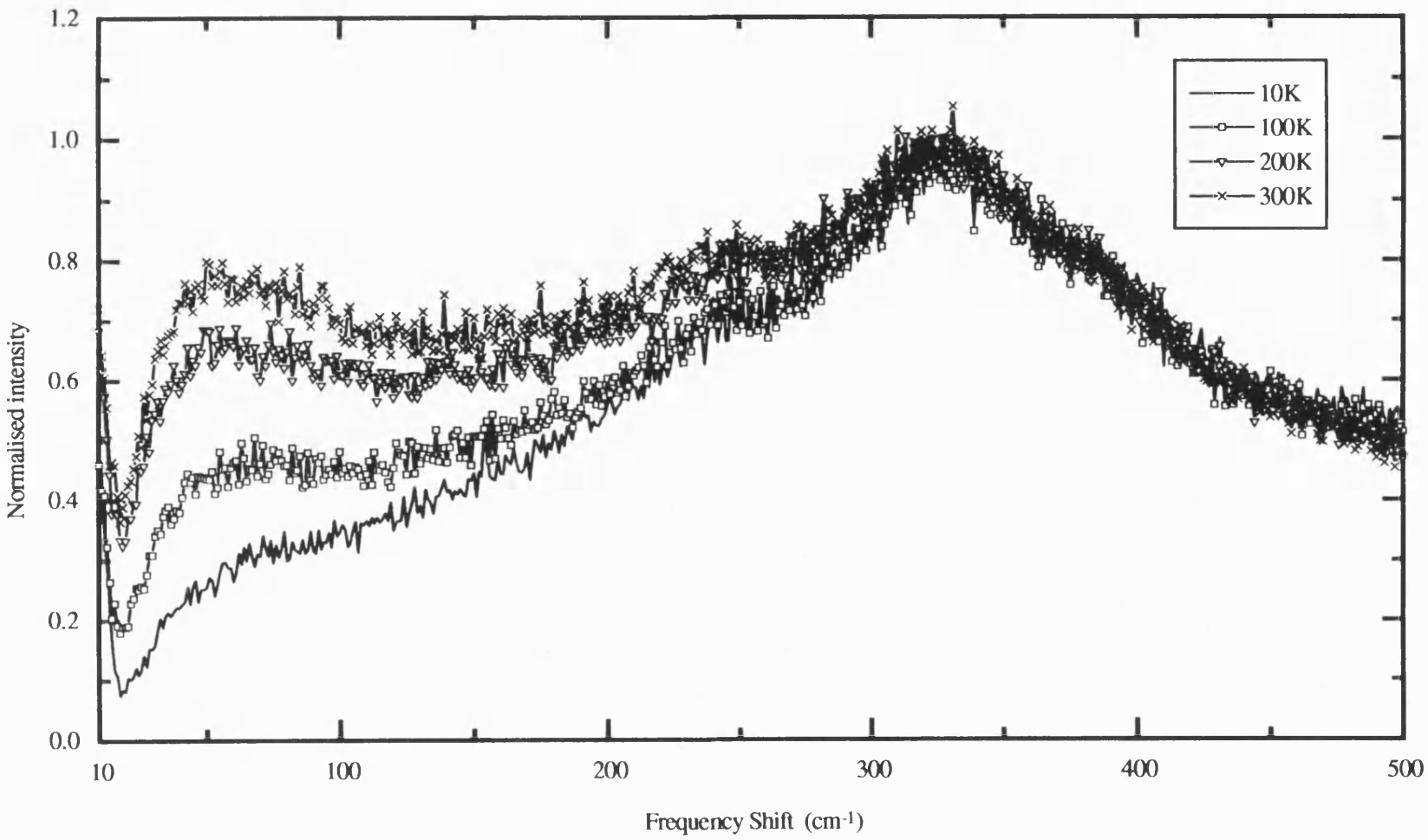

Figure 9.6. Low frequency Raman spectrum of $(Nd_2O_3)_{0.194}(P_2O_5)_{0.806}$ glass at different temperatures.

manufacturing these glasses.

The effect of temperature on the low frequency region of the Raman spectra of the $(Nd_2O_3)_{0.194}(P_2O_5)_{0.806}$ and $(Nd_2O_3)_{0.196}(P_2O_5)_{0.804}$ glasses was examined. The measurements were taken using the 4880Å laser line with 300mW laser power, a scanning speed $1cm^{-1}$ every 4 seconds and 200μ slit widths. Figure 9.6 shows the normalised Raman spectrum of the sample having the composition $(Nd_2O_3)_{0.194}(P_2O_5)_{0.806}$ (normalised against the Raman band at $330cm^{-1}$) recorded at 10, 100, 200, and 300K. Two important effects of temperature on the low frequency region of the spectrum can be seen. First, there is an obvious decrease in the intensity of the Raman band at $60cm^{-1}$ with temperature reduction. Secondly, there is a decrease in the intensity of the tail of the Rayleigh scattering (below $10cm^{-1}$) with temperature reduction (from an intensity value of 0.3 at 300K to 0.1 at 10K).

The temperature effect on the low frequency region of the Raman spectrum of the glass having the higher concentration $[(Nd_2O_3)_{0.196}(P_2O_5)_{0.804}]$ was examined. Figure 9.7 shows the low frequency region of the Raman spectrum of this glass recorded at 10, 100, 200, and 300K and normalised against the band at $320cm^{-1}$. The spectrum of this sample displays the same two effects found in the spectrum of the lower concentration of neodymium (Figure 9.6): a decrease in the intensity of the band at $60cm^{-1}$ (from about 0.86 at 300K to 0.3 at 10K) and a decrease in the intensity of the tail of the Rayleigh scattering (from 0.45 at 300K to 0.09 at 10K) with temperature reduction.

The low frequency Raman spectra (recorded at 300K) of the two samples of the neodymium phosphate glass can be used to find the effect of neodymium concentration on the spectra. In the spectrum of the glass with higher concentration of neodymium $[(Nd_2O_3)_{0.196}(P_2O_5)_{0.804}]$ the intensity of the tail of the Rayleigh scattering and the intensity of the band at $60cm^{-1}$ (Figure 9.7) have higher values than the ones in the lower concentration of neodymium $(Nd_2O_3)_{0.194}(P_2O_5)_{0.806}$ (Figure 9.6). At 10K both the tail of the Rayleigh scattering and the intensity of the band at $60cm^{-1}$ are reduced in both spectra. In comparing the two spectra it is found that their intensities are so similar as to be indistinguishable at this temperature.

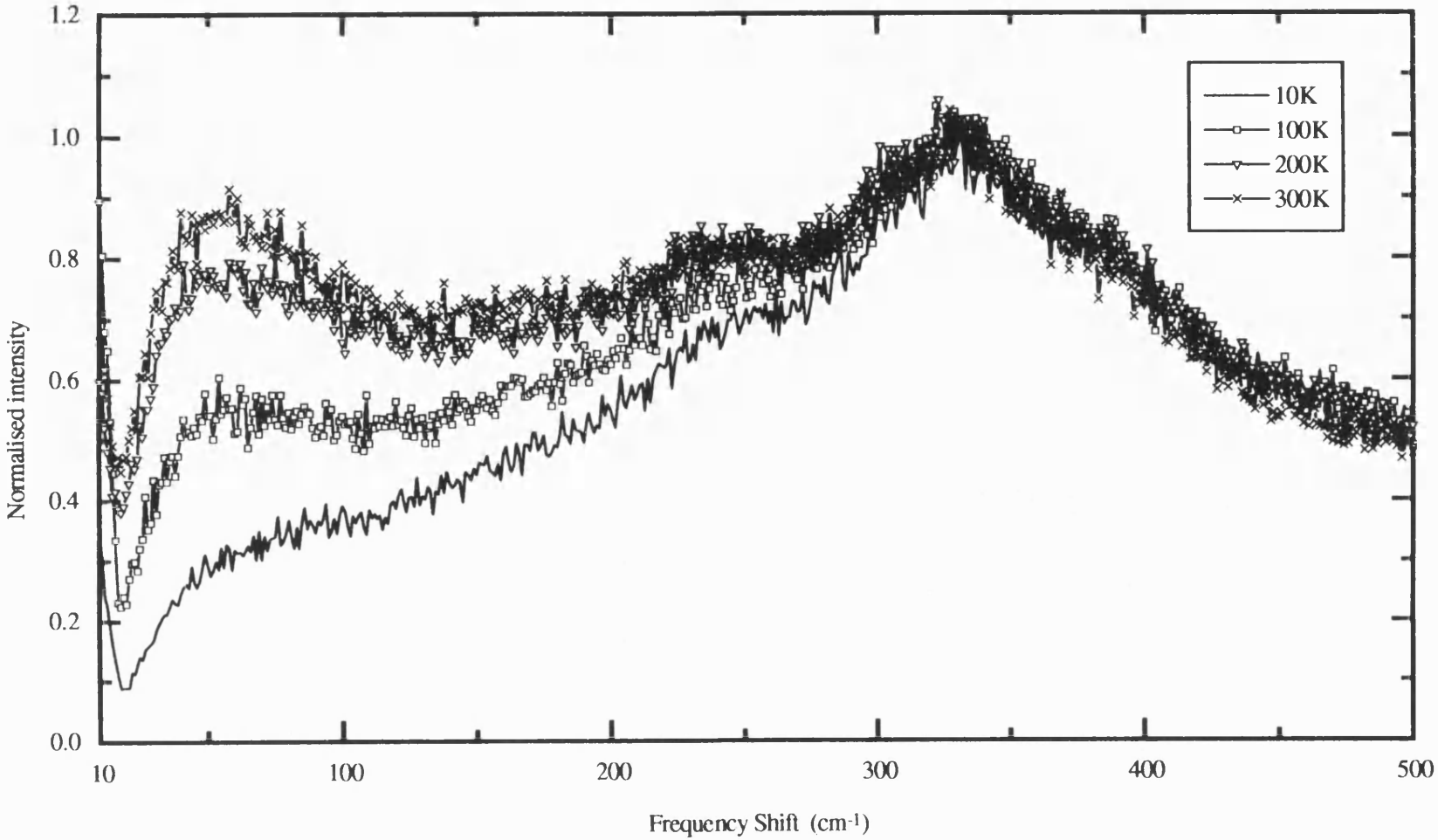

Figure 9.7. Low frequency Raman spectrum of $(Nd_2O_3)_{0.196}(P_2O_5)_{0.804}$ glass at different temperatures.

The low frequency region of the Raman spectrum was employed to measure the power of the coupling constant in the Raman intensity equation of glasses (equation 9.1). The experimental Raman intensity data of the neodymium phosphate glass having the composition $(Nd_2O_3)_{0.194}(P_2O_5)_{0.806}$ at 10K were reduced through multiplication by the frequency shift (ω) and dividing by the Bose-Einstein population factor ($n(\omega,T)+1$) (equation 9.2). There are two reasons for using the data of theRaman spectrum recorded at 10K: first to minimise any disturbance from the light scattering excess (LSE), which is at its minimum at low temperatures, second to obtain a region of acoustic mode which depends on ω^2 (Deby-like frequency dependence), obtainable at low temperatures. Figure 9.8 shows the log-log plot (at 10K) of the reduced intensity of the Raman spectrum of the sample having the composition $(Nd_2O_3)_{0.194}(P_2O_5)_{0.806}$ against the frequency shift in the frequency range 16-40cm^{-1}. The plot is linear with a slope of 3.43. A similar log-log plot for the sample having the composition $(Nd_2O_3)_{0.196}(P_2O_5)_{0.804}$ is shown in Figure 9.9; in this case the slope is 3.41.

9.7. EXPERIMENTAL RAMAN SPECTRA OF EUROPIUM PHOSPHATE GLASS

The Raman spectrum of a sample of europium phosphate glass, having the composition $(Eu_2O_3)_{0.186}(P_2O_5)_{0.814}$, was measured over the temperature range of 10-300K. The spectrum was obtained using 400μ slit widths, 200mW laser power, and scanning steps of 5cm^{-1} for every second. The frequency shifts of the Raman bands were measured with an accuracy of $\pm$1cm^{-1}. The 5145, 4765, and 4579Å argon ion laser lines were used to excite the Raman spectrum of this glass. The purpose of recording the Raman spectrum with three different laser lines was to identify any interference between the fluorescence bands and the Raman bands in the spectrum of this glass. Figure 9.10 shows the Raman spectrum of the europium phosphate glass, having the composition $(Eu_2O_3)_{0.186}(P_2O_5)_{0.814}$, measured at 300K. The spectrum shows six main bands located at 50, 330, 705, 1200, 1235, and 1315cm^{-1}. In addition, the spectrum excited by the 5145Å laser line has two more bands; one broad band extending over the Raman band at 705cm^{-1} and the other extending over the bands at 1235 and 1315cm^{-1}. However these two broad bands do not exist in

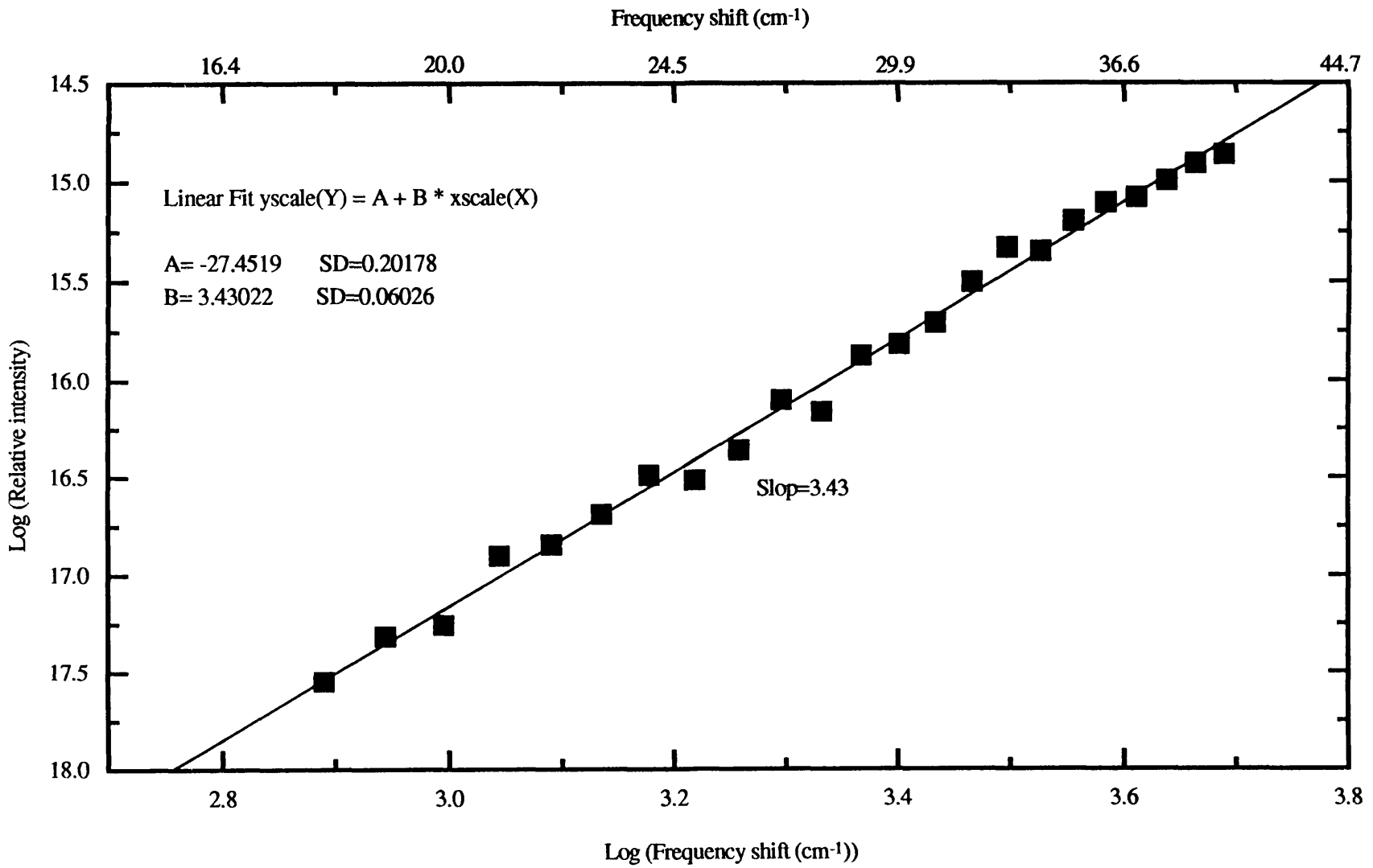

Figure 9.8. The frequency dependence of the reduced Raman intensity for the $(Nd_2O_3)_{0.194}(P_2O_5)_{0.806}$ glass at 10K.

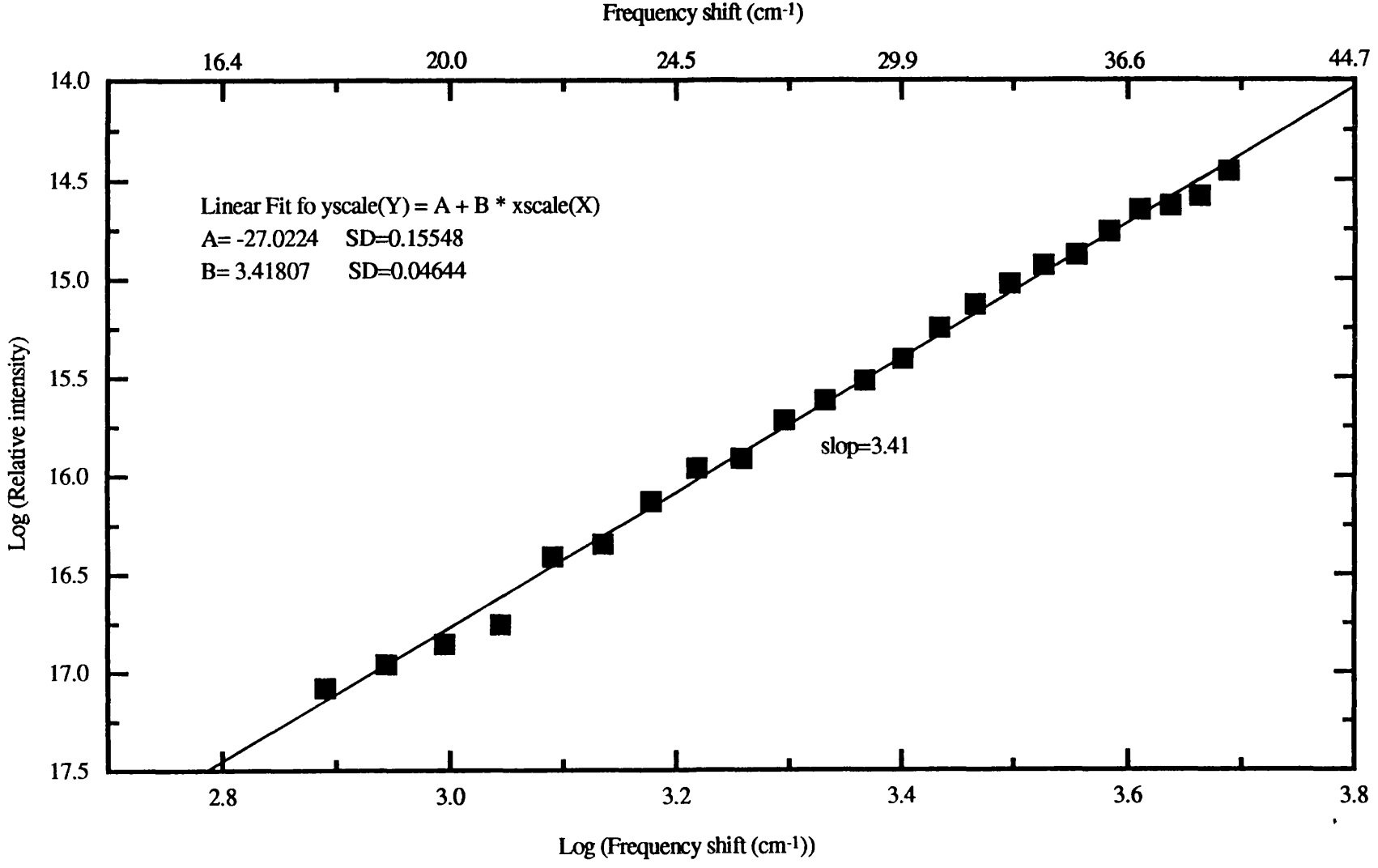

Figure 9.9. The frequency dependence of the reduced Raman intensity for the $(Nd_2O_3)_{0.196}(P_2O_5)_{0.804}$ glass at 10K.

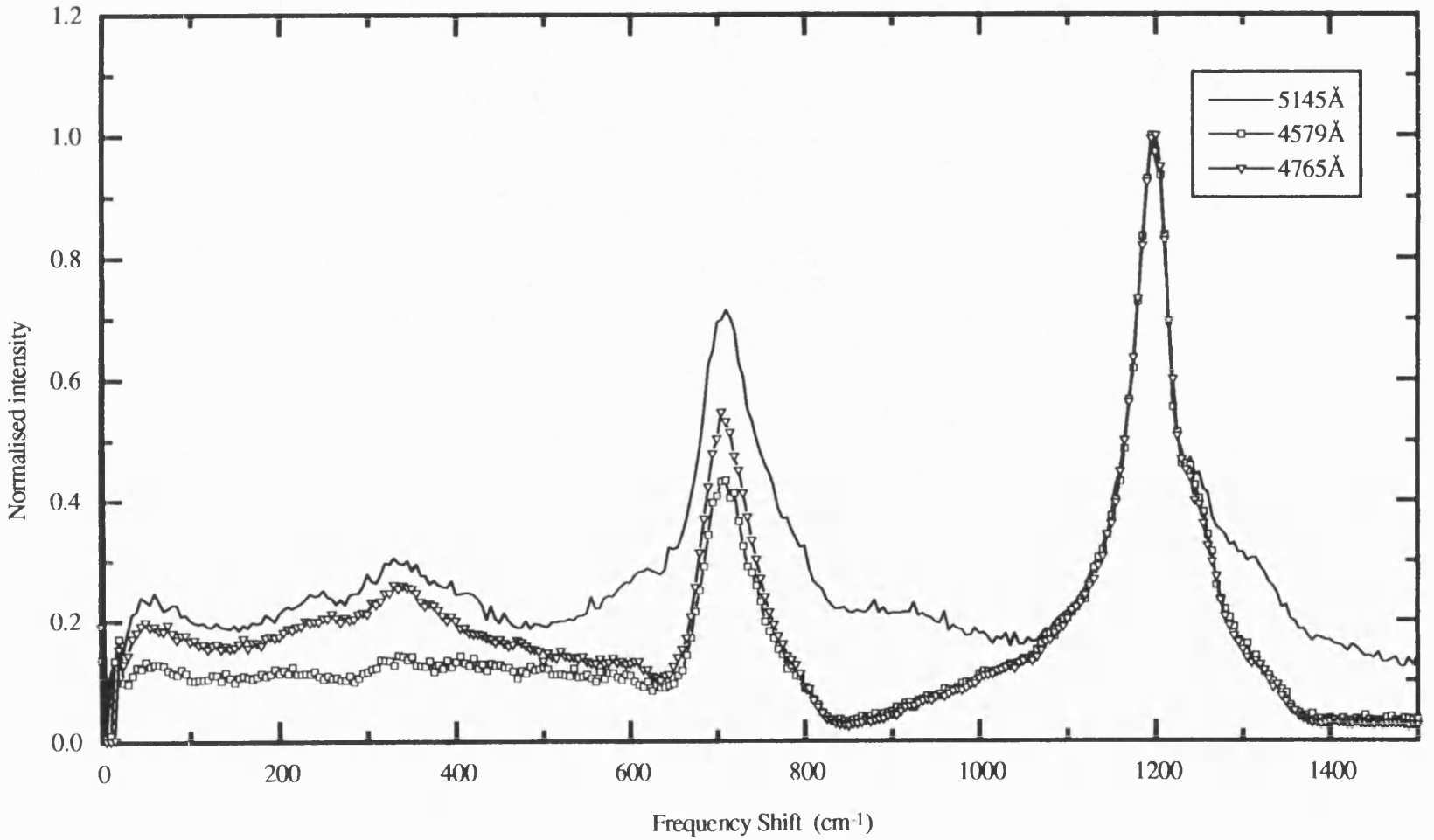

Figure 9.10. The Raman spectrum of $(Eu_2O_3)_{0.186}(P_2O_5)_{0.814}$ glass measured at 300K using different laser lines.

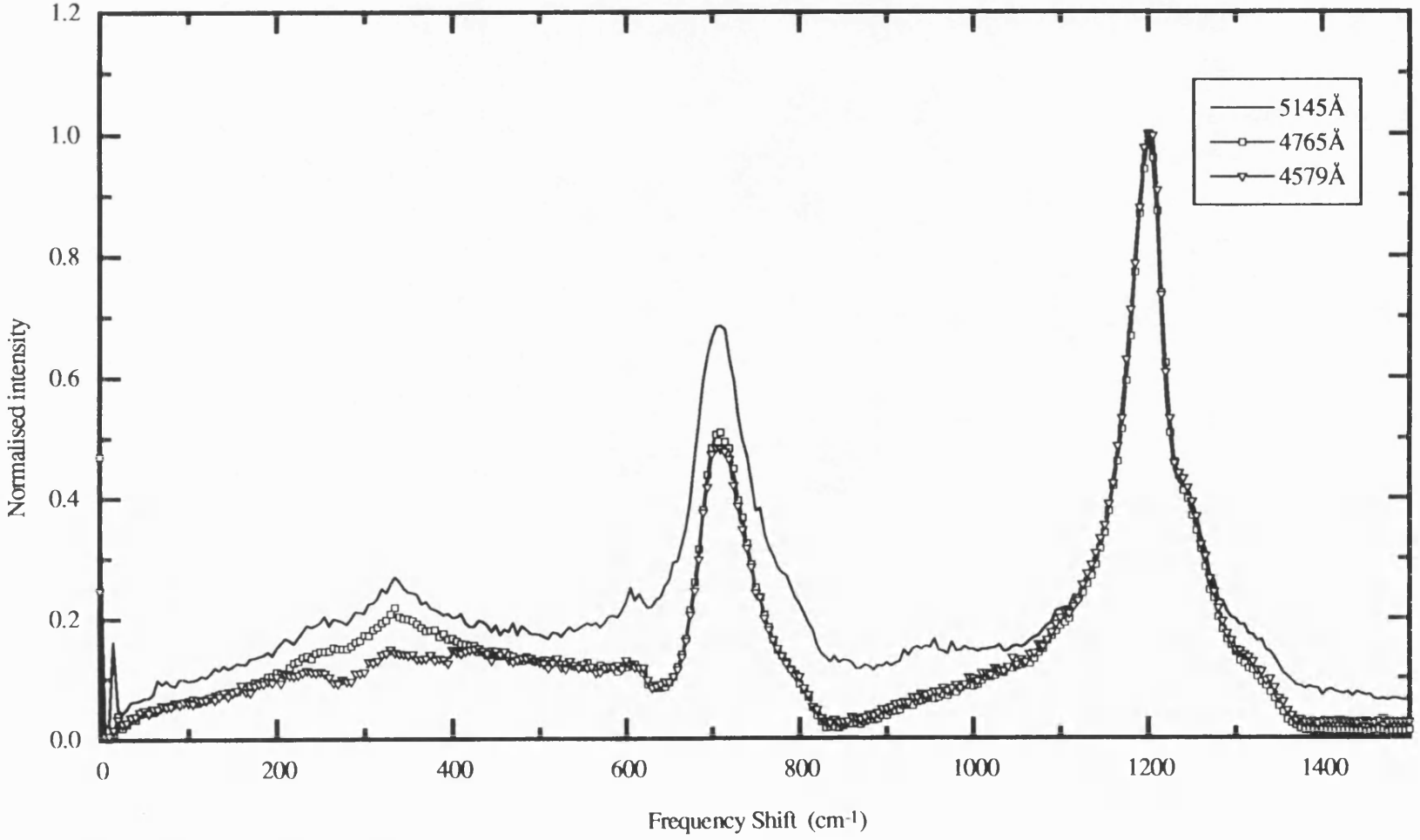

Figure 9.11. The Raman spectrum of $(Eu_2O_3)_{0.186}(P_2O_5)_{0.814}$ glass measured at 10K using different laser lines.

the Raman spectrum of the glass measured using the 4765 and 4579Å laser lines (Figure 9.10). The Raman spectrum of the $(Eu_2O_3)_{0.186}(P_2O_5)_{0.814}$ glass measured at 10K is shown in Figure 9.11. The spectrum shows the same band locations as those found in the spectrum of this glass measured at 300K. It also shows, in the spectrum excited by the 5145Å laser line, the same two broad bands, found in spectrum 300K spectrum, interfering with the Raman bands at 705cm^{-1}, 1235 and 1315cm^{-1}. Again, both these bands disappear in the glass spectrum excited with the 4579 and 4765Å laser lines (Figure 9.11). Therefore, both these bands can be attributed to the fluorescence of the europium ion in this glass.

To visualise the effect of temperature on the Raman spectrum of the glass sample, having the composition $(Eu_2O_3)_{0.186}(P_2O_5)_{0.814}$, the spectrum measured at 10 and 300K (the spectra excited by the 4765Å laser line) are shown overlapped in Figure 9.12; it can be seen that the locations, the widths and the intensities of the high frequency Raman bands of this glass do not alter significantly as temperature is lowered; the low frequency part does show some temperature effects. To have a better insight into the temperature effect on the low frequency region of the Raman spectrum of the europium phosphate glass, this frequency region was examined in detail. Smaller slit widths (200μ) and a slower scanning speed (1cm^{-1} every 4 second) were used. Figure 9.13 shows the low frequency Raman spectrum of glass sample, having the composition $(Eu_2O_3)_{0.186}(P_2O_5)_{0.814}$, measured at 10, 100, 200, 300K and normalised against the Raman band at 330cm^{-1}. This frequency region of the spectrum shows an apparent increase in the intensity of the band at 50cm^{-1} (the boson peak) with increasing temperature. In addition, the tail of the Rayleigh scattering (below 10cm^{-1}) also shows an intensity increase with increasing temperature (from 0.2 at 10K to 0.3 at 300K, Figure 9.13).

The low frequency region of the Raman spectrum of the europium phosphate glass was used to calculate the power of the coupling constant in the Raman intensity equation of glasses (equation 9.1). Equation 9.2 was used to obtain the reduced intensity of the low frequency Raman spectrum of this glass measured at 10K. Figure 9.14 shows the log-log plot of the reduced intensity of the Raman spectrum of the glass sample against the frquency shift in the frequency range 16-40cm^{-1}. A slope of 3.44 was obtained from a linear fit applied to the plot data.

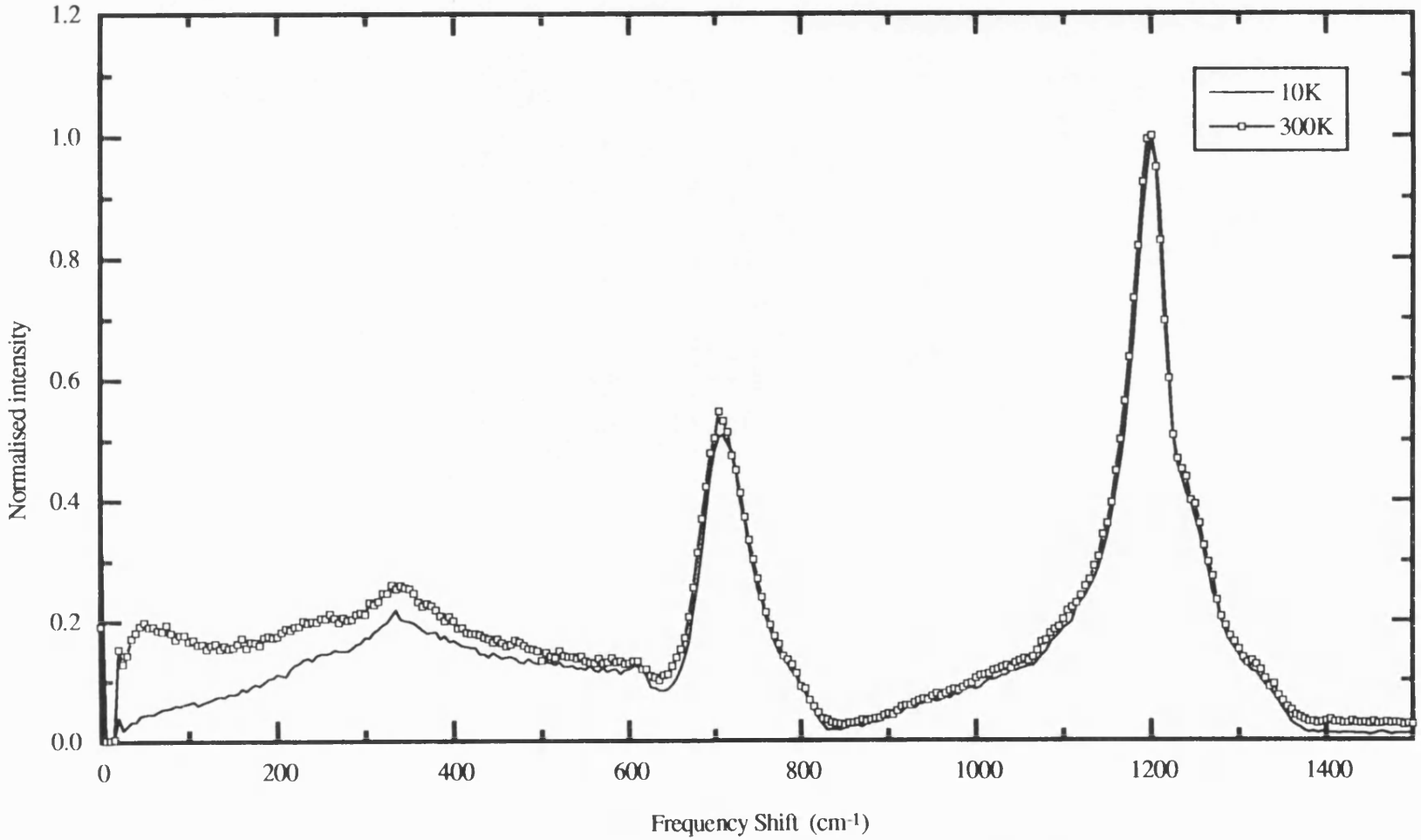

Figure 9.12. The Raman spectrum of $(Eu_2O_3)_{0.186}(P_2O_5)_{0.814}$ glass excited by the 4765Å laser line.

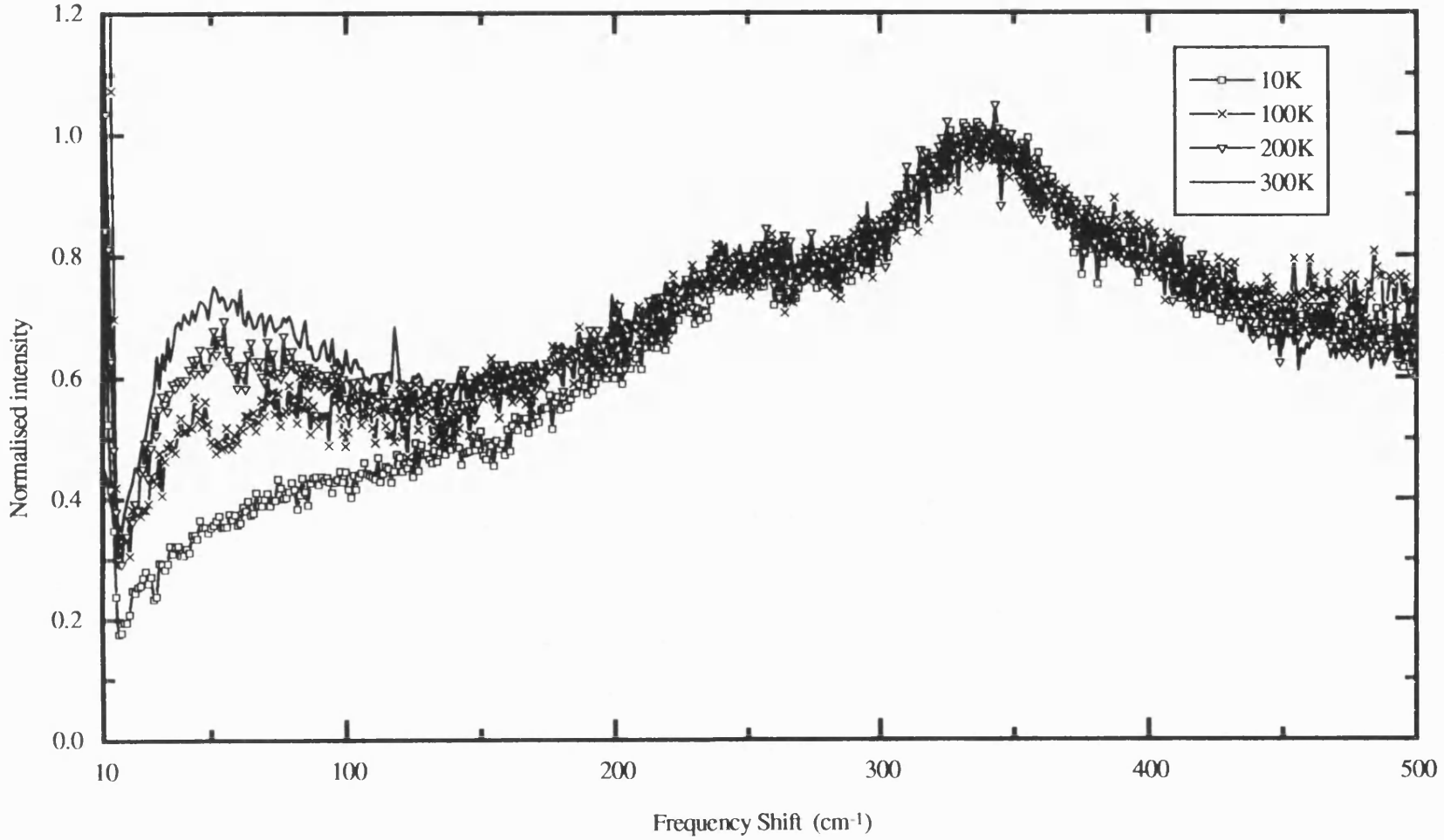

Figure 9.13. The Low frequency Raman spectrum of $(Eu_2O_3)_{0.186}(P_2O_5)_{0.814}$ glass at different temperatures.

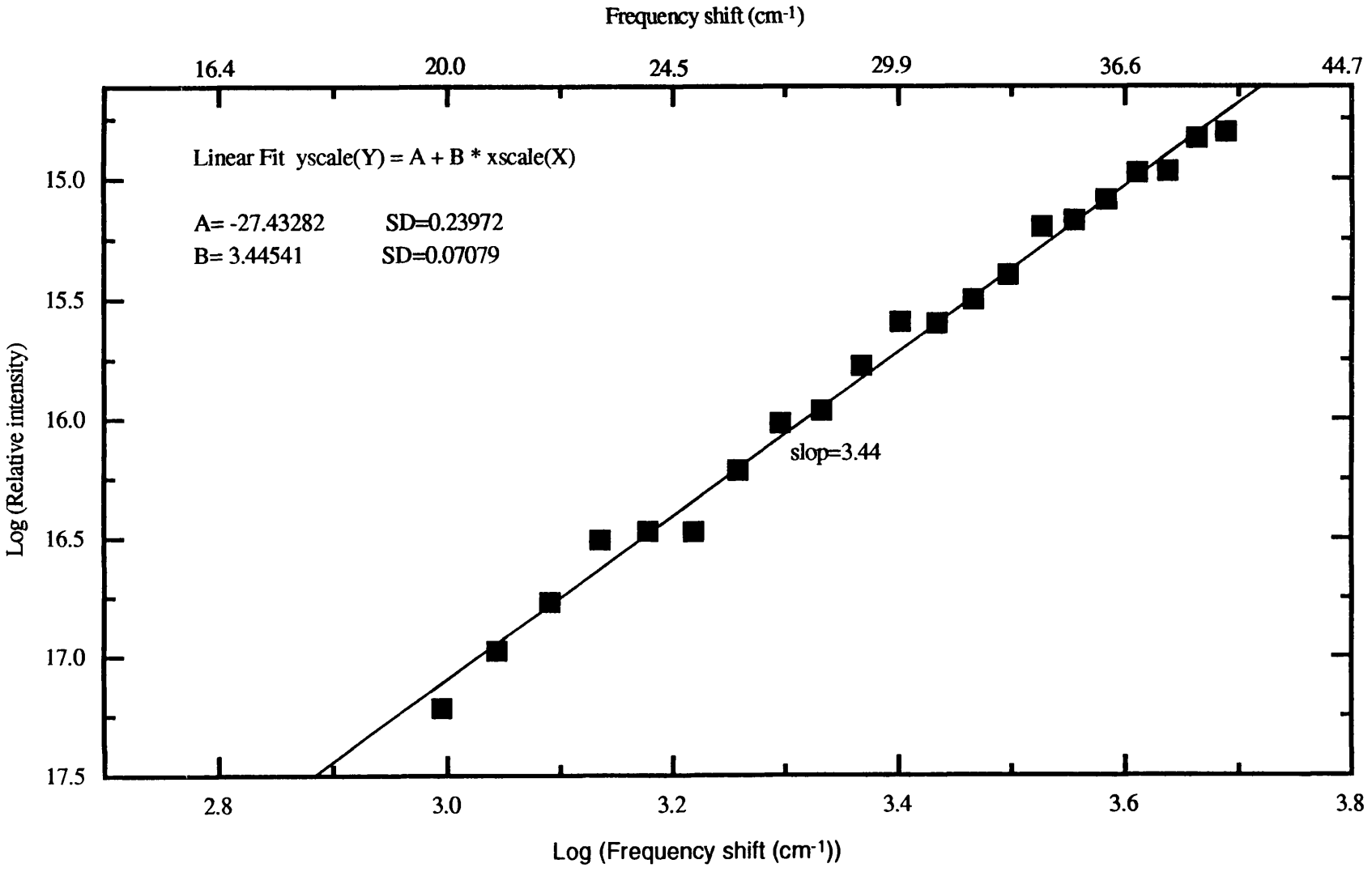

Figure 9.14. The frequency dependence of the reduced Raman intensity for the $(Eu_2O_3)_{0.186}(P_2O_5)_{0.814}$ glass at 10K.

9.8. EXPERIMENTAL RAMAN SPECTRA OF SAMARIUM PHOSPHATE GLASS

The Raman spectra of two different samples of samarium phosphate glass, having the compositions $(Sm_2O_3)_{0.19}(P_2O_5)_{0.81}$ and $(Sm_2O_3)_{0.212}(P_2O_5)_{0.788}$, were measured over the temperature range of 10-300K. The spectral measurements were obtained using 200mW laser power, $5cm^{-1}$ for every second scanning steps, and 400μ slit widths. Figure 9.15 shows the normalised Raman spectrum of the sample of the glass, which has the composition $(Sm_2O_3)_{0.19}(P_2O_5)_{0.81}$, measured at 300K using the 5145, 4880, and 4765Å laser lines. The spectrum of this glass comprises of six major bands located at 55, 315, 675, 1190, 1265, and $1320cm^{-1}$. In Figure 9.16 the normalised Raman spectrum of the glass sample, having the composition $(Sm_2O_3)_{0.212}(P_2O_5)_{0.788}$, measured at 300K using the 5145 4880, and 4765Å laser lines, is shown. The spectrum of this glass sample shows the same six bands as those found in the spectrum of the glass sample having the composition $(Sm_2O_3)_{0.19}(P_2O_5)_{0.81}$, but they are located at 50, 330, 700, 1195, 1240, and $1310cm^{-1}$. It is evident from the Raman spectra of the two glass samples of samarium phosphate glass, shown in the Figures 9.15 and 9.16, that the use of different laser lines has no effect on shapes, widths or number of the Raman bands. Hence, the measured spectra of the two glass samples can be considered to be free of fluorescence band interference.

To visualise the effect of samarium concentration on the Raman spectrum of the samarium phosphate glass, the measured spectra (at 300K) of the samples having the composition $(Sm_2O_3)_{0.19}(P_2O_5)_{0.81}$ and $(Sm_2O_3)_{0.212}(P_2O_5)_{0.788}$ are shown overlapped in Figure 9.17. Figure 9.18 shows another overlap made between the spectra obtained at 10K. In both figures three significant differences can be seen between the Raman spectrum of glass sample having the composition $(Sm_2O_3)_{0.19}(P_2O_5)_{0.81}$ and the spectrum of glass sample having the composition $(Sm_2O_3)_{0.212}(P_2O_5)_{0.788}$: the Raman band situated at $1265cm^{-1}$ shifts to $1240cm^{-1}$ and becomes a shoulder for the band at $1195cm^{-1}$ with lower intensity, the band at $680cm^{-1}$ shifts to $700cm^{-1}$ and becomes narrower on its low frequency side only, and finally, the band at $315cm^{-1}$ shifts to $330cm^{-1}$.

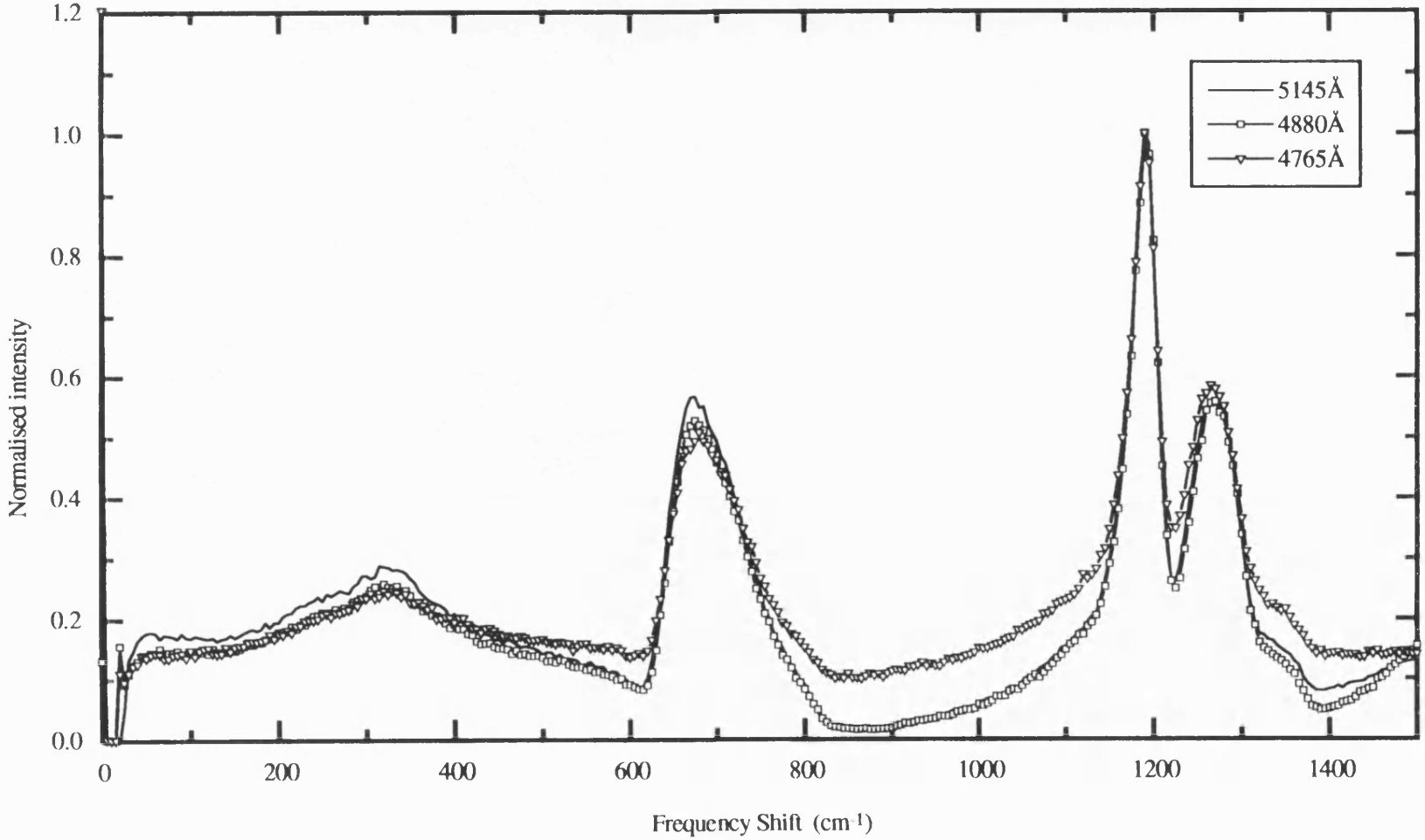

Figure 9.15. The Raman spectrum of $(Sm_2O_3)_{0.19}(P_2O_5)_{0.81}$ glass measured at 300K using different laser lines.

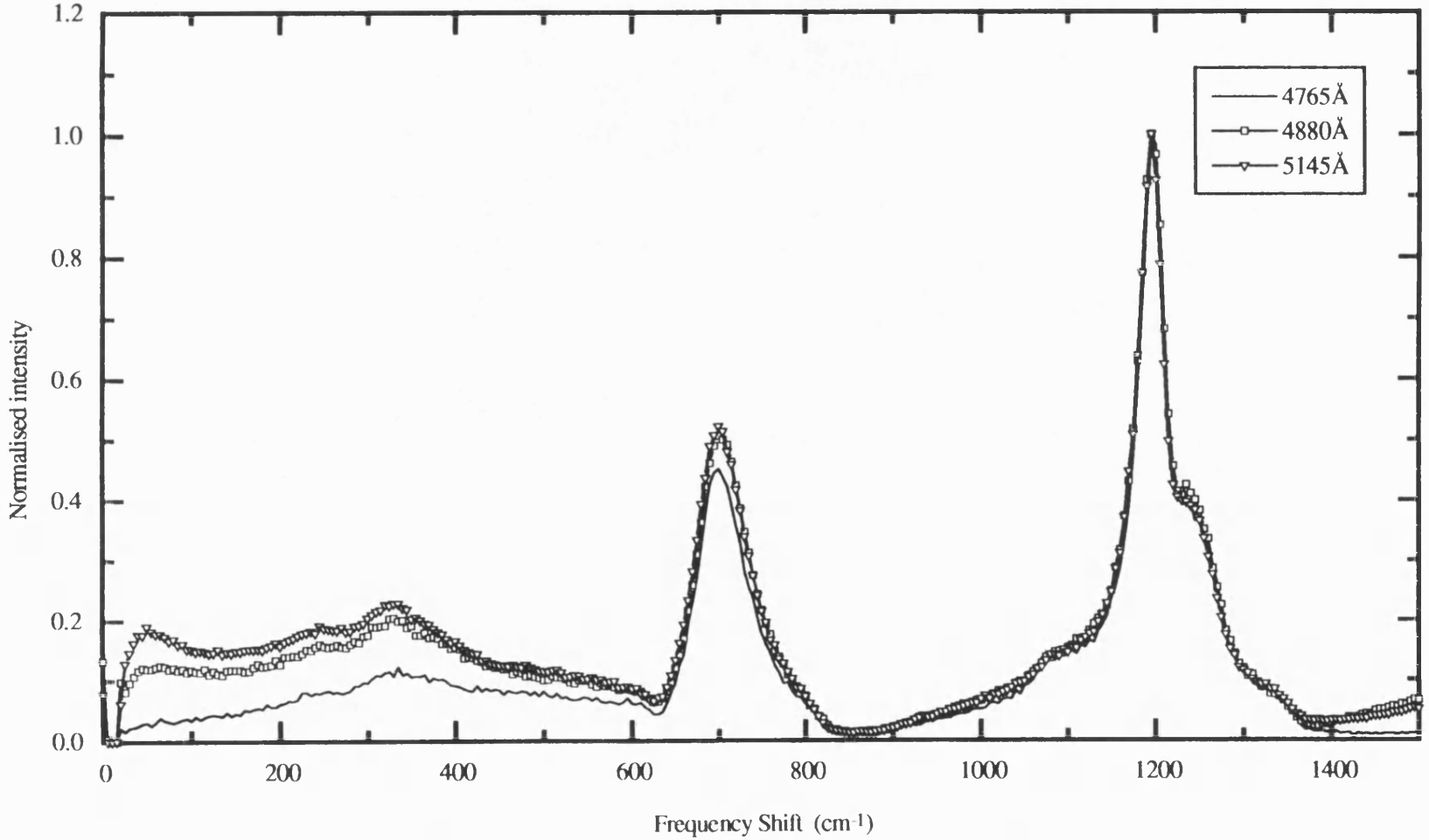

Figure 9.16. The Raman spectrum of $(Sm_2O_3)_{0.212}(P_2O_5)_{0.788}$ glass measured at 300K using different laser lines.

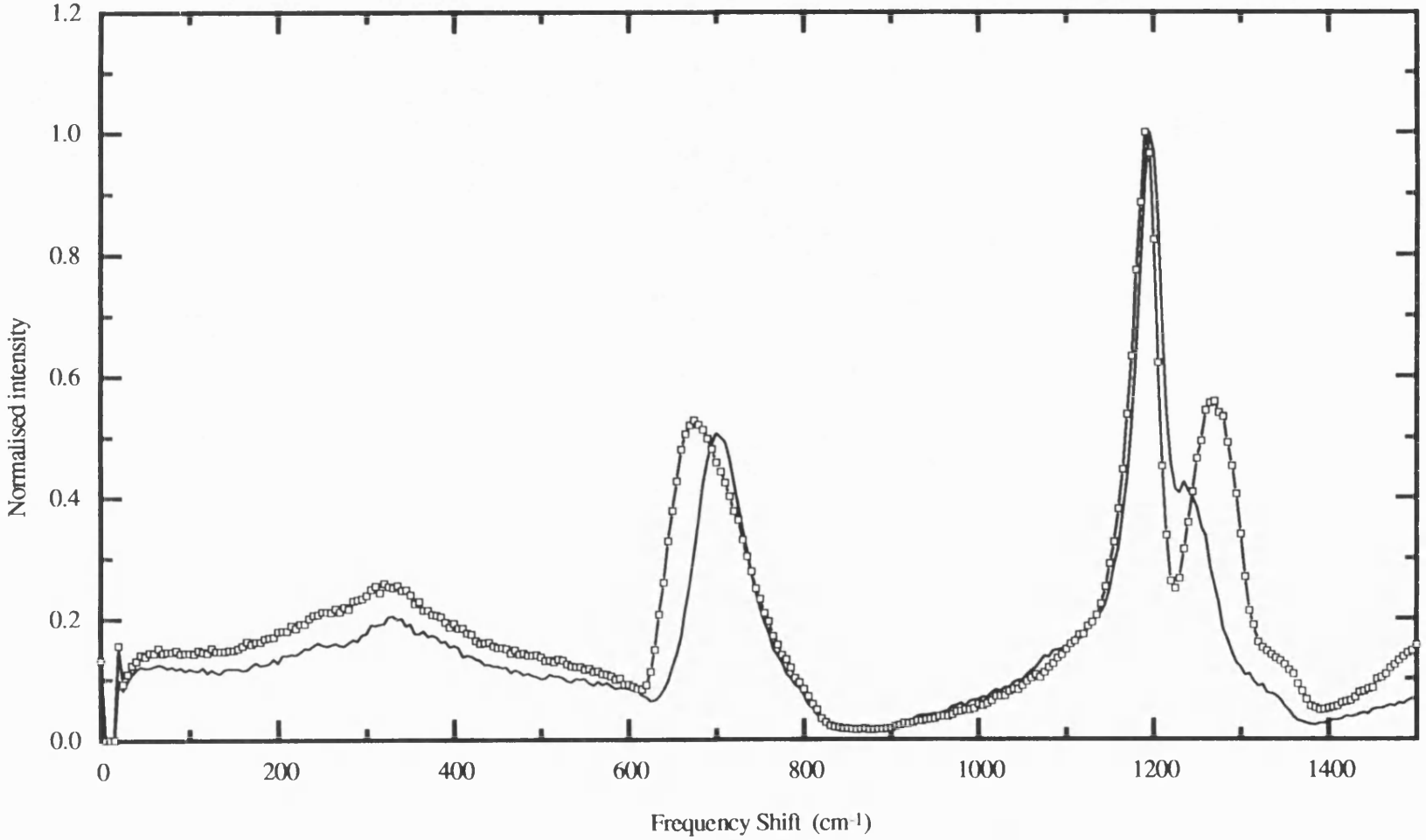

Figure 9.17. A comparison between the Raman spectra of $(Sm_2O_3)_{0.19}(P_2O_5)_{0.81}$ glass (square) and the $(Sm_2O_3)_{0.212}(P_2O_5)_{0.788}$ glass (line) at 300K.

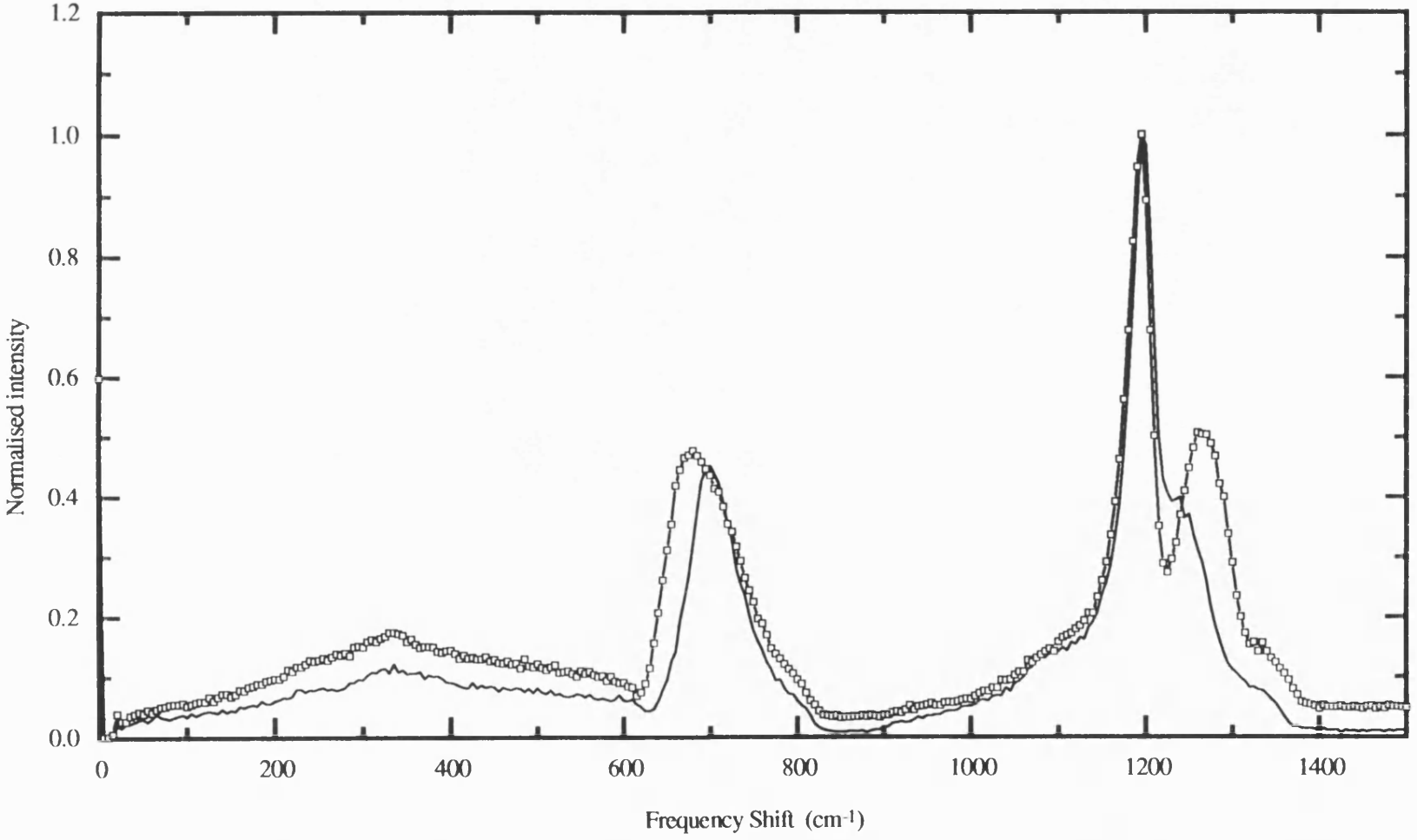

Figure 9.18. A comparison between the Raman spectrua of $(Sm_2O_3)_{0.19}(P_2O_5)_{0.81}$ glass (square) and the $(Sm_2O_3)_{0.212}(P_2O_5)_{0.788}$ glass (line) at 10K.

The temperature effect on the Raman spectrum of the samarium phosphate glasses was investigated. Figure 9.19 shows the Raman spectrum of the samarium phosphate glass (excited by 4765Å laser line) having the composition $(Sm_2O_3)_{0.19}(P_2O_5)_{0.81}$ recorded at 10, 100, 200, and 300K. The spectrum of this glass shows no significant alteration with temperature in the high frequency region. This was also true for the spectrum of the glass having the composition $(Sm_2O_3)_{0.212}(P_2O_5)_{0.788}$ recorded in the same temperature range. However, the low frequency region of the Raman spectra of both samarium phosphate glass compositions shows some temperature effect. To illustrate the temperature effect, the spectrum of the glass in this frequency region was normalised against the Raman band at 315cm^{-1}. Figure 9.20 shows the normalised low frequency region of the spectrum of glass sample $(Sm_2O_3)_{0.19}(P_2O_5)_{0.81}$ at 10, 100, 200 and 300K. The spectrum shows an apparent increase in the intensity of the Raman band at 55cm^{-1} (boson peak) with increasing temperature.

9.9. EXPERIMENTAL RAMAN SPECTRA OF LANTHANUM PHOSPHATE GLASS

The Raman spectrum of a sample of lanthanum phosphate glass was measured over the temperature range of 15-300K, using the 4880Å argon ion laser line with 200mW lasing power, 400μ slit widths, and 5cm^{-1} for 2 seconds scanning steps. Figure 9.21 shows the normalised Raman spectrum of the lanthanum phosphate glass sample, having the composition $(La_2O_3)_{0.263}(P_2O_5)_{0.737,}$ recorded at 15, 100, 200, and 300K. The spectrum shows six major bands located at 55, 340, 695, 1185, 1230, and 1305cm^{-1}. In the high frequency region, the spectrum of this glass does not alter with temperature reduction, the bands retain their number, widths and profiles. However, in the low frequency region, the spectrum of this glass recorded at 15K shows some differences from the spectrum recorded at 300K. Therefore, this low frequency region requires more detailed investigation.

Examination of the low frequency region of the Raman spectrum of the glass sample $(La_2O_3)_{0.263}(P_2O_5)_{0.737}$ at different temperatures was achieved, using a 200μ slit widths, and 1cm^{-1} scanning step every 4 seconds. Figure 9.22 shows the normalised low frequency Raman spectrum (normalised against the 340cm^{-1} band) in the tem-

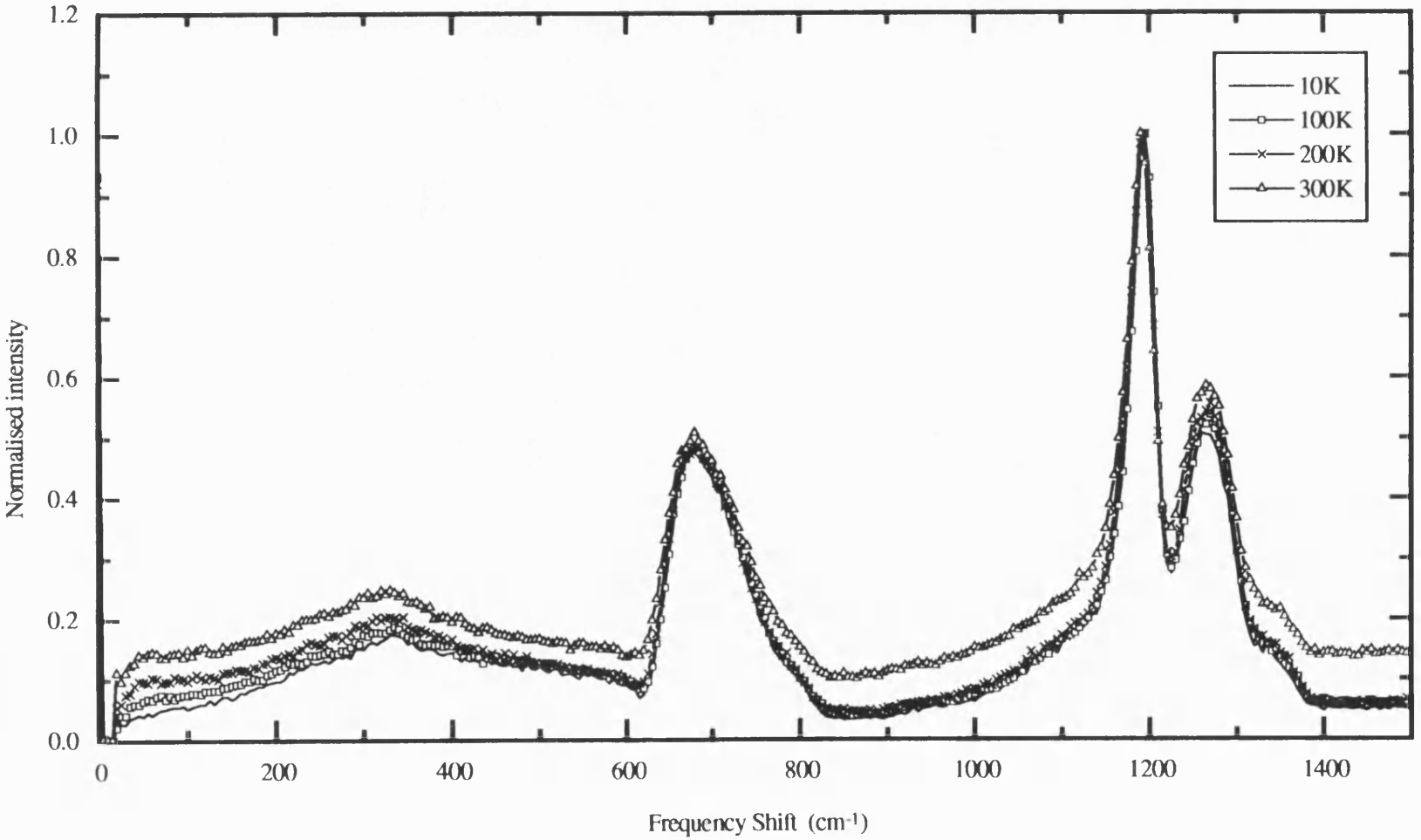

Figure 9.19. The Raman spectrum of $(Sm_2O_3)_{0.19}(P_2O_5)_{0.81}$ glass measured at different temperatures and excited by the 4765Å laser line.

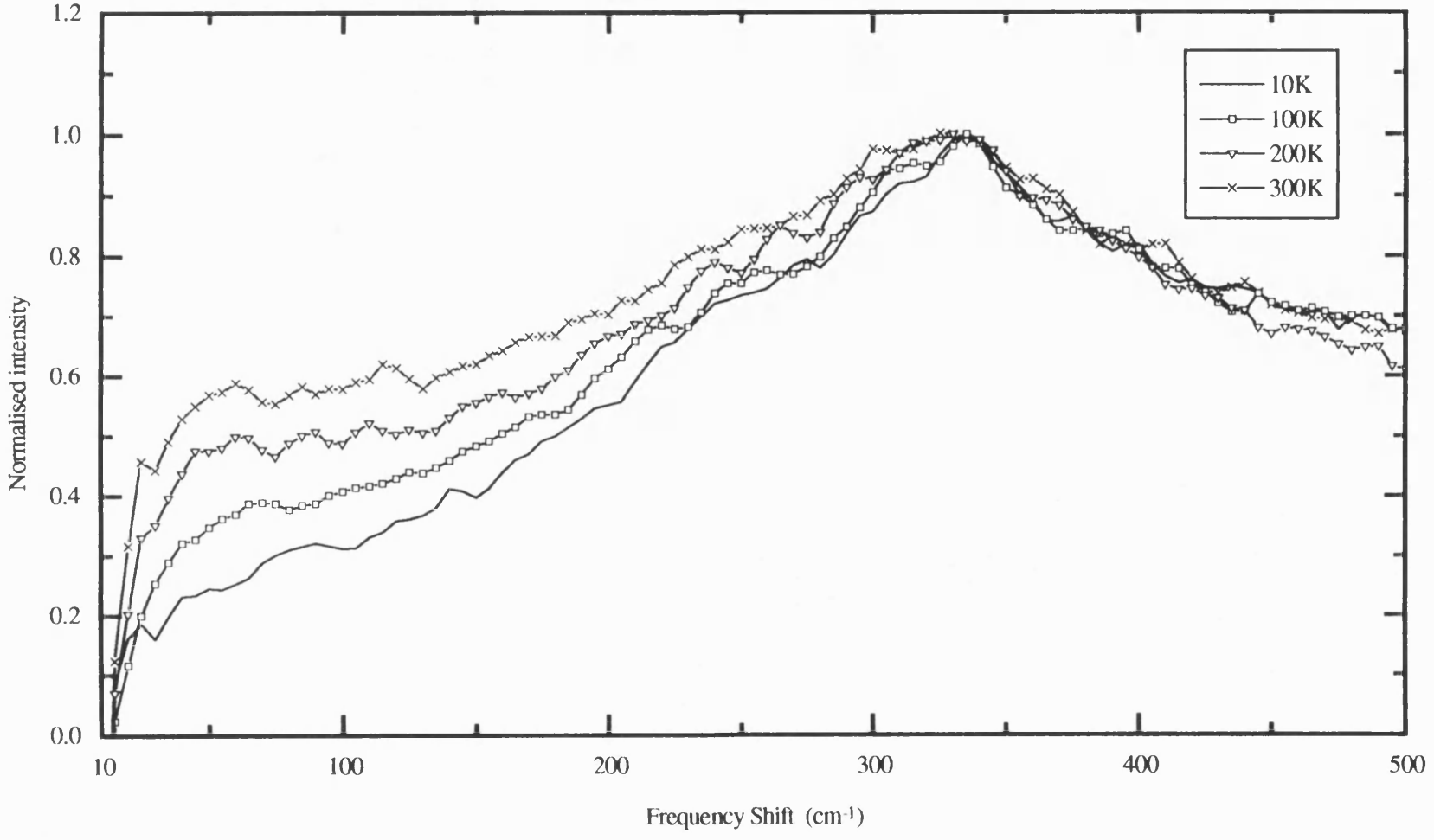

Figure 9.20. The low frequency Raman spectrum of $(Sm_2O_3)_{0.19}(P_2O_5)_{0.81}$ glass measured at differnet temperatures.

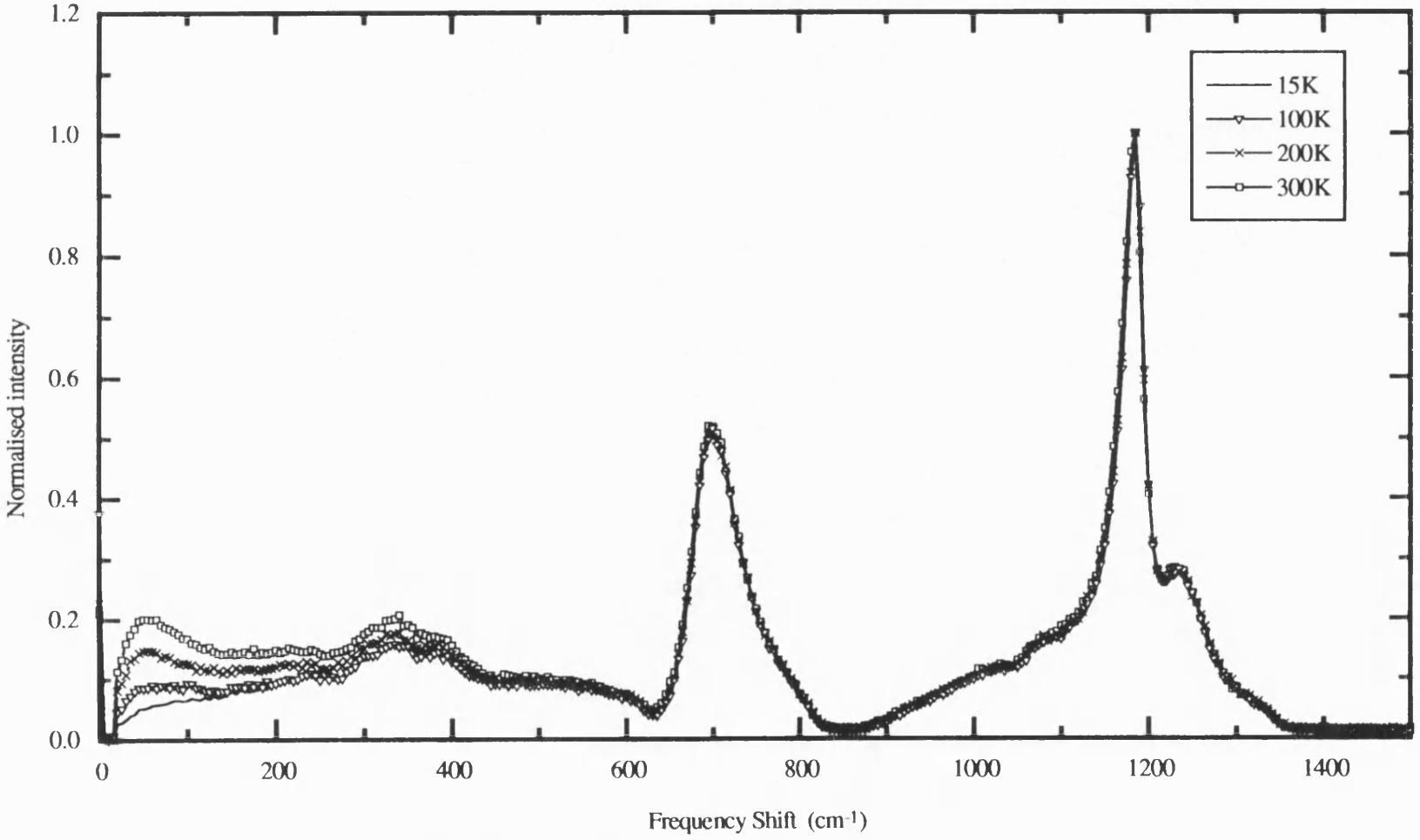

Figure 9.21. The Raman spectrum of $(La_2O_3)_{0.263}(P_2O_5)_{0.737}$ glass at different temperatures.

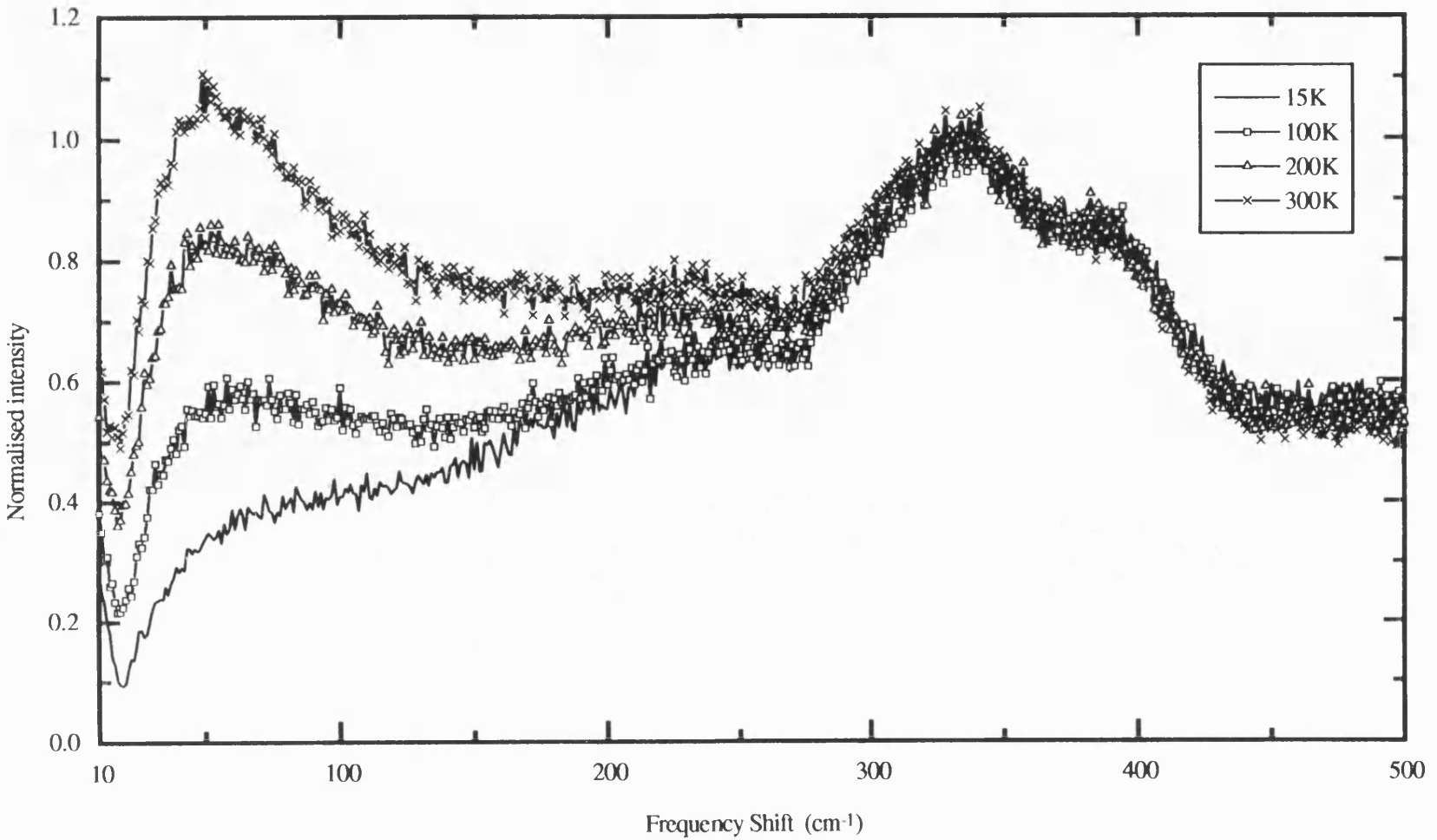

Figure 9.22. The low frequency Raman spectrum of $(La_2O_3)_{0.263}(P_2O_5)_{0.737}$ glass measured at different temperatures.

perature range of 15-300K. Two apparent alterations can be observed in the spectrum of this glass: the increase of the intensity of the band at 55cm^{-1} and the increase of the intensity of the tail of the Rayleigh scattering, with increasing temperature.

To measure the power of the coupling constant in the Raman intensity equation of glasses (eq.9.1), the experimental Raman intensity data of the glass having the composition $(La_2O_3)_{0.263}(P_2O_5)_{0.737}$ (at 15K) was reduced using equation 9.2. Figure 9.23 shows the log-log plot of the reduced intensity against the frequency shift of this glass in the frequency range of 16-40cm^{-1}. A linear fit was applied to the plot in the figure and a slop of 3.38 was obtained for the line.

9.10. EXPERIMENTAL RAMAN SPECTRA OF SAMARIUM PENTAPHOSPHATE CRYSTAL

The Raman spectrum of the samarium pentaphosphate SmP_5O_{14} crystal was measured and recorded at different temperatures. The spectrum was obtained using the 4880Å argon ion laser line with 200mW lasing power, 200μ slit widths, and scanning steps of 1cm^{-1} for every 3 seconds. The frequency shifts of the Raman lines were measured with an accuracy of ±1cm^{-1}. Figure 9.24 shows the experimental Raman spectrum of this crystal obtained at 300 and 12K. The spectrum shows a large number of sharp Raman lines, which are all listed in Table 9.1 columns 1 and 2. The relative intensities of the Raman lines of this crystal can not be relied upon, because some of the lines are polarised and their polarisation depend strongly on the crystal axes orientation relative to the laser beam. Comparison between the spectrum of crystal measured at 12 and 300K, shows some obvious changes; the two spectral lines located above the frequency shift 1400cm^{-1} in the spectrum of the 300K temperature disappeared in the spectrum of the 12K. It is possible that these two lines are related to the fluorescence of the samarium ion in this crystal. To check this possibility the spectrum of the samarium pentaphosphate crystal (SmP_5O_{14}) was measured (at 300K) using the 4765Å laser line. The resulted spectrum showed that the two spectral lines have not kept the same frequency shift locations in the spectrum. Therefore, the two lines beyond 1400cm^{-1} in the Raman spectrum of this crystal are indeed fluorescence lines of the samarium ion.

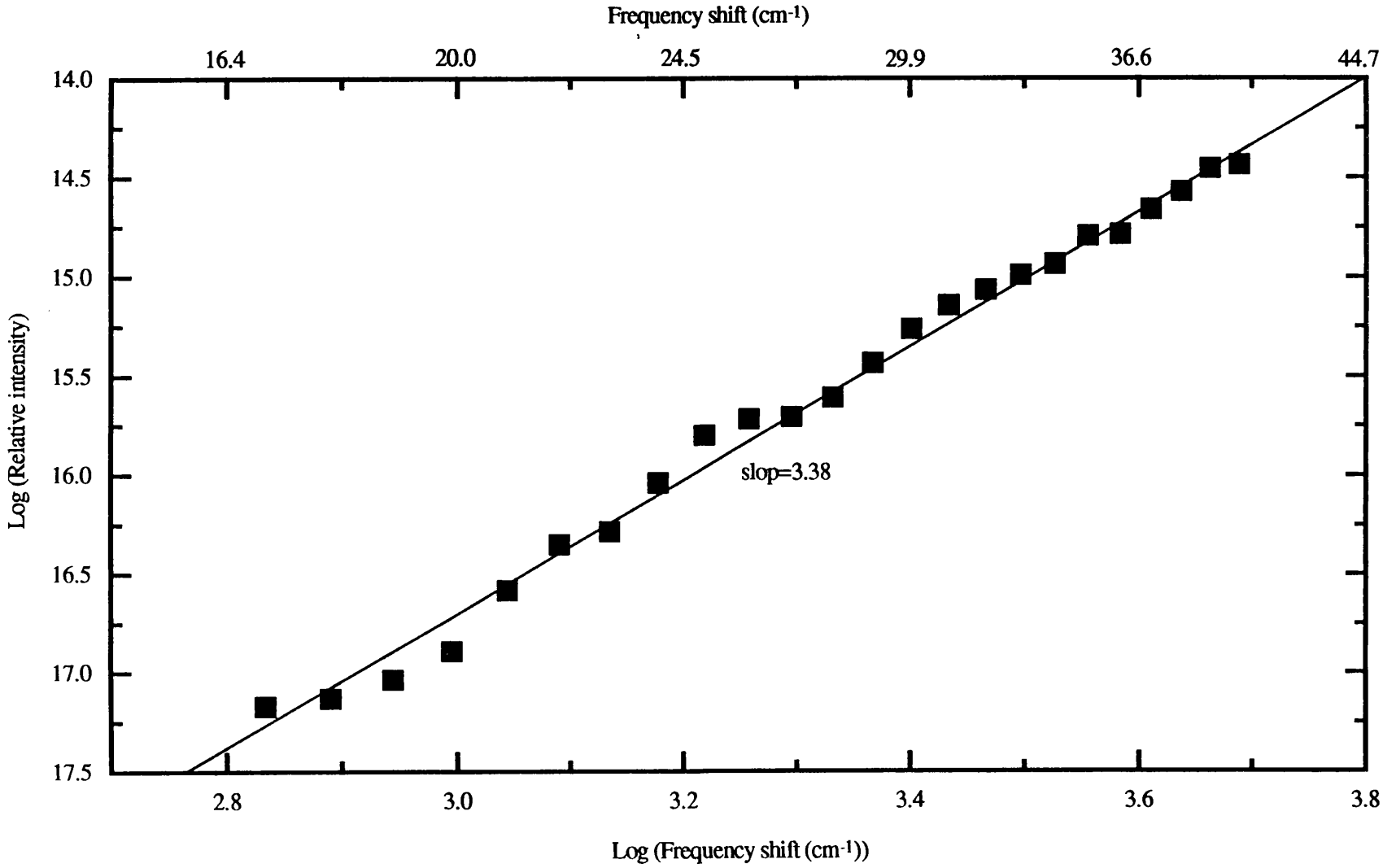

Figure 9.23. The frequency dependence of the reduced Raman intensity for the $(La_2O_3)_{0.263}(P_2O_5)_{0.737}$ glass at 10K.

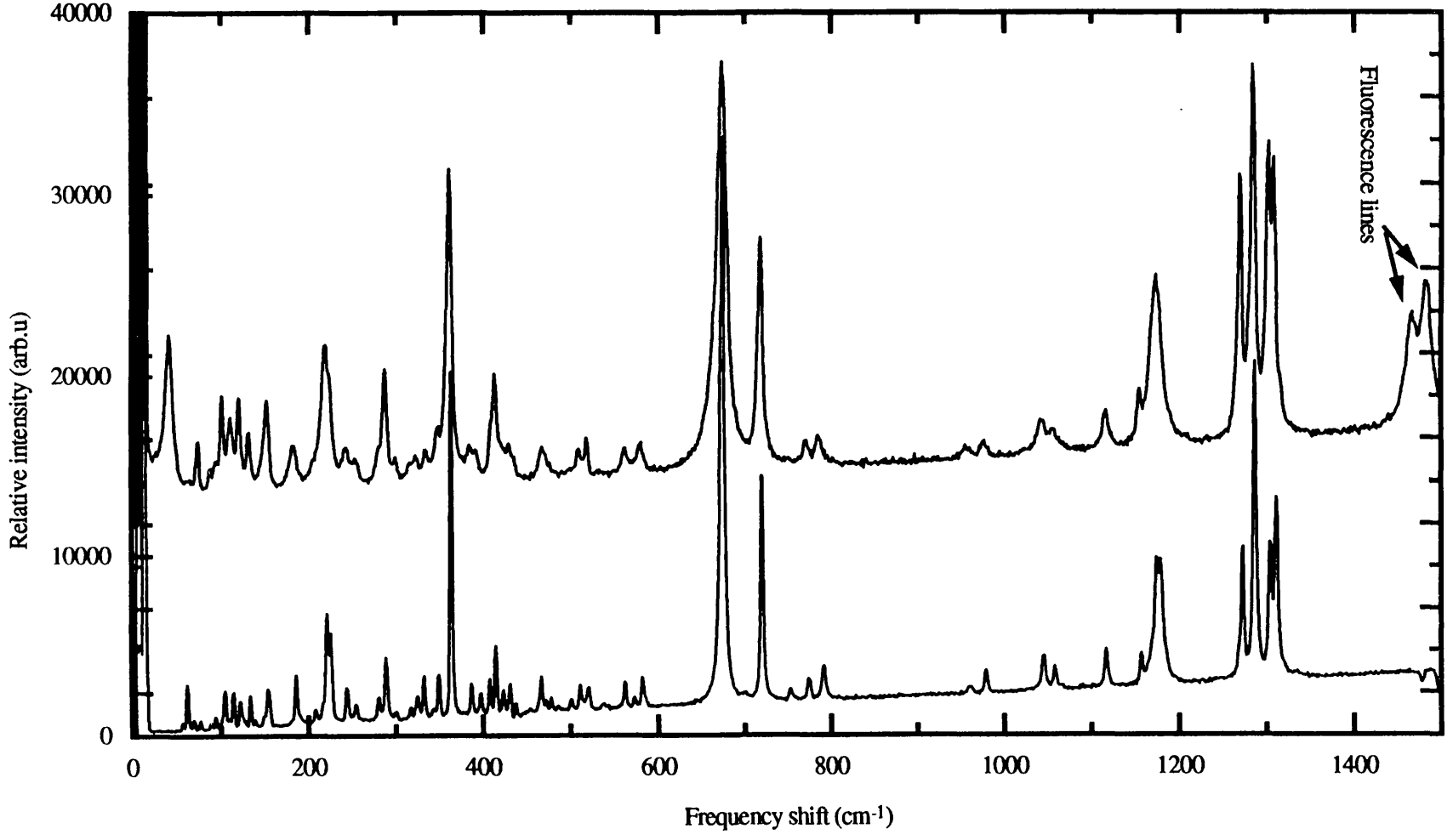

Figure 9.24. The Raman spectrum of samarium pentaphosphate crystal (SmP_5O_{14}) measured at 300K (above) and 12K (below).

Table 9.1. The experimental Raman lines extracted from the spectrum of the SmP_5O_{14}, EuP_5O_{14}, and NdP_5O_{14} crystals excited by the 4880Å argon ion laser line and measured at 12 and 300K. The unit of the measure is cm^{-1}.

Raman lines of SmP_5O_{14} crystal 12K	Raman lines of SmP_5O_{14} crystal 300K	Raman lines of EuP_5O_{14} crystal 12K	Raman lines of EuP_5O_{14} crystal 300K	Raman lines of NdP_5O_{14} crystal 12K	Raman lines of NdP_5O_{14} crystal 300K
1311 s	1308 s	1312	1309	1309	1305
1304 s	1302 s	1306	1303	1302	1300
1287 vs	1284 vs	1289	1286	1286	1283
1273 s	1269 s	1273	1271	1271	1268
1178 s	1173 s	1179	1176	1175	1170
1174 s	1155	1171	1159	1171	
1157		1157		1155	
1117	1117	1117	1118	1114	
1064	1055	1076	1059	1064	
1058	1042	1068	1043	1056	
1045		1065		1042	
		1055		1034	
		1043			
979	977	980	978	977	823
960	955	962	958	923	
		959		910	
		937		905	
				888	
				879	
				865	
				843	
				840	
				825	
792	785	792	787	788	769
774	772	775	773	781	
753		753		772	
				751	
720 s	718 s	721s	720	718s	716
701	----				
675 vs	674 vs	675vs	676vs	672	672

Continuation of Table 9.1.

582 573 562	581 --- 562	582 573 562	581 564	580 571 560	577
537	--	536			
521 511 501 478 472 467	519 510 468	521 511 501 486 478 472 466	520 511 485 467	519 514 510 499 485 476 471 464	470
		454			
437 431 424 415 408 398 387	430 414 392 385	437 432 423 415 408 397 388	430 415	436 429 422 414 406 395 384	428 423 413 389 382 378
364 s 350 344 333 325 317	362 350 334 323 317	364 350 344 333 325	363 350 336 325	363 347 330 321 313	360 346 334 330 321
301 289 281	300 288 282	301 290 282	301 290 282	298 285 277	298 284 270 267

Continuation of Table 9.1.

254	254	257	257	253	251
244	244	245	243	244	242
226	224	227	227	222	222
222	220	222	215	215	218
217	206	217	186	204	216
208	183	208	156	182	209
186	153	188	152	149	204
154	133	180	150	146	195
139	121	156	135	137	189
134	112	152	127	130	181
128	102	141	123	125	178
122	95	135	113	121	175
115	90	126	110	112	172
109	75	115	104	106	169
105	42	111	96	104	157
94		106	90	98	154
89		101	76	93	148
77		95	72	84	142
69		90	54	73	136
62		77	48	60	132
57		69	39	56	130
		63	35		120
		57			109
		39			100
		30			92
					89
					87
					79
					72
					63
					57
					51
					47
					41
					39
					27

*. vs refers to very strong intensity and s to strong intensity.

In the high frequency region (above $100cm^{-1}$), the Raman spectrum of the samarium pentaphosphate crystal shows no significant changes with temperature reduction (Figure 9.24), apart from the apparent increase in the splitting of some of the Raman lines. This confirms that spectrum of this crystal contains only the Raman bands with no interference from fluorescence. Reducing the temperature of the crystal from 300 to 12K has some effect on the width of the Raman lines. For instant, at 300K the Raman lines of the crystal located at 362, 674, and $718cm^{-1}$ manifest half widths of around 10, 14, and $7cm^{-1}$ respectively, yet at 12K these lines have half-widths around 3, 6, and $5cm^{-1}$ respectively. In the data listed in Table 9.1, comparison between the Raman lines recorded at 300K and the 12K shows shifts in the range of 2-$5cm^{-1}$ towards higher frequency in some of the intense Raman lines of the crystal. Most of these shifts exist in the frequency regions where the Raman lines are very close to each other. Therefore, the shifts can be considered as errors in measuring the original peak positions rather than a temperature effect. This conclusion is derived from the fact that Raman lines sharpen at low temperatures and therefore the resolution is increased, which enables the positions of the peaks to be determined more accurately.

The temperature dependence of low frequency region of the Raman spectrum of the samarium pentaphosphate crystal (SmP_5O_{14}) was measured under the same experimental conditions as above. Figure 9.25 displays the spectrum of the crystal in the frequency range of 10-$150cm^{-1}$, measured at 12, 50, 100, 200, and 300K temperatures. The spectrum in this frequency region shows some effect of temperature; the Raman line located at $42cm^{-1}$ shifts gradually towards higher frequency and reaches a frequency shift of $62cm^{-1}$ at 12K temperature. In addition, this particular Raman line sharpens to such an extent that at 12K two extra low intensity Raman lines can be seen on its both sides; their peaks are located at 57 and $69cm^{-1}$ at 12K. There are two possibilities for the origin of these two extra Raman lines; either they were hidden under the broad width of the $42cm^{-1}$ Raman line at 300K and they emerge at 12K due to the line sharpening at low temperatures, or the $42cm^{-1}$ Raman line splits to three Raman lines at low temperatures. The rest of the Raman lines in the low frequency region do not show measurable shifts with temperature. The tail of the Rayleigh scattering in the spectrum of this crystal measured at different tempera-

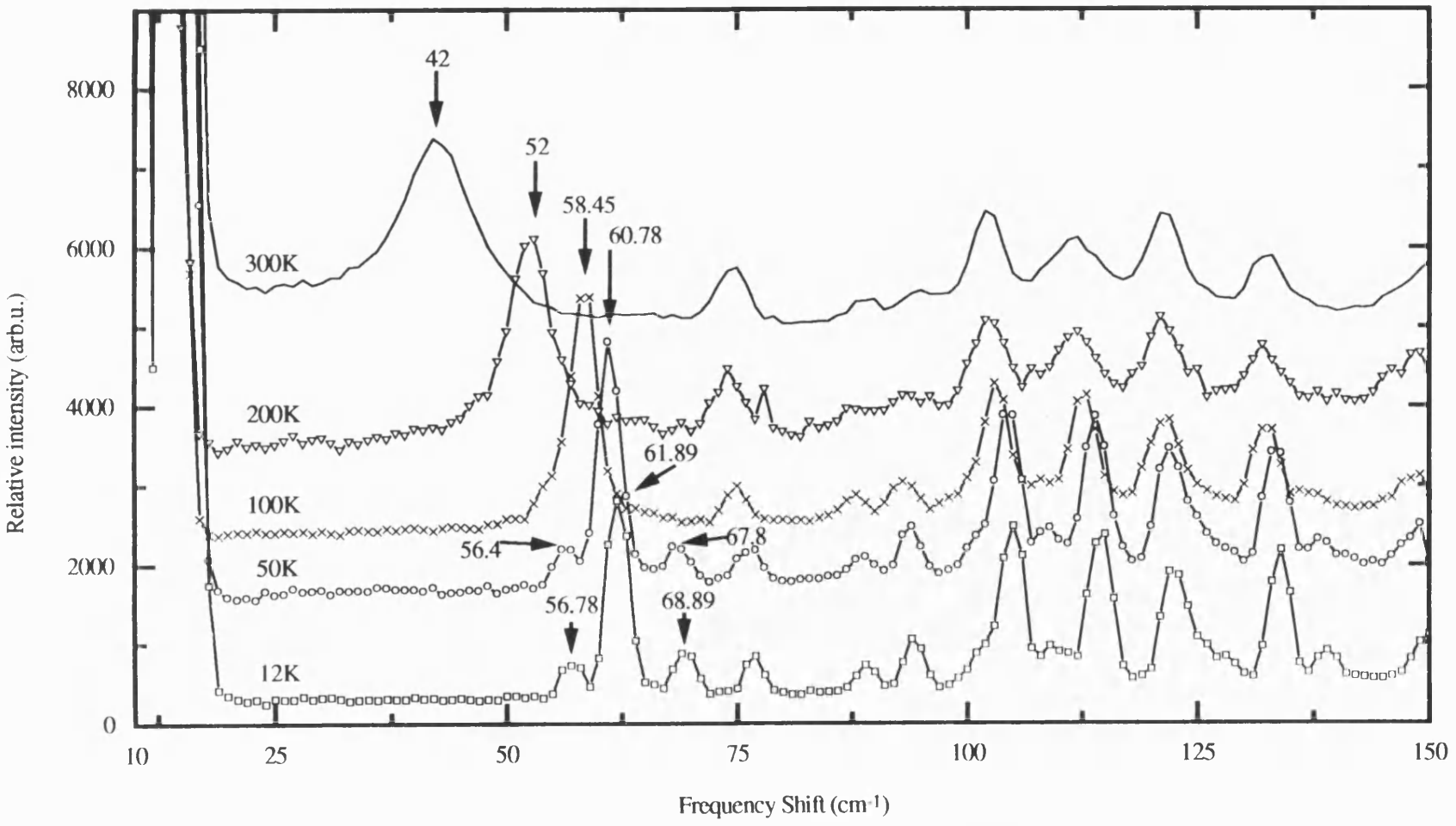

Figure 9.25. The low frequency Raman spectrum of samarium pentaphosphate crystal (SmP_5O_{14}) measured at different temperatures.

tures (Figure 9.25) is always terminated at about 18cm^{-1} frequency shift. This is an indication that temperature lowering has not much effect on the light scattering in this crystal.

9.11. EXPERIMENTAL RAMAN SPECTRA OF EUROPIUM PENTAPHOSPHATE CRYSTAL

The temperature effect on the Raman spectrum of the europium pentaphosphate crystal having the formula EuP_5O_{14} was measured. The Raman spectrum was obtained by using the 4880Å argon ion laser line set at 200mW power, 150μ slit widths, and scanning steps of 1cm^{-1} for every 2 seconds. Figure 9.26 shows the Raman spectrum of this crystal measured at 300 and 12K and Table 9.1 lists the frequency shift of the Raman lines extracted from this spectrum. The Raman spectrum of the crystal (Figure 9.26) shows some apparent changes with temperature reduction: three lines in the vicinity of 1400cm^{-1} in spectrum recorded at 300K disappear in the spectrum recorded at 12K, most of the Raman lines split and some of them show intensity variation. The disappearance of the three lines in the vicinity of 1400cm^{-1} at low temperature suggests that these lines are fluorescence lines of the europium ion. This was confirmed by using a different laser line to obtain the Raman spectrum of this crystal which did not show these three lines in the spectrum. The splitting in the Raman lines can be attributed to line resolution, since Raman lines sharpen at low temperatures. The relative intensity variation of the Raman lines is most probably related to the change in the crystal orientation during the experiment, since some Raman lines have a different direction of polarisation.

The effect of temperature on the low frequency region of the Raman spectrum of EuP_5O_{14} was measured in detail in the temperature range 300-12K. Slower scanning steps of 0.5cm^{-1} for every 2 seconds were employed to obtain a more reliable spectral measurements in low frequency region. Figure 9.27 shows the low frequency spectrum of the europium pentaphosphate crystal registered at 12, 25, 50, 100, 200, and 300K. The spectrum reveals that the Raman line located at 48cm^{-1} in the spectrum measured at 300K shifts gradually with temperature to reach the position 63cm^{-1} at 12K. In addition, two extra low intensity Raman lines can be seen emerging on both sides of the 48cm^{-1} Raman line with temperature reduction; the

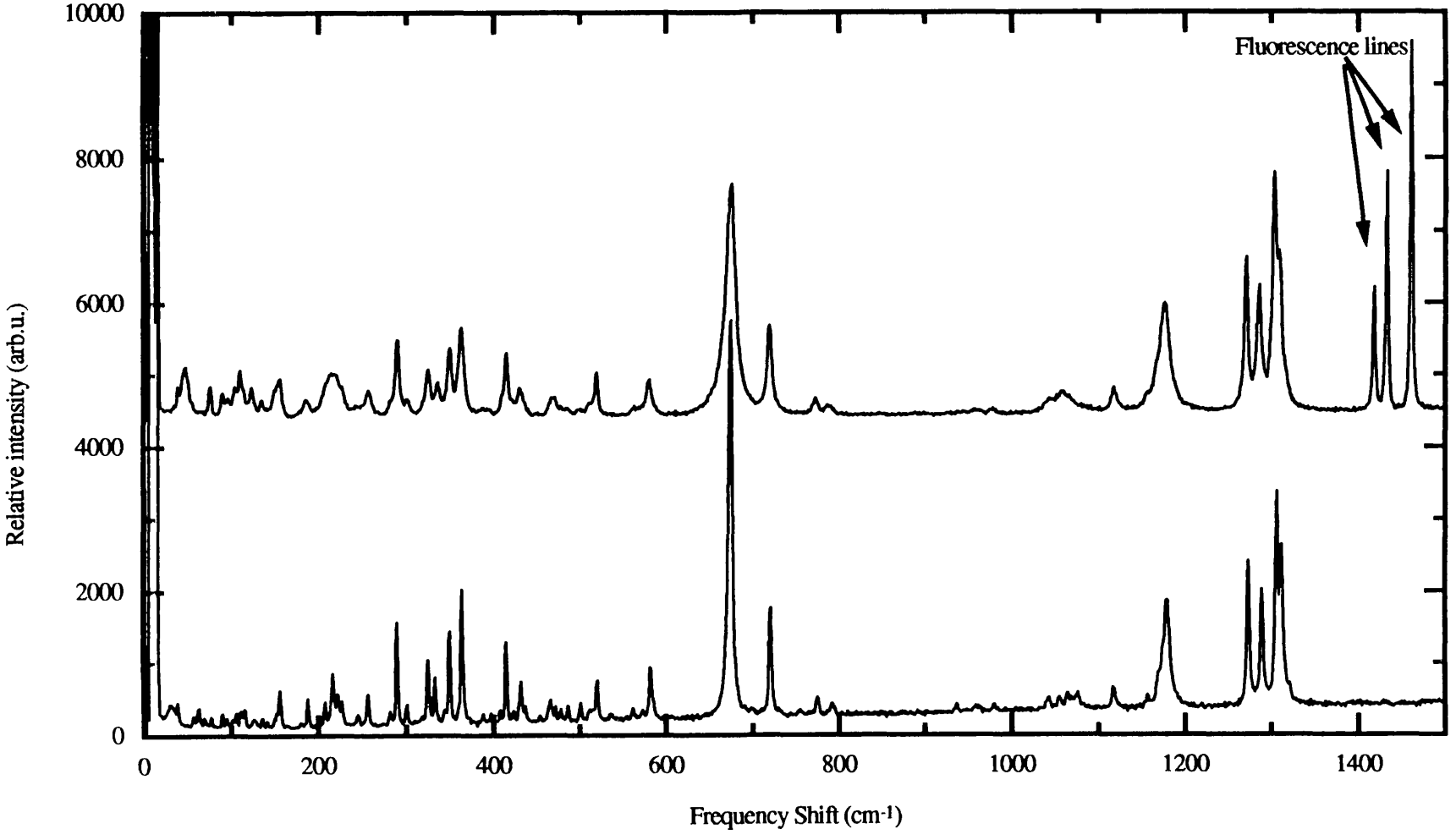

Figure 9.26. The Raman spectrum of europium pentaphosphate crystal (EuP_5O_{14}) measured at 300K (above) and 12K (below).

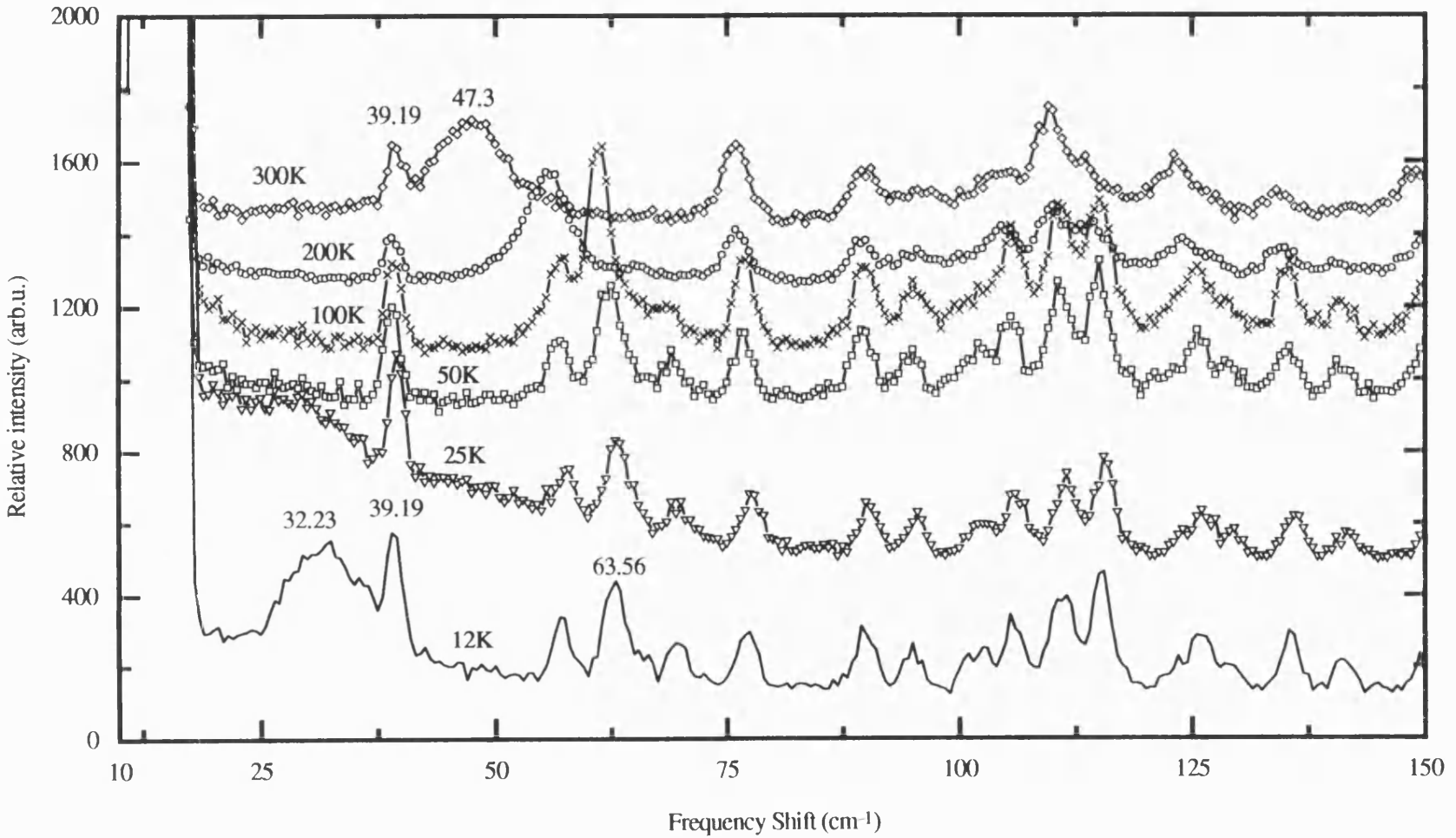

Figure 9.27. The low frequency Raman spectrum of europium pentaphosphate crystal (EuP_5O_{14}) measured at different temperatures.

two extra lines have their peaks located at 57 and 69cm^{-1} in the spectrum measured at 12K. Surprisingly, the Raman line located at 39cm^{-1} does not show any shift with temperature reduction and keeps its width unchanged too. A remarkable change in the Raman spectrum measured at 25 and 12K can be observed; a new broad Raman band at around 32cm^{-1} emerges which was absent in the higher temperatures.

9.12. EXPERIMENTAL RAMAN SPECTRA OF NEODYMIUM PENTAPHOSPHATE CRYSTAL

The Raman spectrum of a sample of neodymium pentaphosphate crystal, having the formula NdP_5O_{14}, was recorded over the temperature range of 12-300K. The spectrum was obtained using the 4880Å laser line set at 200mW power, 200μ slit widths, and scanning steps of 1cm^{-1} for every 3 seconds. Figure 9.28 shows the experimental Raman spectrum of this crystal measured at 300 and 12K. The Raman line locations, extracted from both temperature spectra, are listed in Table 9.1 columns 5 and 6. The spectrum of this crystal at 300K shows many areas of disturbance (particularly at the base of the spectrum); most likely these effects originate from interference between the Raman lines and the fluorescence lines of the neodymium ion. The spectrum of the crystal measured at 12K shows a reduction in disturbance found in the 300K spectrum (Figure 9.28). Further, the 12K spectrum shows some sharp intensity drops (specially above 1200cm^{-1}). It is apparent from the pattern of the intensity drops that these parts of the spectrum are related to the electronic absorption bands of the neodymium ion which interfere with the Raman lines.

The low frequency region of Raman spectrum of the NdP_5O_{14} crystal shows some temperature effects which require careful examination. Figure 9.29 shows the experimental low frequency spectrum of this crystal measured at 12, 50, 100, 200, and 300K. The spectrum reveals a gradual shift in the Raman line located at 39cm^{-1} with temperature lowering which reaches the location 60cm^{-1} at 12K. Further, two more Raman lines emerge, one on each side of the Raman line located at 60cm^{-1}. In the 12K spectrum of the crystal the two extra Raman lines are located at 56 and 63cm^{-1} (Figure 9.29).

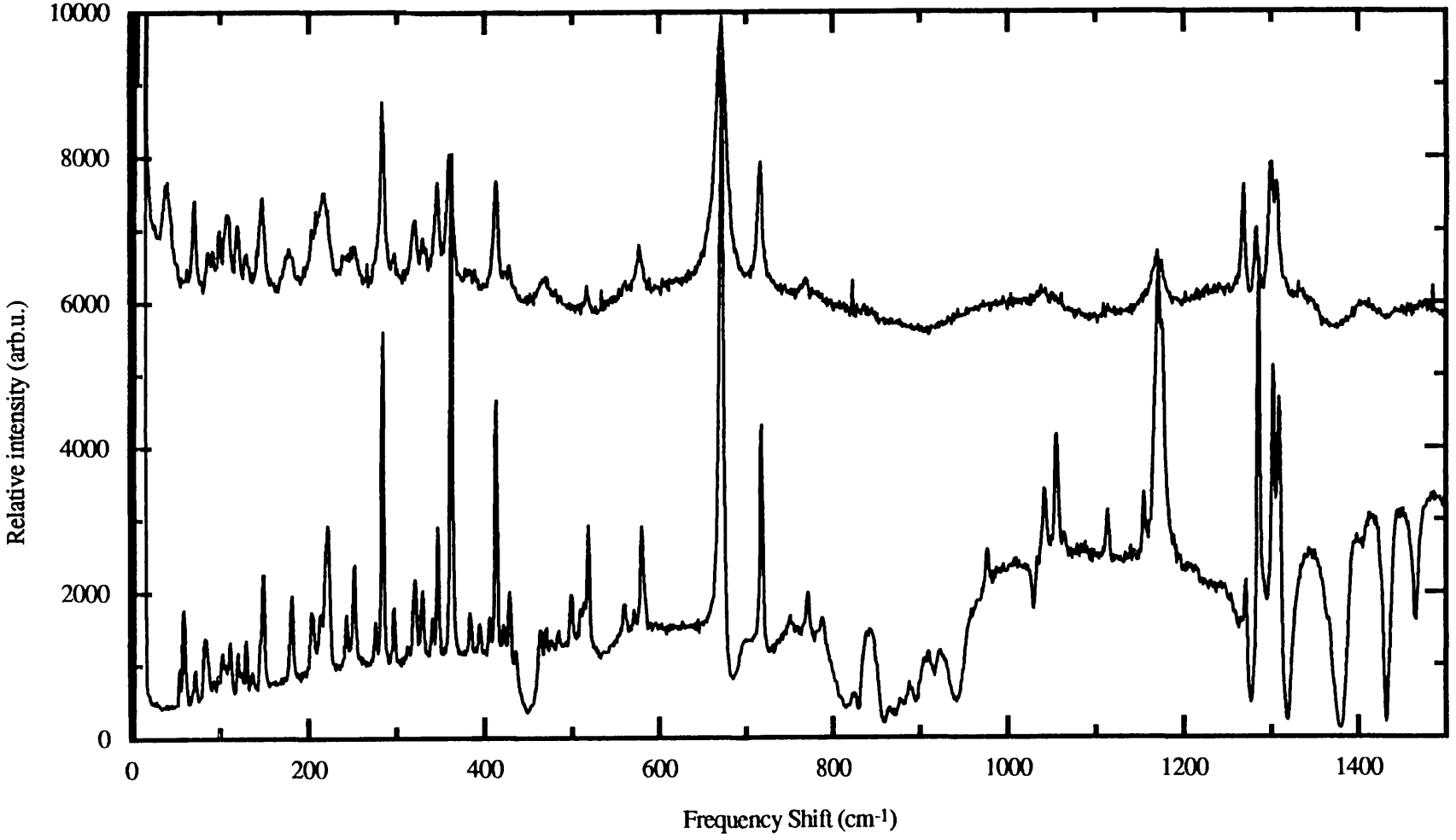

Figure 9.28. The Raman spectrum of neodymium pentaphosphate crystal (NdP_5O_{14}) measured at 300K (above) and 10K (below).

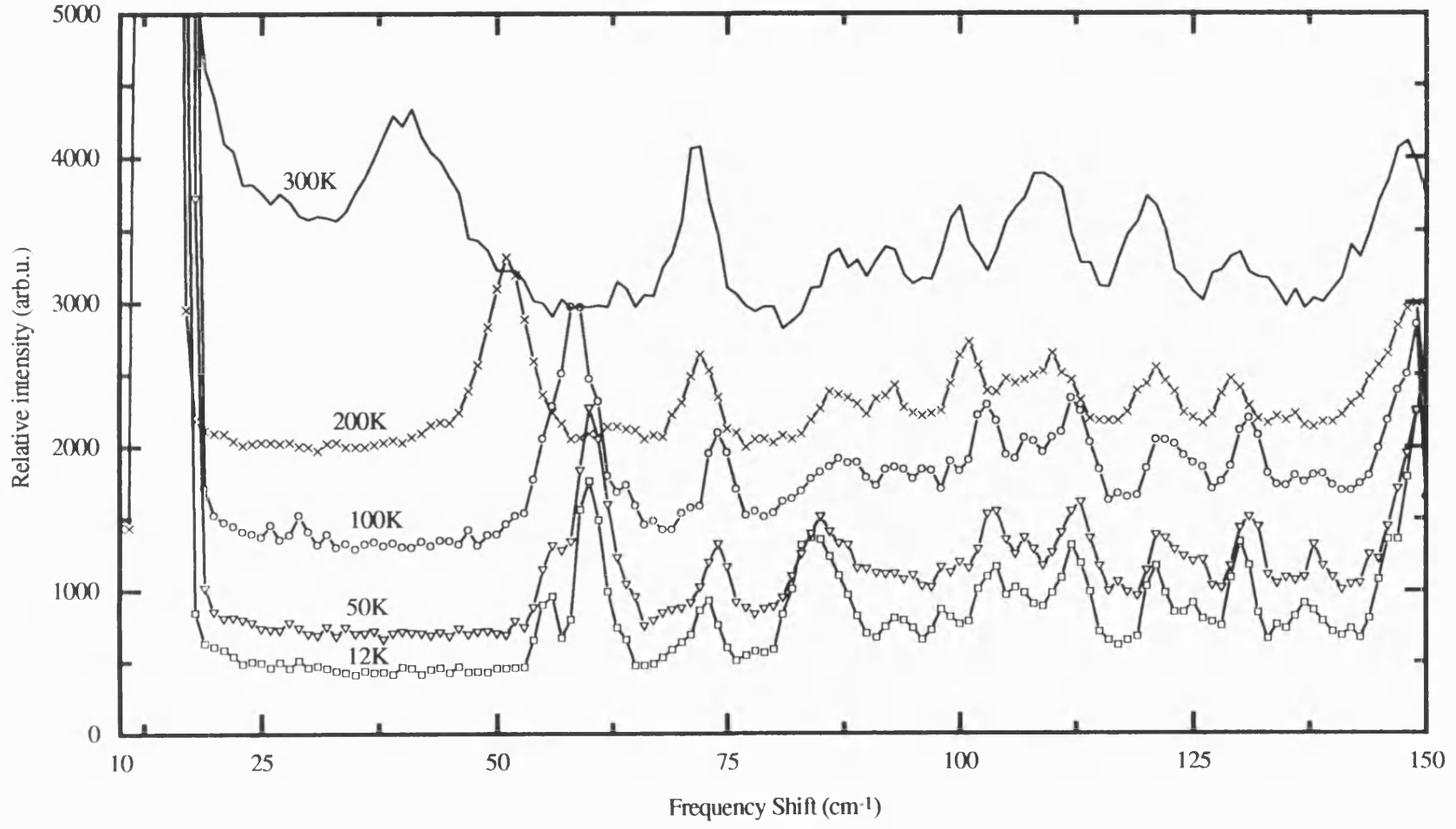

Figure 9.29. The low frequency Raman spectrum of neodymium pentaphosphate crystal (NdP_5O_{14}) measured at different temperatures.

9.13. RESULTS ANALYSES AND DISCUSSION

An inspection of the Raman spectra of the examined rare earth phosphate glass samples, shown in Figures 9.4, 9.10, 9.17 and 9.21, reveals that these spectra are characterised by broad Raman bands. The band broadening is evidence of the existence of the structural disorder, resulting from the large variation in the bond distribution of the PO_4 units. No obvious sign of crystallisation can be seen in the spectra of these glass samples (crystals usually have sharp Raman lines).

To gain further physical insight into the experimental results, and to determine the vibrational modes responsible for the Raman bands of the rare earth phosphate glasses, it is useful to consider the data in Table 9.2. This table contains the Raman bands of the rare earth phosphate glass samples arranged according to the concentration of the incorporated rare earth ion, from low to high. From the table and the spectra of these glasses (Figures 9.4, 9.10, 9.17 and 9.21), one significant remark can be made concerning the structural analysis. In general, the Raman bands of these glasses have the same overall Raman spectral profile and approximately the same peak locations. This spectral similarity is a distinguishing mark which reflects the existence of a common structural skeleton among these rare earth phosphate glasses. Therefore, it is plausible to analyse and discuss the experimental Raman spectra of these glasses on the basis of this structural similarity.

Depending upon the previous Raman studies carried out on various phosphate glasses and crystals (reviewed in section 9.3), the experimental Raman bands of the rare earth phosphate glass samples listed in Table 9.2 can be assigned to the vibrational modes which produce them. Accordingly, the band in the vicinity of $700cm^{-1}$, in the Raman spectra of neodymium, samarium, and europium phosphate glasses can be assigned to the in-chain symmetric stretching of the P-O-P vibration. The band around $1200cm^{-1}$ has been attributed to the out-of-chain symmetric stretching of the PO_2 vibration, whereas the band around $1230cm^{-1}$ has been related to overlap between the out-of-chain antisymmetric stretching of the PO_2 vibration and the P=O bond vibration. The band around $330cm^{-1}$ is due to PO_2 bending, whereas the band near $300cm^{-1}$ arises from in-chain O-P-O bending. In general, the resultant Raman bands of spectra of these glasses are in reasonable agreement with previously reported ones (see section 9.3). Thus, in light of these results, it can be suggested

Table 6.2. The experimental Raman bands and their suggested vibrations extracted from the studied Raman spectra of the rare earth phosphate glass samples. The glasses are arranged according to their rare earth ion concentration from low to high.

Sample composition	Experimental Raman main bands (cm^{-1})				
	Boson peak	PO_2 bending	P-O-P symmetric in-chain	PO_2 symmetric out-of-chain	PO_2 anti-symmetric out-of-chain and the P=O vibration
$(Eu_2O_3)_{0.186}(P_2O_5)_{0.814}$	50	330	710	1200	1240
$(Sm_2O_3)_{0.19}(P_2O_5)_{0.81}$	55	315	680	1190	1265
$(Nd_2O_3)_{0.194}(P_2O_5)_{0.806}$	60	330	700	1200	1250
$(Nd_2O_3)_{0.196}(P_2O_5)_{0.804}$	60	320	700	1195	1240
$(Sm_2O_3)_{0.212}(P_2O_5)_{0.788}$	50	330	700	1195	1240
$(La_2O_3)_{0.263}(P_2O_5)_{0.737}$	55	340	700	1185	1235

that these rare earth phosphate glasses comprise of chains of PO_4 tetrahedra. This suggestion comes from the fact that almost all of the Raman bands for these glasses fit the vibrational modes of phosphate chains.

The R ratio (chapter 4) for the rare earth phosphate glass samples can be calculated and used to illustrate the type of linkage existed between the phosphate tetrahedra (PO_4 units). The proportion of the rare earth oxide (Re_2O_3) to the phosphate oxide (P_2O_5) in the glass samples listed in Table 9.2 is approximately one to three, and since the common valence of the rare earth ion is +3, it can be deduced that the R ratio for these glasses is around one (R =1). Therefore, these rare earth glasses are in the composition region of the metaphosphate (metaphosphates are comprised of long chains of PO_4 unit, Van Wazer and Campanella 1950). However, the concentration of the rare earth ion in the glass samples are not exactly 25% of the total, which is needed for obtaining the long phosphate chains of metaphosphate, the ratio falls just below one (R<1), excluding the lanthanum phosphate glass sample which has its R ratio falls just above one (R>1). Therefore, for the samarium, europium and neodymium phosphate glass samples, cross-linking between the long chains of the phosphate is expected which results in an increase in the intensity of the P=O band (see section 9.3). In fact, it is quite evident that P=O band is relatively intense in the Raman spectra of the neodymium phosphate glass having the composition $(Nd_2O_3)_{0.194}(P_2O_5)_{0.806}$ (1250cm^{-1} band in Figure 9.2), and the samarium phosphate glass having the composition $(Sm_2O_3)_{0.19}(P_2O_5)_{0.81}$ (1265cm^{-1} band in Figure 9.15).

The Raman spectrum of the lanthanum phosphate glass shows (Figure 9.21) the lowest frequency for the PO_2 symmetric out-of-chain band (1185cm^{-1}) and the highest frequency for the PO_2 bending band (340cm^{-1}), among the rare earth phosphate glasses. This is not surprising since this glass sample has lanthanum oxide concentration of 26.3%, the highest among the rare earth glass samples (R>1). Raman spectra of phosphate glasses with such a ratio do not show strong overlap between the PO_2 symmetric out-of-chain band and the P=O band, since the latter band has a low intensity in this ratio due to reduction in cross-linking among the phosphate chains. Thus, the PO_2 symmetric out-of-chain band will have a sharper line width and its shift in the frequency can be attributed to the ion size effect. This is based on the fact that the lanthanum ion has the largest ion size among the samples of the

rare earth phosphate glasses (the other ions are smaller due to the lanthanide contraction) so the PO_2 symmetric out-of-chain band frequency will be the lowest due to an increase in the O-P-O bond angle φ (Nelson and Exarhos, 1979). Another confirmation of this idea comes from the data in Table 9.2, which shows that the europium phosphate glass has the largest frequency for the PO_2 symmetric out-of-chain band ($1200cm^{-1}$); europium is the smallest ion among the rare earth phosphate glass samples studied, therefore the PO_2 symmetric out-of-chain band frequency will be the highest. It has been mentioned in section 9.3, that glasses with the ratio R>1 have some chain shortening, which is manifested in the creation of some PO_3 terminals. In fact, the spectrum of the lanthanum phosphate glass shows a trace of a band just above $1000cm^{-1}$, which is believed to originate from the vibration of the PO_3 terminals.

On comparing the Raman spectrum of the neodymium phosphate glasses of compositions $(Nd_2O_3)_{0.194}(P_2O_5)_{0.806}$ and $(Nd_2O_3)_{0.196}(P_2O_5)_{0.804}$ (Figure 9.4) two differences were identified. First, the Raman band in the vicinity of $1250cm^{-1}$ shows a shift towards lower frequency and its intensity decreases. Secondly, the band at $700cm^{-1}$ narrows on the low frequency side only. Similar differences can also be seen between the spectra of the two samarium phosphate glass samples, having the compositions $(Sm_2O_3)_{0.19}(P_2O_5)_{0.81}$ and $(Sm_2O_3)_{0.212}(P_2O_5)_{0.788}$ (Figure 9.17). These pronounced differences in the Raman spectra are possibly attributed to traces of residual microscopic stresses in these glasses with resultant microscopic structural differences. It has been mentioned above that the Raman band in the vicinity of $1250cm^{-1}$ is the band responsible for the P=O vibration which is a sign of cross-linking in the PO_4 chains (ring -shaped PO_4 connections) of the phosphates. Therefore it can be concluded that some of these rare earth phosphate glasses have a high degree of cross-linkage among chains of the PO_4 tetrahedra. Confirmation of cross linking comes from the widening of the $700cm^{-1}$ band, on the low frequency side only, in spectra of $(Nd_2O_3)_{0.194}(P_2O_5)_{0.806}$, and $(Sm_2O_3)_{0.19}(P_2O_5)_{0.81}$ glass samples (Figures 9.4 and 9.17). The frequency location of the $700cm^{-1}$ band accommodates another Raman band (around $680cm^{-1}$) related to the vibration of the ring-shaped PO_4 units. This $680cm^{-1}$ Raman band can be seen clearly in the spectra of the rare earth pentaphosphate crystals which will be analysed later in this section.

Measurements of fractal dimensionality can be of a significant help in providing useful information about the connectivity of the network of glasses. The fractal dimensionality d vary from 3 for 3-d networks of tetrahedral coordination polyhedra to 2 for 2-d structures and 1 for 1-d chains. Bergman and Kantor (1984) have shown that the effective fractal dimensional d of an inhomogeneous random mixture of fluid and a solid backbone at threshold is given by C_{44}/B where C_{44} is the second order elastic stiffness tensor component and B is the bulk modulus. Bogue and Sladek (1990) have used the fractal dimensionality to assess the network connectivity of glasses. A fractal dimensionality d of close to unity obtained for a pure $AgPO_3$ metaphosphate glass (Bogue and Sladek 1990) is consistent with a skeletal structure comprised of weakly linked chains of interconnected middle PO_4 tetrahedra. By contrast, the measured fractal dimensionality of the rare earth metaphosphate glasses $R(PO_3)_3$ determined from the elastic stiffnesses and bulk moduli, have values between 2.2 and 2.8 (Bowron et al. 1996, Farok et al. 1994, Senin et al. 1994, Mierzejewski et al. 1988, Sidek et al. 1988, 1993). These fractal dimension values imply that all these rare earth metaphosphate glasses have similar structures and also show a near 3 dimensional structure which agrees with the results obtained for the Raman spectra of these glasses that suggests the presence of a marked degree of cross-linkage of PO_4 chains.

The Extended X-ray Absorption Fine Structure Spectroscopy (EXAFS) structural studies carried out on a range of rare earth metaphosphate $R(PO_3)_3$ glasses modified using the rare earth oxides Nd_2O_3, Eu_2O_3, Gd_2O_3, Tb_2O_3, Ho_2O_3 and Pr_6O_{11} have established that the glass skeleton is made up from linked PO_4 tetrahedra (Bowron et al. 1995, 1996). One of the four oxygen atoms in a PO_4 tetrahedron is doubly bonded to the phosphorus and may not take part in the network bonding. The rare earth ions occupy sites with an average coordination number of surrounding oxygen atoms in the range $6 \leq N \leq 8$. This is a common range for oxygen coordination in rare earth oxides and is consistent with a cubic or "pseudo-cubic" local environment for the Rare earth ions. Therefore, the rare-earth ion can be pictured in these metaphosphate glasses as being at the centre of a distorted cube made of cross-linked PO_4 tetrahedra. These EXAFS results are in a good agreement with our Raman spectral results which suggest the presence of high cross-linking of PO_4 tetrahedra

in these glasses necessary for the construction of the proposed distorted cube of oxygen atoms around the rare earth ion.

The Raman spectrum of the samarium phosphate glass (Figure 9.18) indicates that the higher the concentration of the samarium ion the lower the intensity of the P=O vibration band at 1240cm^{-1} and the narrower the width of the band at 700cm^{-1}. This could suggest that the higher the concentration of rare earth ion in the metaphosphate glass samples the less the cross-linking of the PO_4 tetrahedra in structural skeleton. Some evidence for this comes from the Raman spectrum of the lanthanum phosphate glass sample which has the highest concentration of rare earth ion (lanthanum oxide concentration of 26.3%) among the rare earth metaphosphate glasses studied (Table 9.2). Its Raman spectrum (Figure 9.21) shows that the intensity of the P=O vibration band at 1235cm^{-1} is low and the width of the 700cm^{-1} band is relatively narrow. Thus, according to the above suggestion the europium metaphosphate glass sample which has the lowest concentration of rare earth ion (europium oxide concentration of 18.6%) should have the highest cross-linking of PO_4 tetrahedra among the rare eath metaphosphate glass samples. In fact its Raman spectrum shows (Figure 9.11) that the P=O vibrational band at 1240cm^{-1} has moderate intensity and the 710cm^{-1} band has a moderate width revealing a lower degree of cross-linking in comparison with the spectrum of the samarium phosphate glass which has the samarium oxide concentration of 19.0% (Figure 9.15). This contradiction leads to the suggestion that the amount of cross-linking of the PO_4 tetrahedra presence in structural skeleton of the rare earth metaphosphate glasses does not depend only on the rare earth ion concentration but it also depends on which rare earth ion has been incorporporated in the glass.

The Raman spectra of the rare earth phosphate glass samples show that the in-chain PO_2 vibrational band at 700cm^{-1} does not shift appreciably when the rare earth ions are changed (Table 9.2). This is in agreement with the vibrational model, which assumes that the cation has a weak interaction with the bridging oxygens of the polyphosphate chains (Rouse et al. 1978, Nelson and Exarhos 1979). However, the in-chain PO_2 vibrational band does shift in the Raman spectra of the europium phosphate $(Eu_2O_3)_{0.186}(P_2O_5)_{0.814}$ and the samarium phosphate $(Sm_2O_3)_{0.19}(P_2O_5)_{0.81}$. This is not a real shift since this peak, in spectra of these two samples, is a combi-

nation of the in-chain PO_2 vibrational band and the Raman band related to the vibration of rings of PO_4 tetrahedra (around 675cm^{-1}) which is apparent in the Raman spectra of the rare earth pentaphosphate crystals (Figures 9.24, 9.26, and 9.28). Therefore, in measuring the exact location of this in-chain PO_2 band some error will occur.

The low frequency Raman spectral intensity of the neodymium, europium, and lanthanum metaphosphate glasses were analysed, using the Shuker and Gammon equation (eq. 9.2), to add further support to the work done by Carini et al. (1993) and Lipinska-Kalita et al. (1995) on some of our rare earth metaphosphate glass samples having different compositions. The spectral analysis was made to find the frequency dependence of the coupling constant $C(\omega)$ in the equation 9.2. The log-log plots of the reduced Raman intensity against the frequency shift of spectra of these glasses (Figures 9.8, 9.9, 9.14 and 9.23) resulted in slope values of 3.4, 3.4, 3.4, and 3.3 respectively; all in the vicinity of 3.5 within the experimental error of the fitting procedure. Slope values for the Raman intensity data of the samarium metaphosphate glass (Carini et al. 1993), having the composition $(Sm_2O_3)_{0.25}(P_2O_5)_{0.75}$, and for the gadolinium metaphosphate glass (Lipinska-Kalita et al. 1995), having the composition $(Gd_2O_3)_{0.226}(P_2O_5)_{0.774}$, have been obtained as of 3.8 and 3.4 respectively. On comparing these slope values with the values obtained by us on the rare earth metaphosphate glasses a good agreement can be found with the slop value of the $(Gd_2O_3)_{0.226}(P_2O_5)_{0.774}$ glass. Carini et al. (1993) and Lipinska-Kalita et al. (1995) suggested a fourth power relationship based on the assumption that the slopes are closer to 4 and accordingly the coupling constant $C(\omega)$ of these glasses has an ω^2 dependency (Eq. 9.2); at low temperatures the density of states $g(\omega)$ has an ω^2 behaviour (Debye-like). A soft potential model (Parshin 1993), which has been used in providing a general explanation of the anomalous thermal, acoustic and optical vibrational properties of glasses, predicts that the stokes Raman scattering intensity of glasses to have an ω^4 dependence. This prediction is not in a quite good agreement with the results shown in Figures 9.8, 9.9, 9.14 and 9.23 for the rare earth metaphosphate glasses which show that the reduced Raman intensity (in the low frequency region) to have a frequency dependence close to 3.5. This small disagreement between our results and the soft

potential model leads to two possibilities. First, it could be that the cooling temperature of samples (10K) is not enough to eliminate all the thermal effects in the low frequency region which in turn has an effect on the calculated reduced intensity of the spectra. Second, it could be that the coupling constant $C(\omega)$ of these glasses have an $\omega^{1.5}$ dependency instead of the ω^2 dependency concluded from the model.

The measured Raman spectra of the rare earth pentaphosphate crystals SmP_5O_{14}, EuP_5O_{14} and NdP_5O_{14} show a large number of sharp Raman lines. The locations of these Raman lines, extracted from the spectra (measured at 12 and 300K on these crystals) are tabulated in Table 9.1. It can be observed that these Raman spectra (Figures 9.24, 9.26 and 9.28) show considerable similarity, having almost the same profiles, number of lines and line widths. This spectral similarity suggests, to some extent, that these crystals have the same structural skeleton as expected from their similar crystal structures.

The spectra of these rare earth pentaphosphate crystals show that some of the Raman lines split and slightly shift with temperature. The strongest lines in each of the crystal spectra show a shift of around $4cm^{-1}$ with the temperature lowered to 12K (Table 9.1). A shift of around $3cm^{-1}$ is also evident in the main Raman lines, at one temperature. This shift is most probably due to the differences in the rare earth ion. The Raman spectrum of NdP_5O_{14} (Figure 9.28) shows broadening and interference in the lines. This can be ascribed to the interference between the Raman lines of the crystal and the fluorescence bands of the neodymium ion since this frequency region coincides with some of the high electronic energy bands of ion.

The most intense lines in the Raman spectra of SmP_5O_{14}, EuP_5O_{14} and NdP_5O_{14} crystals can be assigned to the vibration of the structural skeleton made from the PO_4 tetrahedra connection. The Raman line at around $360cm^{-1}$ can be attributed to the PO_2 bending vibration, the line at around $720cm^{-1}$ can be assigned to P-O-P symmetric in-chain vibration, the line at around $1175cm^{-1}$ can be attributed to PO_2 symmetric out-chain vibration and the four lines located around $1300cm^{-1}$ can be assigned to the vibrations of PO_2 antisymmetric out-of-chain and the P=O. The most distinguishing feature found is the existence of an intense Raman line at around $675cm^{-1}$. This intense line arises from the vibration of the ring-shaped PO_4

tetrahedra interconnections which exist in the structure of the rare earth pentaphosphate crystals (Hong and Pierce 1974, Parent et al. 1987). The rings of PO_4 tetrahedra (cross-linked PO_4) boost the P=O vibration in the spectra which is quite evident in the high intensity of the four Raman lines at about 1300cm^{-1}.

The Raman spectra of the rare earth pentaphosphate crystals can be of significant assistance in explaining the variations found in the Raman spectra of the rare earth metaphosphate glasses. Apart from the broadening in the Raman bands of rare earth metaphosphate glasses, there is a high degree of resemblance between the spectra of the crystals and the glasses, which is reflected in the approximate locations of the main Raman bands. The differences between Raman bands at around 1250cm^{-1} and 700cm^{-1} in the spectra of the samarium and neodymium metaphosphate glasses (Figures 9.5 and 9.18) can be explained following a comparison with the Raman spectra of the rare earth pentaphosphate crystals. Since the Raman spectra of the rare earth pentaphosphate crystals give rise to lines at around 1250cm^{-1} and 675cm^{-1}, which are related to the ring-shaped interconnections between the PO_4 tetrahedra (Hong and Pierce 1974), it can be deduced that the increase in the intensity of the P=O vibrational band (around 1250cm^{-1}) and the widening of the 700cm^{-1} band on the low frequency side in the spectra of the glass samples having the compositions $(Nd_2O_3)_{0.194}(P_2O_5)_{0.806}$ and $(Sm_2O_3)_{0.19}(P_2O_5)_{0.81}$ (Figures 9.4 and 9.17) are both signs of the existence of ring-shaped interconnections (high cross-linking) between the PO_4 tetrahedra in these glasses.

A part of the spectral study was to measure the temperature dependence of the low frequency Raman modes of the three rare earth pentaphosphate crystals. Figure 9.30 shows the temperature dependence of the square of frequency shift of the lowest Raman modes in the spectra of SmP_5O_{14}, EuP_5O_{14} and NdP_5O_{14} crystals. It is apparent from the figure that there is mode softening which is an evidence of the existence of structural phase transition in these crystals with temperature. These soft modes are associated with the existence of second order ferroelastic transition in these crystals with symmetry change mmm→2/m (or $D^7_{2h} \rightarrow C^5_{2h}$) (Schulz et al. 1974, Budin 1975, Weber 1975, Kobayashi et al. 1976). Some splitting in these soft modes has been observed which can be ascribed to lifting the degeneracy in the vibration due to the structural changes related to the phase transition.

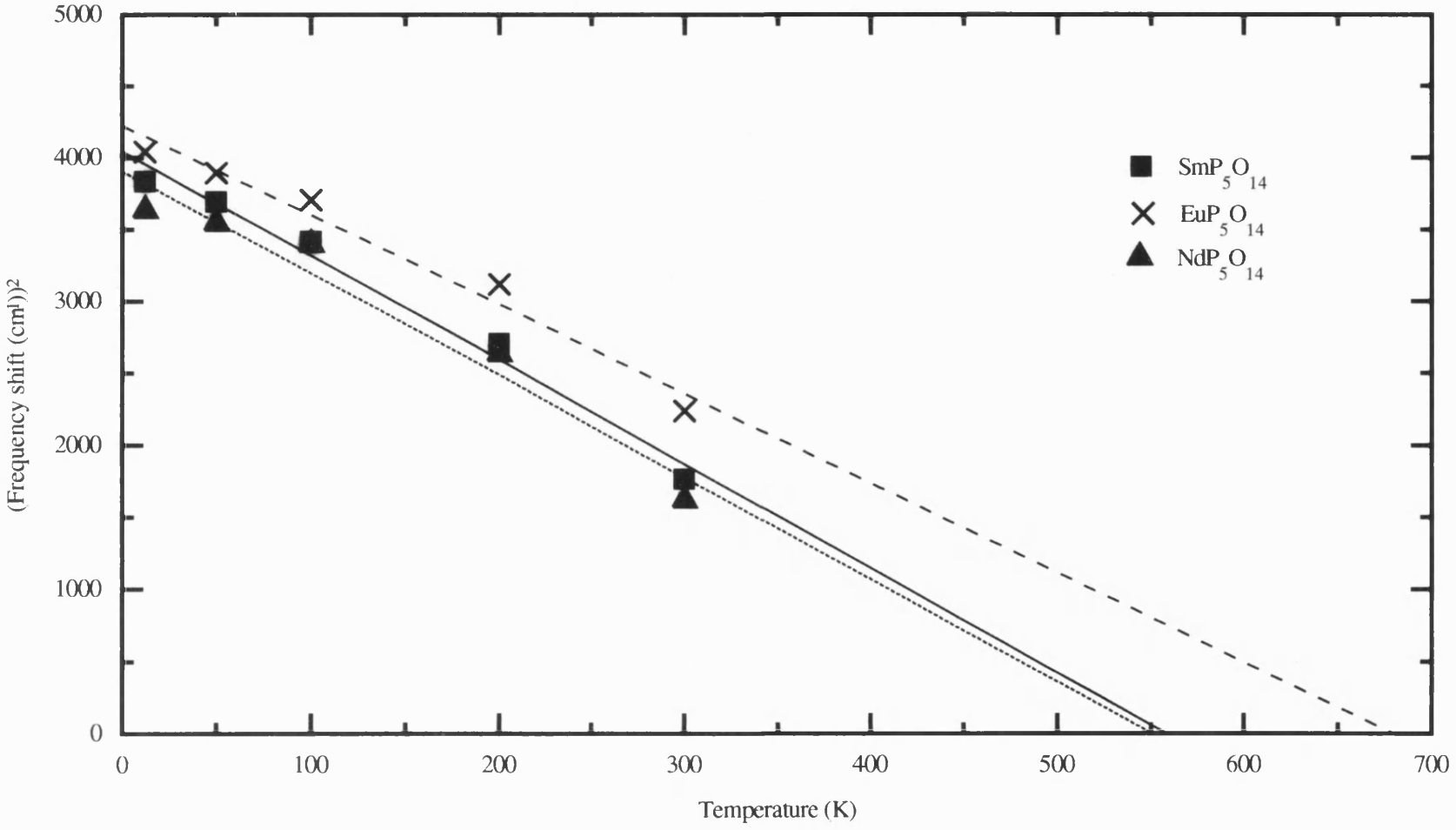

Figure 9.30. The temperature effect on the square of the frequency shift of the soft modes of samarium, europium, and neodymium pentaphosphate crystals.

The change found in the local symmetry of the rare earth ions in the rare earth pentaphosphate crystal with temperature reduction would require a slight structural rearrangement of the linked PO_4 tetrahedra; this would be likely the cause of the mode softening.

CHAPTER TEN

CONCLUSIONS AND FUTURE WORK

The aim of this chapter is to present the conclusions associated with the significant findings of this work. It is divided into three sections according to the order of the thesis chapters: (i) the diamond anvil cell and the optical system constructed to calibrate it using ruby fluorescence, (ii) the fluorescence spectra of the rare earth metaphosphate glasses and pentaphosphate crystals, (iii) the Raman spectra of glasses and crystals. This is followed by suggestions for future work which could be carried out for the rare earth metaphosphate glasses and pentaphosphate crystals.

10.1. DIAMOND ANVIL CELL AND HIGH PRESSURE CALIBRATION OPTICAL SYSTEM

The diamond anvil cell has been described and its principle of operation has been given. Special accessories needed for handling and loading ruby and rare earth metaphosphate glasses and crystals in the cell have been used. The critical procedure of aligning the diamond anvils has been explained in detail. Difficulties in gasket handling (drilling, indentation, centring) and sample loading in the DAC, have been overcome by using special tools (microlitre syringe, fine wires, surgical blades etc.). The DAC has been successfully used to generate very high pressures on tiny samples of ruby and rare earth phosphate glasses and crystals loaded inside it.

An optical system has been assembled to calibrate the DAC, using the ruby fluorescence lines, and to measure the fluorescence spectra of rare earth metaphosphate glasses and pentaphosphate crystals. The specification and description of each of the optical and electrical components of the optical system have been explained. This assembled system has been successfully used to calibrate the DAC and measure the fluorescence spectra of the samples. The findings can be summarised as follows:

1. The two octagonal culet faces of the diamond anvils have been aligned relative to each other; a complete octagonal shape with one interference fringe inside it has-

been observed under the microscope .

2. To avoid the problem of evaporation of the alcohol mixture inside the gasket hole before closing the DAC, we found it effective to cool the mixture with liquid nitrogen before injecting it into the hole to eliminate this problem.

3. The DAC has been successfully used and hydrostatic pressures as high as 50Kbar have been generated.

4. The assembled optical system has been able to produce a very intense fluorescence from a ruby sample as small as 30μ loaded in DAC. This has demonstrated the capability of the chosen lenses, mirrors and filters of the system to gather maximum light from tiny samples located in the tiny gasket hole of the DAC.

5. The chosen photomultiplier and lock-in amplifier have proved to provide good detection and high amplification respectively; they produce high output signals, even with very low level fluorescence from tiny samples. An output signal 50 times higher than the noise has been detected for the lowest fluorescence signal measured.

6. The natural line width of the R lines of the ruby fluorescence have been maintained and line widths of 7.5Å for the R_1 line, in agreement with reported data, have been recorded with sample size as small as 30μ and narrow silt widths of 50μ.

7. The linear shifts in the wavelength of the ruby fluorescence lines, R_1 and R_2, with pressure have been observed and recorded up to 70Kbar. The wavelength shifts have been used to measure the pressure applied on the rare earth metaphosphate glasses and pentaphosphate crystals loaded in the DAC.

8. Errors in pressure measurements have been minimised by using a low power laser to avoid local heating in the samples. Errors associated with reading the peak positions of the ruby lines have been minimised using slow wavelength scanning. An error of 1.37Kbar in the pressure measurements has been registered due to estimated uncertainty of ± 0.5Å in the wavelength peak of the ruby R_1 line.

10.2. THE EFFECT OF TEMPERATURE AND HIGH PRESSURE ON THE FLUORESCENCE SPECTRA OF RARE EARTH METAPHOSPHATE GLASSES AND PENTAPHOSPHATE CRYSTALS

The fluorescence spectra of the rare earth metaphosphate glasses have been measured at 300K and 10K to record the temperature effect on these spectra and to establish the valency of the rare earth ions in these matrices. The fluorescence spectra of the rare earth pentaphosphate crystals have also been measured at 300K and 10K for the purpose of comparison with the spectra of the glasses to identify similarities and differences. The spectra of the glasses and crystals have been recorded under high pressures using the DAC to search for any pressure effect on the valency of the rare earth ions and any phase transition. Below, we list the findings for each rare earth metaphosphate glass with its counterpart of pentaphosphate crystal.

(A) The spectra of $(Eu_2O_3)_{0.186}(P_2O_5)_{0.814}$ glass and EuP_5O_{14} crystal

1. The absorption and fluorescence spectra of the europium metaphosphate glass having the composition $(Eu_2O_3)_{0.186}(P_2O_5)_{0.814}$ at room and low temperatures show that the europium ion has 3+ valency. Also, the fluorescence spectrum of the europium pentaphosphate crystal EuP_5O_{14} at room and low temperatures show a valency of 3+ for the europium ion. Both materials have a relatively strong fluorescence.

2. The fluorescence spectrum of the europium metaphosphate glass excited with 2600Å ultra-violet line has shown no sign of divalent europium ion in this glass only trivalent.

3. The fluorescence spectrum of the glass and the crystal are similar except the broadening observed in the glass spectra; the spectra split into five groups of well-separated bands originating from transition between the $^5D_0$ excited state and the $^7F_0$, $^7F_1$, $^7F_2$, $^7F_3$, $^7F_4$ lower states.

4. The fluorescence spectrum of the europium pentaphosphate crystal reveals that the local symmetry of the europium ion is low (C_s, C_v). On comparing this spectrum with the spectrum of the europium metaphosphate glass it has been found that the local symmetry of the europium ion in the glass is low too.

5. The spectrum of the glass suggests that the europium ions are sited in two different low symmetry environments at least having an energy difference of about ΔE=0.0031eV.

6. Up to 50Kbar neither the crystal nor the glass spectra show any changes which might be associated with phase transition or valency change; both high pressure spectra are typical of fluorescence originating from trivalent europium ions. When a high pressure is applied to the crystal, the fluorescence lines originating from the $^5D_0 \rightarrow {}^5F_1$ transition shift towards longer wavelengths with pressure derivatives ($d\lambda/dP$) ranging between 0.06 and 0.43 Å/kbar.

(B) The spectra of $(Sm_2O_3)_{0.248}(P_2O_5)_{0.752}$ glass and SmP_5O_{14} crystal

1. The laser induced fluorescence spectra of metaphosphate glass of composition $(Sm_2O_3)_{0.248}(P_2O_5)_{0.752}$ and an pentaphosphate crystal SmP_5O_{14} at room temperature show that in both materials the samarium ions are in the 3+ state. Both materials have relatively strong fluorescence.

2. The spectrum of the glass suggests that the samarium ions are sited in two different locations separated by an average energy difference of about ΔE=0.016eV.

3. The fluorescence spectrum of samarium ion in the SmP_5O_{14} crystal splits into five groups of well separated bands. The number of lines in each band indicates that the local symmetry can be treated as being pseudocubic. This is consistent with the crystal structure; the Sm^{3+} ions can be considered to a first approximation to be at the centre of a pseudocube comprised of eight oxygen atoms belonging to PO_4 tetrahedra.

4. When the temperature of the crystal is reduced to 12K, some of the fluorescence lines at the short wavelengths in each band disappear. One possible explanation of this is the occurrence of a symmetry non-breaking transition which takes the local environment of the Sm^{3+} ions from pseudocubic to another more regular pseudocubic local symmetry with consequent slight difference in crystal field.

5. When a high pressure is applied to the crystal, the fluorescence lines in the first two bands shift towards longer wavelengths with a pressure derivatives ($d\lambda/dP$)

ranging between 0.15 and 0.4 Å/kbar.

6. The fluorescence spectrum of samarium ion in the $(Sm_2O_3)_{0.248}(P_2O_5)_{0.752}$ glass also splits into five groups of well-separated bands. When the glass is cooled down to 10K, there is disappearance of the tail on the short wavelength side for each of the five fluorescence bands. This appears to be a counterpart of the disappearance of the shorter wavelength lines in the crystal fluorescence at low temperature.

7. Neither the crystal nor the glass show any effects under pressure which might be associated with any phase transition.

(C) The spectra of $(Tb_2O_3)_{0.186}(P_2O_5)_{0.814}$ glass and TbP_5O_{14} crystal

1. The laser induced fluorescence spectra of metaphosphate glass of composition $(Tb_2O_3)_{0.186}(P_2O_5)_{0.814}$ and an pentaphosphate crystal TbP_5O_{14} at 300K and 12K show that in both materials the terbium ions are in the 3+ state.

2. The fine structure of the fluorescence bands of the TbP_5O_{14} crystal reveals that the local symmetry of the Tb^{3+} ion in this crystal can be considered to be either hexagonal or tetragonal. For small distortions both these local symmetries are close to pseudocubic. An interpretation of the fluorescent spectral lines of the TbP_5O_{14} crystal that the local symmetry around the Tb^{3+} ion is pseudocubic is in accord with the shape of the co-ordination polyhedron of the eight oxygen atoms surrounding a Tb^{3+} ion in crystal structure, which can be thought of as a distorted cube.

3. The fluorescence spectrum of terbium ion in the $(Tb_2O_3)_{0.186}(P_2O_5)_{0.814}$ glass and TbP_5O_{14} crystal splits into seven groups of well-separated bands. The bands are attributed to transitions between the $^5D_4$ excited state and the multiplets of the $^7F_{6,5,4,3,2,1,0}$ states. . Both materials show intense fluorescence especially at low temperatures; the fluorescence spectrum of the terbium pentaphosphate crystal shows a higher fluorescence intensity than the glass even with using a very low power laser and narrow slitwidths.

4. When the glass is cooled down to 12K, the fluorescence spectrum excited by the 5154Å laser line shows the typical overall profile of Raman bands of rare earth

metaphosphate glass which was embedded under the strong fluorescence bands of the Tb^{3+} ion.

5. Fluorescence measurements on the glass and crystal show intense fluorescence tail and sharp peaks respectively, above the laser line frequency. It is speculated that this tail and peaks of fluorescence on the higher frequency side could be caused by phonon-assisted fluorescence. It is possible that some of the laser photons could gain further energy by absorbing Raman phonons created by light scattering inside the glass and crystal.

6. The local symmetry of the Tb^{3+} ion in the TbP_5O_{14} crystal experiences a change, from a low value to hexagonal or tetragonal, with temperature reduction. Comparison between the spectrum of the crystal and that of the glass suggests that the local symmetry of the Tb^{3+} ion in the metaphosphate glass experiences the same local symmetry change with temperature reduction. The EXAFS measurements made for the $(Tb_2O_3)_{0.26}(P_2O_5)_{0.74}$ glass showed that the an average co-ordination number of 7±1 for oxygen atoms surrounding the Tb^{3+} ion (Bowron et al. 1995); the structural parameters in other rare earth metaphosphate glasses are similar (Bowron et al. 1996). Therefore, picturing the terbium ion in metaphosphate glass as being at the centre of a distorted cube is in accord with the EXAFS results.

7. Application of high pressures(up to 52Kbar) using the DAC did not show great effects on the spectrum of the glass; the same spectral profile which is typical of the Tb^{3+} ion fluorescence bands was retained through out. These pressure measurements suggest that there is no phase transition in the glass and the valency of the Tb remains trivalent up to the higher pressure measured.

(D) The alexandrite effect in $(Ho_2O_3)_{0.22}(P_2O_5)_{0.758}$ glass

1. Thanks to the observation by Mrs W Lambson an alexandrite effect has been identify in holmium metaphosphate glass having the composition $(Ho_2O_3)_{0.22}(P_2O_5)_{0.758}$. The glass colour changes from dark salmon pink in artificial light to yellow in daylight.

2. The optical absorption and laser induced fluorescence spectra of holmium metaphosphate glass measured at room temperature show bands belonging to trivalent

holmium ion only.

3. The fluorescence spectrum of the glass is very weak compared with the spectra of the other rare earth metaphosphate glasses studied here.

4. The alexandrite effect has been ascribed to the two windows in the optical absorption spectrum of the glass in the yellow-orange and green regions.

10.3. THE RAMAN SPECTRA OF THE RARE EARTH METAPHOSPHATE GLASSES AND PENTAPHOSPHATE CRYSTALS

The Raman spectra of rare earth metaphosphate glasses and pentaphosphate crystals have been measured in the temperature range 10-300K to assign the vibrational modes in these materials. The effects of temperature on the low frequency Raman spectra of the glasses have been measured in detail and the Shuker and Gammon equation has been applied to find the frequency dependence of the coupling constant $C(\omega)$ at low frequency. Also, the effects of temperature on the low frequency Raman spectra of the rare earth pentaphosphate crystals have been measured to search for any soft modes. The findings can be summarised as follows:

1. The Raman bands of neodymium, samarium, europium and lanthanum metaphosphate glasses have all the same overall Raman spectral profile and approximately the same peak locations. This spectral similarity reflects the existence of a common structural skeleton among these glasses.

2. The analysis of concentrations of the rare earth phosphate glasses shows that they have compositions in the region of metaphosphate.

3. The vibrational modes responsible for the Raman bands found in the spectra of rare earth metaphosphate glasses have been assigned as below:

Band	Assignment
$300cm^{-1}$	PO_2 bending
$700cm^{-1}$	in-chain symmetric of O-P-O
$1200cm^{-1}$	out-of-chain symmetric stretching of the PO_2
$1230cm^{-1}$	out-of-chain antisymmetric stretching of the PO_2 vibration overlapped on the P=O bond vibration

These vibrational modes suggest that the rare earth metaphosphate glasses are comprised of cross-linked chains of PO_4 tetrahedra. This is in accord with the reported fractal dimension values of these glasses which show a near 3 dimensional structure and also with the EXAFS structural studies which established that the rare earth ions occupy sites with an average co-ordination number of surrounding oxygen atoms in the range $6 \leq N \leq 8$. The local environment for the rare earth ions in these metaphosphate glasses can be pictured as being at the centre of a distorted cube made of cross-linked PO_4 tetrahedra.

4. The increase in the intensity of the 1250cm^{-1} band (P=O vibration) and the widening of the low frequency side of the 700cm^{-1} band, are both signs of the existence of cross-linking among the PO_4 tetrahedra (ring-shaped PO_4 connections) of these metaphosphates. It has been observed that some of rare earth phosphate glasses have slightly higher degree of cross-linkage of the PO_4 tetrahedra than others.

5. The amount of cross-linking of the PO_4 tetrahedra presence in structural skeleton of the rare earth metaphosphate glasses does not depend only on the rare earth ion concentration but it also depends on which rare earth ion has been incorporporated in the glass.

6. The Raman spectra of the rare earth metaphosphate glass samples show that the in-chain PO_2 vibrational band at 700cm^{-1} does not shift appreciably when the rare earth ions are changed. This is in agreement with the vibrational model, which assumes that the cation has a weak interaction with the bridging oxygens of the polyphosphate chains.

7. The Shuker and Gammon equation has been applied for the low frequency Raman regions of these glasses to verify the ω^2 dependency of the coupling constant $C(\omega)$ at low frequency found by others. The log-log plots of the reduced Raman intensity against the frequency shift of spectra of these glasses resulted in slope values close to 4. The results found are in a good agreement with the prediction of an ω^4 dependence in the soft potential model for the Stokes Raman scattering intensity of glasses.

8. The measured Raman spectra of the rare earth pentaphosphate crystals SmP_5O_{14}, EuP_5O_{14} and NdP_5O_{14} show a large number of sharp Raman lines and considerable

similarity which confirm that these crystals have the same structural skeleton as expected from their similar crystal structures.

9. The most intense lines in the Raman spectra of SmP_5O_{14}, EuP_5O_{14} and NdP_5O_{14} crystals have be assigned to the vibration of the structural skeleton made from the PO_4 tetrahedra connection as follows:

Band	Assignment
$360cm^{-1}$	PO_2 bending vibration
$675cm^{-1}$	ring-shaped PO_4 tetrahedra interconnections vibrations
$720cm^{-1}$	P-O-P symmetric in-chain vibration
$1175cm^{-1}$	PO_2 symmetric out-chain vibration
$1300cm^{-1}$	4 lines, PO_2 antisymmetric out-of-chain and the P=O

The intense Raman lines at around $675cm^{-1}$ and $1300cm^{-1}$ arise from the vibration of the ring-shaped PO_4 tetrahedra interconnections which exist in the structure of the rare earth pentaphosphate crystals (cross-linked PO_4).

10. The Raman bands of rare earth metaphosphate glasses are much broader than the ones for the pentaphosphate crystals. However, there is a high degree of resemblance between both the spectra which can be seen in the overall profile and the approximate locations of the main Raman bands. The spectra of the crystals show higher degree of cross-linking of the PO_4 tetrahedra than the spectra of the glasses; this due to the existence of ring-shaped interconnections between the PO_4 tetrahedra in the rare earth pentaphosphate crystals.

11. The temperature dependence of the low frequency Raman modes of the SmP_5O_{14}, EuP_5O_{14} and NdP_5O_{14} crystals show some soft modes. These soft modes are associated with the existence of second order ferroelastic transition in these crystals with symmetry change mmm→2/m (or $D^7_{2h} \rightarrow C^5_{2h}$) (Schulz et al. 1974, Budin 1975, Weber 1975, Kobayashi et al. 1976). Some splitting in these soft modes has been observed which can be ascribed to lifting the degeneracy in the vibration due to the structural changes related to the phase transition.

10.4. FUTURE INVESTIGATIONS AND SUGGESTIONS

Some preliminary work has already been done on the absorption and fluorescence spectra of praseodymium (Pr), dysprosium (Dy), and erbium (Er), metaphosphate glasses. The spectrum of the praseodymium metaphosphate glass is relatively strong while the spectra of the dysprosium and erbium metaphosphate glasses are rather weak, but they all can be studied at low temperature and possibly under high pressures. Some quick scans have also been recorded for the spectrum of the praseodymium pentaphosphate crystal; the spectrum is rather intense and needs a detailed investigation. However, these preliminary spectra need to be studied thoroughly under different temperatures and pressures to obtain a better view about these materials.

In the literature there were reported some successful attempts to grow metaphosphate crystals of rare earths having the formula ReP_3O_9. Therefore, we would find it useful to obtain such crystals and measure their fluorescence and Raman spectra so they can be used for a more direct comparison with the spectra of their counterpart of rare earth metaphosphate glasses. We believe that metaphosphate crystals of samarium, europium, terbium, praseodymium would have intense fluorescence and Raman spectra.

The optical system assembled for high pressure measurements can be modified for Raman spectral measurements. This is can be achieved by changing the present monochromator with a dual or triple grating monochromator, to reduce the level of light scattering close to the laser line used, and by cooling the photomultiplier. Also, the system can be modified to be used for simultaneous high pressure and low temperature studies of the fluorescence and the Raman spectra of any material. To achieve that, there is a need for a cryogenic and a miniature DAC which can be fitted in it; especially designed micropositioners can be fitted inside the cryogenic to hold the DAC in position and to focus the laser light. Currently, the optical system is being used by one of our colleague to measure the life-time of the fluorescence of the rare earth metaphosphate glasses. The system has been modified to produce pulse laser by using acousto-optic modulator crystal. The primary experimental results on samples of europium and samarium metaphosphate glasses are promising.

REFERENCES

Adams D, 1990. Chemistry Department, University of Leisceter. Private Communications.

Almeida R M, 1988. J.Non-Cryst.Solids. **106** 347.

Alonso M and Finn E, 1971. Fundamental University Physics III.(Addison-Wesley) 276.

Anderson P W, Halperin B I and Varma C M, 1972. Philos.Mag. **25** 1.

Babb S Jr and Scott G J, 1964. J.Chem.Phys.**40** 3666.

Bapat V N, 1977. J. Phys. C: Solid State Physics **10** L465.

Barnett J D and Bosco C D, 1969. J.Appl.Phys.**40** 3144.

Barnett J D, Block S and Piermarini.G J, 1973. Rev.Sci.Instrum.**44** 1.

Bassett W, Takahashi T and Mao H K, 1968. J.Appl.Phys.**39** 319.

Bassett W, Takahashi T and Stock P W, 1967.Rev.Sci.Instrum.**38** 37.

Behrens E G, Durville F M and Powell R C, 1986. Opt. Lett. **11** 653.

Behrens E G, Durville F M, Powell R C and Blackburn D H, 1989. Phys. Rev. B **39** 6076.

Behrens E G, Powell R C, and Blackburn D H, 1990. J.Opt.Soc.Am. B **7** 1437.

Bell PM and Mao H K, 1975. Carnegie Inst. Washington, Year Book **74** 399.

Belliveau T F and Simkin D J, 1989. J.Non-Cryst. Solids. **110** 127.

Bergman D J and Kantor Y, 1984. Phys. Rev. Lett. **53** 511.

Bethe H, 1929. Ann.Phys. **3** 133.

Beucher M, 1970. Les Elements Des Terres Rares, Coll. No. 180, **1** 331.

Biscoe J, Pincus A G, Smith C S and Warren B E, 1941. J.Am.Cerm.Soc. **24** 116.

Bobovich Y S, 1962.Opt.Spectra (English Translation), **13** 274.

Bogue R and Sladek R J, 1990. Phys. Rev.B **42** 5280.

Bowron D T, Newport R J, Rainford B D, Saunders G A and Senin H B, 1995. Phys.Rev.B **51** 5739.

Bowron D T, Saunders G A, Newport R J, Rainford B D and Senin H B, 1996. Phys.Rev.B **53**, 5268.

Brady G W, 1958. J.Chem.Phys. **28** 48.

Brand O and Löhneysen H V, 1991. Eur.Phys.Lett. **16** 455.

Brecher C J, 1974. Chem. Phys. **61** 2297.

Bridgman P, 1964. Collected Experimental Papers. (Harvard University, Provo, Cambridge, Mass.). Vol Vi, Paper No 166, P 3903.

Broer M M, Bruce A J and Grodkiewicz W H, 1992. Phys.Rev.B **45** 7077.

Bruno M S and Dunn K J, 1984. Rev.Sci.Instrum. **55** 940.

Buchenau U 1993. Eur.Phys.News **24** 77.

Buchenau U, Galperin Yu, Gurevinch V L, Parshin D A, Ramos M A and Schober H R, 1992. Phys.Rev.B **46** 2798.

Buchenau U, Prager M, Nucker N, Dianoux A J, Ahmad N and Phillips W A, 1986. Phys.Rev. B **34** 5665.

Buchenau U, Zhou H M, Nucker N, Gilroy K S and Phillips W A. 1988. Phys.Rev.Lett. **60** 1318.

Budin J P, Milatos Roufos A, Duc Chinh N and Le Roux G, 1975. J.Appl.Phys.**46**, 2867.

Bues W and Gehrk H, 1956. Z.Anorg.Allg.Chem. **288** 307.

Burgemeister E, 1978. Physica B.**93** 165.

Capobianco J A, Proulx P P, Bettinelli M, and Negrisolo F, 1990. Phys. Rev. B **42** 5936.

Carini G, Cutroni M, D'angelo G, Federico M, Galli G, Tripodo G, Saunders G A and Wang Q, 1990. J. Non-Cryst. Solids **121** 288.

Carini G, D'Angelo G, Federico M, Tripodo G, Saunders G A and Senin H B, 1994. Phys.Rev.B **50** 2858.

Carini G, Federico M, Fontana A and Saunders G A, 1993. Phys.Rev.B **47** 3005.

Caspers H H and Rast H E, 1970. J.Chem.Phys. **53** 3208.

Cobridge D E, 1974. The Structure Chemistry Of Phosphorus.(Elsevier, New York).

Ctyroký V, 1940. Glastechnische Berichte, **18** 1.

Danielmeyer H G and Weber H P, 1972. IEEE J. Quantum Electron. **QE8** 805.

Davies H W, 1968. J.Res.Natl.Bur.Stand.A **72** 149.

Deshazer L G and Dieke G H, 1963. J. Chem. Phys. **38** 2190.

Dieke G H and Crosswhite H M, 1963. Applied Optics. **2** 675.

Dieke G H and Sarup R, 1962. J.Chem.Phys. **36** 371.

Dieke G H, 1969. Spectra of Energy Levels of Rare Earth Ions in Crystals. (John Wiley and Sons, Inc, NewYork).

Doremus R H, 1973. Glass Science. (John Wiley and Sons).

Dunstan D. and Spain I, 1989. J.Phys.E:Sci.Instrum. **22** 913.

Durville F M, Behrens E G and Powell R C, 1986. Phys. Rev.B **34** 4213.

Eastham D, 1986. Atomic Physics of Lasers. (Taylor and Francis). P156

Elliott S R, 1990. Physics of Amorphous Materials.(Longman Scientific and Technical).

Errandonea G and Sapriel J, 1979. Sol.Stat.Comms. **32** 391.

Exarhos G J and Risen Jr W M, 1971. Chem.Phys. Letters. **10** 484.

Exarhos G J and Risen Jr W M, 1972. Sol.Stat.Comm. **11** 755.

Farok H M, Senin H B, Saunders G A, Poon W and Vass H, 1994. J.Mat.Sci. **29** 2847.

Farrell E F and Newnham R E, 1965. Amer. Mineral. **50** 1972.

Farrell E F, Fang J H and Newnham R E, 1963. Amer. Mineral. **48** 804.

Fawcett V, Long D A and Taylor L H, 1976. Proc.5th.Int.Conf.Raman Spectroscopy. Frieburgh **112.**

Forman R A, Piermarini G J, Barnett J D and Block S, 1972. Science.**176** 284.

Freed S, and Katcoff S, 1948. Physica **14** 17.

French V A, Powell R C, Blackburn D H and Cranmer D C, 1991. J. Appl. Phys. **69** 913.

Friedel M G, 1924. Bull. Soc. Fr. Mineral. Cristallogr. **47** 60.

Galeener F L and Mikkelsen Jr J C, 1979. Sol.Stat.Comm. **30** 505.

Gilson T R and Hendra P J, 1970. Laser Raman Spectroscopy. Wiley-Interscience, London.

Grace J M and Anderson A C, 1989. Phys.Rev.B **40** 1901.

Guitel J C and Tordjman. 1976. Acta Crystallogr.Part **B32** 2960.

Hazen R and Finger W, 1984. Comparative Crystal Chemistry (John Wiley).

Hirao K and Soga N, 1985. J.Am.Ceram.Soc. **68** 515.

Hirst L L, 1970. Phys. Kondens. Mater. **11** 255.

Hollas J, 1987. Modern Spectroscopy. (John Wiley and Sons).

Hong H Y-P and Pierce J W, 1974. Mat.Res.Bull. **9** 179.

Hong H Y-P, 1974. Acta Cryst. **B30** 1857.

Imbusch G F, 1987. Physica Scripta.**T19** 354.

Jäckle J, 1981. Topics In Current Physics, Amorphous Solids. Vol.24. P135. Edition Phillips W A Editor, (Springer-Verlag, Berlin).

Jayaraman A, 1983. Rev. Mod. Phys. **55** 65.

Jayaraman A, Dernier P and Longinotti L D, 1975. Phys.Rev.B **11** 2783.

Jayaraman A, Narayanamurti V, Bucher E and Maines R G, 1970. Phys.Rev.Lett. **25** 1430.

Jørgensen C K, 1955. J.Inorg.Nucl.Chem.1 301.

Jost K H, 1963. Acta Crust. **16** 623.

Kaiser W and Bond W L, 1959. Phys.Rev.**115** 857.

Kaiser W, Garrett C G B and Wood D L, 1961. Phys.Rev. **123** 766.

Karpov V G, Klinger M I and Ignatev F N, 1983. Sov.Phys.JETP **57** 439.

Kirk J L, Vedam K, Narayanamurti V, Jayaraman A and Bucher E, 1972. Phys.Rev. B **6** 3023.

KishanKumar V S, Sastry S B and Acharyulu B S, 1989. Phys. Stat. Sol. B **155** 679.

Kobayashi T, Sawada T, Ikeo H, Muto K and Kai J, 1976. J.Phys.Soc.Japan. **40** 595.

Kordes E, 1939. Z.Anorg.Allgem.Chem. **241** 171.

Lasjaunias J C, Ravex A, Vandorpe M and Hunklinger S, 1975. Sol.Stat.Comm. **17** 1045.

Lawson A and Tang T, 1950. Rev.Sci.Instrum. **21** 815.

Lipinska-Kalita K E, Fontana A, Leonardi A, Carini G, D'Angelo G, Tripodo G, and Saunders G A, 1995. Philo.Mag.B **71** 571.

Long D A, 1977. Raman Spectroscopy. Mcgraw-Hill International Book Company. London.

Malinovsky V K and Sokolov A P, 1986. Sol.Stat.Comm. **57** 757.

Malinovsky V K, Novikov V N, Parshin P P, Sokolov A P and Zemlyanov 1990. Eur.Phys.Lett. **11** 43.

Mao H and Bell P, 1978.Carnegie.Institution Of Washington. Year Book. **77** 904.

Maple M B and Wohlleben D, 1971. Phys. Rev. Lett. **27** 511.

Marion J E and Weber M J, 1991. Eur.J.Sol.Stat.Inorg.Chem. **28** 271.

Martin S W, 1991. Eur.J.Solid State Inorg.Chem. **28** 163.

Martin W C, 1978. Atomic Energy Levels: The Rare-Earth Elements. U.S. Department of Commerce, National Bureau of Standards, P182.

Mcclure D S and Kiss Z, 1963. J. Chem. Phys. **39** 3251.

Mierzejewski A, Saunders G A, Sidek H A, Hampton R N and Al-Mummar I J 1988. J.Sol Stat. Ion. **28-30** 778.

Milberg M and Daly M, 1963. J.Chem.Phys.**39** 2966.

Miller A E, Nassau K, Lyons K B and Lines M E, 1988. J.Non-Crys.Solids. **99** 289.

Morgan S H, Magruder I R H and Silberman E, 1987. J. Am.Cerm.Soc. **70** C378.

Naock R and Holzapfel, 1978. Proc.6th.Airapt.Conf.High Pressure.(Plenum Press, New York) P748.

Nelson B N, and Exarhos G J, 1979. J.Chem.Phys.**71** 2739.

Parent C, Lurin C, Guillen F, LeFlem G, Hagenmuller P and Couzi M, 1987. J.Phys.Chem.Solids. **48** 207.

Parshin D A and Sahling S, 1993. Phys.Rev.B **47** 5677.

Petrovskii G T, Feofilov P P and Tsurikova G A, 1966. Opts Spectrosc. **20** 289.

Pfaender H G, 1983. Schott Guide to Glass. (Van Nostrand Reinhold).

Phillips W A, 1972. J.Lo.Temp.Phys.**7** 351.

Piermarini G J and Block S, 1975. Rev. Sci. Instrum. **46** 973.

Piermarini G J, Block S and Barnett J D, 1973. J.Appl.Phys. **44** 5377.

Piermarini G J, Block S, Barnett J D and Forman R A, 1975. J.Appl.Phys. **46** 2774.

Pissarenko V F and Bykovskii P I, 1968. Physica Status Solidi. **26** K13.

Pohl R O, 1981. Amorphous Solids Low-Temperatures Properties, Topics in Current Physics, Ed. Phillips W A (Springer-Verlag, Berlin) Vol.24 P.27.

Prins J A, 1965. In Physics of Non-Crystalline Solids,. Prins J A Ed. John Wiley and Sons, Inc, New York,. P1.

Ramos M A, Gil L, Bringer A and Buchenau U, 1993. Phys.Stat.Sol. A **135** 477.

Reisfeld R and Boehm L, 1972. J. Sol. Stat. Chem. **4** 417.

Reisfeld R and Eckstein Y, 1972. J.Sol. Stat. Chem. **5** 174.

Reisfeld R, 1972. J. Res. Nat. Bureau. Standards. A **76** 613.

Reisfeld R, 1973. Struct.Bind. **13** 53.

Reisfeld R, Greenberg E and Biron E, 1974. J. Sol. Stat.Chem. **9** 224.

Reisfeld R, Velapoldi R A, Boehm L and Ish-Shalom M, 1971. J. Phys. Chem. **75** 3981.

Rice D K and Deshazer L G, 1969. Phys. Rev. **186** 387.

Riseberg L A, 1972. Phys. Rev. Lett. **28** 786.

Riseberg L A, 1972. Sol. Stat. Comm. **11** 469.

Rouse G B Jr, Miller P J and Risen W M Jr, 1978. Non-Crys.Sol. **28** 193.

Runciman W A, 1956. Philos. Mag. **1** 1075.

Runciman W A, 1958.Repts. Progr. Phys. **21**, 30.

Sales B C, 1990. J.Non-Cryst.Sol. **119** 136.

Sales B C, Ramsey R S, Bates J B and Boatner L A, 1986. J.Non-Cryst.Sol. **87** 137.

Schulz H, Thiemann K H, and Fenner J, 1974. Mat.Res.Bull. **9** 1525.

Senin H B, 1994. PhD Thesis. The Elastic and Nonlinear Acoustic Vibrational Properties of Vitreous SiO_2 and Rare Earth Phosphate Glasses. University of Bath.

Senin H B, Wang Q, Saunders G A and Lambson E F, 1993. J. Non-Cryst.Sol. **152** 83.

Sherman W F and Stadmuller A A, 1987. Experimental Techniques in High-Pressure Research.(John Wiley and Sons).

Shuker R and Gammon R W, 1970. Phys.Rev.Lett. **25** 222.

Sidek H A, Saunders G A, Hampton R N, Draper R C and Bridge B, 1988. Philos.Mag.Lett. **57** 49.

Sidek H A, Senin H B, Saunders G A and Ford P J, 1993. J.Fiz Mal. **14** 11.

Spain I and Dunstan D, 1989. J.Phys.E:Sci.Instrum. **22** 923.

Stevels J M, 1946. Philips Technical Review. **8** 231.

Stokowski S E, Martin W E and Yarema S M, 1980. J.Non.Cryst.Sol. **40** 481.

Sun K and Risen W M Jr, 1986. Sol.Stat.Comm. **60** 697.

Szabo A, 1970. Phys.Rev.Lett. **25** 924.

Szabo A, 1971. Phys.Rev.Lett. **27** 323.

Thomas R and Nampoori V P N, 1990. Sol. Stat. Comm. **73** 803.

Tu Hailing, Saunders G A, and Bach H, 1984. Phys.Rev. B **29** 1848.

VanValenburg A, 1965. Conf.Int.Sur Les Haute Pressions, Le Creusot (Saone Et Loire, France).

VanWazer J and Campanella D, 1950. J.Am.Chem.Soc. **72** 655.

VanWazer J R, 1964. Phosphorus and Its Compounds, Vol. I (Interscience Publishers).

Walling J C, Jenssen H P, Morris R C, O'Dell E W and Peterson O G, 1979. Opt.Lett. **4** 182.

Weber H P, Damen T C, Danielmeyer H G and Tofield B C, 1972. Appl. Phys. Lett. **22** 534.

Weber H P, Tofield B C and Liao P F, 1975. Phys.Rev.B **11** 1152.

Weber M J and Matsinger B H, 1972. J. Chem. Phys. **57** 562.

Weber M J, 1990. J.Non-Cryst.Solids. **123** 208.

Weir C E, Lippincott E R, VanValkenburgh A and Bunting E N, 1959. J.Res.N.B.Standards. A **63A** 55.

Welber B and Jayaraman A, 1977. J.Appl.Phys. **50** 462.

Westman A E, 1960. Modern Aspects of Vitreous State. Ed. Mackenzie J (Butterworths, London) P.63.

Weyl W A, 1951. Coloured Glasses. Society of Glass Technology, Sheffield.

White W B, Roy R and Crichton J M, 1967. Amer. Mineral. **52** 867.

Winterling G, 1975. Phys.Rev.B **12** 2432.

Zachariasen W H, 1932. J.Am.Chem.Soc. **54** 3841.

Zeller R C and Pohl R O, 1971. Solids.Phys.Rev.B **4** 2029.

PAPERS PUBLISHED IN SCIENTIFIC JOURNALS AND CONFERENCE PROCEEDINGS

1- An 'alexandrite' effect and optical properties of holmium metaphosphate glass.
H M Farok, G A Saunders, W A Lambson, R Krüger, H B Senin, S Bartlett and S Takel, Physics and Chemistry of Glasses. **37** (1996) 125.

2- Optical and ultrasonic properpties of europium phosphate glasses.
H M Farok, H B Senin, G A Saunders, W Poon and H Vass, Journal of Material Science. **29** (1994) 2859.

3- Low temperature fluorescence, valence state and elastic anomalies of samarium phosphate glasses.
H M Farok, G A Saunders, W Poon and H Vass, Journal of Non-Crystalline Solids, **142** (1992) 175.

4- Ultrasonic Studies of Rare Earth Phosphate Glasses.
B Senin,Q Wang, G A Saunders, R C J Draper, **H M Farok**, P J Ford, W Poon, H Vass and B Bridge. Developments in Acoustic and Ultrasonics, ed. M. Povey and J. McClements, Institute of Physics, London, pp. 197 (1992).

5- Ultrasonic Studies of Rare Earth Phosphate Glasses.
H B Senin, Q Wang, G A Saunders, R C J Draper, **H M Farok**, M Cankurtaran and P J Ford. Proc. of the *8th* Ann. Solid State Science (UPM) pp. 157 (1991).

6- Manufacture and Physical Properties of Rare Earth Phosphate Glasses.
H B Senin, Q Wang, G A Saunders, R C Draper, E F Lambson, M Cankurtaran, P J Ford, **H M Farok**, H A Sidek and W Lambson. Glass Technology, **34** (1993) 75.

7- Vibrational Properties of Europium Phosphate Glasses.
H B Senin, **H M Farok**, H A A Sidek, G A Saunders and P J Ford. Journal of Solid State Science and Technology (Malaysia) 118 (1993).

PAPERS PRESENTED AT SCIENTIFIC CONFERENCES

1- Ultrasonic Studies of Rare Earth Phosphate Glasses

H B Senin, Q Wang, G A Saunders, R C J Draper, **H M Farok**, P J Ford, W Poon, H Vass and B Bridge. Developments in Acoustic and Ultrasonics Conference, University of Leeds, UK, 24-25 September 1991.

2- Ultrasonic Studies of Rare Earth Phosphate Glasses.

H B Senin, Q Wang, G A Saunders, R C J Draper, **H M Farok**, P J Ford and B Bridge.Annual Conference of Solid State Physics (Malaysia) 1993, Universiti Pertanian Malaysia, Malaysia, 24-26 October 1991.

3- Acoustic and Optical Properties of Rare Earth Phosphate Glasses.

H B Senin, **H M Farok**, G A Saunders, Q Wang, R C J Draper, M Cankurtaran, P J Ford, W Poon, H Vass and B Bridge. Condensed Matter Division Annual General Conference - 1991, University of Birmingham, UK, 17-19 December 1991.

4- Manufacture and Physical Properties of Rare Earth Phosphate Glasses.

H B Senin, Q Wang, G A Saunders, R C J Draper, E F Lambson, M Cankurtaran, P J Ford, **H M Farok**, H A A Sidek and W A Lambson. Symposium on Science and Art in Glass, Royal Institution, London, UK, 19-21 October 1992.

5- Optical and Acoustic Properties of Europium Phosphate Glasses.

H B Senin, **H M Farok**, G A Saunders, P J Ford, W Poon and H Vass.13*th* General Conference of the Condensed Matter Division, European Physical Society, Universität Regensburg, Germany, 29 March - 2 April 1993.

PH30035 MP 2/6.

1310 - 1500. 3/4.

PH30032 LMO 3/6.

1300 - 1500 3/4.

PH30029. TD / Stat. M 9/6.

1300 - 1500. A = 5
B = 2/3

PH30030 QM. 11/6.

16:30 - 1830. 3/4.

PH30025 Eqn. 10/6.

1630 - 1830 3/4

Farok, Haitham Mohammed.

Fluorescence & Raman Spectra of rare earth metaphosphate glasses & .....

Bath. Univ. 1997.

~~Thesis~~ Thesis (Ph.D).

PG. Thesis - Physic.

ISSUE DESK.